UNIVERSITAT DE BARCELONA

Diarylethene-based Pt(II) molecular switches: a novel approach to photoactivated chemotherapy

Andreu Presa i Rodríguez

Facultat de Química

Departament de Química Inorgànica i Orgànica, Secció de Química Inorgànica

Programa de doctorat en Química Inorgànica Molecular

Diarylethene-based Pt(II) molecular switches: A novel approach to photoactivated chemotherapy

---

Andreu Presa i Rodríguez

2016

Grup de Química Bioinorgànica

Prof. Patrick Gamez Enamorado — Director

Dra. Amparo Caubet Marin — Tutora

Patrick Gamez Enamorado, investigador ICREA Senior i professor associat del Departament de Química Inorgànica i Orgànica, Secció de Química Inorgànica, de la Universitat de Barcelona,

CERTIFICO que el treball "Diarylethene-based Pt(II) molecular switches: A novel approach to photoactivated chemotherapy", que presenta Andreu Presa i Rodríguez per optar al grau de Doctor, ha estat realitzat sota la meva direcció al Departament de Química Inorgànica i Orgànica, Secció de Química Inorgànica, de la Universitat de Barcelona.

Barcelona, novembre de 2016

Patrick Gamez Enamorado

Amparo Caubet Marin, professora titular del Departament de Química Inorgànica i Orgànica, Secció de Química Inorgànica, de la Universitat de Barcelona,

CERTIFICO que el treball "Diarylethene-based Pt(II) molecular switches: A novel approach to photoactivated chemotherapy", que presenta Andreu Presa i Rodríguez per optar al grau de Doctor, ha estat realitzat sota la meva tutela al Departament de Química Inorgànica i Orgànica, Secció de Química Inorgànica, de la Universitat de Barcelona.

Barcelona, novembre de 2016

Amparo Caubet Marin

Parts of this PhD thesis can be found in the following publications:

'Photoswitching the cytotoxic properties of platinum(II) compounds'

Andreu Presa, Rosa F. Brissos, Ana Belén Caballero, Ivana Borilovic, Luís Korrodi-Gregório, Ricardo Pérez-Tomás, Olivier Roubeau and Patrick Gamez.
Angew. Chem. Int. Ed. **2015**, *54* (15), 4561-4565.

'Non-switching 1,2-dithienylethene-based diplatinum(II) complex showing high cytotoxicity'

Andreu Presa, Leoní Barrios, Jordi Cirera, Luís Korrodi-Gregório, Ricardo Pérez-Tomás, Simon J. Teat and Patrick Gamez.
Inorg. Chem. **2016**, *55* (11), 5356-5364.

‘It’s a dangerous business, Frodo, going out your door.
You step into the road, and if you don’t keep your feet,
there’s no knowing where you may be swept off to.’

— The Lord of the Rings: The Fellowship of the Ring

Agraïments

En primer lloc, voldria expressar el meu agraïment al Prof. Patrick Gamez, actual cap del grup de Química Bioinorgànica de la Universitat de Barcelona i director d'aquesta tesi doctoral, per haver confiat en mi a l'hora d'iniciar una nova i estimulant línia de recerca. Així mateix, vull donar les gràcies a la Prof. Virtudes Moreno, anterior cap del grup, per haver despertat el meu interès per la química bioinorgànica amb les seves classes i, posteriorment, donar-me la oportunitat d'iniciar el meu treball científic.

El meu agraïment és també per a la Dra. Amparo Caubet i la resta de membres del grup de Química Bioinorgànica. La Rosa, que ha estat sempre disposada a ajudar en tot el que fos necessari; l'Ana Belén, que ha aconseguit imposar una mica de criteri i cordura al laboratori; i el Guillem, que va ser prou llest com per abandonar els diariletens a temps.

Agraeixo la inestimable col·laboració del Dr. Jordi Cirera, del Grup d'Estructura Electrònica, per haver dut a terme els càlculs computacionals recollits en aquest treball. Agraeixo també al Prof. Ricardo Pérez Tomás que m'obrís les portes del Cancer Cell Biology Research Group de la facultat de medicina, per tal de poder-hi realitzar els assaigs cel·lulars presentats en aquesta tesi, i al Dr. Luís Korrodi-Gregório i la resta de membres d'aquest grup la seva bona predisposició per acollir-me i ajudar-me durant la meva estada.

Gràcies a tots els companys i companyes del departament (ara secció) de Química Inorgànica, que durant tots aquests anys m'han fet sentir com a casa. Especialment al Pau i la Marta, que han après a suportar-me i han aconseguit fer de l'hora del cafè un dels millors moments del dia.

Finalment, dono les gràcies als meus pares, sense el suport dels quals no hauria estat possible assolir aquesta fita. I també a tu, Maria, perquè tot i que el camí no ha estat fácil sempre m'has fet costat.

Moltes gràcies a tots.

Contents

Chapter 3: Spectroscopic, structural and computational analyses

Chapter 4: Biological evaluation

Summary and conclusions

Abbreviations

A.U.	Arbitrary units
Ar	Aryl group
b.p.	Boiling point
bp	Base pair
bipy	Bipyridine
CD	Circular dichroism
ct	*Calf thymus*
DFT	Density functional theory
DMEM	Dulbecco's modified eagle medium
DMF	Dimethylformamide
DMSO	Dimethylsulfoxide
DNA	Deoxyribonucleic acid
DTC	Dithienylcyclopentene
DTFC	Dithienylperfluorocyclopentene
EA	Elemental analysis
EB	Ethidium bromide
en	Ethylenediamine
equiv.	Equivalents (concentration)
ESI	Electrospray ionization
Et_2O	Diethyl ether
HOMO	Highest occupied molecular orbital

IC_{50}	Half maximal inhibitory concentration
IR	Infrared
LUMO	Lowest unoccupied molecular orbital
Me	Methyl
MeOH	Methanol
MRI	Magnetic resonance imaging
MS	Mass spectrometry
MTT	3-(4,5-Dimethylthiazol-2-yl)-2,5-diphenyltetrazolium bromide
NMR	Nuclear magnetic resonance
PACT	Photoactivated chemotherapy
ppm	Parts per million (frequency)
PDT	Photodynamic therapy
Phen	Phenanthroline
PSS	Photostationary state
py	Pyridine
R_f	Retention factor
TD-DFT	Time-dependent density functional theory
terpy	Terpyridine
THF	Tetrahydrofuran
TLC	Thin-layer chromatography
UV	Ultraviolet
Vis	Visible

Abstract

The photoactivation of metal complexes with potential anticancer activity is a hot topic of current research, as it may lead to the development of more selective and efficient drugs. Photoactivated chemotherapy (PACT) with coordination compounds is usually based on photochemical processes taking place at the metal center. In contrast, an innovative ligand-mediated photoactivation approach that exploits the outstanding photochemical properties of diarylethenes has been developed in the present PhD thesis. Platinum(II) complexes from dithienylcyclopentene-based photoswitchable ligands have been designed and prepared. These systems exhibit two thermally stable, interconvertible photoisomeric forms, which present clearly distinct properties. The photochemical behavior of all ligands and metal complexes has been examined by means of ^{1}H NMR and UV-Vis spectroscopies, and a number of crystal structures have been determined. Additionally, DFT calculations have been performed to analyze the effect produced by the attachment of different metal-binding units on the photochemical performance of the diarylethene synthon. Subsequently, the interaction of each photoisomer of the platinum(II) complexes with DNA has been thoroughly investigated using different techniques. These studies revealed that the light-triggered transformation of these systems effectively translates into different DNA binding modes and affinities, as desired for a photoactivatable drug. The antiproliferative activity of the complexes prepared has then been evaluated through various cell viability *in vitro* assays, which validated the potential applications of such diarylethene-based photoswitches for the development of a new class of photochemotherapeutic metallodrugs.

CHAPTER 1

Introduction

1.1. Medicinal bioinorganic chemistry

Metallic elements play a critical role in the metabolism of living organisms.[1] Positively charged metal ions are able to interact with a variety of electron-rich structures, such as proteins, nucleic acids, molecular oxygen and other relevant anionic species, and regulate countless biological processes. It is well known, for instance, that hemoglobin contains an iron center that is responsible for dioxygen binding and transport. Manganese is indispensable for oxygenic photosynthesis, since it is required for the oxidation of water in photosystem II, and zinc provides the structural framework that governs the DNA-binding specificity of a number of proteins. Many other metal ions are also found in the active site of a wide variety of metalloproteins and enzymes, and are thus essential for life. Up to fifteen metallic elements (Na, K, Mg, Ca, V, Cr, Mn, Fe, Co, Ni, Cu, Zn, Mo, Cd and Sn) are currently known to be required for normal biological function in human beings, and the involvement of a few other metals is still under investigation.[2,3]

In addition, metal ions are also a fundamental part of pharmacology. In fact, although the rational design of metal-containing drugs is still a relatively recent field of research, metals have been used as medicinal agents for several millennia. Copper, for example, was already used for the sterilization of water and physical wounds in Ancient Egypt

around 2500 BC, and later civilizations such as the Greeks and the Aztecs were also aware of its beneficial properties.[4] Gold is found in a number of preparations in Chinese and Arabic traditional medicine, and there is evidence that the Romans used iron oxide, antimony sulfide and various zinc carbonates for healing purposes.[5] Centuries later, after the relative stagnation of chemical research during the Middle Ages, both mercury(I) and mercury(II) chlorides were applied as medicines in the early modern period; the former was commonly administered as a diuretic and laxative agent, and the latter was widely used for syphilis treatment before the advent of antibiotics.[6] However, their actual efficacy was never proven and they often led to even worse effects due to mercury toxicity, which would not be eventually discovered until the nineteenth century.

It was not until the early twentieth century that the first major discovery of a synthetic, metal-based pharmacological agent finally took place. Arsphenamine, an organoarsenic complex bearing 2-aminophenol ligands and typically known as salvarsan, was introduced in 1910 by Paul Ehrlich as the first truly effective treatment for syphilis.[7] The proposed chemical structure of salvarsan, which could not be determined until recent years, is depicted in Figure 1.1, along with that of its subsequent sulfoxylated, water-soluble derivative neosalvarsan. Both arsenic compounds were replaced by penicillin after World War II, but they still represent the first example of structure-activity relationship and chemical optimization of a synthetic drug. Ehrlich, who was awarded the Nobel Prize in 1908 for his contributions to

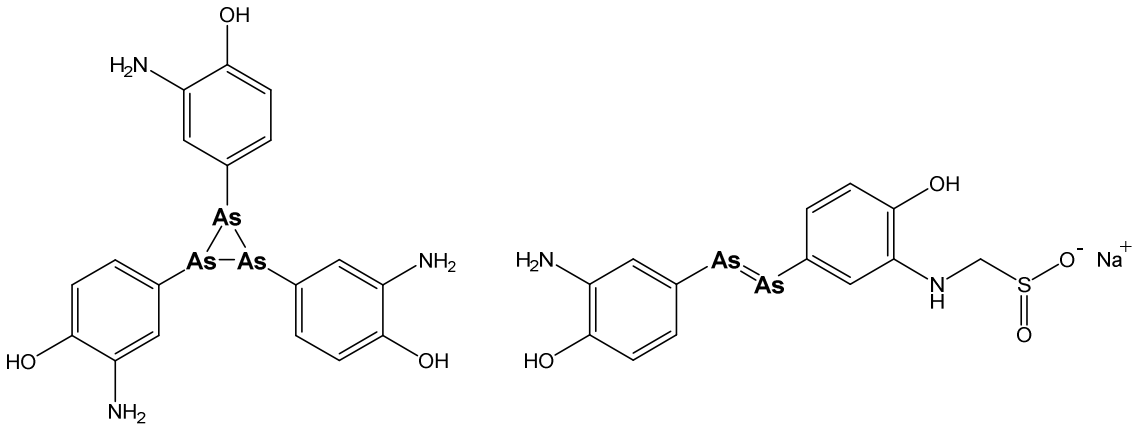

Figure 1.1. *Proposed chemical structures of salvarsan (left) and neosalvarsan (right).*[7]

immunology, also introduced the "magic bullet" concept to describe a chemical compound able to hit a specific target without harming the whole organism, and is thus considered one of the main founders of chemotherapy.

The clear landmark event that gave rise to medicinal bioinorganic chemistry as a discipline is the key discovery of the antitumoral properties of *cis*-$[PtCl_2(NH_3)_2]$, universally known as cisplatin, by Barnett Rosenberg in 1965.[8] Cisplatin, already described in 1844 by Michele Peyrone and therefore referred to as Peyrone's salt for a long time,[9] exhibited promising inhibition of cell replication in *Escherichia Coli* cultures. Further studies in mice demonstrated its effectiveness in tumor growth regression,[10] and the treatment of human patients started in 1971; in current terms, this represented a remarkably short period of time since the original discovery. Finally, cisplatin received worldwide clinical approval for testicular and ovarian cancer treatment between 1978 and 1979, greatly increasing their cure rates. Nowadays, despite its severe side effects and limitations, cisplatin is routinely used to treat bladder and cervix cancer, as well as several types of sarcomas and carcinomas, and it is currently included in the World's Health Organization Model List of Essential Medicines.

From this important breakthrough, the development of novel pharmacological agents based on transition metals became a whole new field of research which has attracted ever-growing attention over the last decades. As a result of all these efforts, the amount of metallic elements that have found application as both therapeutic or diagnosis agents, along with the number of pathologies towards which these therapies can be applied, have increased exponentially.[11] A few representative examples of compounds used clinically are depicted in Figure 1.2. Several gold(I) complexes are commonly used in the treatment of rheumatoid arthritis, auranofin being the most prominent.[12] A great number of ^{99m}Tc compounds are currently employed as imaging agents that target specific organs or fluids, and highly paramagnetic gadolinium(III) or manganese(II) complexes are used as injectable contrast agents for MRI scans.[13,14] Compounds containing copper, gallium, bismuth, vanadium, iron, ruthenium or silver have also shown notable activities against several pathologies, such as cancer, diabetes, cardiovascular disorders or parasitic diseases, and are either in clinical use or in advanced clinical trials.[15]

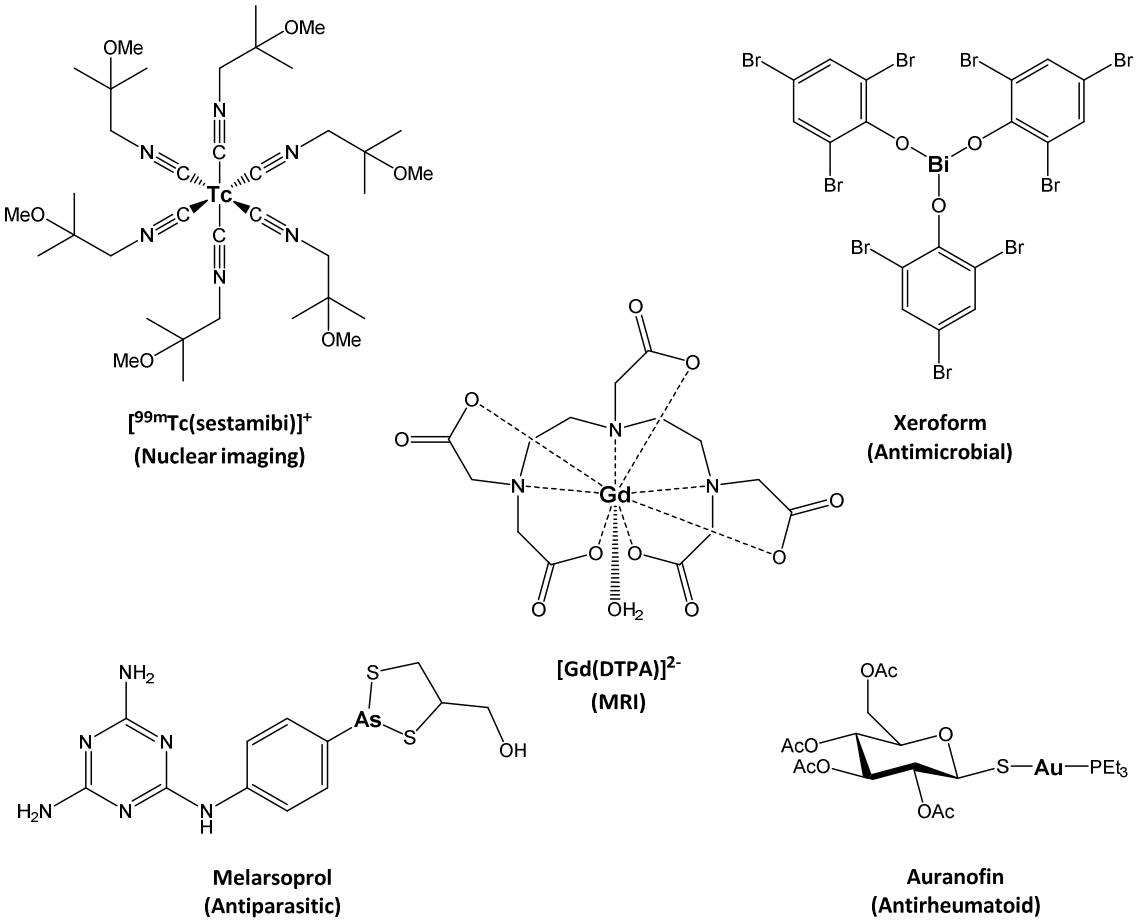

Figure 1.2. *Selected examples of metal complexes in current clinical use.*[12–15]

The key to this success lies in the intrinsic properties of metal ions. Transition-metal complexes offer a wide range of accessible oxidation states and coordination geometries, as well as particular thermodynamic and kinetic features closely linked to the electronic structure of the chosen metal center. Moreover, they can also effectively act as scaffolds or prodrugs that can undergo ligand-exchange or redox reactions under specific conditions or external stimuli, which allows the selective generation of active species upon reaching specific targets. In summary, metal complexes represent a rich synthetic toolbox to achieve singular reactivities, in combination with the vast range of functional groups and molecular recognition motifs that organic molecules can offer. Metallodrugs hold a tremendous potential to help overcoming currently intractable conditions and to lead to novel mechanisms of action able to surpass drug resistance. Accordingly, they are expected to continue playing a crucial role in the development of novel treatments in the coming years.

1.2. Platinum anticancer drugs

1.2.1. Cancer incidence and treatment

Despite the constant widening of the spectrum of diseases towards which metal-containing drug development is addressed, cancer is still one of the main focuses of research in medicinal bioinorganic chemistry. Cancer is currently the second leading cause of death among the adult population after cardiovascular disease; about 15 million new cases of cancer were diagnosed in 2013, accounting for over 8 million deaths worldwide.[16] Regrettably, these numbers are expected to continue growing in the coming years.

Cancer can be defined as a group of more than a hundred of related pathologies involving abnormal and uncontrolled cell growth, which results in the formation of masses of tissue known as tumors. Tumors interfere with the normal biological function of adjacent organs, ultimately producing their failure. In some cases, they are even able to invade distant tissues in the body via the migration of malignant cells through the blood stream and the lymphatic system, a process known as metastasis. Malignant cancerous cells exhibit a series of specific features such as their ability to stimulate their own growth and ignore the normal regulatory signals and cell-death mechanisms, thus exhibiting a limitless replication potential.[17]

At the subcellular level, cancer originates from the undesired alteration of the cell-growth regulation mechanisms in a healthy tissue, which may result from the eventual mutation of specific genes during the normal cell-replication cycle.[18] Two conceptually different kinds of genes may be affected for cancer to occur; the oncogenes, which promote different cell-growth and replication-related processes, and the so-called tumor-suppressor genes, whose expression either inhibits cell division or promotes regulation and cell-death mechanisms. The malignant transformation of healthy cells into cancerous cells generally involves a cascade of mutations and DNA-replication errors along subsequent cell-division cycles, ultimately leading to the overexpression of oncogenes, the disabling of various tumor-suppressor genes and the failure of DNA-repair mechanisms. Although many of these changes may be serendipitous, the presence of carcinogenic substances in the cellular environment, e.g. as a result of a

continuous exposure, greatly contributes to this process, since such species are generally able to induce additional damage to the genome or disrupt the DNA-repair pathways.[19]

Owing to the nature of this disease, cancer treatment focuses on the effective destruction of malignant cells. Common current treatments include surgery, radiotherapy, chemotherapy, immunotherapy, hormonal therapy and targeted therapy, whose application depends on the location of the main tumoral mass and the global stage of development of the pathology. Chemotherapeutic agents, such as cisplatin, generally aim to destroy cancer cells by blocking their abnormally high proliferation rates and inducing cell-death mechanisms, nuclear DNA being the main target to achieve that goal.

1.2.2. The mechanism of action of cisplatin

Despite the fact that the full elucidation of the processes that govern cisplatin's antitumoral activity is still the focus of several lines of research, it is widely accepted that its biochemical mechanism of action stems from its binding to DNA, within the cancer cell nucleus. This association interferes with the transcription and replication mechanisms, triggering a cascade of events that ultimately leads to the activation of irreversible cell-death programs, namely apoptosis or necrosis.[20]

Owing to its limited oral bioavailability, cisplatin is commonly administered by intravenous injection, rapidly diffusing into tissues. The high chloride concentration in the blood stream (ca. 100 mM) prevents hydrolysis and maintains the compound in its neutral state until reaching the tumoral cells. The high affinity of platinum(II) towards sulfur-containing amino acids, such as methionine or cysteine, allows cisplatin binding to albumin and other plasma proteins; this association, which is estimated to affect 65-90% of the administered platinum, reduces the drug's initial excretion, therefore increasing its subsequent deposition in tissues.[21]

The exact mechanism by which cisplatin crosses the cell membrane is still not fully understood, although it is known that its accumulation does not saturate with increasing drug concentration nor is it inhibited by structural analogues. Several

studies indicate that the drug enters the cell via a combination of passive diffusion and active transport mediated by membrane proteins, with a significant contribution of the copper transporter CTR1.[22] Once within the cytoplasm, where the chloride concentration falls below 20 mM, cisplatin is activated by hydrolysis; the water-mediated substitution of a chlorido ligand results in the formation of the more reactive *cis*-$[PtCl(H_2O)(NH_3)_2]^+$ species, which readily interacts with a number of electron-rich biological targets. In fact, although chromosomal DNA has been unequivocally identified as the drug's primary objective, most of the internalized cisplatin binds to various metalloproteins and other cellular components before actually reaching the cell nucleus. Glutathione (GSH), a relatively abundant cysteine-containing tripeptide with antioxidant functions, is considered the most important non-DNA cellular target of cisplatin. Binding to GSH leads to the inactivation of cisplatin followed by subsequent excretion, and its overproduction has been related with the development of drug-resistance mechanisms.[23] Other excretion pathways include the recognition by copper transporters, such as ATP7A and ATP7B.[24] A schematic representation of all these cisplatin's uptake-related processes is depicted in Figure 1.3.

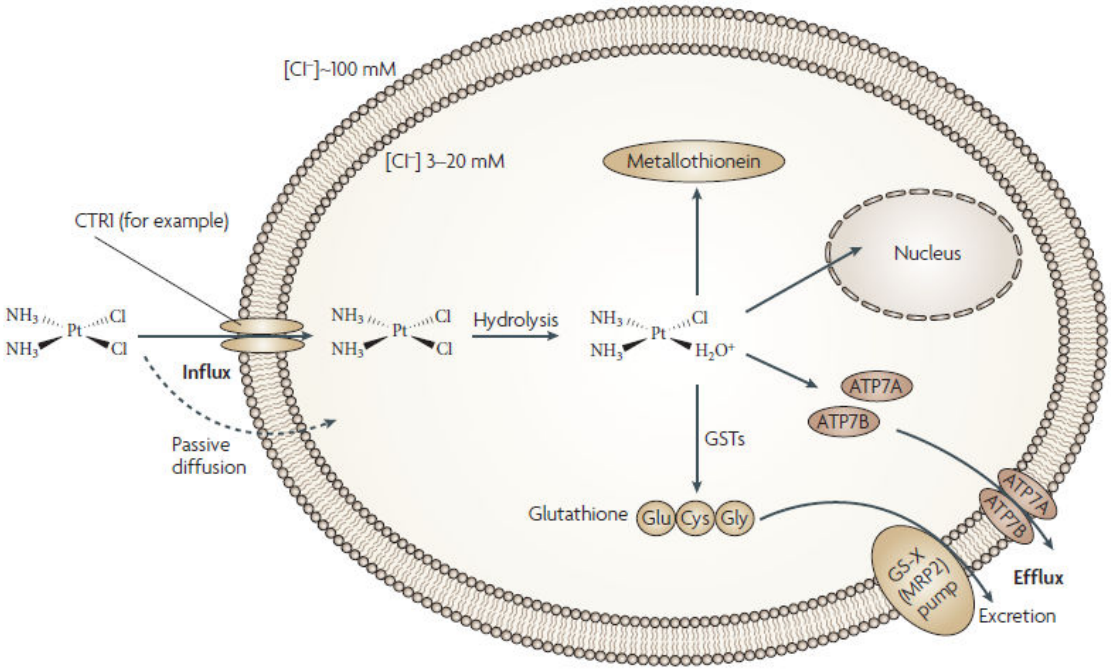

Figure 1.3. *Schematic representation of the most important processes governing cisplatin's cellular uptake, ligand-exchange activation and excretion.*[24]

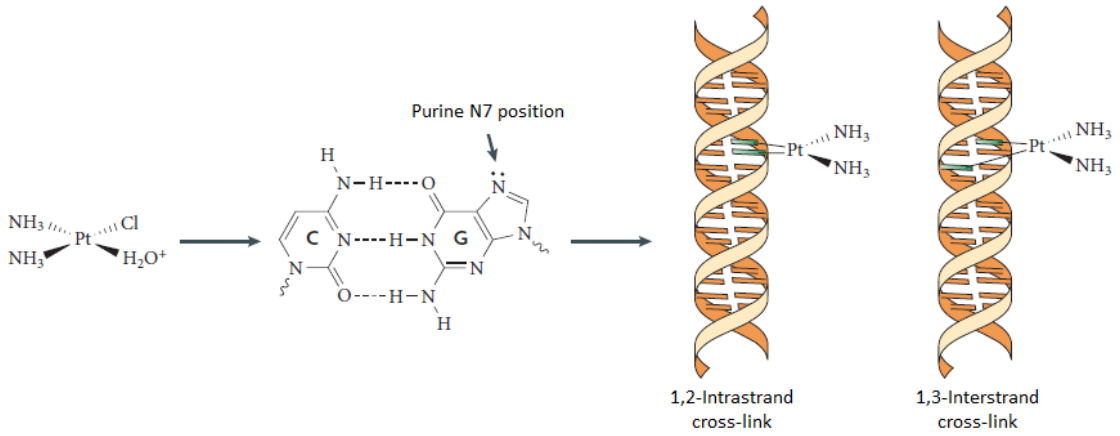

Figure 1.4. *Schematic representation of the main bifunctional adducts resulting from the covalent binding of cisplatin to DNA.*[24]

The nucleophilic N7 position of the purine bases (i.e. adenine and guanine), which is readily accessible through the major groove of the double helix, constitutes the preferential DNA binding site of cisplatin once the aquated drug enters the cell nucleus. Following coordination through the substitution of the aqua ligand, the remaining chlorido leaving group is subsequently substituted by another purine residue, with a remarkable preference for guanine, thus forming a bifunctional DNA cross-link. As depicted in Figure 1.4, the formation of the two covalent bonds may involve purine bases in the same DNA strand or in separate strands, which gives rise to intrastrand or interstrand cross-links, respectively.[25] It has been found that 1,2-d(GpG) intrastrand cross-links, involving two guanine residues adjacent to each other, are the most prevalent adducts formed by cisplatin (65%), followed by the 1,2-d(ApG) adduct (25%). Other less-frequent platination products include the intrastrand and interstrand 1,3-d(GpXpG) cross-links, involving two non-adjacent guanine residues, whereas monofunctional adducts and protein-DNA cross-links have also been reported.[26]

Cisplatin-induced cross-links severely distort the structure of duplex DNA, producing its local unwinding and bending. Such alterations interfere with DNA replication and transcription processes, due to the blockage of the required strand separation and protein binding.[27] Even though most of these genomic lesions can be recognized by mismatch-repair proteins and removed by the nucleotide excision repair (NER) machinery, if the cell is unable to fully overhaul DNA damage, a complex network of

signal transduction pathways leads to G2 phase cell-cycle arrest.[28] Ultimately, apoptotic or necrotic cell death occurs.[29]

However, as notable as its clinical impact may be, particularly against testicular or ovarian cancer, it is also widely known that the treatment with cisplatin has important limitations. Its relatively low accumulation specificity towards cancer cells accounts for severe affectation of other tissues displaying high cell-replication rates, most remarkably in the gastrointestinal tract. Additional dose-limiting side effects include affectation of the kidney (nephrotoxicity), the nervous system (neurotoxicity) and the auditory nerve (ototoxicity), as well as hemolytic anemia.[30]

Additionally, some types of tumors, such as non-small cell lung carcinoma (NSCLC), exhibit intrinsic resistance to cisplatin treatment, whereas in other cases the drug resistance is gradually acquired upon chronic exposure.[31] The mechanisms of such acquisition of platinum resistance are still scarcely understood, but from a general perspective they usually result in an insufficient amount of platinum actually reaching the cell nucleus, in addition to the inability to trigger apoptotic pathways upon DNA cross-link formation. In this regard, it has been pointed out that the main metabolic responses causing acquired resistance to platinum-based metallodrugs include the eventual increase of the cellular levels of sulfur-containing detoxification components —such as glutathione and metallothioneins—, as well as the overexpression of NER-related proteins like ERCC1.[32,33]

1.2.3. Novel generations of platinum-based chemotherapeutics

Understanding the molecular mechanisms by which cancer cells react to cisplatin-induced damage, as well as the origin of undesired side effects and drug resistance, led to the design of subsequent generations of novel, more efficient platinum antitumoral agents aiming to circumvent those limitations. Hence, over twenty novel platinum compounds entered clinical trials in the last decades, although a very few of them managed to be finally granted marketing approval.[34] A summary of all the platinum drugs in current clinical use, together with the most promising compounds presently undergoing clinical trials, is depicted in Figure 1.5.

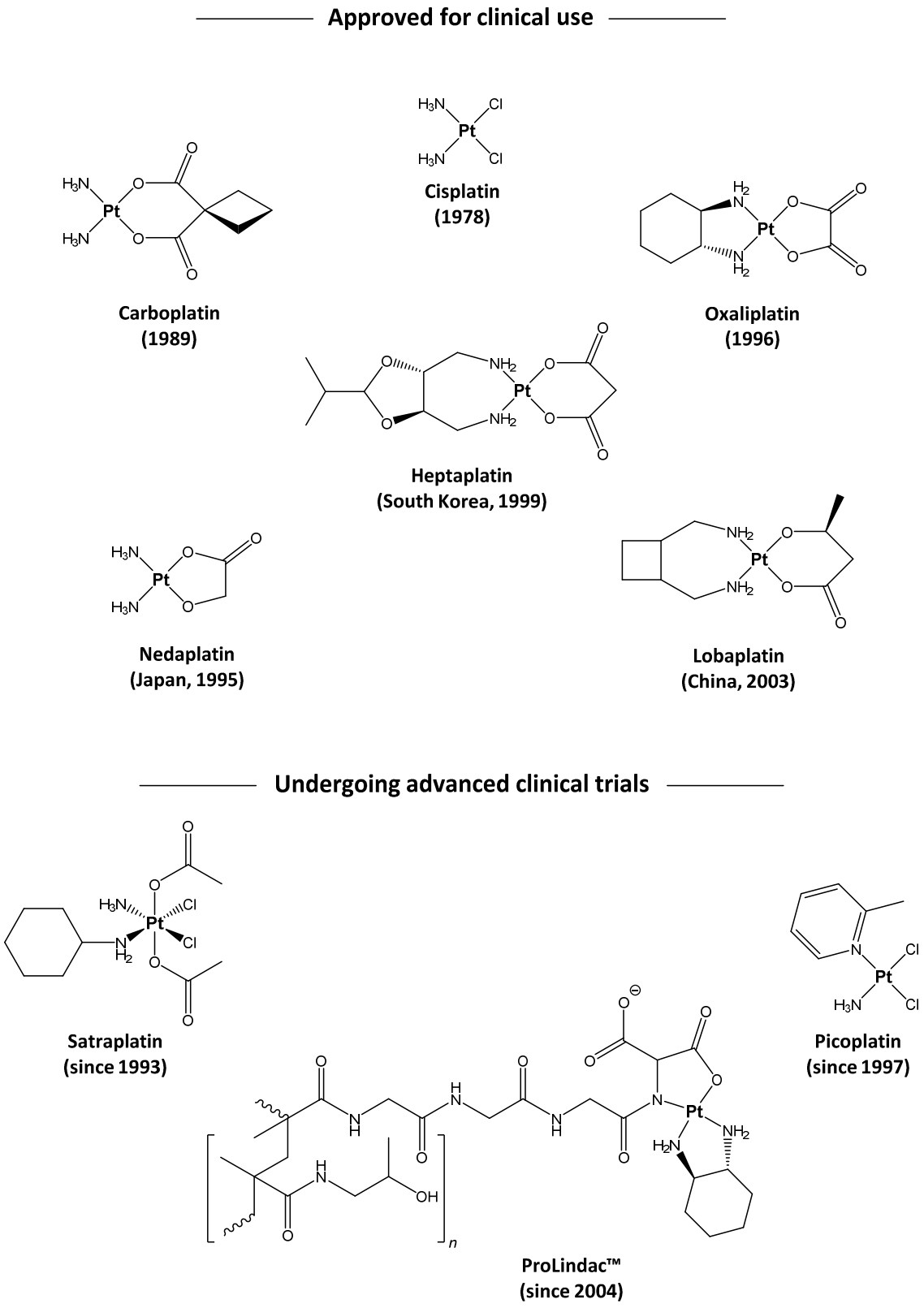

Figure 1.5. *Currently approved platinum drugs in clinical use (top) and promising platinum drugs presently undergoing advanced clinical trials (bottom). The year of first approval or of clinical-trial entry, as well as region-limited approvals, are indicated in parentheses.*[34]

Carboplatin, introduced in the early 1980s, was the first successful platinum drug specifically developed to reduce the side effects associated to cisplatin treatment. The hypothesis behind carboplatin's design was that the replacement of the chlorido ligands with a more stable carboxylate leaving group would account for lower aquation rates and hence reduced systemic toxicity, although the active species resulting from this slower process would still remain the same as those of cisplatin.[35] Interestingly, this assumption turned out to be quite accurate; carboplatin can be essentially considered as a cisplatin analogue with equivalent antitumoral properties, but showing remarkably more tolerable side effects. In addition to being far less aggressive to the nervous system and the gastrointestinal tract, it is devoid of excretion-related nephrotoxicity, and can be administered in much higher doses with respect to its parent compound. Carboplatin is now the drug of choice for the treatment of ovarian cancer, and further expansion of its clinical application is yet under examination.[36]

The third platinum drug receiving worldwide approval for cancer treatment was the third-generation compound oxaliplatin. If carboplatin managed to overcome toxicity by incorporating the carboxylate motif, oxaliplatin was developed with the additional aim of circumventing resistance mechanisms, through the additional replacement of the ammine ligands with a (*R*,*R*)-1,2-diaminocyclohexane (DACH) moiety (see Figure 1.5). Due to the presence of this bulky hydrophobic group, oxaliplatin-induced 1,2-intrastrand cross-links result in a greater conformational alteration of DNA, preventing the recognition and binding of DNA-repair proteins.[37] Furthermore, it has also been shown that oxaliplatin's uptake is far less dependent on copper transporters compared to that of cisplatin and oxaliplatin, thus being able to overcome CTR1 underexpression-mediated acquired resistance.[38] Currently, oxaliplatin is widely used in the treatment of colorectal cancer in combination with 5-fluorouracil, and its efficacy towards other types of cancer is still being investigated.

Nedaplatin, lobaplatin and heptaplatin (see Figure 1.5) are also second- and third-generation platinum drugs in clinical use, although their marketing approvals are still limited to Japan, China and South Korea, respectively. Being a glycolate-containing, more water-soluble analogue of cisplatin, nedaplatin exhibits features comparable to those of carboplatin. The substitution of the chlorido leaving groups with the chelating ligand provided comparable effectiveness with respect to its parent compound, but

with reduced renal and gastrointestinal toxicity. Nedaplatin is now commonly used in the treatment of lung, esophageal, head and neck cancers.[39] Lobaplatin and heptaplatin, on the other hand, are third-generation derivatives bearing a chelating carboxylate and a diamine bidentate ligand, and are thus structurally and functionally equivalent to oxaliplatin. Both drugs show lower levels of toxicity and more potent anticancer activity against cisplatin-resistant cells, and are applied in the treatment of breast, lung and gastric cancers.[40,41]

In addition, a few platinum compounds that are currently undergoing phase II and III clinical trials are also worth of attention, owing to the interesting approaches that led to their development (see Figure 1.5, bottom). For instance, satraplatin is a platinum(IV) octahedral complex specifically developed to display improved oral bioavailability, which results from the inclusion of lipophilic axial acetato ligands. Within the blood stream, satraplatin is reduced to majorly produce the active *cis*-$[PtCl_2(C_6H_5NH_2)(NH_3)]$ species, whose mechanism of action is comparable to that of the previously described complexes.[42] Due to the fact that its uptake is independent of copper transporters, satraplatin retains good activity against tumors exhibiting influx-related acquired resistance to cisplatin, including lung, prostate, ovarian and cervix cancers.[43] Nevertheless, its approval was rejected on the basis of not showing significant benefits in overall patient survival. Currently, satraplatin is undergoing additional clinical trials for combined therapy, in several stages of development.[44,45]

Picoplatin was specifically designed to circumvent excretion and drug resistance associated to glutathione and metallothioneine binding, by providing steric bulk around the platinum center with a 2-methylpyridine ligand.[46] Preclinical studies showed that picoplatin was strongly active against cisplatin-resistant and carboplatin-resistant cell lines, and it exhibited promising antitumor activity against ovarian and prostate cancer in phase II trials. However, picoplatin was also withdrawn from several studies due to its low patient-survival improvement. It is now under examination for combined therapy against colorectal cancer.

Lastly, ProLindac™ is an innovative formulation containing the $[Pt\{(R,R)\text{-}1,2\text{-}DACH\}]^{2+}$ active species from oxaliplatin, attached to a hydrophilic, biocompatible polymer, the objective being to exploit the enhanced permeability and retention effect of

macromolecules in malignant cells.[47] Additionally, it takes advantage of the more acidic conditions typically found in the extracellular environment of solid tumors, which facilitate the protonation of the amidomalonate chelate and subsequent local release of the active compound.[48] At present, ProLindac™ has completed several phase II clinical trials for the treatment of ovarian, head and neck cancers, with promising results in patients unsuccessfully treated with other platinum formulations. Furthermore, it also shows strong synergistic effects in combination with the organic anticancer drug paclitaxel (Taxol®).

Actually, ProLindac™ constitutes a very illustrative example of the ever-growing importance of introducing novel biochemical strategies in cancer treatment, in order to develop more selective drugs able to overcome resistance and toxicity. In recent years, much effort has been directed towards the design of targeted systems capable of selectively transporting active species to tumors, through the application of a variety of responsive approaches.[49] In this context, several types of drug-loaded scaffolds able to be preferentially delivered and internalized by cancer cells have been developed. For instance, the iron-storage protein ferritin has been used to selectively deliver cisplatin to malignant cells, owing to their much higher iron requirements, and cell membrane-derived microparticles displaying high affinity for tumors have also been reported to accomplish the same function.[50,51] Attaching active drugs to various molecular recognition motifs, hence targeting specifically overexpressed cancer-cell receptors, is also an interesting strategy. Folate or estrogen receptors, to name a few relevant examples, are commonly overexpressed in several types of human cancer cells, and can therefore be exploited to efficiently deliver conveniently functionalized drug derivatives, leading to high tumor specificity.[52,53]

Another elegant approach aimed at enhancing tumor selectivity, while reducing systemic toxicity, is photochemical control. Recent advances in laser and fiber-optic technologies have spurred the development of several medical applications based on the use of light, including the design of novel metal-containing prodrugs that can be conveniently activated upon irradiation. Photoactivated chemotherapy (PACT) is a prominent investigation field able to provide both temporal and spatial control over drug activity, which offers tremendous potential for the treatment of different types of cancer.[54]

1.3. Light-activated metallodrugs

1.3.1. Basic principles of photochemistry

Photochemistry is the chemistry of excited electronic states. Light irradiation produces alteration of the inner electronic structure of absorbing molecules, modifying both their physical and chemical properties. Typically, when a molecule absorbs a photon, an electron is promoted to an orbital of higher energy, generating a short-lived excited state. The excess of energy accumulated in this way shall therefore be dissipated for the system to return to its starting, more stable ground state; this process may take place through different modes of energetic deactivation, some of them involving the emission of light at a longer wavelength with respect to that used for the excitation.[55]

A schematic representation of the processes related to light absorption in a singlet ground-state model system is depicted in Figure 1.6. Following excitation through light absorption, a partial relaxation from higher vibrational levels may take place through different non-radiative modes of deactivation, namely vibrational relaxation and

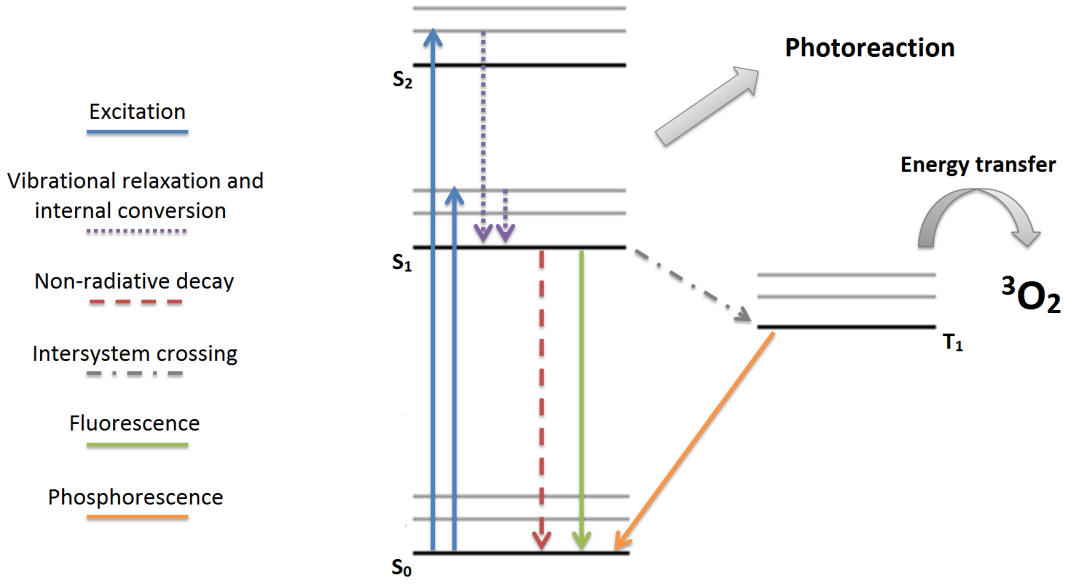

Figure 1.6. *Jablonski energy diagram, depicting different processes triggered by light excitation of a singlet ground-state (S_0) model system. Radiative and non-radiative processes are indicated with solid (—) and dashed (--) lines, respectively.*

internal conversion, which lead to the most stable electronic excited state. Several processes may occur at this point. The system may revert to the ground state by emitting energy in the form of light, thus producing fluorescence; alternatively, the remaining energy may be dissipated in the form of heat, through a non-radiative decay.

The excited system may also experience a forbidden non-radiative transition to another excited state with different spin multiplicity. This phenomenon, known as intersystem crossing, becomes favored when the vibrational levels of different electronic states overlap. From this long-lived alternative excited state, the system may directly return to the ground state via a forbidden radiative transition, producing phosphorescence emission. Otherwise, relaxation may also be attained by intermolecular energy transfer to another species, which hence becomes excited. This latter process, called photosensitization, may only take place between systems displaying the same spin multiplicity, triplet oxygen being the most common target.

In addition, due to the electronic and structural changes induced by light absorption, the system may eventually transit to a reactive state, which can lead to products unattainable by other means. Metal complexes, in particular, exhibit a rich and diverse photoreactivity, which can be efficiently tuned by varying the metal center and/or the coordinated ligands. Photoactivation offers potential for initiating unusual ligand substitution and redox reactions in otherwise non-reactive species, which can be exploited to achieve new mechanisms of anticancer activity.[56]

1.3.2. Current strategies in inorganic PACT

Inorganic photoactivated chemotherapy takes advantage of some of the non-radiative processes triggered by light-mediated excitation of a metal center, in order to generate pharmacologically active species. An optimal photochemotherapeutic agent should be stable and non-toxic to cells before activation, while exhibiting remarkable antiproliferative activity after external light irradiation. Such pharmacological activity may take place through different mechanisms of action, according to which three broad categories of metal-based PACT agents can be distinguished: photosensitizers,

photothermal therapy agents and photoactivatable prodrugs, the latter ones including metal complexes designed to carry and release small organic molecules with therapeutic action.[57]

Photosensitizers

Photosensitizing compounds constitute the basis of photodynamic therapy (PDT), a technique already used clinically to treat a wide range of disorders. Upon light irradiation, photosensitizers efficiently undergo energy transfer from a long-lived excited triplet state (attained by intersystem crossing) to neighboring dioxygen molecules, which hence become excited. This activation results in the formation of highly reactive singlet oxygen ($^1O_2$), which promotes the formation of other reactive oxygen species (ROS) like hydroxyl radicals (•OH) and superoxide anions (O_2^-). Such ROS violently react with cellular membranes, nucleic acids and other cellular components, inducing apoptotic or necrotic cell death by massive oxidative damage in the surrounding area.[58] Owing to the lack of toxicity of photosensitizing agents, PDT offers crucial advantages over more conventional treatments, namely its non-invasive character and the lack of associated side effects or cross-resistance. However, its dioxygen dependence considerably hampers its application in the hypoxic environment of several types of solid tumors.

Although most PDT agents are organic porphyrins and phthalocyanine-related molecules, several examples of photosensitizing transition-metal complexes can also be found in the literature.[59] A low-energy triplet excited state with a long lifetime is needed for a metal complex to behave as an efficient photosensitizer. Pt(II) and Ir(III) cyclometalated complexes, for instance, fulfill these requirements and have lately been reported to efficiently produce singlet oxygen upon irradiation with UV light.[60] Ru(II) polypyridyl compounds, which have been extensively studied for their rich photochemistry, as well as several classes of pentacoordinated Cu(II) compounds, can also behave as singlet oxygen producers.[61,62] Other examples include a number of macrocyclic complexes coordinated to various metal or metalloid centers, like Pd(II) or Si(IV), which have been used to tune the photochemistry of such systems.[63,64] A few of these inorganic photosensitizers are illustrated in Figure 1.7.

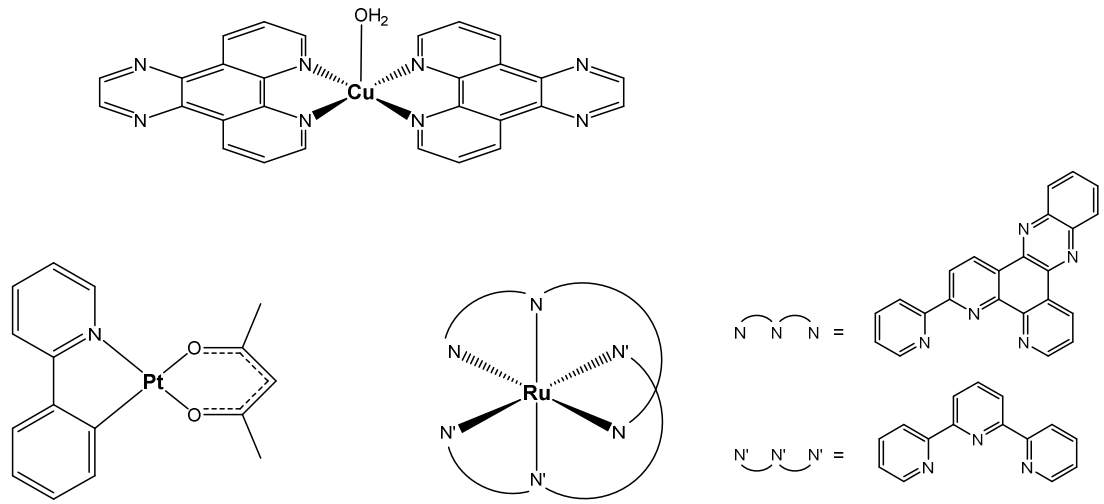

Figure 1.7. *Selected examples of photosensitizing metal complexes for PDT.*[60–62]

Photothermal therapy agents

Photothermal therapy (PTT) focuses on the destruction of malignant cells by means of light-induced hyperthermia, which stems from the thermal energy dissipated through the non-radiative decay of an electronically excited sensitizer.[65] Several classes of photothermal sensitizers have been developed and applied, including carbon nanotubes and various porphyrin-based metal complexes.[66] However, most PTT agents developed to date are based on inorganic nanomaterials, which are preferentially accumulated by cancer cells owing to the so-called enhanced permeability and retention effect exhibited by tumors.[67] Gold, in particular, has proven to be remarkably valuable for such an application, due to the highly efficient photon-to-thermal energy conversion exhibited by nanoparticles of this metal.[68] Gold-based nanostructures for PTT, such as nanorods, nanoshells and nanocages, have gained notable attention over the last decade, and recently some of these systems have even managed to successfully enter clinical trials.[69]

Photoactivatable prodrugs

Metal-based prodrugs are chemical systems designed to undergo light-mediated ligand exchange, rearrangement or dissociation reactions, often associated to the redox properties of the metal center. The pharmacologically active species liberated in these

processes may either be the photoreleased ligand(s) or a more reactive metal complex, which can readily interact with neighboring biological targets such as DNA. Several remarkable examples of photoactivatable inorganic prodrugs are shown in Figure 1.8.

Besides their performance as dioxygen photosensitizers, octahedral Ru(II) polypyridyl complexes have also been studied for their potential application as light-activatable prodrugs.[70] The photoactivation of these systems generates a strongly oxidizing excited state able to produce oxidative cleavage of the DNA strands; therefore, they have been proposed as oxygen-independent photosensitizers. In addition, it has been shown that irradiation of Ru(II) complexes bearing highly π-deficient polyaromatic ligands induces the formation of non-conventional covalent adducts with the nucleobases, most likely through a radical recombination process (see Figure 1.8). As in the case of classical platinum drugs, such genomic lesions interfere with DNA replication and transcription mechanisms, thus promoting apoptosis.[71]

The design of platinum-based prodrugs able to generate cisplatin analogues upon photoexcitation has been receiving more attention in recent years.[72] This strategy, pioneered by the groups of Bednarski and Sadler, takes advantage of a range of chemically inert octahedral platinum(IV) complexes bearing photolabile ligands. Such systems can be selectively irradiated to promote the reduction of the metal center and the subsequent release of ligands, hence producing the corresponding bioactive, square-planar Pt(II) species. Diazido Pt(IV) complexes were recently developed; they display strong cytotoxic activities *in vitro* after irradiation with UV light, while remaining non-toxic in the dark. For instance, *trans*,*trans*,*trans*-$[Pt(OH)_2(N_3)_2(NH_3)(py)]$ (see Figure 1.8) proved to be remarkably effective against cisplatin-resistant ovarian cancer cells, owing to its ability to induce distinct DNA damage and cell-signaling responses, with respect to classical platinum drugs.[73]

Photoactivatable prodrugs can also be applied to control the release of therapeutically active small ligands, such as nitric oxide (NO) and carbon monoxide (CO). Both gases are endogenously produced in living organisms and have important functions as signaling molecules. In addition to this naturally occurring role, there is strong evidence that NO and CO administration may be useful in the treatment of several diseases, including anticancer applications.[74] Numerous nitrosyl and carbonyl metal

complexes with Fe(III), Cr(III), Co(III), Ru(II) or Mn(II) have been described to be able to release NO and CO upon light activation, due to the labilization of the metal-to-ligand bond in the excited state. Current investigation in this area of research encompasses the fine tuning of the coordination sphere of these metal-based prodrugs, so as to properly modulate their photochemical properties. Moreover, their conjugation with different targeting groups is also being examined, with the objective to achieve better cancer-cell selectivities.[75]

Light-upconverting drug carriers

Upconverting carriers are not pharmacological agents, but rather a new class of drug-delivery systems specifically designed to overcome one of the major drawbacks of most inorganic photochemotherapeutics. Indeed, not any kind of light can penetrate tissues deep enough to treat all types of solid tumors in cancer patients; blue light is more efficiently absorbed by hemoglobin or melanine, compared to lower-energy radiations, and hence the optimal phototherapeutic window is considered to lie within the range 600-1000 nm.[76] However, since most metal-based prodrugs typically require high-energy UV or visible light for their photoactivation to occur, the broadening of their clinical application is still a considerable challenge.

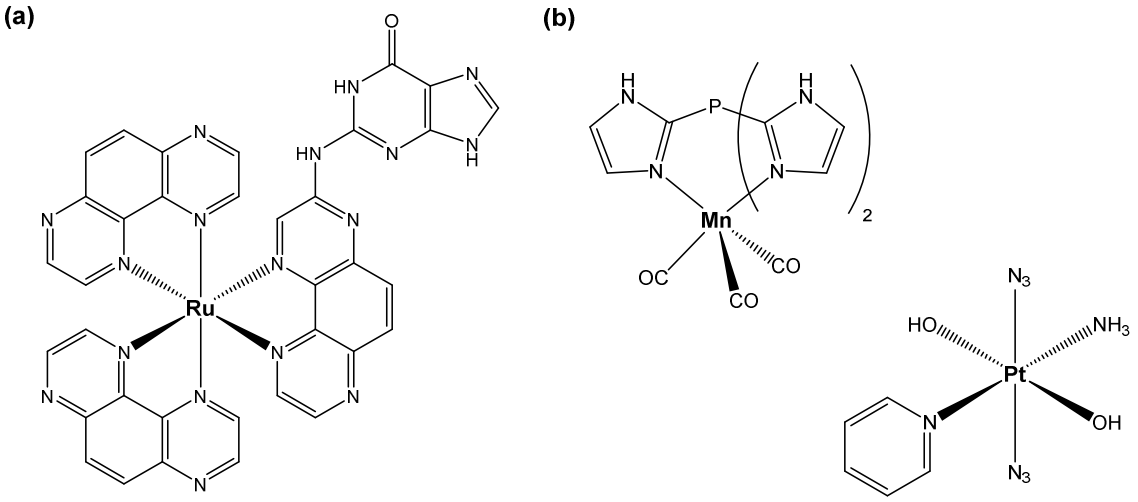

Figure 1.8. *Non-conventional covalent adduct between a Ru(II) polypyridyl complex and guanine (a), and selected examples of metal-based photoactivatable prodrugs (b).*[73,75]

In this regard, despite still being in early stages of development, light-upconverting drug carriers have recently emerged as a very promising tool for PACT applications. These systems are capable of absorbing penetrating near-IR light and dissipating the accumulated energy in the form of a radiative emission of a shorter wavelength, through different photochemical mechanisms. This phenomenon can hence be used to achieve the local activation of photoresponsive drugs attached to their surface. Currently, lanthanide-doped nanoparticles constitute one of the most promising classes of light-upconverting systems; they have been used to promote the activation of Mn, Fe, Ru or Pt complexes using red light, albeit with limited efficiencies.[77] Similarly, liposomes carrying triplet-triplet annihilation molecular pairs have lately been reported to show auspicius light-upconverting properties, which can be applied in photomedical applications requiring *in situ* generation of blue light.[78]

1.3.3. Photoresponsive molecules for ligand-based activation

A common feature for all the inorganic light-activatable systems described so far is the fundamentally metal-centered nature of their photochemistry. However, in a context of continuous development of novel biochemical and mechanistic strategies, which may provide new tools to help overcoming the current limitations of these molecules, ligand-mediated photoactivation of metal complexes has very recently started to gain attention as a novel approach to the design of PACT drugs.

Several classes of organic molecular photoswitches, like those depicted in Figure 1.9, offer the potential to serve as photoresponsive ligands in metal complexes. Such systems exhibit a rich chemical diversity that may lead to novel mechanisms of action, as well as an interesting photochemistry mostly based on reversible double-bond isomerization or intramolecular pericyclic reactions. These transformations produce remarkable changes not only in the chemical structure of the molecular switches, but also in their optical and electronic properties.[79] Accordingly, they have been used in several areas of research, from catalysis to material sciences, and more recently in the development of photocontrollable biological systems.[80] Their utilization in drug design, however, is still in its infancy, and more in-depth investigation is clearly required.

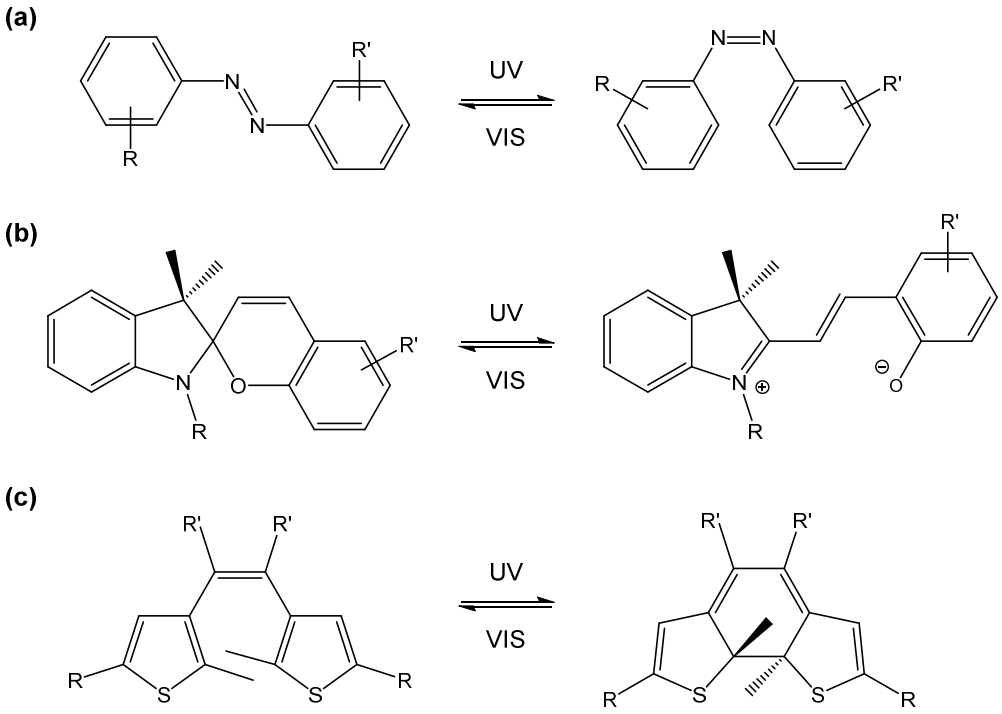

Figure 1.9. *Photoswitches based on azobenzenes (a), spiropyrans (b) and diarylethenes (c).*[79]

One of the key aspects concerning the biological application of such molecules is their thermal stability. Azobenzenes and spiropyrans, among other organic photoswitches, are thermally unstable and gradually revert to their initial state in the absence of light. While spontaneous deactivation can be useful for certain uses,[81] it certainly hampers the implementation of these systems when a stable activation is desirable, as in the case of DNA-targeting drugs. Diarylethenes, in contrast, might be more suitable for this purpose. These remarkable systems exhibit negligible thermal relaxation and thus have arisen as one of the most promising classes of photoresponsive molecular devices, owing to their potentially broader range of applications.[82]

In the present PhD thesis, aimed at providing new insight into this emerging field of inorganic photoactivated chemotherapy, the potential application of diarylethenes to the design of ligand-mediated light-activatable metallodrugs has been investigated. The premise behind this innovative approach was that the distinct properties exhibited by the two thermally stable states of these molecular switches might allow to selectively modulate the biological activity of their metal complexes, thus leading to a novel mechanism of photochemical control.

1.4. Diarylethene systems

1.4.1. Photochemical properties

Diarylethenes are photochromic molecules; they exhibit a light-induced reversible transformation between two isomeric forms, each one exhibiting clearly different absorption spectra. As previously stated, the photoisomers resulting from this process differ not only in their geometrical structure and color, but also in all their intrinsic features, including redox potentials, refractive indices, luminescent properties and even chirality.[83]

The photochemistry of diarylethenes is based on that of 1,3,5-hexatriene. Systems containing this remarkable synthon, such as (*Z*)-stilbene (which is actually the most simple diarylethene) are well-known to undergo photochemically induced electrocyclic reactions, leading to the formation of the corresponding 1,3-cyclohexadiene products. This process is promoted by the rearrangement of the terminal carbon bonds of the hexatriene synthon, which, according to the Woodward-Hoffman rules for the photoinduced cyclization of a [4n+2] π electrons system, proceeds via a conrotatory mechanism at the LUMO excited state.[84] A schematic representation of the reversible photocyclization of (*Z*)-stilbene is illustrated in Figure 1.10.

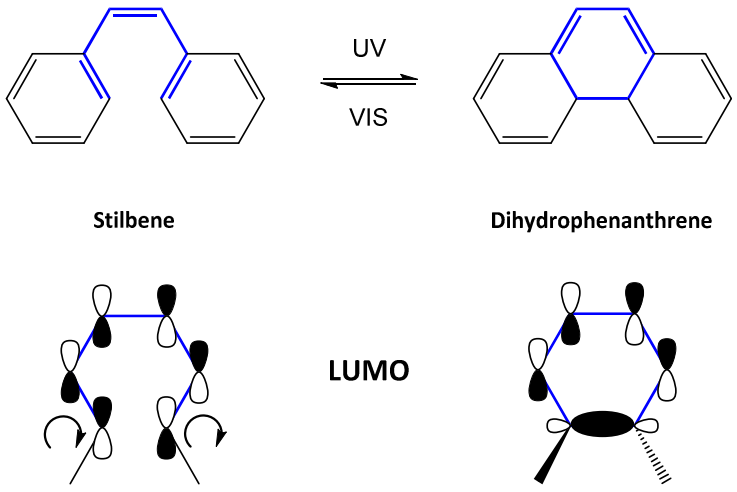

Figure 1.10. *Reversible photocyclization of (Z)-stilbene into dihydrophenanthrene. The photoreactive 1,3,5-hexatriene system is highlighted in blue.*

(*Z*)-Stilbene, however, is far from being an optimal molecular switch because dihydrophenanthrene is not a thermally stable product. Thermal reversibility is directly related to the activation barrier of the cycloreversion process, which correlates with the ground-state energy difference between the open and closed isomers, and is dependent on the aryl group.[85] When this difference is large, as for (*Z*)-stilbene, the thermally induced cycloreversion reaction is favored and readily occurs. In contrast, when the aryl groups are furan, thiophene or thiazole rings, which have low aromatic stabilization energies, the activation barrier for the cycloreversion increases, and hence the closed-ring species become thermally stable.

It should also be noted that stilbene, like azobenzene, can readily undergo an alternative *cis*/*trans* (*Z*/*E*) isomerization of the central double bond upon light irradiation, which directly interferes with the photocyclization process. However, this undesired transformation can be prevented if the alkene is part of a cyclic structure. Studies carried out with different diarylethene systems showed that those containing a cyclopentene or other five-membered cyclic alkenes between the aryl units tend to display higher photoconversion quantum yields and efficiencies.[86,87] On the other hand, it is also known that the closed-ring species can be irreversibly oxidized to form a central benzene ring by hydrogen elimination. Accordingly, hydrogen atoms must be avoided in the terminal carbons of the hexatriene synthon so as to prevent this decomposition pathway; they are usually replaced with methyl groups, which in the closed-ring form adopt a *trans* relative disposition as a result of the conrotatory photocyclization mechanism.

Dithienylcyclopentenes (DTCs) and dithienylperfluorocyclopentenes (DTFCs), depicted in Figure 1.11, were designed taking into account all these considerations, and hence constitute the most prominent class of diarylethenes.[88] Mainly developed by the groups of Irie and Feringa, these photochromic switches exhibit optimal thermal stability and a very high fatigue resistance, being able to undergo up to 10^4 coloration/bleaching cycles without noticeable decomposition.[89] Furthermore, they have also been reported to display remarkably high response times; both the photocyclization and cycloreversion reactions of DTC systems proceed at the picosecond scale, which is of special relevance in terms of their potential use in the field of optoelectronics.[90]

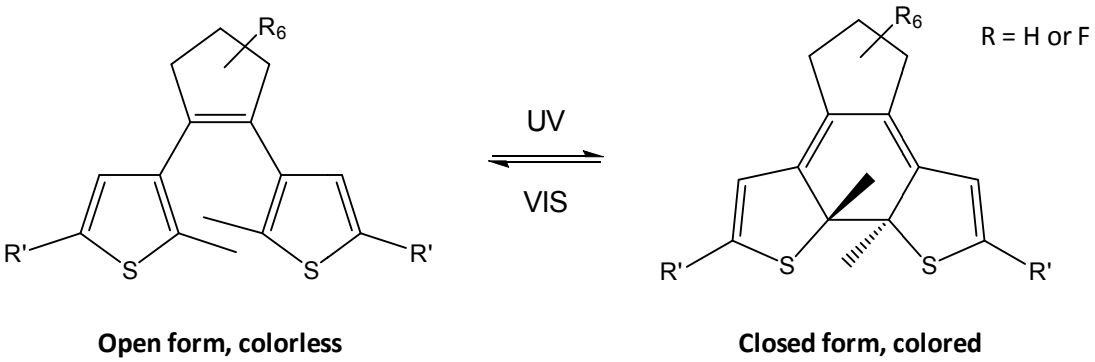

Figure 1.11. *Reversible photocyclization of dithienylcyclopentenes (R = H) and dithienylperfluorocyclopentenes (R = F).*

The typical absorption spectral changes of a DTC system, corresponding to one of the photoswitches prepared in this work (for which R = H and R' = pyridine; see Chapter 3) is shown in Figure 1.12. The open form exclusively absorbs in the UV region, and hence irradiation with light in this wavelength range induces its intramolecular electrocyclic reaction. In contrast, the closed form typically exhibits a distinct absorption in the visible region, owing to the destabilization of the ground state and thus to the lessening of the HOMO/LUMO energy gap. This red shift of the closed species is dependent on both the bridging structure connecting the aryl groups and the various substituents attached to them, which means that the photochemical application

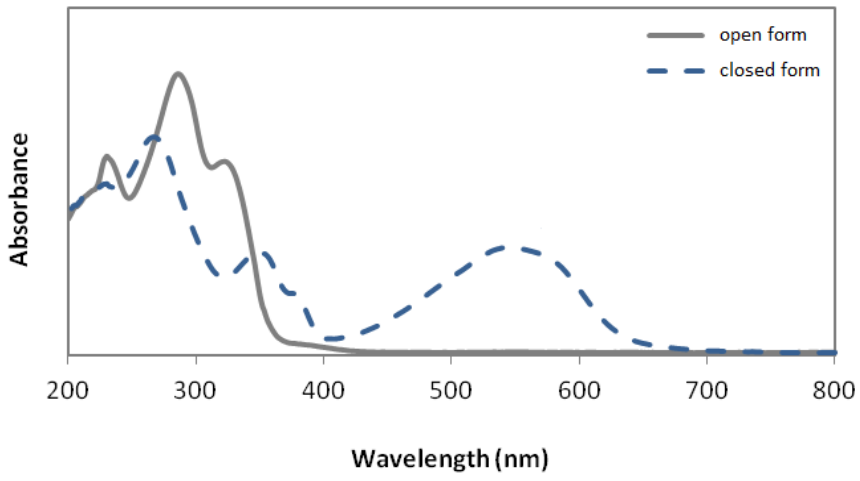

Figure 1.12. *Typical UV-Vis absorption spectra of the open (solid line) and closed (dashed line) forms of a DTC-based molecular switch.*

window of these systems can be properly tailored by rationally modifying their chemical structure. In fact, while the photoreactive absorption of the open-ring form is generally found in the 300-375 nm region, the position of the HOMO→LUMO transition of the closed-ring species can range from 500 to 800 nm (being thus located in the optimal phototherapeutic window), longer wavelengths being even attainable in a few cases. Up to now, the longest reported wavelength for a DTC system in its closed state is 828 nm.[91]

Furthermore, the distinct structural features of the interchangeable isomeric forms of these molecules are of special relevance considering their implementation in biological environments. The open-ring species is noticeably more voluminous than the closed one, being both longer and thicker. Moreover, the open form exhibits a much higher degree of conformational flexibility, whereas the closed isomer is clearly more planar and rigid, due to its more effective π conjugation. These differences may necessarily translate into completely different intracellular interactions and molecular recognition patterns, thus opening up new options in the development of biologically relevant light-controlled tools.

In view of all these considerations, it is no surprise that the implementation of DTCs and closely related systems in biology has been receiving growing attention in recent years. The final part of this introductory chapter is aimed at providing a brief insight into this emerging field, underlining some of the most promising current investigations regarding the biological applications of these remarkable molecular switches.

1.4.2. Biological applications of dithienylcyclopentenes

The potential incorporation of photoresponsive moieties into nucleic acids is one of the most attractive biological applications of molecular photoswitches. Such systems can be used to provide light-mediated spatial and temporal control over replication and transcription processes, by altering the structure and binding properties of this vital biomacromolecule. Actually, different photochromic molecules have been introduced in the various structural motifs of the DNA architecture, i.e. the phosphate backbone, the nucleobases or the deoxyribose moieties.

Jäschke and co-workers recently described an innovative class of DTC-based adenosine derivatives, in which a nucleobase is directly incorporated into the photoswitching framework, as depicted in Figure 1.13.[92] These systems combine the photochemical properties of the DTC structure with the ability to establish Watson-Crick base pairing with the complementary thymidine residues of DNA, which could be exploited to induce greater-scale conformational changes into the double helix. Uridine and cytidine were also successfully incorporated into the photoswitchable unit in subsequent investigations, and a partial control over transcription was demonstrated by incorporating the photoresponsive nucleosides in promoter oligonucleotides.[93]

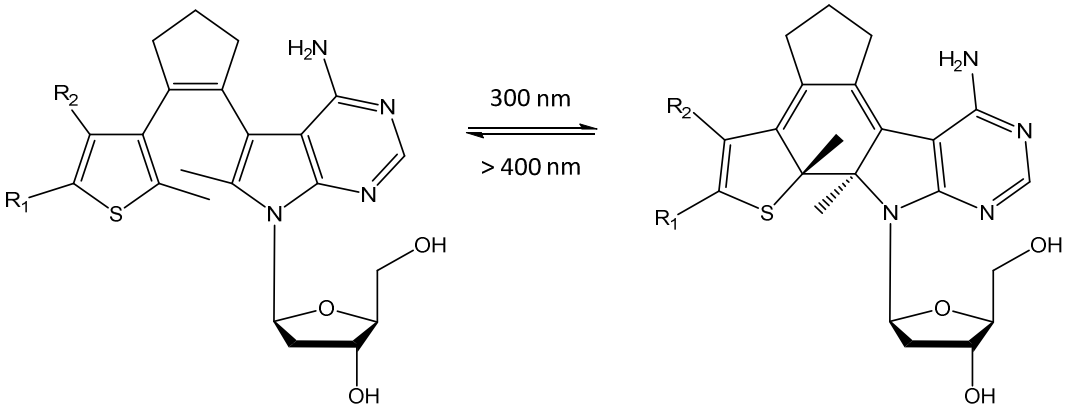

Figure 1.13. *Photoswitchable diarylethene system incorporating a deoxyadenosine motif, developed by Jäschke and co-workers.*[92]

In a completely different approach, Andréasson and co-workers have designed positively charged dithienylperfluorocyclopentenes able to selectively bind to linear DNA. This association was used to induce chirality transfer from DNA to the photoswitchable molecules, producing an enantiomeric enhancement of the closed-ring products, which are normally composed of a racemic mixture of the *R*,*R* and *S*,*S* stereoisomers resulting from the *trans* disposition of the methyl groups.[94] This chirality transfer from DNA has potential to be applied in asymmetric synthetic procedures requiring enantioselective catalysts.

Diarylethenes can also be used to design light-controlled biocatalysts and enzyme-targeting inhibitors, with potential applications in therapeutics, diagnostics and

biosensoring. For instance, König and co-workers used a DTC derivative for the photocontrolled inhibition of human carbonic anhydrase I (hCAI), an enzyme that has been established as a target in the treatment of glaucoma, neurological disorders and cancer.[95] To that end, the photoswitchable scaffold was functionalized with a sulfonamide group that acts as the inhibitory moiety, as well as a copper(II) iminodiacetate binding unit, able to coordinate to the histidine residues near the active site of the enzyme (Figure 1.14).[96] Due to its much higher conformational flexibility, the open form appeared to be a much more potent hCAI inhibitor than the closed one, whose activity was severely limited by its geometrical constraints.

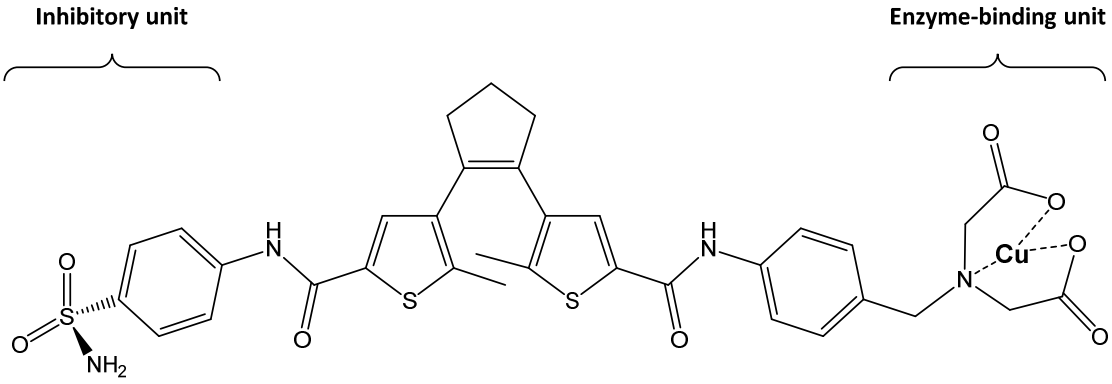

Figure 1.14. *Photoswitchable carbonic anhydrase I inhibitor developed by König and co-workers.*[96]

The electronic redistribution caused by the photoisomerization of diarylethenes can be used to selectively modify the luminescent properties of emissive systems, which can have potential applications in bioimaging. Recently, Tian's research group reported a diarylethene-based iridium(III) complex exhibiting intense phosphorescent emission upon irradiation with visible light (488 nm), solely in its open-ring state (Figure 1.15).[97] Most remarkably, due to the notable red shift of the HOMO-to-LUMO transition induced by the metal coordination, the ring-closing reaction and thus the selective quenching of the luminescence could also be prompted by light in the visible region (440 nm). The non-toxic complex was readily internalized by nasopharyngeal epidermal carcinoma cells, after which its photocontrollable luminescent functionality remained unaltered.

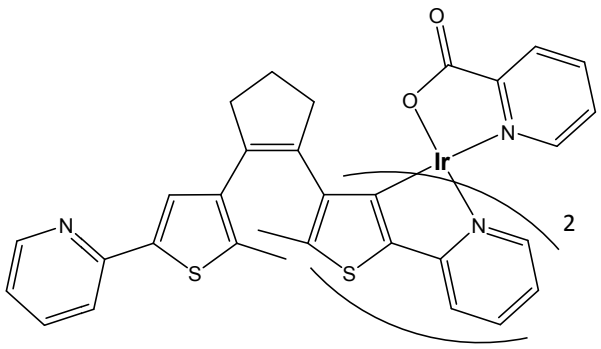

Figure 1.15. *DTC-based iridium(III) luminescent complex developed by Tian and co-workers.*[97]

Lastly, the incorporation of a functional DTC scaffold within the aminoacid chain of several antimicrobial cyclic peptidomimetics has been lately described by the group of Ulrich (Figure 1.16).[98] The resulting photoswitchable peptides, whose structure was analogous to that of the well-known antimicrobial agent gramicidin S, displayed biological activities comparable to those of its parent compound in their open-ring state, but significantly lower efficacies after undergoing ring closure. Furthermore, the results obtained demonstrated that the peptidomimetics' activity is dependent on the actual position of the photoresponsive moiety within the aminoacid chain, due to specific alteration of the global conformation of the drug.

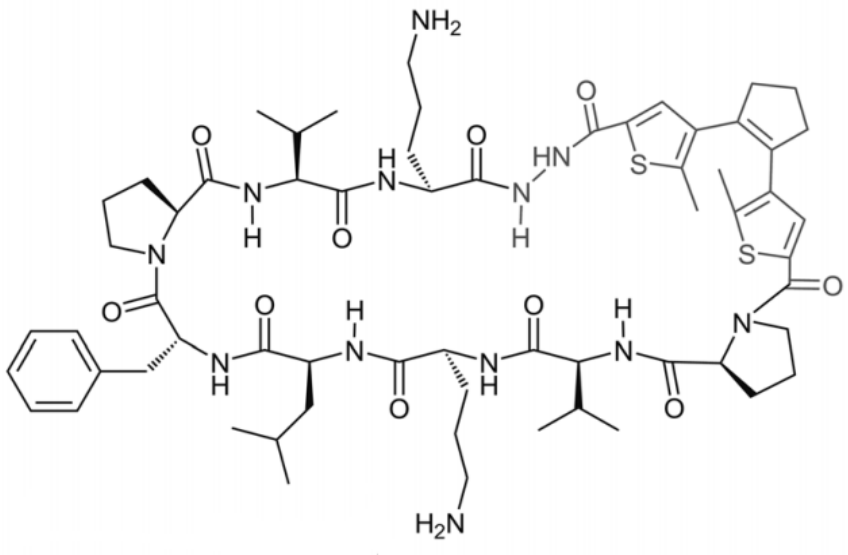

Figure 1.16. *An antimicrobial diarylethene-containing cyclic peptidomimetic developed by Ulrich and co-workers.*[98]

1.5. Aim and outline of the thesis

As mentioned earlier in this introduction, photoactivated chemotherapy represents one of the most promising approaches towards spatial and temporal control over anticancer drug activity. The current strategies concerning the development of photocontrollable metal compounds aim to take advantage of the rich photochemical properties of metal ions. In contrast, the implementation of photoresponsive ligands in light-activatable metallodrug design is still a fairly unexplored field. Accordingly, thorough examination of this alternative possibility clearly needs to be conducted.

The key aim of this PhD thesis is to introduce a novel approach to this field, by developing an unprecedented class of dinuclear platinum(II) complexes bearing bridging, photoswitchable dithienylcyclopentene-based ligands. It is expected that the distinct structural and electronic changes taking place upon the light-induced transformation of these complexes may result in a modulation of their DNA binding affinity, leading to a new type of photochemical control over the drug activity.

Hence, the second chapter of this thesis covers the design and chemical synthesis of several dithienylcyclopentene-based ligands, as well as the preparation of the corresponding dinuclear platinum(II) complexes. Different synthetic strategies have been followed to introduce several structural variations in the photoresponsive ligands, with the objective to properly evaluate their influence on the biological activity of the metal complexes.

The third chapter deals with the investigation of the photochromic properties of all the photoswitchable ligands prepared and of their corresponding metal complexes, as well as the structural characterization of several of the Pt(II) compounds. In addition, a computational study carried out to analyze the unexpected photochemical inertness of one of the synthesized systems is also included in this chapter.

Finally, the biological evaluation of the metal complexes prepared is described in the fourth chapter. The distinct interaction with DNA of their open and closed photoisomers has been thoroughly investigated using different techniques. Several *in vitro* studies against selected cancer cell lines were subsequently performed, the ultimate goal being to validate the innovative strategy proposed in this PhD thesis.

1.6. References

(1) Lippard, S. J. *Nat. Chem. Biol.* **2006**, *2* (10), 504–507.

(2) Lippard, S. J. In *Bioinorganic Chemistry*; Bertini, I., Gray, H. B., Lippard, S. J., Valentine, J.; University Science Books: Mill Valley, CA, 1994; pp 505–583.

(3) Lassner, E.; Schubert, W. D. In *Tungsten: Properties, Chemistry, Technology of the Element, Alloys and Chemical Compounds*; Springer US: Boston, MA, 1999; pp 409–416.

(4) Grass, G.; Rensing, C.; Solioz, M. *Appl. Environ. Microbiol.* **2011**, *77* (5), 1541–1547.

(5) Giachi, G.; Pallecchi, P.; Romualdi, A.; Ribechini, E.; Lucejko, J. J.; Colombini, M. P.; Mariotti Lippi, M. *Proc. Natl. Acad. Sci.* **2013**, *110* (4), 1193–1196.

(6) Frith, J. *J. Mil. Veterans. Health* **2012**, *20* (4), 49–58.

(7) Williams, K. J. *J. R. Soc. Med.* **2009**, *102* (8), 343–348.

(8) Rosenberg, B.; VanCamp, L.; Krigas, T. *Nature* **1965**, *205* (4972), 698–699.

(9) Peyrone, M. *Justus Liebigs Ann. Chem.* **1844**, *51* (1), 1–29.

(10) Rosenberg, B.; VanCamp, L.; Trosko, J. E.; Mansour, V. H. *Nature* **1969**, *222* (5191), 385–386.

(11) Desoize, B. *Anticancer Res.* **2004**, *24* (3A), 1529–1544.

(12) Kean, W. F.; Hart, L.; Buchanan, W. W. *Rheumatol.* **1997**, *36* (5), 560–572.

(13) Bhattacharyya, S.; Dixit, M. *Dalton Trans.* **2011**, *40* (23), 6112–6128.

(14) Heffern, M. C.; Matosziuk, L. M.; Meade, T. J. *Chem. Rev.* **2014**, *114* (8), 4496–4539.

(15) Mjos, K. D.; Orvig, C. *Chem. Rev.* **2014**, *114* (8), 4540–4563.

(16) Global Burden of Disease Cancer Collaboration. *JAMA Oncol.* **2015**, *1* (4), 505–527.

(17) Hanahan, D.; Weinberg, R. A. *Cell* **2000**, *100* (1), 57–70.

(18) Croce, C. M. *N. Engl. J. Med.* **2008**, *358* (5), 502–511.

(19) Anand, P.; Kunnumakara, A. B.; Sundaram, C.; Harikumar, K. B.; Tharakan, S. T.; Lai, O. S.; Sung, B.; Aggarwal, B. B. *Pharm. Res.* **2008**, *25* (9), 2097–2116.

(20) Siddik, Z. H. *Oncogene* **2003**, *22* (47), 7265–7279.

(21) DeConti, R. C.; Toftness, B. R.; Lange, R. C.; Creasey, W. A. *Cancer Res.* **1973**, *33* (6), 1310–1315.

(22) Ishida, S.; Lee, J.; Thiele, D. J.; Herskowitz, I. *Proc. Natl. Acad. Sci. USA* **2002**, *99* (22), 14298–14302.

(23) Ishikawa, T.; Ali-Osman, F. *J. Biol. Chem.* **1993**, *268* (27), 20116–20125.

(24) Kelland, L. R. *Nat. Rev. Cancer* **2007**, *7* (8), 573–584.

(25) Cepeda, V.; Fuertes, M. A.; Castilla, J.; Alonso, C.; Quevedo, C.; Pérez, J. M. *Anti-Cancer Agents Med. Chem.* **2007**, *7* (1), 3–18.

(26) Fichtinger-Schepman, A. M. J.; Van der Veer, J. L.; Den Hartog, J. H. J.; Lohman, P. H. M.; Reedijk, J. *Biochemistry* **1985**, *24* (3), 707–713.

(27) Wang, D.; Lippard, S. J. *Nat. Rev. Drug Discov.* **2005**, *4* (4), 307–320.

(28) Chaney, S. G.; Campbell, S. L.; Temple, B.; Bassett, E.; Wu, Y.; Faldu, M. *J. Inorg. Biochem.* **2004**, *98* (10), 1551–1559.

(29) Jung, Y.; Lippard, S. J. *Chem. Rev.* **2007**, *107* (5), 1387–1407.

(30) Levi, J. A.; Aroney, R. S.; Dalley, D. N. *Br. Med. J. (Clin. Res. Ed.)* **1981**, *282* (6281), 2003–2004.

(31) Giaccone, G. *Drugs* **2000**, *59* (4), 9–17.

(32) Mistry, P.; Kelland, L. R.; Abel, G.; Sidhar, S.; Harrap, K. R. *Br. J. Cancer* **1991**, *64* (2), 215–220.

(33) Ferry, K. V; Hamilton, T. C.; Johnson, S. W. *Biochem. Pharmacol.* **2000**, *60* (9), 1305–1313.

(34) Wheate, N. J.; Walker, S.; Craig, G. E.; Oun, R. *Dalton Trans.* **2010**, *39* (35), 8113–8127.

(35) Go, R. S.; Adjei, A. A. *J. Clin. Oncol.* **1999**, *17* (1), 409.

(36) Penson, R. T.; Dizon, D. S.; Cannistra, S. A.; Roche, M. R.; Krasner, C. N.; Berlin, S. T.; Horowitz, N. S.; DiSilvestro, P. A.; Matulonis, U. A.; Lee, H.; King, M. A.; Campos, S. M. *J. Clin. Oncol.* **2010**, *28* (1), 154–159.

(37) Kasparkova, J.; Vojtiskova, M.; Natile, G.; Brabec, V. *Chem. Eur. J.* **2008**, *14* (4), 1330–1341.

(38) Holzer, A. K.; Manorek, G. H.; Howell, S. B. *Mol. Pharmacol.* **2006**, *70* (4), 1390–1394.

(39) Shimada, M.; Itamochi, H.; Kigawa, J. *Cancer Manag. Res.* **2013**, *5*, 67–76.

(40) McKeage, M. J. *Expert Opin. Investig. Drugs* **2001**, *10* (1), 119–128.

(41) Kim, D. K.; Kim, H. T.; Cho, Y. B.; Tai, J. H.; Ahn, J. S.; Kim, T. S.; Kim, K. H.; Hong, W. S. *Cancer Chemother. Pharmacol.* **1995**, *35* (5), 441–445.

(42) Kelland, L. R. *Expert Opin. Investig. Drugs* **2000**, *9* (6), 1373–1382.

(43) Bhargava, A.; Vaishampayan, U. N. *Expert Opin. Investig. Drugs* **2009**, *18* (11), 1787–1797.

(44) Choy, H.; Park, C.; Yao, M. *Clin. Cancer Res.* **2008**, *14* (6), 1633–1638.

(45) Vaishampayan, U. N.; Fontana, J.; Heilbrun, L. K.; Smith, D.; Heath, E.; Dickow, B.; Figg, W. D. *Urol. Oncol.* **2016**, *32* (1), 31.e25-31.e33.

(46) Holford, J.; Sharp, S. Y.; Murrer, B. A.; Abrams, M.; Kelland, L. R. *Br. J. Cancer* **1998**, *77* (3), 366–373.

(47) Nowotnik, D. P.; Cvitkovic, E. *Adv. Drug Deliv. Rev.* **2009**, *61* (13), 1214–1219.

(48) Rice, J. R.; Gerberich, J. L.; Nowotnik, D. P.; Howell, S. B. *Clin. Cancer Res.* **2006**, *12* (7), 2248–2254.

(49) Bruijnincx, P. C. A.; Sadler, P. J. *Curr. Opin. Chem. Biol.* **2008**, *12* (2), 197–206.

(50) Yang, Z.; Wang, X.; Diao, H.; Zhang, J.; Li, H.; Sun, H.; Guo, Z. *Chem. Commun.* **2007**, No. 33, 3453–3455.

(51) Tang, K.; Zhang, Y.; Zhang, H.; Xu, P.; Liu, J.; Ma, J.; Lv, M.; Li, D.; Katirai, F.; Shen, G.-X.; Zhang, G.; Feng, Z.-H.; Ye, D.; Huang, B. *Nat. Commun.* **2012**, *3*, 1282.

(52) Aronov, O.; Horowitz, A. T.; Gabizon, A.; Gibson, D. *Bioconjug. Chem.* **2003**, *14* (3), 563–574.

(53) Galanski, M.; Keppler, B. K. *Anti-Cancer Agents Med. Chem.* **2007**, *7* (1), 55–73.

(54) Farrer, N. J.; Sadler, P. J. *Aust. J. Chem.* **2008**, *61* (9), 669–674.

(55) Szaciłowski, K.; Macyk, W.; Drzewiecka-Matuszek, A.; Brindell, M.; Stochel, G. *Chem. Rev.* **2005**, *105* (6), 2647–2694.

(56) Smith, N. A.; Sadler, P. J. *Phil. Trans. R. Soc. A.* **2013**, *371* (1995), 20120519.

(57) Crespy, D.; Landfester, K.; Schubert, U. S.; Schiller, A. *Chem. Commun.* **2010**, *46* (36), 6651–6662.

(58) Huang, Z.; Xu, H.; Meyers, A. D.; Musani, A. I.; Wang, L.; Tagg, R.; Barqawi, A. B.; Chen, Y. K. *Technol. Cancer Res. Treat.* **2008**, *7* (4), 309–320.

(59) O'Connor, A. E.; Gallagher, W. M.; Byrne, A. T. *Photochem. Photobiol.* **2009**, *85* (5), 1053–1074.

(60) Djurovich, P. I.; Murphy, D.; Thompson, M. E.; Hernandez, B.; Gao, R.; Hunt, P. L.; Selke, M. *Dalton Trans.* **2007**, No. 34, 3763–3770.

(61) Liu, Y.; Hammitt, R.; Lutterman, D. A.; Joyce, L. E.; Thummel, R. P.; Turro, C. *Inorg. Chem.* **2009**, *48* (1), 375–385.

(62) Dhar, S.; Senapati, D.; Reddy, P. A. N.; Das, P. K.; Chakravarty, A. R. *Chem. Commun.* **2003**, No. 19, 2452–2453.

(63) Donzello, M. P.; Viola, E.; Bergami, C.; Dini, D.; Ercolani, C.; Giustini, M.; Kadish, K. M.; Meneghetti, M.; Monacelli, F.; Rosa, A.; Ricciardi, G. *Inorg. Chem.* **2008**, *47* (19), 8757–8766.

(64) Jiang, X.-J.; Lo, P.-C.; Yeung, S.-L.; Fong, W.-P.; Ng, D. K. P. *Chem. Commun.* **2010**, *46* (18), 3188–3190.

(65) Jori, G.; Spikes, J. D. *J. Photochem. Photobiol. B* **1990**, *6* (1), 93–101.

(66) Soncin, M.; Busetti, A.; Fusi, F.; Jori, G.; Rodgers, M. A. J. *Photochem. Photobiol.* **1999**, *69* (6), 708–712.

(67) Maeda, H. *Adv. Enzyme Regul.* **2001**, *41* (1), 189–207.

(68) Cobley, C. M.; Au, L.; Chen, J.; Xia, Y. *Expert Opin. Drug Deliv.* **2010**, *7* (5), 577–587.

(69) Abadeer, N. S.; Murphy, C. J. *J. Phys. Chem. C* **2016**, *120* (9), 4691–4716.

(70) Herman, L.; Ghosh, S.; Defrancq, E.; Mesmaekera, A. K.-D. *J. Phys. Org. Chem.* **2008**, *21* (7–8), 670–681.

(71) Moucheron, C. *New J. Chem.* **2009**, *33* (2), 235–245.

(72) Bednarski, P. J.; Mackay, F. S.; Sadler, P. J. *Anti-Cancer Agents Med. Chem.* **2007**, *7* (1), 75–93.

(73) Mackay, F. S.; Woods, J. A.; Heringová, P.; Kašpárková, J.; Pizarro, A. M.; Moggach, S. A.; Parsons, S.; Brabec, V.; Sadler, P. J. *Proc. Natl. Acad. Sci.* **2007**, *104* (52), 20743–20748.

(74) Mann, B. E.; Motterlini, R. *Chem. Commun.* **2007**, No. 41, 4197–4208.

(75) Schatzschneider, U. *Eur. J. Inorg. Chem.* **2010**, *2010* (10), 1451–1467.

(76) Farrer, N. J.; Salassa, L.; Sadler, P. J. *Dalton Trans.* **2009**, No. 48, 10690–10701.

(77) Ruggiero, E.; Alonso-de Castro, S.; Habtemariam, A.; Salassa, L. *Dalton Trans.* **2016**, *45* (33), 13012–13020.

(78) Askes, S. H. C.; Bahreman, A.; Bonnet, S. *Angew. Chem. Int. Ed.* **2014**, *53* (4), 1029–1033.

(79) Brieke, C.; Rohrbach, F.; Gottschalk, A.; Mayer, G.; Heckel, A. *Angew. Chem. Int. Ed.* **2012**, *51* (34), 8446–8476.

(80) Szymański, W.; Beierle, J. M.; Kistemaker, H. A. V; Velema, W. A.; Feringa, B. L. *Chem. Rev.* **2013**, *113* (8), 6114–6178.

(81) Zatsepin, T. S.; Abrosimova, L. A.; Monakhova, M. V; Hien, L. T.; Pingoud, A.; Kubareva, E. A.; Oretskaya, T. S. *Russ. Chem. Rev.* **2013**, *82* (10), 942.

(82) Irie, M. *Proc. Jpn. Acad. Ser. B. Phys. Biol. Sci.* **2010**, *86* (5), 472–483.

(83) Feringa, B. L. *Molecular Switches*; Wiley-VCH: Darmstadt, 2001.

(84) Woodward, R. B.; Hoffmann, R. *J. Am. Chem. Soc.* **1965**, *87* (1959), 395–397.

(85) Nakamura, S.; Irie, M. *J. Org. Chem.* **1988**, *53* (26), 6136–6138.

(86) Hohlneicher, G.; Mueller, M.; Demmer, M.; Lex, J.; Penn, J. H.; Gan, L. X.; Loesel, P. D. *J. Am. Chem. Soc.* **1988**, *110* (14), 4483–4494.

(87) Hanazawa, M.; Sumiya, R.; Horikawa, Y.; Irie, M. *J. Chem. Soc. Chem. Commun.* **1992**, No. 3, 206–207.

(88) Tian, H.; Yang, S. *Chem. Soc. Rev.* **2004**, *33* (2), 85–97.

(89) Irie, M. *Chem. Rev.* **2000**, *100* (5), 1685–1716.

(90) Jean-Ruel, H.; Gao, M.; Kochman, M. A.; Lu, C.; Liu, L. C.; Cooney, R. R.; Morrison, C. A.; Miller, R. J. D. *J. Phys. Chem. B* **2013**, *117* (49), 15894–15902.

(91) Gilat, S. L.; Kawai, S. H.; Lehn, J.-M. *Chem. Eur. J.* **1995**, *1* (5), 275–284.

(92) Singer, M.; Jäschke, A. *J. Am. Chem. Soc.* **2010**, *132* (24), 8372–8377.

(93) Cahová, H.; Jäschke, A. *Angew. Chem. Int. Ed.* **2013**, *52* (11), 3186–3190.

(94) Pace, T. C. S.; Müller, V.; Li, S.; Lincoln, P.; Andréasson, J. *Angew. Chem. Int. Ed.* **2013**, *52* (16), 4393–4396.

(95) Supuran, C. T.; Scozzafava, A.; Casini, A. *Med. Res. Rev.* **2003**, *23* (2), 146–189.

(96) Vomasta, D.; Högner, C.; Branda, N. R.; König, B. *Angew. Chem. Int. Ed.* **2008**, *47* (40), 7644–7647.

(97) Tan, W.; Zhou, J.; Li, F.; Yi, T.; Tian, H. *Chem. Asian J.* **2011**, *6* (5), 1263–1268.

(98) Babii, O.; Afonin, S.; Berditsch, M.; Reiβer, S.; Mykhailiuk, P. K.; Kubyshkin, V. S.; Steinbrecher, T.; Ulrich, A. S.; Komarov, I. V. *Angew. Chem. Int. Ed.* **2014**, *53* (13), 3392–3395.

CHAPTER 2

Preparation of platinum(II) molecular switches

2.1. Synthesis of photoswitchable ligands

2.1.1. General approaches to the synthesis of DTC systems

As discussed in the previous chapter, dithienylcyclopentenes (DTCs) and their fluorinated analogues, dithienylperfluorocyclopentenes (DTFCs), constitute one of the most remarkable classes of photochromic molecules, owing to their outstanding photochemical properties.[1,2] Accordingly, these were the chosen scaffolds to design a new series of photoresponsive, DNA-targeting platinum(II) complexes, with the aim of evaluating their applicability in the development of photoactivatable metallodrugs. However, despite their ever-growing popularity in several areas of research, the chemical preparation of these molecules is far from being trivial.

The synthesis of the bisthienylcyclopentenyl synthon, which is responsible for the reversible ring opening and closing photoswitching process, can be approached via two conceptually different methods that mainly differ from each other in the introduction of the bridging five-membered unit. That is, it is either possible to use a readily available and conveniently functionalized cyclopentene ring as a starting material, or obtaining that motif on a latter step of the synthetic route through an intramolecular reaction. Both approaches were explored over the course of this work.

A common strategy for obtaining dithienylcyclopentenes with a perfluorinated backbone consists in a formal substitution reaction between octafluorocyclopentene and a thiophene derivative bearing an exchangeable halogen at the 4-position, namely bromine (Scheme 2.1).[3] This process, often referred to as the Dixon reaction,[4] proceeds under a general addition-elimination mechanism, which is promoted by the selective lithiation of the most reactive bromide position. Then the resulting carbanion undergoes nucleophilic attack over the electron-deficient ring, promoting the elimination of a fluorine atom and producing the new carbon-carbon bond.

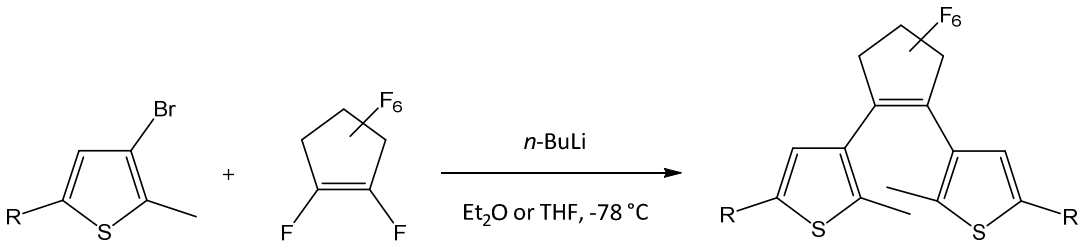

Scheme 2.1. *General preparation of dithienylperfluorocyclopentenes*.

Even though this procedure has been —and actually is— extensively used in the preparation of a wide range of photoswitches, it does present notable drawbacks. The extremely high volatility of octafluorocyclopentene (b.p.: 26-28 °C) often accounts for difficult handling and unsuitable stoichiometric control of the reaction, which ultimately leads to poor yields and to the formation of undesired byproducts. In addition, recent studies indicate that electronic effects from the substituents introduced in the thiophene ring must be also considered, since they may also contribute to further yield decrease due to the partial deactivation of the resulting thienyl nucleophile.[5] Moreover, since 1,2-difluorocyclopentene is not a readily available nor easily synthesizable reagent, this strategy does not allow the preparation of perhydro switches, but only perfluorinated ones.

In view of the above considerations, an alternative synthetic pathway for obtaining the photoswitchable dithienylcyclopentene core was proposed by Ben Feringa and co-workers in 1998.[6] The key aspect of this novel approach, initially adopted to produce perhydrogenated switches, is the formation of the cyclopentenyl ring via an

intramolecular McMurry reaction with a proper 1,5-dithienyl-1,5-diketone substrate, prepared by a simple Friedel-Crafts acylation reaction (Scheme 2.2). The main advantage of Feringa's strategy relies on the fact that all reactions involved are well-established and can be conducted in larger scales with moderate-to-high yields, whereas at the same time the formation of undesired monosubstituted products is also avoided. Indeed, this method was applied successfully to prepare an enormous variety of DTC-based switches, and is now the procedure of choice in most current investigations owing to its high efficiency and versatility.

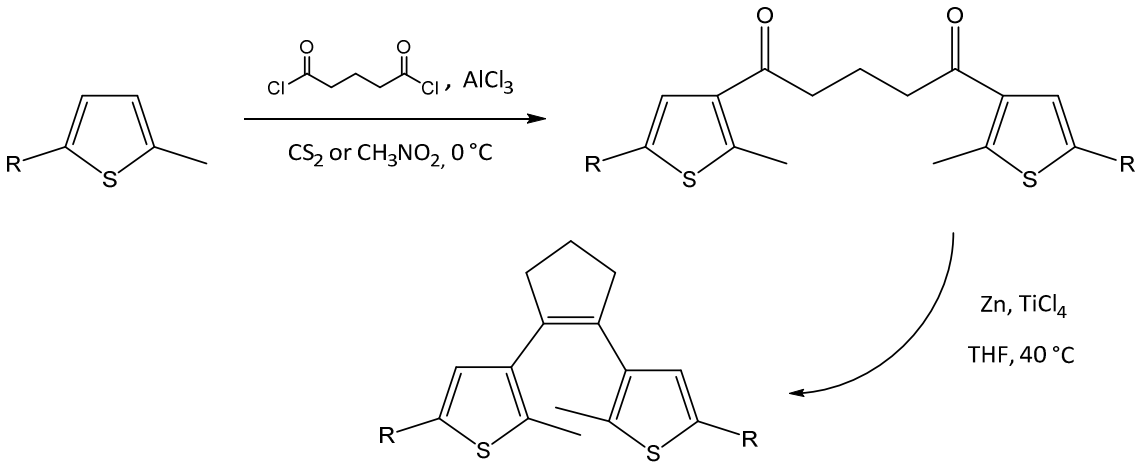

Scheme 2.2. *Preparation of dithienylcyclopentenes via an intramolecular McMurry reaction*.

Nonetheless, in spite of the apparent simplicity of this approach, there is also room for some considerations; in particular, the directing effect of each of the substituents of the thiophene rings in the Friedel-Crafts acylation step shall be carefully considered. Due to the presence of its electron-rich sulfur atom, thiophene is a strongly activated molecule towards electrophilic attack from the acylium cation, which is generated by reaction of the acyl chloride and the Lewis acid. However, the 2- and 5-positions of the ring, which are the sulfur neighboring locations, constitute the most reactive sites as a result of a higher resonance stabilization of the carbocationic intermediate, as illustrated in Figure 2.1. Therefore, a proper functionalization of these carbon atoms is strictly necessary for the reaction at the 3-position to occur. Besides the prevention of

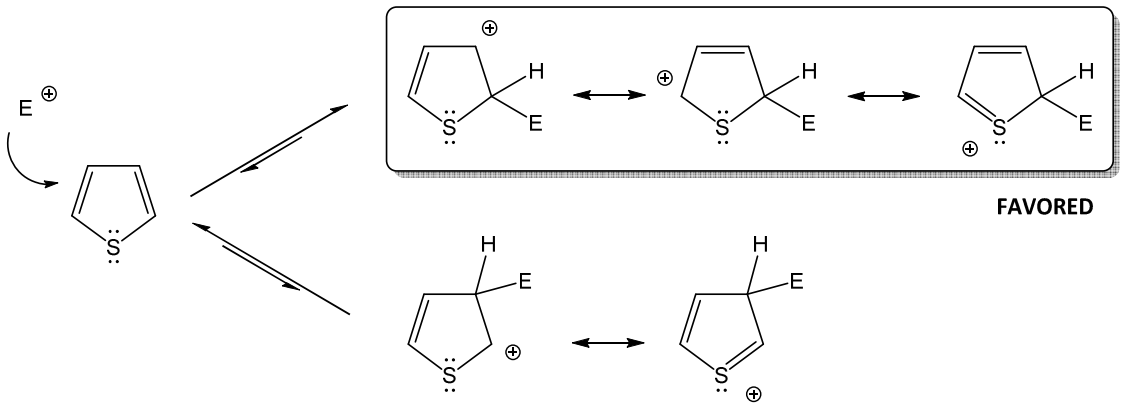

Figure 2.1. *Resonance stabilization of thiophene's carbocationic intermediate after an electrophilic attack at its 2- or 3-position.*

the irreversible oxidation of the ring-closed species (see Chapter 1),[7] the methyl groups at the 2-position of the thiophene rings of most DTC systems also favors this synthetic strategy, since their slightly activating character promotes the electrophilic substitution at the neighboring *ortho* position. Accordingly, the substituent at the 5-position of the thiophene ring shall be *meta*-directing, or at least less activating than the opposite group, for the exclusive acylation at carbon 3 to occur. Halogens and aldehydes may accomplish this function and constitute the functional groups of choice towards the preparation of more complex DTC switches, due to vast range of possibilities for their subsequent derivatization.

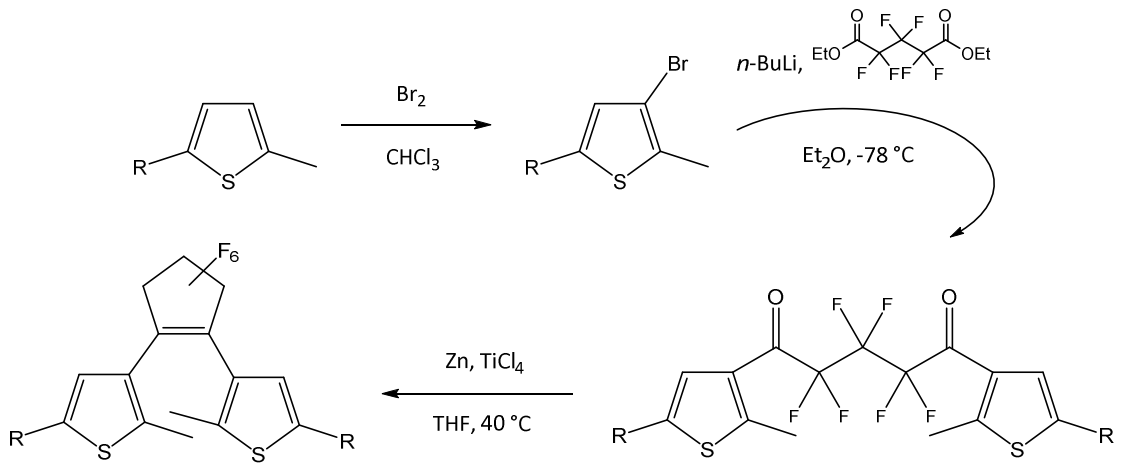

Scheme 2.3. *Adaptation of the intramolecular McMurry reaction approach for the preparation of perfluorinated DTCs.*

Moreover, it is worth noting that Feringa's approach can also be applied to the preparation of perfluorinated DTCs with some modifications.[8] Due to the electron-withdrawing perfluorinated backbone that hinders the formation of the required acylium ion, the corresponding diketone intermediate is in this case not obtained through Friedel-Crafts acylation, but rather by an addition-elimination reaction between diethyl hexafluoroglutarate and a properly functionalized 3-bromothiophene (Scheme 2.3). This product may then undergo intramolecular McMurry reaction, thus forming the perfluorinated ring through the establishment of a new carbon-carbon bond between both carbonyl positions.

2.1.2. Synthesis of symmetrical DTC ligands

Synthesis of the photoswitching core

Due to its apparent simplicity and attractive potential to serve as a versatile building block, the first synthetic target of this work was 1,2-bis(5-chloro-2-methyl-3-thienyl)cyclopentene (**2**), which was prepared following the procedure described by Feringa with subtle modifications (Scheme 2.4). The starting compounds for **2** were commercially available 2-chloro-5-methylthiophene and glutaryl dichloride, which were connected via Friedel-Crafts acylation in cold nitromethane; aluminium chloride

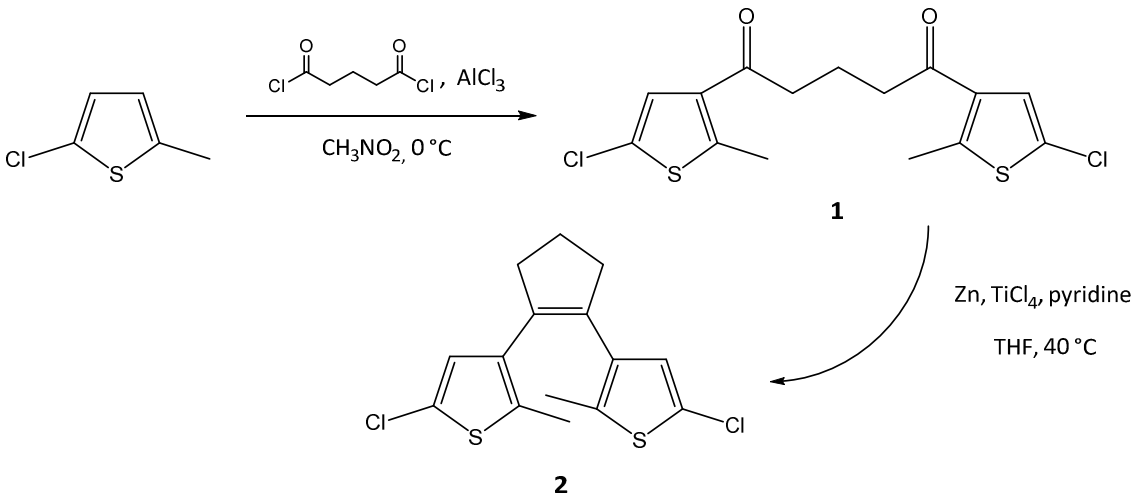

Scheme 2.4. *Preparation of 1,2-bis(5-chloro-2-methyl-3-thienyl)cyclopentene (**2**).*

was then used to promote the formation of the acylium species by reaction with the acyl chloride. Addition of ice-cold water to the reaction mixture and vigorous stirring in an ice bath led to the formation of an abundant precipitate, corresponding to the spectroscopically pure diketone **1**, obtained with a yield of 81%. This product was then used in a subsequent intramolecular McMurry reaction in THF, using the well-known system composed of titanium(IV) chloride, Zn dust as the reducing agent and pyridine as a low-valent titanium stabilizing ligand, in a nitrogen atmopshere.[9] Extraction of the slurry reaction crude with diethyl ether afforded the expected molecular switch **2** as a colorless solid, with a yield of up to 72% after column chromatography purification with cyclohexane. This synthetic route was remarkably consistent, and could be repeatedly performed on multigram scale without significant loss in yield.

Synthesis of imine-based derivatives

The obtained 2,2'-dichloro DTC is an outstanding starting reagent which can be derivatized in different ways by lithium-chlorine exchange and subsequent electrophilic substitution. In this regard, a wide range of examples can be found in the literature illustrating the functionalization with aldehyde, carboxylic acid, thioether, silane or phosphine moieties, among many other possibilities.[10–12] The aldehyde function was considered to be particularly interesting for the purpose of this study, owing to the fact that it should allow to systematically attach different metal-binding groups to the photoswitching core by simple condensation reactions with appropriate amine derivatives (Scheme 2.5).

Initial attempts to functionalize compound **2** showed that the required double lithium-chlorine exchange could not be achieved under the commonly used dry-ice temperature conditions; actually, monofunctional products were rather obtained even upon addition of an excess of *n*-buthyllithium. However, the lithiation of both chlorine positions was successfully achieved by performing this reaction at room temperature, as indicated by the slow apparition of a pale brown precipitate attributed to the DTC dilithium salt. Quenching of this intermediate with anhydrous dimethylformamide, followed by subsequent acid hydrolysis, produced the bis-aldehyde compound **3** with a yield of 65%.

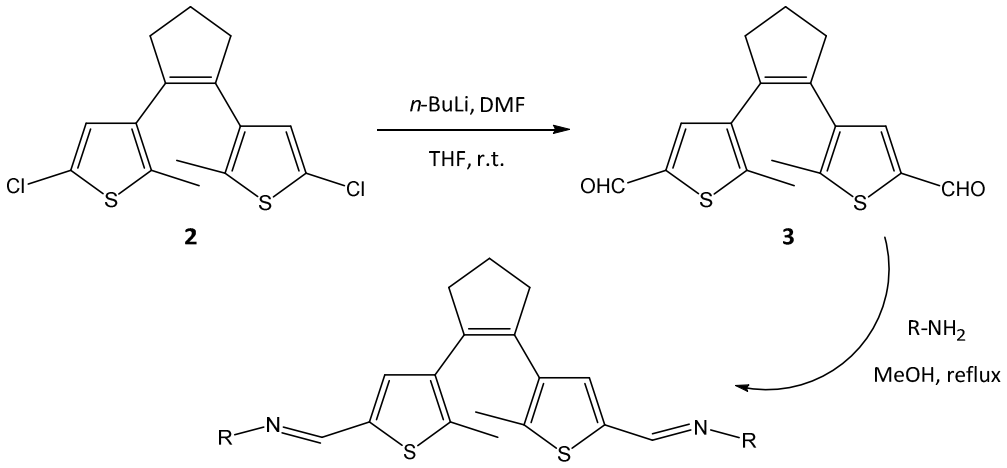

Scheme 2.5. *Proposed synthetic route for the preparation of photoswitchable imine derivatives.*

Compound **3** was then used in a common condensation reaction with 1,10-phenantrolin-5-amine in refluxing methanol, in order to generate a photoswitchable bis-bidentate Schiff-base ligand. However, this simple process did not take place, and TLC analysis of the reaction crude revealed the sole presence of both unaltered starting reagents. Similar unsuccessful results were also obtained applying various modifications of the reaction conditions, including the use of different solvents (i.e. methanol or toluene), extended reaction times and the introduction of either a drying agent or a Dean-Stark trap. Most strikingly, this lack of reactivity was also repeatedly observed with other heterocycle-containing amine substrates, and even with more activated reagents such as 2-hydrazinopyridine (Scheme 2.6).

Close inspection of literature reports revealed that, although a number of imine derivatives starting from compound **3** have been actually described by several

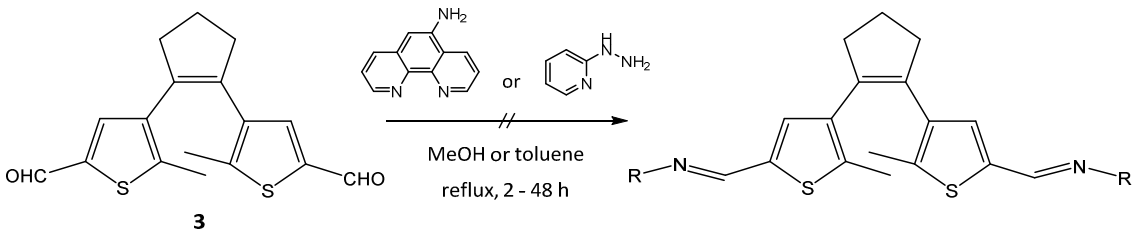

Scheme 2.6. *Unsuccessful preparation of several imine derivatives*.

authors, successful preparations mostly rely on the inclusion of aryl or alkyl groups.[13,14] Certainly, the lack of reported imine derivatives bearing heterocyclic residues is consistent with the observed inertness towards this kind of substrates, and suggests that the aldehyde groups of **3** may not be reactive enough to undergo condensation with slightly deactivated amines carrying aromatic N-donor groups. This synthetic methodology was therefore ruled out in favor of an alternative and more effective approach to derivatize compound **2**, based on the Suzuki cross-coupling reaction.

Derivatization of the DTC core using the Suzuki reaction

The Suzuki cross-coupling reaction, also known as Suzuki-Miyaura reaction, is a process first described in 1979 by Akira Suzuki,[15] in which a halide derivative is connected to an organoboron species in the presence of a palladium catalyst and a base (Scheme 2.7). Some of the most striking features of this transformation include its remarkably mild reaction conditions and its tolerance to a wide range of functionalized substrates, as well as the relatively low toxicity of the boronic acid derivatives; in addition, moderate-to-high yields are generally obtained. As a result, the Suzuki cross-coupling reaction constitutes one of the most common procedures for the formation of carbon-carbon bonds in several areas of chemical research, being a particularly important process in the pharmaceutical industry.[16]

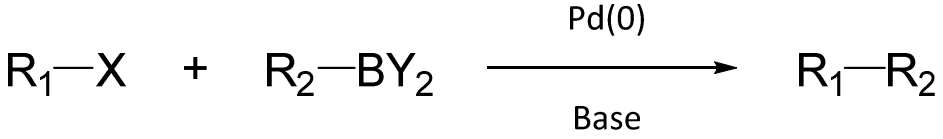

Scheme 2.7. *General overview of the Suzuki cross-coupling reaction*.

A detailed view of the mechanism of this reaction is depicted in Figure 2.2. As other metal-catalyzed processes, the Suzuki cross-coupling involves a series of consecutive basic inorganic reactions and is originated by the metal's ability to activate the R_1-X bond through oxidative addition, generating the organopalladium R_1-Pd(II)-X species.[17] Common palladium(0) sources for this purpose include $Pd(PPh_3)_4$ and $Pd(dba)_2$ (dba =

dibenzylideneacetone), but the active catalytic species might also be generated *in situ* from less air-sensitive Pd(II) complexes such as $Pd(OAc)_2$ or $PdCl_2(PPh_3)_2$.[18]

Following palladium's insertion, the coordination of the R_2 group to the transition metal center takes place via transmetalation with the organoboron species. Although the exact mechanism of this step remains to be elucidated, it is well known that the presence of a base is needed for the reaction to occur. Namely, it has been recently proposed that the base is able to generate a more active intermediate upon replacement of the halide in the palladium complex, which then undergoes ligand exchange with the boronic acid derivative.[19] Finally, the new carbon-carbon bond is formed in the latter step by reductive elimination of the coupled R_1-R_2 product, and the Pd(0) catalyst is regenerated.

Although a deeper insight into the enormous relevance of this process in several areas greatly surpasses the purpose of this brief overview and can be found elsewhere,[20,21] it is indeed worth stressing that, among the numerous applications that the Suzuki reaction has found in chemical research, the preparation of a wide variety of

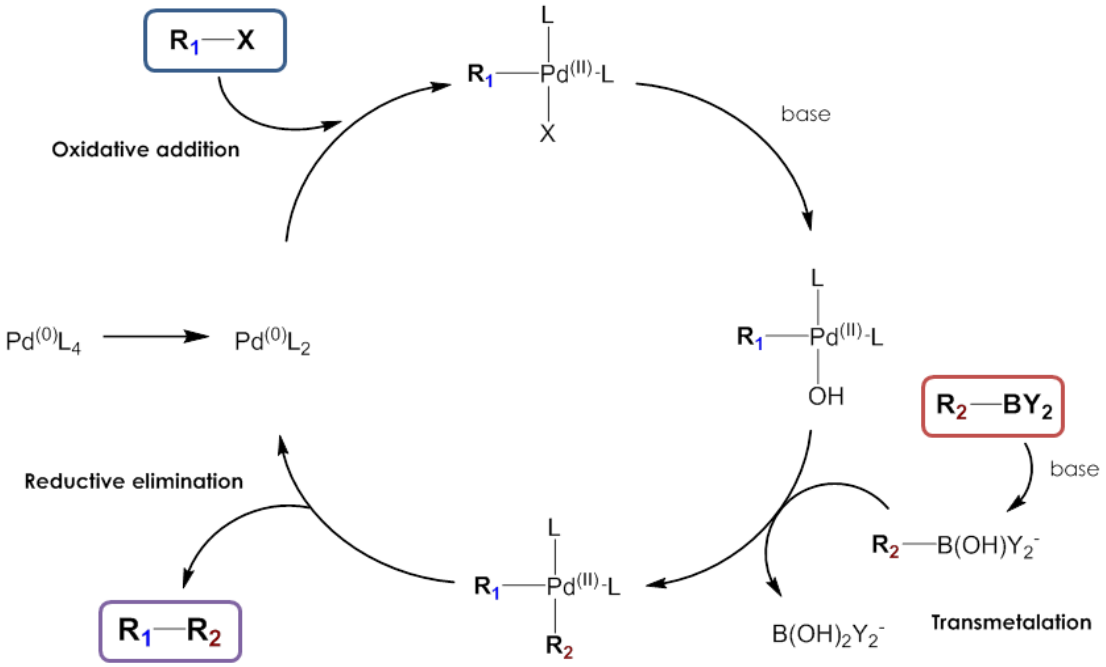

Figure 2.2. *Detailed reaction mechanism of the Suzuki-Miyaura cross-coupling reaction*.

diarylethene switches is no exception. Feringa and co-workers used this approach in the synthesis of a series of various aryl-containing dithienylcyclopentenes in moderate-to-high yields,[22] and similar procedures have been extensively used to gain access to a number of more complex switches showing remarkable photochromic properties.[23,24]

However, due to the lower reactivity of most carbon-chlorine bonds towards oxidative addition, compared to that of bromide, iodide or triflate substrates,[25] the DTC precursor **2** is not a suitable reagent to directly undergo Suzuki cross-coupling reaction with an organoboron species. One possible solution to this problem would be to transform compound **2** into its much more reactive dibromide analogue, as done in a few recent studies,[26] and another possibility would be to convert it into the coupling organoboron derivative. This latter approach seems to be preferred by most authors, judging by its much higher impact in the literature, and was also the chosen strategy in this work owing to the wider scope of commercially available aryl bromides to react with.

The introduction of a pyridine ring, which is one of the simplest metal-binding units as well as one of the very few heterocycles reported to have been connected to a dithienylcyclopentene structure,[27] was the first to be tested. Thereby, the 2,2'-dichloro precursor **2** was lithiated at room temperature under a nitrogen atmosphere, and the resulting dilithium salt suspension was then treated with tributyl borate to generate the bis-boronic ester derivative **2b** (Scheme 2.8). Since this kind of intermediate organoboron species has been described to be air-unstable and to easily undergo deboronization into its hydrogenated analogue,[28] the unaltered reaction crude was subsequently coupled with 4-bromopyridine hydrochloride. This reaction was performed in the presence of catalytic amounts of $Pd(PPh_3)_4$ as the palladium source and K_2CO_3 as the needed base, using a solvent mixture of THF and water. Such conditions proved to be quite effective and the formation of the expected pyridine-containing molecular switch **4** was confirmed by TLC analysis of the crude product, due to its characteristic colorless-to-blue color change upon exposure to UV radiation. Column chromatography purification, using ethyl acetate as the eluent and a few drops of ammonia so as to diminish the affinity of the pyridine residues towards the slightly acidic silica gel matrix, afforded the pure ligand as an off-white solid with a yield of up to 48%.

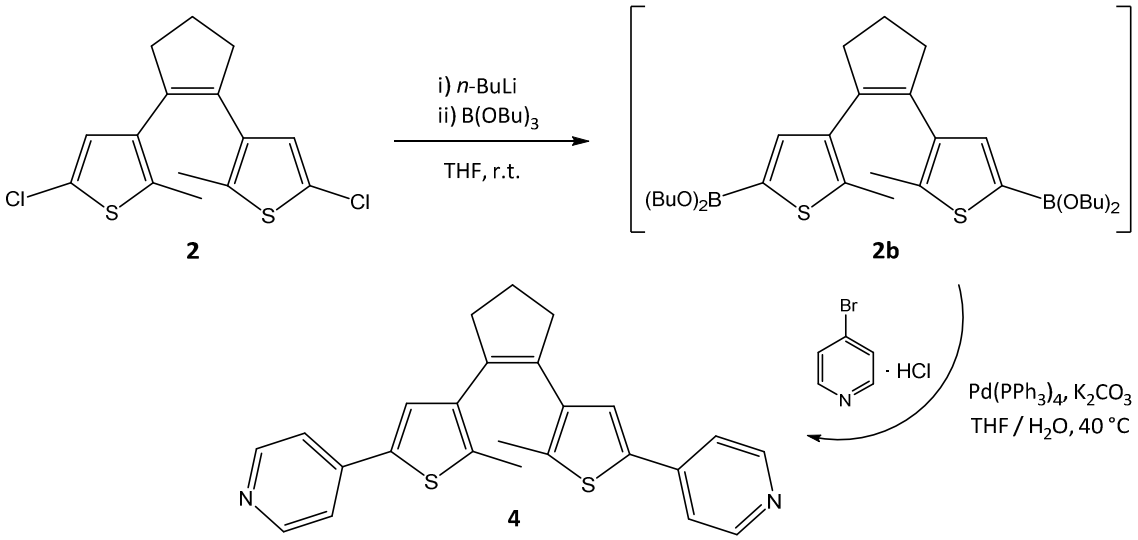

Scheme 2.8. *Introduction of a pyridine function using the Suzuki cross-coupling reaction*.

This effective pathway was subsequently used to prepare the series of ligands **5**-**9**, bearing various metal-binding moieties introduced via the coupling of **2b** with the corresponding bromide derivatives, under almost identical reaction conditions. The resulting products, most of which are hitherto unreported in the literature, were isolated in moderate yields (37-68%) after purification as either off-white or slightly colored solids, and were fully characterized by means of common techniques, including ^{1}H NMR spectroscopy, mass spectrometry and elemental analysis. Figure 2.3 depicts the chemical structure of the molecules prepared; these were designed to exhibit extended or modified conjugated systems, as well as different metal-binding

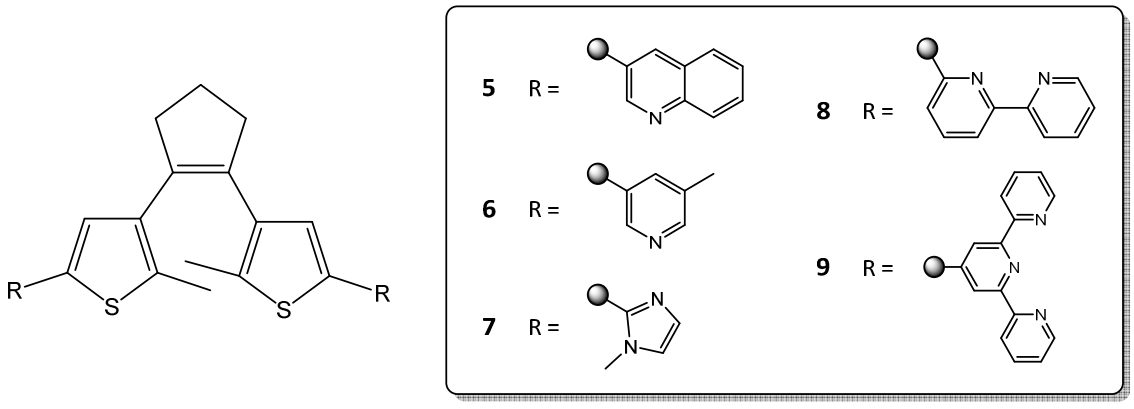

Figure 2.3. *Synthesized series of symmetrical DTC-based ligands*.

modes, with the ultimate aim of thoroughly studying the influence of the structure of the photoswitching ligands on the biological performance of the corresponding metal complexes.

Furthermore, the alternative bis-aldehyde compound **10** was also prepared with a yield of 58% by reaction of the DTC precursor **2** with 4-bromobenzaldehyde, so as to further explore the formation of photoswitching, metal-binding ligands through Schiff-base condensation reactions (Scheme 2.9). This strategy was encouraged by recent reports on the perfluorinated analogue of compound **10**, which was used as an effective starting material for the synthesis of photoswitchable Schiff bases, although as in the case of bis-aldehyde **3** such preparations were again limited to a number of aryl and alkyl derivatives.[29]

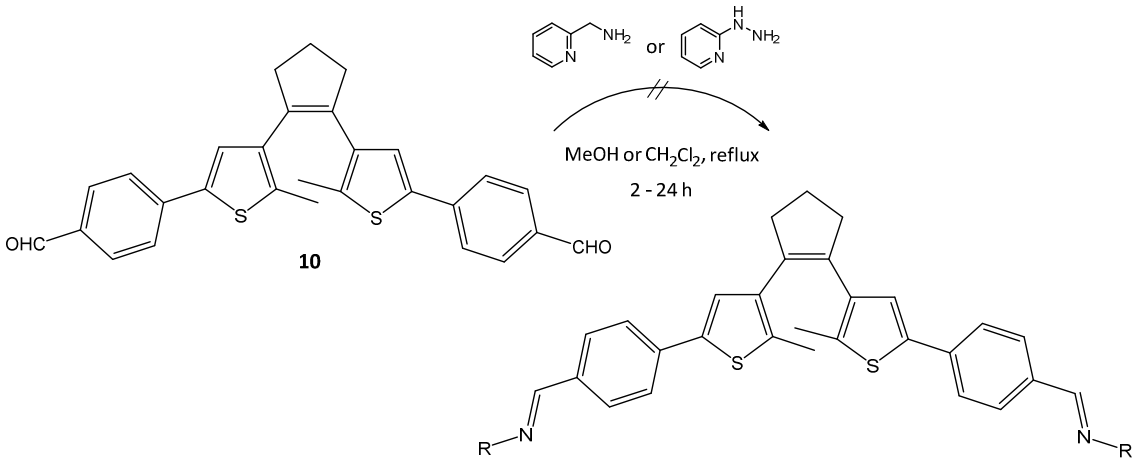

Scheme 2.9. *Ineffective imine-based derivatization of the alternative bis-aldehyde molecular switch* **10**.

Regrettably, as for compound **3**, the subsequent functionalization of this alternative bis-aldehyde precursor using different amine substrates (i.e. 2-aminomethylpyridine or 2-hydrazinopyridine) was unsuccessful under all the tested experimental conditions, and only unaltered starting materials were identified by TLC analysis after all attempts. Tiny amounts of additional photoreactive products could be detected in a few cases, but they could not be properly isolated nor identified by spectroscopic means. Accordingly, this strategy was abandoned.

2.1.3. Synthesis of symmetrical, perfluorinated DTC ligands

The preparation of perfluorinated analogues of the previously synthesized ligands, so as to further analyze the influence of the ligand's structural features on the biological interactions of the metal complexes, was carried out using the Dixon reaction approach described at the beginning of this chapter (see Scheme 2.1).

For this purpose, the corresponding substituted bromothiophenes were prepared beforehand by means of the Suzuki cross-coupling reaction, starting from readily available 3,5-dibromo-2-methylthiophene (Scheme 2.10). Treatment of this product with one equivalent of *n*-buthyllithium at low temperature, followed by subsequent addition of tributyl borate, led to the exclusive formation of a boronic ester function at the more reactive 5-position of the thiophene ring. In contrast with compound **2b**, this organoboron intermediate was air stable and could be isolated as the corresponding, spectroscopically pure boronic acid derivative **11** in almost quantitative yield, upon precipitation with hydrochloric acid. In a following step, reaction of this intermediate with 4-bromopyridine hydrochloride produced the expected pyridine-bearing bromothiophene **12**, with a yield of up to 82% after column chromatography purification with dichloromethane.

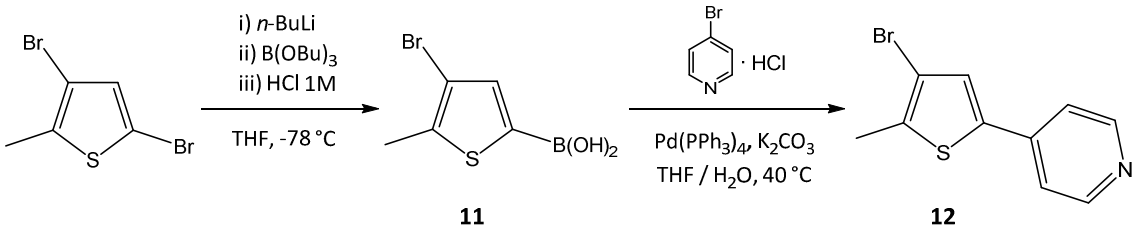

Scheme 2.10. *Synthesis of 4-bromo-5-methyl-2-(4-pyridyl)thiophene (**12**).*

The insertion of **12** into the fluorinated ring motif had to be optimized. The established procedures in THF or dioxane yielded mixtures of various unidentifiable photoswitching products, as revealed by TLC analysis of the reaction crudes. It was eventually found that previous dilution of the highly volatile octafluorocyclopentene in the appropriate anhydrous solvent considerably helped in reducing the apparition of such byproducts; upon applying this slight modification, the pyridine-containing

ligand **13** (analogous to the non-fluorinated ligand **4**) was finally obtained by reaction in anhydrous diethyl ether, with a low yield of 26% (Scheme 2.11), in agreement with the lower efficiencies reported for such preparations. The presence of the fluorinated backbone was verified by ^{19}F NMR spectroscopy, revealing the expected two sets of signals at ca. -132 and -110 ppm.

Using 3-bromoquinoline, the corresponding thiophene derivative **14** was obtained with a yield of 59%, and ligand **15** was subsequently prepared in anhydrous THF (Scheme 2.11). In this latter case, the quinolyl ligand was isolated among several unidentified byproducts, with a poor yield of 14%. Unfortunately, even poorer results were achieved when trying to apply this methodology for the preparation of the rest of the perfluorinated series. Even though the derivatization of the boronic acid precursor **11** with the corresponding bromo derivatives was successful, the following substitution reactions with octafluorocyclopentene did not generate substantial quantities of the expected molecular switches, regardless of all tested modifications of the reaction conditions.

On the basis of these results, an alternative pathway for the preparation of the perfluorinated ligands was employed (Scheme 2.12). Following a recently published procedure,[30] bromination of commercially available 2-chloro-5-methylthiophene produced 3-bromo-5-chloro-2-methylthiophene (**16**), which was then connected to octafluorocyclopentene to afford compound **17** with a yield of 64%. As a perfluorinated analogue of the bis-chloride precursor **2**, this compound was hence used as a photoswitchable building block in a new series of Suzuki cross-coupling reactions.

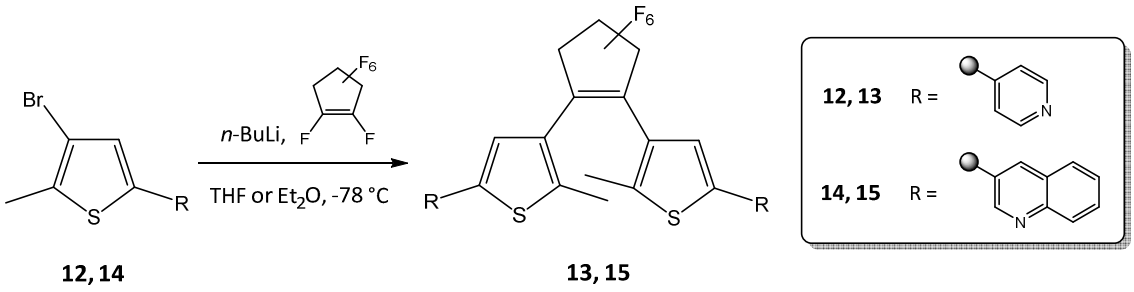

12, 14 **13, 15**

Scheme 2.11. *Preparation of several dithienylperfluorocyclopentene ligands*.

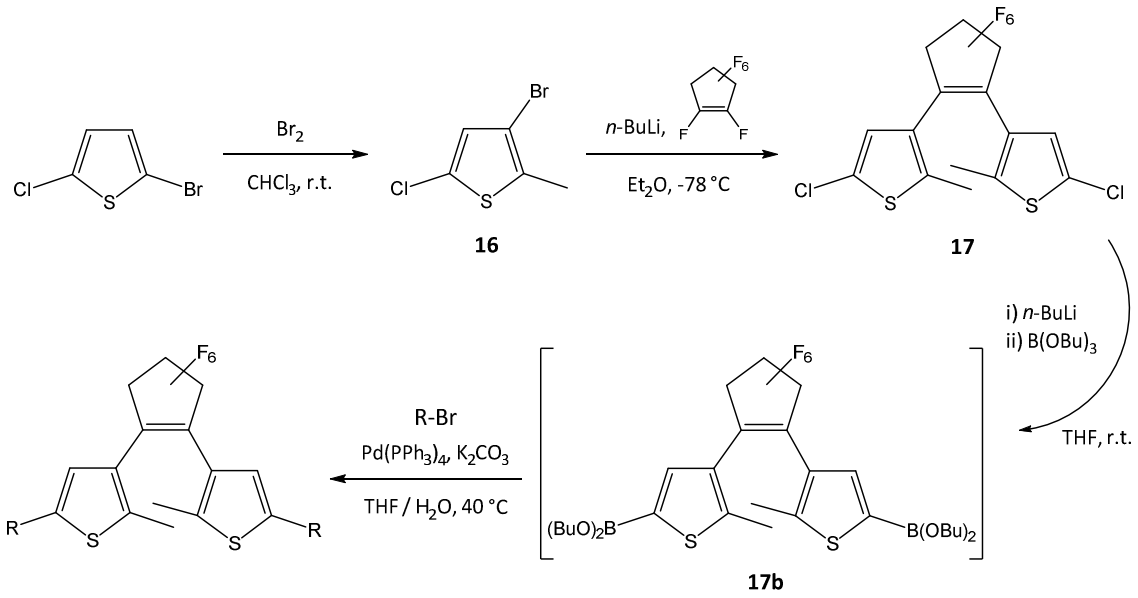

Scheme 2.12. *Proposed preparation of perfluorinated DTC ligands using the Suzuki reaction*.

In fact, a comparative study regarding the preparation of several aryl-containing dithienylcyclopentenes via Suzuki cross-coupling reaction, starting from the related compounds **2** and **17**, was already described by Feringa's group in 2003.[22] The results obtained showed that remarkably lower yields were systematically achieved for the derivatization of the fluorinated precursor (e.g. 70% vs. 7% for the coupling with bromophenyl), and some of the expected products could not even be properly obtained. On account of these precedents, it was decided to first synthesize again ligands **13** and **15** starting from compound **17**, in order to establish a comparison between this alternative synthetic route and the Dixon reaction.

Ligand **13** could be isolated with a yield of 12% through this method. As expected, the reaction was clearly less efficient compared with that of its non-fluorinated analogue **4** (48%), but in addition the yield was also substantially poorer than that achieved by employing the addition-elimination Dixon reaction over octafluorocyclopentene (26%). Moreover, ligand **15** could only be detected as a minor product by TLC analysis after reaction of **17b** with 3-bromoquinoline, and no substantial quantities could be properly isolated. Comparable results were obtained with all other bromo derivatives tested, and consequently the preparation of perfluorinated analogues remained limited to ligands **13** and **15**.

2.1.4. Synthesis of unsymmetrical DTC ligands

Besides the symmetrical ligands **4**-**9**, **13** and **15**, presenting two identical coordination pockets that would generate dinuclear metal complexes upon coordination, the preparation of unsymmetrical ligands was also considered of interest so as to evaluate the biological activity of the resulting mononuclear complexes. For the sake of comparison, it was chosen to prepare the unsymmetrical analogues of the simpler pyridine-containing ligands **4** and **13**. Hence, aiming to preserve maximal structural equivalence, it was decided to replace one of the metal-binding units with a non-coordinating phenyl ring.

The synthesis of the non-symmetrical hydrogenated ligand was performed by means of two consecutive Suzuki cross-coupling reactions, starting from compound **2** (Scheme 2.13). This strategy had also been successfully applied by Feringa's group for the preparation of non-symmetrical switches.[31] However, in the present work, the order in which the different substituents were attached to the DTC core turned out to be

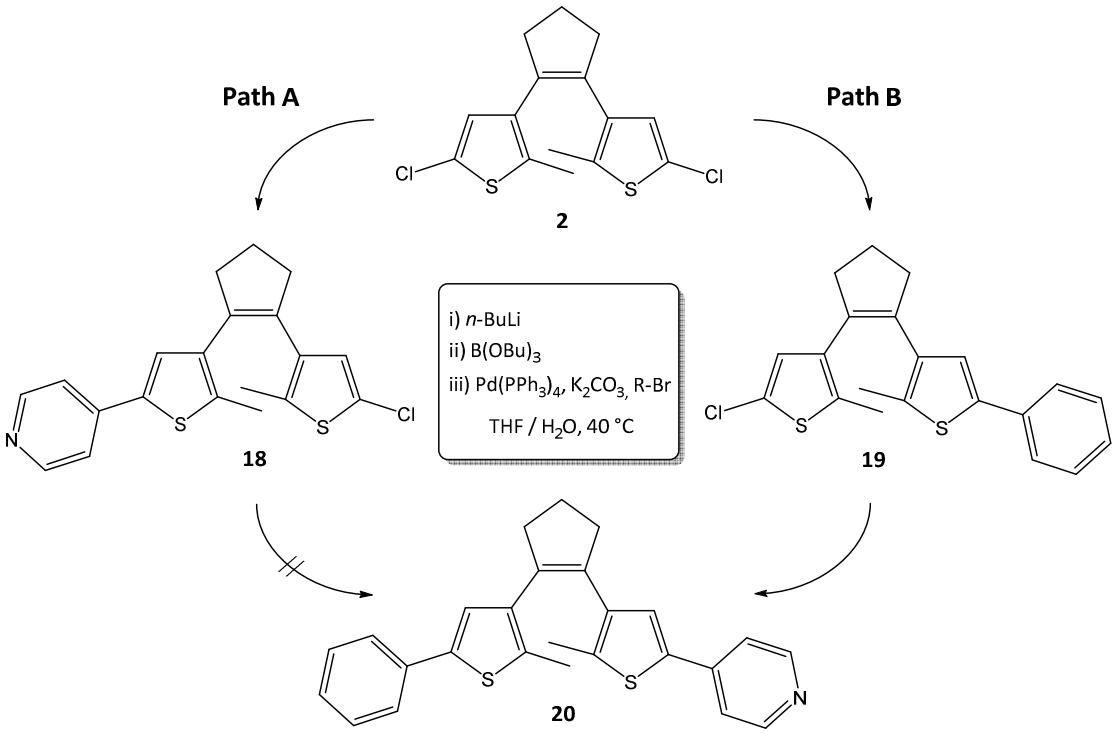

Scheme 2.13. *Proposed synthetic pathways towards the desymmetrization of the photoswitching precursor **2**.*

non trivial. Initially, compound **2** was treated with 1.1 equivalents of *n*-buthyllithium to generate lithium-halide exchange in just one of the chloride positions. This lithiathion step was first carried out at dry-ice temperature, with the objective to favour the exclusive formation of the monosubstituted species, although it was eventually found that lithiation performed at room temperature produced higher yields and similar byproduct ratios. Addition of tributyl borate and subsequent one-pot reaction of the unsymmetrical boronic ester intermediate with 4-bromopyridine hydrochloride afforded the monosubstituted compound **18**, which was obtained as a slightly orange oil with a yield of 79% (Scheme 2.13, path A).

However, the successive substitution of the remaining chloride position with bromophenyl did not proceed; instead of the expected unsymmetrical ligand, a major pyridine-containing, photochromic byproduct could be isolated but not unequivocally identified, even after ^{1}H NMR and mass spectrometry analysis. The same product was also obtained when bromophenyl was replaced with other aryl bromides, thereby suggesting that its formation starting from **18** was somehow favored, and was not occurring through Suzuki cross-coupling. In agreement with these observations, it may be noted that compound **18** has been described as an intermediate in the preparation of photochromic organogels,[32] but no further derivatization of its remaining halide position has ever been successfully reported in the literature. Consequently, the synthetic approach was readjusted to introduce the pyridyl function at a latter step, after the coupling of the phenyl group (Scheme 2.13, path B). Hence, reaction of **2** with bromobenzene produced compound **19** as a light-colored oil, with a yield of 66%. After purification, this product was then put to react with bromopyridine hydrochloride in a second Suzuki cross-coupling process, from which the desired unsymmetrical ligand **20**, hitherto non-described in the literature, was obtained with a yield of 72%.

The synthesis of the analogous perfluorinated unsymmetrical ligand was initially addressed applying a similar method described by Irie,[33] consisting of two consecutive nucleophilic substitutions of derivatized bromothiophenes on the central fluorinated ring. Hence, 4-bromo-5-methyl-2-(4-pyridyl)thiophene (**12**) was reacted with an equimolar amount of octafluorocyclopentene with the aim of yielding the corresponding monosubstituted compound (Scheme 2.14).

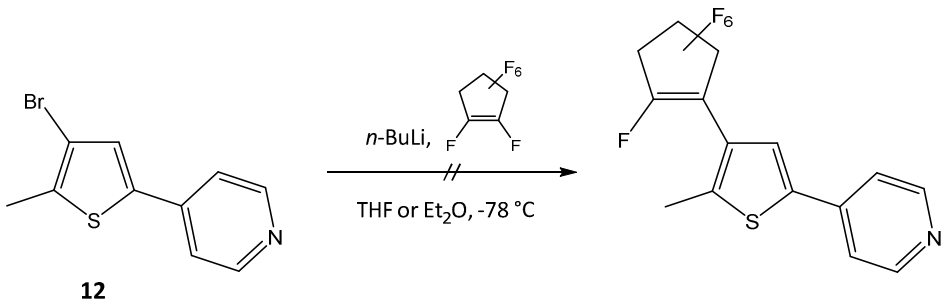

Scheme 2.14. *Inefficient monosubstitution over octafluorocyclopentene*.

However, the reaction did not proceed satisfactorily and the subsequent coupling step with 3-bromo-2-methyl-5-phenylthiophene (**21**), prepared as compound **12** with a yield of 52%, could not be carried out. Since comparable results were achieved upon swapping the order of the two substitutions, it was decided to perform a modified one-pot synthesis. Thereby, the bromothiophene derivatives **12** and **21** were simultaneously lithiated and immediately reacted with octafluorocyclopentene, the aim being to produce at most 50% of the unsymmetrically substituted ligand with respect to the corresponding symmetrical ones (Scheme 2.15). This approach was successful, as indicated by TLC analysis of the reaction crude; three clearly distinguishable photochromic products could be identified, the one with an intermediate R_f, ascribed to the unsymmetrical compound, being apparently more abundant. Separation of this product via column chromatography afforded the expected unsymmetrical ligand **22** as a dark green solid, with a reasonable yield of 25%, thus completing the series of ligands synthesized.

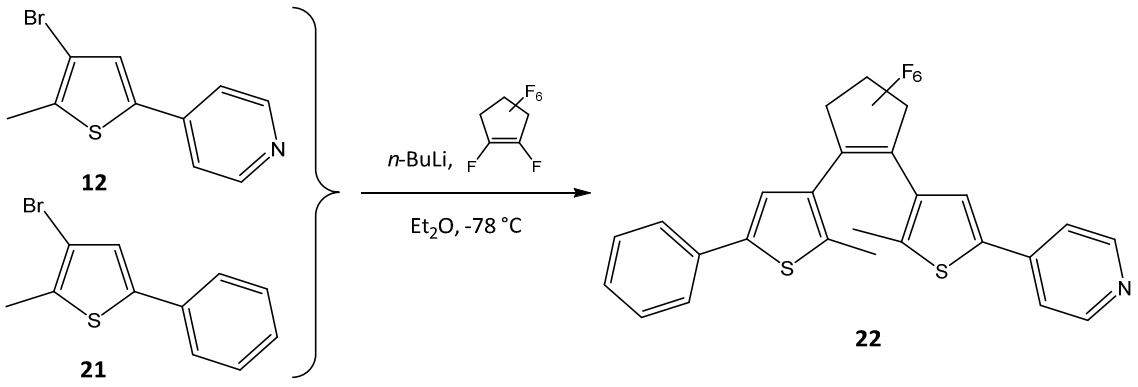

Scheme 2.15. *One-pot preparation of the unsymmetrical perfluoro derivative*.

2.2. Synthesis of the platinum(II) complexes

All the photochromic ligands prepared are depicted in Figure 2.4 together with their code names, which will be used from this point onwards. It can be pointed out here that, apart from **L1^{H}** and **L1^{F}**, which were previously reported by other autors, and **L5^{F}**, which was actually described as a synthetic intermediate,[34] the rest of the series is hitherto unreported.

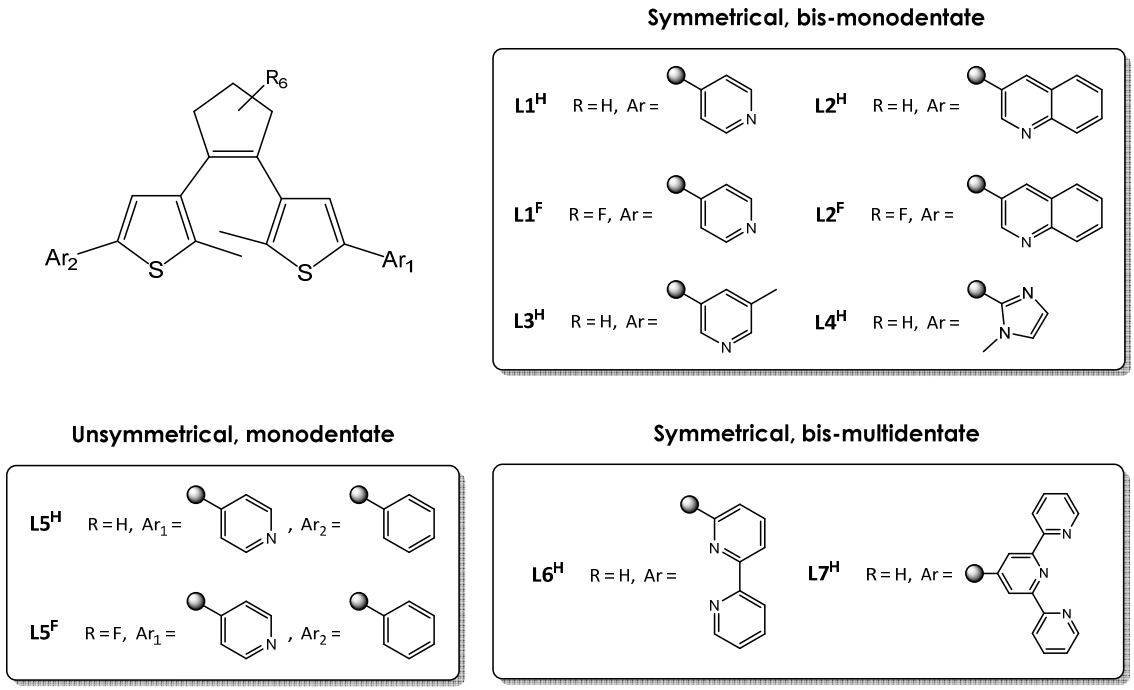

Figure 2.4. *Illustration of the designed and synthesized series of photochromic ligands*.

Following the synthesis and full characterization of these molecular switches, the preparation of platinum(II) complexes of biological interest was subsequently addressed, with the objective to assess the potential application of such systems in the field of photoactivated chemotherapy (PACT). The coordination compounds were obtained through direct ligand-substitution reactions with the appropriate metallic precursor, namely *cis*-[$PtCl_2(DMSO)_2$], which was previously synthesized according to standard published procedures.[35]

Owing to the monodentate nature of most of the ligands prepared, it was decided to maintain unaltered one of the DMSO molecules of the metal precursor to complete the coordination sphere of the platinum(II) centers. This was chosen for a number of reasons. The aim of the present work focuses on the evaluation of the biological properties and potential application of the photochromic ligands; therefore, for the proof of concept, all the systems investigated were kept as simple as possible. Moreover, keeping this position unaltered was also interesting in terms of activity; indeed, antitumor and antimethastatic properties have been reported for a number of complexes containing DMSO and other sulfoxide ligands,[36–38] including the well-known NAMI-A ruthenium(II) compound, which was able to reach Phase II clinical trials before its recent withdrawal.[39] Lastly, it was also considered that the presence of the S-DMSO ligand in the coordination sphere would contribute to reducing undesired substitution reactions (e.g. solvolysis) upon solubilization in dimethylsulfoxide, since this solvent is commonly used in biological studies of platinum compounds prior to their dilution in buffered aqueous media.

The first metal complex was obtained by addition of ligand **L1^{H}** onto a refluxing methanolic solution containing a slight excess of *cis*-[$PtCl_2(DMSO)_2$], previously hot filtered to remove any traces of Pt(0) impurities. The resulting mixture was stirred in the dark at room temperature to eventually produce a green precipitate. This solid, recovered in an almost quantitative yield (i.e. 94%), was identified as the neutral 16-electron species [{*trans*-$PtCl_2(DMSO)$}$_2$(μ-L1^{H})], noted as complex **C1^{H}** (Scheme 2.16).

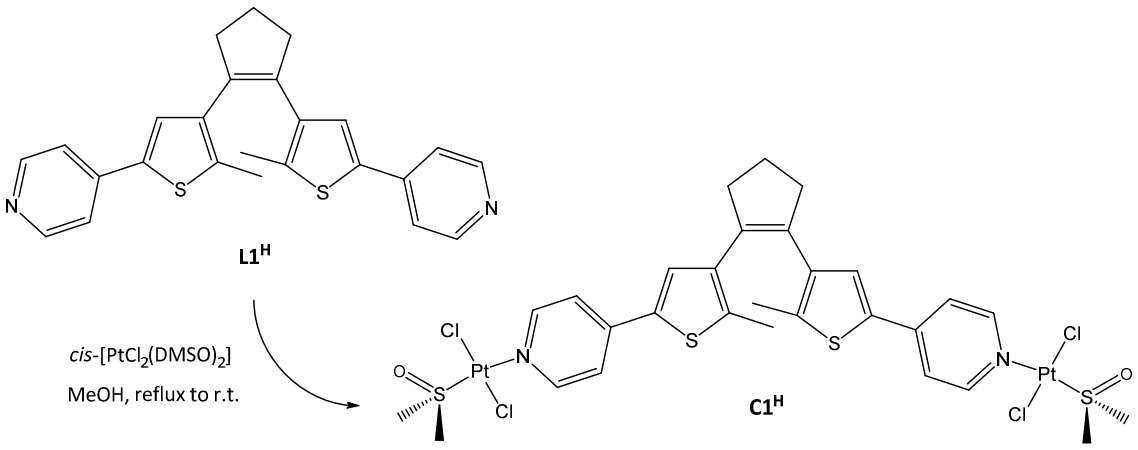

Scheme 2.16. *Preparation of the photochromic complex [{trans-$PtCl_2(DMSO)$}$_2$(μ-L1^{H})],* ***C1^{H}***.

The dinuclear nature of this complex was confirmed by ^{1}H NMR spectroscopy; no changes in the symmetry of the organic ligand were detected, thus implying identical coordination environments at each side of the molecule, and an intense additional peak at 3.47 ppm could be ascribed to the chemically equivalent DMSO groups. Moreover, a subtle chemical shift increase of ca. 0.05 ppm was detected for the thiophene and pyridine signals of the photochromic ligand, as a result of the deshielding effect induced by the coordination to the metal center.

The same procedure applied to all the other symmetrical bis-monodentate ligands produced the corresponding [{*trans*-$PtCl_2$(DMSO)}$_2$(μ-LX^Y)] complexes, respectively noted as **C1^F**, **C2^H**, **C3^H**, **C3^F** and **C4^H**, with yields in the range 79-95% and spectroscopic features comparable to those of **C1^H**. The *trans* disposition of the chlorido ligands in all these complexes was confirmed by the resolution of several crystal structures (see Chapter 3), thus implying a configurational change in the stereochemistry of the platinum centers during the substitution reaction. Such *cis*-to-*trans* isomerization has actually been previously reported in a number of publications, and may be explained by both the well-known strong *trans*-directing effect of the π-acidic S-DMSO ligand and its affinity towards the soft Pt(II) atoms.[40–42] It is likely that, upon substitution with the entering ligand, non-coordinated DMSO molecules might subsequently induce consecutive substitution processes that ultimately lead to the formation of the thermodynamically favored product, which in this case is illustrated by the formation of the less soluble species. Similar isomerization processes of S-DMSO ligands have also been observed for several ruthenium or osmium complexes.[43]

Similarly, reaction of *cis*-[$PtCl_2$(DMSO)$_2$] with the unsymmetrical ligand **L5^H** afforded the corresponding mononuclear complex **C5^H**, identified as *trans*-[$PtCl_2$(DMSO)(L5^H)], which was isolated with a comparably lower yield of 42%. As for the previous species, the presence of the [$PtCl_2$(DMSO)] fragment was confirmed by the appearance of a characteristic ^{1}H NMR peak at 3.47 ppm, ascribed to the dimethylsulfoxide group. Surprisingly, addition of the analogous perfluorinated ligand **L5^F** to a solution of the metal precursor did not produce the desired platinum(II) complex, even under reflux or after several days of reaction. This unforeseen lack of reactivity may be due to a much lower σ-donating character of this particular ligand, which may be related with the inductive effect of the fluorinated backbone.

The unexpected chemical inertness of the bis-bidentate ligand **L6^{H}** towards platination was even more surprising. Despite the fact that the substitution of both neutral ligands of *cis*-[$PtCl_2(DMSO)_2$] by bidentate N-N and N-O donors is commonly found in the literature, producing the corresponding *cis*-[$PtCl_2$(N-X)] neutral complexes,[44,45] no reaction was observed between the bipyridyl ligand and the platinum(II) precursor under all tested conditions. Lastly, lack of reactivity was also observed for the terpyridyl ligand **L7^{H}**, although in this particular case it could be attributed to the extremely low solubility of this compound in all the solvents tried.

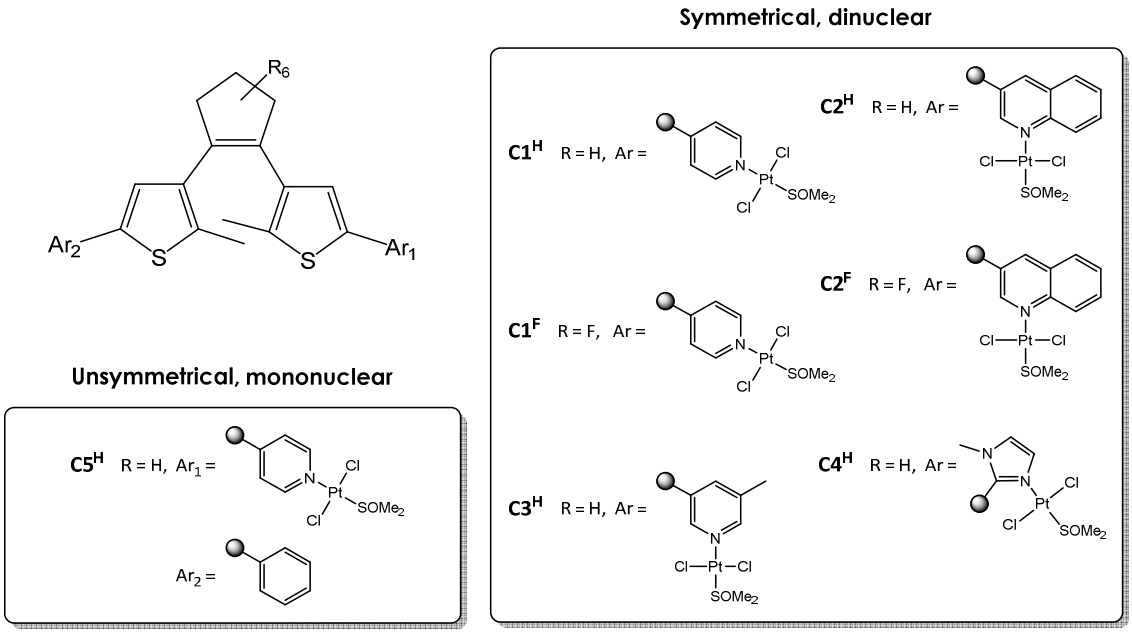

Figure 2.5. *Illustration of the series of photoswitchable Pt(II) complexes synthesized.*

In summary, the expected dinuclear complexes were successfully obtained with high efficiencies for most of the monodentate ligands, although platination of ligands **L5^{F}**, **L6^{H}** and **L7^{H}** could not be achieved. As a result, the subsequent photochemical and biological studies were carried out with complexes **C1^{H}**, **C1^{F}**, **C2^{H}**, **C3^{H}**, **C3^{F}**, **C4^{H}** and **C5^{H}**, which are depicted in Figure 2.5.

2.3. Experimental section

2.3.1. Materials and methods

Chemicals and HPLC-grade solvents were purchased from commercial sources and used as received. Anhydrous solvents were distilled under an inert atmosphere using a PureSolv solvent purification system from Innovative Technologies. When needed, reactions were performed under an atmosphere of N_2 using standard procedures. Column chromatography purifications were carried out in air, using ultrapure silica gel (60-200 µm, 60A) from Acros Organics, and monitored by analytical thin-layer chromatography using pre-coated aluminium plates.

Nuclear magnetic resonance (NMR) spectra were registered at 298 K on a Varian Mercury 400 MHz spectrometer. Chemical shifts (δ) are reported in ppm and coupling constants (J) are given in Hz. Proton chemical shifts are referenced to the corresponding non-deuterated solvent peak ($CHCl_3$: 7.26 ppm; DMSO: 2.50 ppm); fluorine chemical shifts are referenced to trifluoroacetic acid (-76.55 ppm). Signal multiplicities are defined as s (singlet), d (doublet), t (triplet), q (quartet), quint (quintet), br (broad signal) and m (multiplet).

ESI mass spectrometry was carried out using a LC/MSD-TOF spectrometer from Agilent Technologies equipped with an electrospray ionization (ESI) source, at the Centres Científics i Tecnològics de la Universitat de Barcelona. Samples were commonly eluted using a H_2O/CH_3CN 1:1 mixture and measured in the positive mode. C, H, N and S elemental analyses were also performed at the Centres Científics i Tecnològics de la Universitat de Barcelona, using a Thermo EA 1108 CHNS/O analyzer from Carlo Erba Instruments.

2.3.2. Synthesis and characterization

1,5-Bis(5-chloro-2-methyl-3-thienyl)pentane-1,5-dione (1)

$AlCl_3$ (29.0 g, 217 mmol) was slowly added to an ice-cooled mixture of 2-chloro-5-methylthiophene (25.0 g, 189 mmol) and glutaryl dichloride (12.0 mL, 94 mmol) in 200

mL of nitromethane. After the addition of $AlCl_3$, the resulting dark red solution was stirred for 3 h at room temperature and 150 mL of ice-cold water were added in small portions. This mixture was then placed in an ice bath and vigorously stirred for 1 h, until an abundant precipitate formed. This precipitate was then poured over a glass filter, washed with cold *n*-pentane and finally dried under reduced pressure to yield the crude final product as a pale brown solid **(27.6 g, 81%)**.

^{1}H NMR (400 MHz, $CDCl_3$): δ = 2.06 (m, 2H, J = 6.8 Hz, CH_2), 2.66 (s, 6H, Me), 2.86 (t, 4H, J = 6.8 Hz, $COCH_2$), 7.18 (s, 2H, thiophene). **MS (ESI)**: m/z = 361 $[M+H]^+$. **EA** calculated for $C_{15}H_{14}Cl_2O_2S_2$ (%): C 49.86, H 3.91, S 17.75; found: C 50.19, H 3.94, S 16.56.

1,2-Bis(5-chloro-2-methyl-3-thienyl)cyclopentene (2)

To an ice-cooled suspension of zinc dust (5.2 g, 80 mmol) in 150 mL of anhydrous THF, $TiCl_4$ (4.4 mL, 40 mmol) was carefully added under a nitrogen atmosphere using a syringe. The resulting grey-blue mixture was slowly heated to 50 °C and stirred for 2 h, after which pyridine (3.2 mL, 40 mmol) was added dropwise to yield a brown solution. After 10 min, 1,5-bis(5-chloro-2-methyl-3-thienyl)pentane-1,5-dione (7.2 g, 20 mmol) was added and the reaction mixture was stirred in the dark overnight. The solution was then cooled in an ice bath and quenched with 20% aqueous K_2CO_3 solution (25 mL), producing an abundant black precipitate. The mixture was vigorously stirred with diethyl ether (40 mL) and poured over a glass filter, and the filtrate was washed with additional diethyl ether (2 x 25 mL). The combined organic phase was placed in an ice bath for 30 min and filtered again to eliminate the resulting undesired white precipitate, then washed with acidified water (2 x 20 mL), dried (Na_2SO_4), filtered and concentrated under reduced pressure to afford an orange oil. This oil was purified by column chromatography on silica gel with cyclohexane as the eluent, yielding an oil that slowly turned into a colorless solid **(4.75 g, 72%)**.

^{1}H NMR (400 MHz, $CDCl_3$): δ = 1.88 (s, 6H, Me), 2.02 (m, 2H, J = 7.6 Hz, cyclopentene), 2.71 (t, 4H, J = 7.6 Hz, cyclopentene), 6.57 (s, 2H, thiophene). **MS (ESI)**: m/z = 329 $[M+H]^+$. **EA** calculated for $C_{15}H_{14}Cl_2S_2$ (%): C 54.71, H 4.29, S 19.47; found: C 54.89, H 4.37, S 18.78.

1,2-Bis(5-formyl-2-methyl-3-thienyl)cyclopentene (3)

1,2-Bis(5-chloro-2-methyl-3-thienyl)cyclopentene (1.0 g, 3.0 mmol) was dissolved in anhydrous THF (10 mL) under a nitrogen atmosphere and treated with *n*-buthyllithium (4.0 mL of a 1.6 M solution in hexane, 6.4 mmol) at room temperature. The reaction mixture was stirred in the dark for about 45 min until a light brown precipitate appeared, and anhydrous dimethylformamide (0.5 mL, 6.5 mmol) was subsequently added. The resulting yellow solution was stirred for 2 h, quenched with diluted hydrochloric acid (30 mL of a 2 M solution) and extracted with diethyl ether (3 x 25 mL). The combined organic phase was then washed with saturated $NaHCO_3$ solution (2 x 25 mL) and water (25 mL), dried (Na_2SO_4), filtered and concentrated under reduced pressure, affording a pale-brown solid. This solid was purified by column chromatography on silica gel with a 3:1 mixture of cyclohexane and ethyl acetate as the eluent, yielding a white product **(143 mg, 15%)**.

^{1}H NMR (400 MHz, $CDCl_3$): δ = 2.05 (s, 6H, Me), 2.12 (m, 2H, J = 7.6 Hz, cyclopentene), 2.83 (t, 4H, J = 7.6 Hz, cyclopentene), 7.42 (s, 2H, thiophene), 9.74 (s, 2H, CHO). **MS (ESI)**: m/z = 317 $[M+H]^+$.

1,2-Bis(2-methyl-5-(4-pyridyl)-3-thienyl)cyclopentene (4, L1^H)

1,2-Bis(5-chloro-2-methyl-3-thienyl)cyclopentene (1.0 g, 3.0 mmol) was dissolved in anhydrous THF (10 mL) under a nitrogen atmosphere and treated with *n*-buthyllithium (4.0 mL of a 1.6 M solution in hexane, 6.4 mmol) at room temperature. The reaction mixture was stirred in the dark for about 45 min until a light brown precipitate appeared, and then tributyl borate (2.4 mL, 8.9 mmol) was added. The resulting bright orange solution was stirred in the dark for 1 h and subsequently used for the Suzuki cross-coupling reaction. Meanwhile, in a separate flask, $[Pd(PPh_3)_4]$ (360 mg, 5% mol) and 4-bromopyridine hydrochloride (1.46 g, 7.5 mmol) were dissolved in a mixture of anhydrous THF (20 mL) and 20% aqueous K_2CO_3 solution (20 mL) under a nitrogen atmosphere. This two-phase system was stirred at 50 °C for 15 min and the previous freshly prepared boronic derivative solution was added dropwise with a syringe. The resulting mixture was then stirred in the dark overnight, after which it was cooled to

room temperature and treated with dichloromethane (25 mL) and water (15 mL). The organic layer was separated, washed with brine (25 mL), dried (Na_2SO_4), filtered and concentrated under reduced pressure. The crude product was purified by column chromatography on silica gel with ethyl acetate (containing 1% NH_3) as the eluent, yielding the final product as a white solid **(0.60 g, 48%)**.

^{1}H NMR (400 MHz, $CDCl_3$): δ = 2.03 (s, 6H, Me), 2.11 (m, 2H, J = 7.6 Hz, cyclopentene), 2.85 (t, 4H, J = 7.6 Hz, cyclopentene), 7.22 (s, 2H, thiophene), 7.35 (m, 4H, J_{app} = 6.4 Hz, pyridine), 8.53 (m, 4H, J_{app} = 6.4 Hz, pyridine). **MS (ESI)**: m/z = 415.1 $[M+H]^+$. **EA** calculated for $C_{25}H_{22}N_2S_2$ (%): C 72.43, H 5.35, N 6.76, S 15.47; found: C 72.75, H 5.40, N 6.59, S 15.30.

1,2-Bis(2-methyl-5-(3-quinolyl)-3-thienyl)cyclopentene (5, $L2^H$)

Compound **5** was prepared following the procedure described for compound **4**, but using 3-bromoquinoline (1.0 mL, 7.5 mmol) as the bromide derivative in the Suzuki cross-coupling reaction. The crude product was then purified by column chromatography on silica gel with a 4:1 mixture of dichloromethane and ethyl acetate as the eluent to yield the final product as a bright white solid **(0.87 g, 56%)**.

^{1}H NMR (400 MHz, $CDCl_3$): δ = 2.10 (s, 6H, Me), 2.15 (m, 2H, J = 7.6 Hz, cyclopentene), 2.91 (t, 4H, J = 7.6 Hz, cyclopentene), 7.23 (s, 2H, thiophene), 7.53 (m, 2H, J_1 = 6.8 Hz, J_2 = 1.2 Hz, quinoline), 7.66 (m, 2H, J_1 = 6.8 Hz, J_2 = 1.2 Hz, quinoline), 7.79 (d, 2H, J = 8.0 Hz, quinoline), 8.07 (d, 2H, J = 8.0 Hz, quinoline), 8.14 (d, 2H, J = 2.0 Hz, quinoline), 9.09 (d, 2H, J = 2.0 Hz, quinoline). **MS (ESI)**: m/z = 515.1 $[M+H]^+$. **EA** calculated for $C_{33}H_{26}N_2S_2$ (%): C 77.01, H 5.09, N 5.44, S 12.46; found: C 76.73, H 5.22, N 5.59, S 12.29.

1,2-Bis(2-methyl-5-(5-methyl-3-pyridyl)-3-thienyl)cyclopentene (6, $L3^H$)

Compound **6** was prepared following the procedure described for compound **4**, but using 3-bromo-5-methylpyridine (0.85 mL, 7.5 mmol) as the bromide derivative in the Suzuki cross-coupling reaction. The crude product was then purified by column chromatography on silica gel with a 3:1 mixture of ethyl acetate and dichloromethane as the eluent to yield the final product as a white solid **(0.69 g, 52%)**.

^{1}H NMR (400 MHz, $CDCl_3$): δ = 2.02 (s, 6H, Me), 2.10 (m, 2H, J = 7.6 Hz, cyclopentene), 2.34 (s, 6H, Me), 2.85 (t, 4H, J = 7.6 Hz, cyclopentene), 7.05 (s, 2H, thiophene), 7.55 (s, 2H, pyridine), 8.29 (s, 2H, pyridine), 8.56 (s, 2H, pyridine). **MS (ESI)**: m/z = 443.1 $[M+H]^+$. **EA** calculated for $C_{27}H_{26}N_2S_2$ (%): C 73.26, H 5.92, N 6.33, S 14.49; found: C 72.31, H 6.17, N 6.33, S 14.09.

1,2-Bis(2-methyl-5-(1-methyl-1*H*-imidazol-2-yl)-3-thienyl)cyclopentene (7, $L4^H$)

Compound **7** was prepared following the procedure described for compound **4**, but using 2-bromo-1-methyl-1*H*-imidazole (1.0 g, 6.2 mmol) as the bromide derivative in the Suzuki cross-coupling reaction. The crude product was then purified by column chromatography on silica gel with ethyl acetate (containing 1% NH_3) as the eluent, to yield the final product as a slightly pink solid **(0.47 g, 37%)**.

^{1}H NMR (400 MHz, $CDCl_3$): δ = 2.08 (m, 2H, J = 7.6 Hz, cyclopentene), 2.10 (s, 6H, Me), 2.83 (t, 4H, J = 7.6 Hz, cyclopentene), 3.65 (s, 6H, N-Me), 6.84 (d, 2H, J = 1.2 Hz, imidazole), 6.96 (s, 2H, thiophene), 7.01 (d, 2H, J = 1.2 Hz, imidazole). **MS (ESI)**: m/z = 421.1 $[M+H]^+$. **EA** calculated for $C_{23}H_{24}N_4S_2$ (%): C 65.68, H 5.75, N 13.32, S 15.25; found: C 65.38, H 6.07, N 13.21, S 15.43.

1,2-Bis(2-methyl-5-(6-[2,2'-bipyridyl])-3-thienyl)cyclopentene (8, $L6^H$)

Compound **8** was prepared following the procedure described for compound **4**, but using 6-bromo-2,2'-bipyridine (1.75 g, 7.5 mmol) as the bromide derivative for the Suzuki cross-coupling reaction. The crude product was then purified by column chromatography on silica gel with a 4:1 mixture of dichloromethane and ethyl acetate as the eluent to yield a dark oil, which was then vigorously stirred in the presence of pentane until precipitation of the final product as a grey solid **(0.67 g, 65%)**.

^{1}H NMR (400 MHz, $CDCl_3$): δ = 2.07 (s, 6H, Me), 2.13 (m, 2H, J = 7.6 Hz, cyclopentene), 2.90 (t, 4H, J = 7.6 Hz, cyclopentene), 7.31 (m, 2H, J_{app} = 6.0 Hz, bipy), 7.41 (s, 2H, thiophene), 7.54 (d, 2H, J = 7.6 Hz, bipy), 7.77 (m, 2H, J_{app} = 7.6 Hz, bipy), 7.82 (m, 2H, J_{app} = 7.6 Hz, bipy), 8.27 (d_{app}, 2H, J = 7.6 Hz, bipy), 8.54 (d, 2H, J = 7.6 Hz, bipy), 8.67 (m, 2H, J_{app} = 4.0 Hz, bipy). **MS (ESI)**: m/z = 569.2 $[M+H]^+$. **EA** calculated for $C_{35}H_{28}N_4S_2$ (%): C 73.91, H 4.96, N 9.85, S 11.27; found: C 73.23, H 5.36, N 9.66, S 10.96.

1,2-Bis(2-methyl-5-(4'-[2,2':6',2''-terpyridyl])-3-thienyl)cyclopentene (9, $L7^H$)

Compound **9** was prepared following the procedure described for compound **4**, but using 4'-bromo-2,2':6',2''-terpyridine (2.35 g, 7.5 mmol) as the bromide derivative for the Suzuki cross-coupling reaction. The crude product was then stirred in a 9:1 mixture of dichloromethane and diethyl ether until the apparition of a pale precipitate, which was filtered, washed with additional dichloromethane and dried under reduced pressure to yield the final product as a slightly pink solid **(0.64 g, 68%)**.

^{1}H NMR (400 MHz, $CDCl_3$): δ = 1.97 (s, 6H, Me), 2.14 (m, 2H, J = 7.6 Hz, cyclopentene), 2.91 (t, 4H, J = 7.6 Hz, cyclopentene), 7.32 (m, 4H, J_{app} = 4.8 Hz, terpy), 7.58 (s, 2H, thiophene), 7.85 (m, 4H, J_{app} = 8.0 Hz), 8.58 (s, 4H, terpy), 8.61 (d, 4H, J = 8.0 Hz, terpy), 8.71 (d, 4H, J = 4.8 Hz, terpy). **MS (ESI)**: m/z = 723.2 $[M+H]^+$. **EA** calculated for $C_{45}H_{34}N_6S_2$ (%): C 74.76, H 4.74, N 11.63, S 8.87; found: C 74.07, H 5.00, N 11.59, S 8.78.

1,2-Bis(2-methyl-5-(4-formylphenyl)-3-thienyl)cyclopentene (10)

Compound **10** was prepared following the procedure described for compound **4**, but using 4-bromobenzaldehyde (1.39 g, 7.5 mmol) as the bromide derivative in the Suzuki cross-coupling reaction. The crude product was then purified by column chromatography on silica gel with a 4:1 mixture of cyclohexane and ethyl acetate as the eluent, to yield the final product as a slightly blue solid **(0.82 g, 58%)**.

^{1}H NMR (400 MHz, $CDCl_3$): δ = 2.04 (s, 6H, Me), 2.12 (m, 2H, J = 7.6 Hz, cyclopentene), 2.86 (t, 4H, J = 7.6 Hz, cyclopentene), 7.19 (s, 2H, thiophene), 7.63 (d, J = 8.4 Hz, phenyl), 7.84 (d, J = 8.4 Hz, phenyl), 9.97 (s, 2H, CHO). **MS (ESI)**: m/z = 469.1 $[M+H]^+$.

4-Bromo-5-methylthiophene-2-boronic acid (11)

Under a nitrogen atmosphere, *n*-buthyllithium (10 mL of a 1.6 M solution in hexane, 16.0 mmol) was added dropwise to a solution of 3,5-dibromo-2-methylthiophene (2.0 mL, 15.6 mmol) in anhydrous diethyl ether (25 mL) at -78 °C, after which the initially colorless solution turned bright orange. The mixture was stirred for 30 min, and then tributyl borate (8.0 mL, 29.6 mmol) was added. After stirring the resulting solution at

room temperature overnight, 5% HCl aqueous solution (20 mL) was added to redissolve the formed pale yellow precipitate. The organic phase was then separated and extracted with aqueous NaOH solution (1 M, 2 x 20 mL), and the resulting combined aqueous phase was acidified (HCl, 37%) under vigorous stirring until the apparition of an off-white precipitate. The product was then filtered, washed with acidified water and dried under reduced pressure **(3.3 g, 96%)**.

^{1}H NMR (400 MHz, DMSO-d^6): δ = 2.36 (s, 3H, Me), 7.49 (s, 1H, thiophene), 8.32 (s, 2H, $B(OH)_2$). **MS (ESI)**: m/z = 220.9 - 222.9 $[M+H]^+$.

4-Bromo-5-methyl-2-(4-pyridyl)thiophene (12)

To a mixture of anhydrous THF (20 mL) and 20% aqueous K_2CO_3 solution (20 mL), $[Pd(PPh_3)_4]$ (260 mg, 5% mol), 4-bromopyridine hydrochloride (1.3 g, 6.7 mmol) and 4-bromo-5-methylthiophene-2-boronic acid (1.0 g, 4.5 mmol) were subsequently added under a nitrogen atmosphere. The resulting two-phase system was heated to 50 °C, stirred in the dark overnight and then cooled to room temperature before dichloromethane (25 mL) and water (15 mL) were added. The organic layer was separated, washed with brine (25 mL), dried (Na_2SO_4), filtered and concentrated under reduced pressure. The crude product was purified by column chromatography on silica gel with dichloromethane as the eluent, to yield the final product as an off-white solid **(0.94 g, 82%)**.

^{1}H NMR (400 MHz, $CDCl_3$): δ = 2.45 (s, 3H, Me), 7.32 (s, 1H, thiophene), 7.38 (m, 2H, J_1 = 6.0 Hz, J_2 = 2.4 Hz, pyridine), 8.59 (m, 2H, J_1 = 6.0 Hz, J_2 = 2.4 Hz, pyridine). **MS (ESI)**: m/z = 254.0 - 256.0 $[M+H]^+$.

1,2-Bis(2-methyl-5-(4-pyridyl)-3-thienyl)perfluorocyclopentene (13, $L1^F$)

4-Bromo-5-methyl-2-(4-pyridyl)thiophene (1.0 g, 4.0 mmol) was suspended in anhydrous diethyl ether (15 mL) under a nitrogen atmosphere and treated dropwise with *n*-buthyllithium (2.6 mL of a 1.6 M solution in hexane, 4.2 mmol) at -78 °C. After stirring the resulting pink suspension for 30 min, octafluorocyclopentene (1.35 mL of a 20% solution in anhydrous Et_2O, 2.0 mmol) was added and the reaction mixture was

stirred for 1 h at -78 °C. The cooling bath was then removed and the stirring continued at room temperature for 3 h, after which dichloromethane (25 mL) and water (25 mL) were added. The organic layer was separated, washed with brine (25 mL), dried (Na_2SO_4), filtered and concentrated under reduced pressure. The crude product was purified by column chromatography on silica gel using ethyl acetate (containing 1% NH_3) as the eluent, yielding the final product as a pale brown solid **(0.27 g, 26%)**.

^{1}H NMR (400 MHz, $CDCl_3$): δ = 2.00 (s, 6H, Me), 7.41 (m, 4H, J_1 = 4.4 Hz, J_2 = 1.6 Hz, pyridine), 7.47 (s, 2H, thiophene), 8.61 (m, 4H, J_1 = 4.4 Hz, J_2 = 1.6 Hz, pyridine). **^{19}F NMR** (400 MHz, $CDCl_3$): δ = -131.81 (quint, 2H, J = 5.6 Hz), -110.11 (t, 4H, J = 5.6 Hz). **MS (ESI)**: m/z = 523.1 $[M+H]^+$. **EA** calculated for $C_{25}H_{16}F_6N_2S_2$ (%): C 57.47, H 3.09, N 5.36, S 12.27; found: C 58.14, H 3.43, N 5.42, S 12.14.

4-Bromo-5-methyl-2-(3-quinolyl)thiophene (14)

Compound **14** was prepared following the procedure described for compound **12**, but using 3-bromoquinoline (0.9 mL, 6.7 mmol) as the bromide derivative. The crude product was purified by column chromatography on silica gel with dichloromethane as the eluent, to yield the final product as an off-white solid **(0.81 g, 59%)**.

^{1}H NMR (400 MHz, $CDCl_3$): δ = 2.48 (s, 3H, Me), 7.31 (s, 1H, thiophene), 7.58 (m, 2H, quinoline), 7.71 (m, 2H, quinoline), 7.84 (d, 2H, J = 8.8 Hz, quinoline), 8.12 (d, 2H, J = 8.8 Hz, quinoline), 8.21 (d, 2H, J = 2.4 Hz, quinoline), 9.11 (d, 2H, J = 2.4 Hz, quinoline). **MS (ESI)**: m/z = 304.0 – 306.0 $[M+H]^+$.

1,2-Bis(2-methyl-5-(3-quinolyl)-3-thienyl)perfluorocyclopentene (15, L2^F)

4-Bromo-5-methyl-2-(3-quinolyl)thiophene (1.2 g, 4.0 mmol) was suspended in anhydrous THF (15 mL) under a nitrogen atmosphere and treated dropwise with *n*-buthyllithium (2.6 mL of a 1.6 M solution in hexane, 4.2 mmol) at -78 °C. After stirring the resulting pink suspension for 30 min, octafluorocyclopentene (1.35 mL of a 20% solution in anhydrous THF, 2.0 mmol) was added and the reaction mixture was stirred for 1 h at -78 °C. The cooling bath was then removed and the stirring continued at room temperature for 3 h, after which dichloromethane (25 mL) and water (25 mL)

were added. The organic layer was separated, washed with brine, dried (Na_2SO_4), filtered and concentrated under reduced pressure. The crude product was purified by column chromatography on silica gel using ethyl acetate as the eluent, yielding the final product as a pale blue solid **(0.18 g, 14%)**.

^{1}H NMR (400 MHz, $CDCl_3$): δ = 2.08 (s, 6H, Me), 7.47 (s, 2H, thiophene), 7.58 (m, 4H, quinoline), 7.72 (m, 4H, quinoline), 7.84 (d, 2H, J = 8.0 Hz, quinoline), 8.11 (d, 2H, J = 8.0 Hz, quinoline), 8.24 (br, 2H, quinoline), 9.12 (d, 2H, J = 2.0 Hz, quinoline). **^{19}F NMR** (400 MHz, $CDCl_3$): δ = -131.82 (quint, 2H, J = 5.6 Hz), -109.97 (t, 4H, J = 5.6 Hz). **MS (ESI)**: m/z = 623.1 $[M+H]^+$. **EA** calculated for $C_{33}H_{20}F_6N_2S_2$ (%): C 63.66, H 3.24, N 4.50, S 10.30; found: C 63.59, H 3.70, N 4.47, S 9.76.

3-Bromo-5-chloro-2-methylthiophene (16)

2-Chloro-5-methylthiophene (5.0 mL, 45.6 mmol) was dissolved in chloroform (25 mL) and treated with bromine (1.4 mL, 0.6 eq.) at room temperature under a nitrogen atmosphere. After stirring this mixture overnight, the solvent was evaporated under reduced pressure and the resulting crude was then purified by column chromatography on silica gel using cyclohexane as the eluent, affording the product as a colorless liquid **(7.4 g, 76%)**.

^{1}H NMR (400 MHz, $CDCl_3$): δ = 2.32 (s, 3H, Me), 6.73 (s, 1H, thiophene). **MS (ESI)**: m/z = 210.9 – 212.9 $[M+H]^+$.

1,2-Bis(5-chloro-2-methyl-3-thienyl)perfluorocyclopentene (17)

3-Bromo-5-choro-2-methylthiophene (2.15 g, 10 mmol) was dissolved in anhydrous diethyl ether (25 mL) under a nitrogen atmosphere and treated dropwise with *n*-buthyllithium (6.5 mL of a 1.6 M solution in hexane, 10.4 mmol) at -78 °C. After stirring the resulting solution for 30 min, octafluorocyclopentene (3.4 mL of a 20% solution in anhydrous Et_2O, 5 mmol) was added and the reaction mixture was stirred for 1 h at -78 °C. The cooling bath was then removed and the stirring continued at room temperature for 3 h, after which water (25 mL) was added. The organic layer was separated, washed with brine (25 mL), dried (Na_2SO_4), filtered and concentrated under

reduced pressure. The crude product was purified by column chromatography on silica gel using cyclohexane as the eluent, yielding the final product as a yellow solid **(1.4 g, 64%)**.

^{1}H NMR (400 MHz, $CDCl_3$): δ = 1.89 (s, 6H, Me), 6.88 (s, 2H, thiophene). **^{19}F NMR** (400 MHz, $CDCl_3$): δ = -131.96 (quint, 2H, J = 5.6 Hz), -110.36 (t, 4H, J = 5.6 Hz). **MS (ESI)**: m/z = 436.9 $[M+H]^+$.

1-(2-Methyl-5-chloro-3-thienyl)-2-(2-methyl-5-(4-pyridyl)-3-thienyl)-cyclopentene (18)

1,2-Bis(5-chloro-2-methyl-3-thienyl)cyclopentene (1.0 g, 3.0 mmol) was dissolved in anhydrous THF (10 mL) under nitrogen atmosphere and treated with *n*-buthyllithium (2.0 mL of a 1.6 M solution in hexane, 3.2 mmol) at room temperature. After stirring in the dark for about 45 min, tributyl borate (1.2 mL, 4.5 mmol) was added and the resulting bright orange solution was then stirred in the dark for 1 h and subsequently used for the Suzuki cross-coupling reaction. Meanwhile, in a separate flask, $[Pd(PPh_3)_4]$ (180 mg, 5% mol) and 4-bromopyridine hydrochloride (0.73 g, 3.75 mmol) were dissolved in a mixture of anhydrous THF (20 mL) and 20% aqueous K_2CO_3 solution (20 mL) under a nitrogen atmosphere. This two-phase system was stirred at 50 °C for 15 min and the previous freshly prepared boronic derivative solution was added dropwise with a syringe. The resulting mixture was then stirred in the dark overnight, after which it was cooled to room temperature and treated with dichloromethane (25 mL) and water (15 mL). The organic layer was separated, washed with brine (25 mL), dried (Na_2SO_4), filtered and concentrated under reduced pressure. The crude product was purified by column chromatography on silica gel with ethyl acetate as the eluent, yielding the final product as a slightly colored oil **(0.88 g, 79%)**.

^{1}H NMR (400 MHz, $CDCl_3$): δ = 1.88 (s, 3H, Me), 2.03 (s, 3H, Me), 2.07 (m, 2H, 7.6 Hz, cyclopentene), 2.75 (m, 2H, J_{app} = 7.6 Hz, cyclopentene), 2.81 (m, 2H, J_{app} = 7.6 Hz, cyclopentene), 6.61 (s, 1H, thiophene), 7.18 (s, 1H, thiophene), 7.34 (m, 4H, J_{app} = 6.4 Hz, pyridine), 8.54 (m, 4H, J_{app} = 6.4 Hz, pyridine). **MS (ESI)**: m/z = 372.1 $[M+H]^+$.

1-(2-Methyl-5-chloro-3-thienyl)-2-(2-methyl-5-phenyl-3-thienyl)-cyclopentene (19)

1,2-Bis(5-chloro-2-methyl-3-thienyl)cyclopentene (1.0 g, 3.0 mmol) was dissolved in anhydrous THF (10 mL) under a nitrogen atmosphere and treated with *n*-buthyllithium (2.0 mL of a 1.6 M solution in hexane, 3.2 mmol) at room temperature. After stirring in the dark for about 45 min, tributyl borate (1.2 mL, 4.5 mmol) was added and the resulting bright orange solution was then stirred in the dark for 1 h, and subsequently used for the Suzuki cross-coupling reaction. Meanwhile, in a separate flask, $[Pd(PPh_3)_4]$ (180 mg, 5% mol) and bromobenzene (0.4 mL, 3.75 mmol) were dissolved in a mixture of anhydrous THF (20 mL) and 20% aqueous K_2CO_3 solution (20 mL) under a nitrogen atmosphere. This two-phase system was stirred at 50 °C for 15 min and the previous freshly prepared boronic derivative solution was added dropwise with a syringe. The resulting mixture was then stirred in the dark overnight, after which it was cooled to room temperature and treated with dichloromethane (25 mL) and water (15 mL). The organic layer was separated, washed with brine (25 mL), dried (Na_2SO_4), filtered and concentrated under reduced pressure. The crude product was purified by column chromatography on silica gel with a 19:1 mixture of cyclohexane and ethyl acetate as the eluent, yielding the final product as a slightly colored oil **(0.74 g, 66%)**.

^{1}H NMR (400 MHz, $CDCl_3$): δ = 1.88 (s, 3H, Me), 2.00 (s, 3H, Me), 2.05 (m, 2H, 7.6 Hz, cyclopentene), 2.75 (m, 2H, J_{app} = 7.6 Hz, cyclopentene), 2.81 (m, 2H, J_{app} = 7.6 Hz, cyclopentene), 6.62 (s, 1H, thiophene), 6.99 (s, 1H, thiophene), 7.23 (m, 1H, J_{app} = 7.2 Hz, phenyl), 7.34 (m, 2H, J_{app} = 7.2 Hz, phenyl), 7.49 (m, 2H, J_{app} = 7.2 Hz, phenyl). **MS (ESI)**: m/z = 371.1 $[M+H]^+$.

1-(2-Methyl-5-(4-pyridiyl)-3-thienyl)-2-(2-methyl-5-phenyl-3-thienyl)-cyclopentene (20, L5^H)

1-(2-Methyl-5-chloro-3-thienyl)-2-(2-methyl-5-phenyl-3-thienyl)cyclopentene (0.7 g, 1.9 mmol) was dissolved in anhydrous THF (10 mL) under a nitrogen atmosphere and treated with *n*-buthyllithium (1.3 mL of a 1.6 M solution in hexane, 2.1 mmol) at room temperature. After stirring in the dark for about 45 min, tributyl borate (0.8 mL, 3.0 mmol) was added and the resulting bright red solution was then stirred in the dark for

1 h, and subsequently used for the Suzuki cross-coupling reaction. Meanwhile, in a separate flask, [$Pd(PPh_3)_4$] (115 mg, 5% mol) and 4-bromopyridine hydrochloride (0.47 g, 2.4 mmol) were dissolved in a mixture of anhydrous THF (20 mL) and 20% aqueous K_2CO_3 solution (20 mL) under a nitrogen atmosphere. This two-phase system was stirred at 50 °C for 15 min and the previous freshly prepared boronic derivative solution was added dropwise with a syringe. The resulting mixture was then stirred in the dark overnight, after which it was cooled to room temperature and treated with dichloromethane (25 mL) and water (15 mL). The organic layer was separated, washed with brine (25 mL), dried (Na_2SO_4), filtered and concentrated under reduced pressure. The crude product was purified by column chromatography on silica gel with ethyl acetate as the eluent, yielding the final product as a brown solid **(0.57 g, 72%)**.

^{1}H NMR (400 MHz, $CDCl_3$): δ = 1.99 (s, 3H, Me), 2.07 (s, 3H, Me), 2.11 (m, 2H, 7.6 Hz, cyclopentene), 2.85 (t, 4H, J = 7.6 Hz, cyclopentene), 7.01 (s, 1H, thiophene), 7.23 (m, 1H, J_{app} = 7.2 Hz, phenyl), 7.29 (s, 1H, thiophene), 7.34 (m, 2H, J_{app} = 7.2 Hz, phenyl), 7.44 (m, 2H, J_1 = 4.8 Hz, J_2 = 1.6 Hz, pyridine), 7.49 (m, 2H, J_{app} = 7.2 Hz, phenyl), 8.51 (m, 2H, J_1 = 4.8 Hz, J_2 = 1.6 Hz, pyridine). **MS (ESI)**: m/z = 414.1 $[M+H]^+$.

3-Bromo-2-methyl-5-phenylthiophene (21)

To a mixture of anhydrous THF (20 mL) and 20% aqueous K_2CO_3 solution (20 mL), [$Pd(PPh_3)_4$] (260 mg, 5% mol), 4-bromobenzene (0.72 mL, 6.7 mmol) and 4-Bromo-5-methylthiophene-2-boronic acid (1.0 g, 4.5 mmol) were subsequently added under a nitrogen atmosphere. The resulting two-phase system was heated to 50 °C, stirred in the dark overnight and then cooled to room temperature before dichloromethane (25 mL) and water (15 mL) were added. The organic layer was separated, washed with brine (25 mL), dried (Na_2SO_4), filtered and concentrated under reduced pressure. The crude product was purified by column chromatography on silica gel with a 1:1 mixture of dichloromethane and cyclohexane as the eluent, to yield the final product as a white solid **(0.59 g, 52%)**.

^{1}H NMR (400 MHz, $CDCl_3$): δ = 2.42 (s, 3H, Me), 7.11 (s, 1H, thiophene), 7.28 (m, 1H, J_{app} = 7.2 Hz, phenyl), 7.37 (m, 2H, J_{app} = 7.2 Hz, phenyl), 7.51 (d, 2H, J = 7.2 Hz, phenyl). **MS (ESI)**: m/z = 253.0 - 255.0 $[M+H]^+$.

1-(2-Methyl-5-(4-pyridyl)-3-thienyl)-2-(2-methyl-5-phenyl-3-thienyl)-perfluorocyclopentene (22, $L5^F$)

4-Bromo-5-methyl-2-(4-pyridyl)thiophene (1.0 g, 4.0 mmol) and 3-Bromo-2-methyl-5-phenylthiophene (1.0 g, 4.0 mmol) were suspended in anhydrous diethyl ether (20 mL) under a nitrogen atmosphere and treated dropwise with *n*-buthyllithium (5.2 mL of a 1.6 M solution in hexane, 8.3 mmol) at -78 °C. After stirring the resulting pale yellow suspension for 30 min, octafluorocyclopentene (2.7 mL of a 20% solution in anhydrous Et_2O, 4.0 mmol) was added and the reaction mixture was stirred for 1 h at -78 °C. The cooling bath was then removed and the stirring continued at room temperature for 3 h, after which dichloromethane (25 mL) and water (25 mL) were added. The organic layer was separated, washed with brine, dried (Na_2SO_4), filtered and concentrated under reduced pressure. The crude product was purified by column chromatography on silica gel with a 3:2 mixture of dichloromethane and ethyl acetate as the eluent, yielding the final product as a dark green solid **(0.51 g, 25%)**.

^{1}H NMR (400 MHz, $CDCl_3$): δ = 1.98-2.04 (2s, 6H, 2 Me), 7.26 (s_{app}, 2H, thiophene), 7.32 (m, 1H, J_{app} = 7.2 Hz, phenyl), 7.39 (m, 2H, J_{app} = 7.2 Hz, phenyl), 7.54 (d, 2H, J_{app} = 7.2 Hz, phenyl), 7.57 (d_{app}, 2H, J_{app} = 6.4 Hz, pyridine), 8.62 (d_{app}, 2H, J_{app} = 6.4 Hz, pyridine). **^{19}F NMR** (400 MHz, $CDCl_3$): δ = -131.85 (quint, 2H, J = 5.6 Hz), -110.24 (br, 2H), -109.91 (br, 2H). **MS (ESI)**: m/z = 522.1 $[M+H]^+$. **EA** calculated for $C_{26}H_{17}F_6NS_2$ (%): C 59.88, H 3.29, N 2.69, S 12.29; found: C 59.87, H 3.70, N 2.88, S 12.01.

[{*trans*-$PtCl_2$(DMSO)}$_2$(μ-$L1^H$)] ($C1^H$)

cis-[$PtCl_2(DMSO)_2$] (211 mg, 0.5 mmol) was suspended in methanol (40 mL), and the system was refluxed until the complex was completely dissolved. After hot filtering the resulting yellow solution to remove any Pt(0) impurities, ligand **$L1^H$** (104 mg, 0.25 mmol) was immediately added and the mixture was stirred in the dark at room temperature overnight, yielding a pale-green solid, which was filtered, washed with methanol and dried under reduced pressure **(260 mg, 94%)**.

^{1}H NMR (400 MHz, $CDCl_3$): δ = 2.03 (s, 6H, Me), 2.13 (m, 2H, J = 7.6 Hz, cyclopentene), 2.85 (t, 4H, J = 7.6 Hz, cyclopentene), 3.47 (s, 12H, DMSO), 7.28 (s, 2H, thiophene), 7.39

(m, 4H, J_{app} = 6.4 Hz, pyridine), 8.59 (m, 4H, J_{app} = 6.4 Hz, pyridine). **MS (ESI)**: m/z = 1123.9 $[M+Na]^+$. **EA** calculated for $C_{29}H_{34}Cl_4N_2O_2Pt_2S_4$ (%): C 31.58, H 3.11, N 2.54, S 11.63; found: C 31.11, H 3.09, N 2.52, S 11.53.

[{*trans*-$PtCl_2$(DMSO)}$_2$(μ-L1^F)] (C1^F)

Complex **C1^F** was prepared following the procedure described for the synthesis of **C1^H**, but using ligand **L1^F** (136 mg, 0.25 mmol) to obtain the corresponding product as an off-white solid **(295 mg, 95%)**.

^{1}H NMR (400 MHz, $CDCl_3$): δ = 2.03 (s, 6H, Me), 3.48 (s, 12H, DMSO), 7.50 (m, 4H, J_1 = 5.6 Hz, J_2 = 1.6 Hz, pyridine), 7.55 (s, 2H, thiophene), 8.71 (m, 4H, J_1 = 5.6 Hz, J_2 = 1.6 Hz, pyridine). **^{19}F NMR** (400 MHz, $CDCl_3$): δ = -131.78 (quint, 2H, J = 5.6 Hz), -110.10 (t, 4H, J = 5.6 Hz). **MS (ESI)**: m/z = 1231.9 $[M+Na]^+$. **EA** calculated for $C_{29}H_{28}Cl_4F_6N_2O_2Pt_2S_4$ (%): C 28.77, H 2.33, N 2.31, S 10.59; found: C 29.01, H 2.30, N 2.48, S 10.36.

[{*trans*-$PtCl_2$(DMSO)}$_2$(μ-L2^H)] (C2^H)

Complex **C2^H** was prepared following the procedure described for the synthesis of **C1^H** but using ligand **L2^H** (129 mg, 0.25 mmol) to obtain the corresponding product as a pale-green solid **(255 mg, 85%)**.

^{1}H NMR (400 MHz, $CDCl_3$): δ = 2.09 (s, 6H, Me), 2.17 (m, 2H, J = 7.6 Hz, cyclopentene), 2.93 (t, 4H, J = 7.6 Hz, cyclopentene), 3.47 (s, 12H, DMSO), 7.30 (s, 2H, thiophene), 7.65 (m, 2H, J_{app} = 7.6 Hz, quinoline), 7.82-7.88 (m, 4H, quinoline), 8.29 (d, 2H, J = 2.0 Hz, quinoline), 9.25 (d, 2H, J = 2.0 Hz, quinoline), 9.30 (d, 2H, J = 8.8 Hz, quinoline). **MS (ESI)**: m/z = 1224.0 $[M+Na]^+$. **EA** calculated for $C_{37}H_{38}Cl_4N_2O_2Pt_2S_4$ (%): C 36.94, H 3.18, N 2.33, S 10.66; found: C 36.44, H 3.18, N 2.35, S 10.11.

[{*trans*-$PtCl_2$(DMSO)}$_2$(μ-L2^F)] (C2^F)

Complex **C2^F** was prepared following the procedure described for the synthesis of **C1^H**, but using ligand **L2^F** (156 mg, 0.25 mmol) to obtain the corresponding product as an off-white solid **(260 mg, 79%)**.

^{1}H NMR (400 MHz, $CDCl_3$): δ = 2.12 (s, 6H, Me), 3.52 (s, 12H, DMSO), 7.51 (s, 2H, thiophene), 7.71 (m, 2H, J_{app} = 7.6 Hz, quinoline), 7.89-7.93 (m, 4H, quinoline), 8.39 (d, 2H, J = 2.0 Hz, quinoline), 9.27 (d, 2H, J = 2.0 Hz, quinoline), 9.37 (d, 2H, J = 9.2 Hz, quinoline). **^{19}F NMR** (400 MHz, $CDCl_3$): δ = -131.84 (quint, 2H, J = 5.6 Hz), -109.87 (t, 4H, J = 5.6 Hz). **MS (ESI)**: m/z = 1331.9 $[M+Na]^+$. **EA** calculated for $C_{37}H_{32}Cl_4F_6N_2O_2Pt_2S_4$ (%): C 33.90, H 2.46, N 2.14, S 9.78; found: C 33.86, H 2.47, N 2.33, S 9.64.

[{*trans*-$PtCl_2$(DMSO)}$_2$(μ-L3^H)] (C3^H)

Complex **C3^H** was prepared following the procedure described for the synthesis of **C1^H**, but using ligand **L3^H** (111 mg, 0.25 mmol) to obtain the corresponding product as an off-white solid **(235 mg, 83%)**.

^{1}H NMR (400 MHz, $CDCl_3$): δ = 2.02 (s, 6H, Me), 2.11 (m, 2H, J = 7.6 Hz, cyclopentene), 2.38 (s, 6H, Me), 2.84 (t, 4H, J = 7.6 Hz, cyclopentene), 3.46 (s, 12H, DMSO), 7.10 (s, 2H, thiophene), 7.66 (s, 2H, pyridine), 8.35 (s, 2H, pyridine), 8.66 (d, 2H, J = 1.6 Hz, pyridine). **MS (ESI)**: m/z = 1154.0 $[M+H]^+$. **EA** calculated for $C_{31}H_{38}Cl_4N_2O_2Pt_2S_4$ (%): C 32.93, H 3.39, N 2.48, S 11.34; found: C 33.03, H 3.64, N 2.62, S 11.12.

[{*trans*-$PtCl_2$(DMSO)}$_2$(μ-L4^H)] (C4^H)

Complex **C4^H** was prepared following the procedure described for the synthesis of **C1^H**, but using ligand **L4^H** (105 mg, 0.25 mmol) to obtain the corresponding product as an off-white solid **(205 mg, 74%)**.

^{1}H NMR (400 MHz, $CDCl_3$): δ = 2.12 (m, 2H, cyclopentene), 2.23 (s, 6H, Me), 2.89 (t, 4H, cyclopentene), 3.33 (s, 12H, DMSO), 3.68 (s, 6H, N-Me), 6.95 (d, 2H, J = 1.2 Hz, imidazole), 7.15 (d, 2H, J = 1.2 Hz, imidazole), 7.25 (s, 2H, thiophene). **MS (ESI)**: m/z = 1107 $[M+H]^+$. **EA** calculated for $C_{27}H_{36}Cl_4N_4O_2Pt_2S_4$ (%): C 29.25, H 3.27, N 5.05, S 11.57; found: C 29.21, H 3.37, N 5.04, S 11.69.

trans-[$PtCl_2$(DMSO)(L5^H)] (C5^H)

Complex **C5^H** was prepared following the procedure described for the synthesis of **C1^H**,

but using equimolar amounts of *cis*-[$PtCl_2(dmso)_2$] (105 mg, 0.25 mmol) and ligand **L5^H** (103 mg, 0.25 mmol) to obtain the corresponding mononuclear product as a dark green solid **(80 mg, 42%)**.

^{1}H NMR (400 MHz, $CDCl_3$): δ = 1.97 (s, 3H, Me), 2.07 (s, 3H, Me), 2.11 (m, 2H, 7.6 Hz, cyclopentene), 2.84 (m, 4H, cyclopentene), 3.47 (s, 6H, DMSO), 6.99 (s, 1H, thiophene), 7.24 (m, 1H, J_1 = 7.6 Hz, J_2 = 1.2 Hz, phenyl), 7.31 (s, 1H, thiophene), 7.34 (m, 2H, J_{app} = 7.6 Hz, phenyl), 7.39 (m, 2H, J_1 = 5.6 Hz, J_2 = 1.6 Hz, pyridine), 7.48 (m, 2H, J_{app} = 7.6 Hz, phenyl), 8.56 (m, 2H, J_1 = 5.6 Hz, J_2 = 1.6 Hz, pyridine). **MS (ESI)**: m/z = 780.0 $[M+H]^+$. **EA** calculated for $C_{28}H_{29}Cl_2NOPtS_3$ (%): C 44.38, H 3.86, N 1.85, S 12.69; found: C 43.28, H 3.94, N 2.04, S 12.46.

2.4. References

(1) Irie, M. *Chem. Rev.* **2000**, *100* (5), 1685–1716.

(2) Feringa, B. L. *Molecular Switches*; Wiley-VCH: Darmstadt, 2001.

(3) Hanazawa, M.; Sumiya, R.; Horikawa, Y.; Irie, M. *J. Chem. Soc. Chem. Commun.* **1992**, No. 3, 206–207.

(4) Dixon, S. *J. Org. Chem.* **1956**, *21* (4), 400–403.

(5) Szalõki, G.; Pozzo, J. L. *Chem. Eur. J.* **2013**, *19* (34), 11124–11132.

(6) Lucas, L. N.; van Esch, J. H.; Kellogg, R. M.; Feringa, B. L. *Chem. Commun.* **1998**, *3* (21), 2313–2314.

(7) Higashiguchi, K.; Matsuda, K.; Kobatake, S.; Yamada, T.; Kawai, T.; Irie, M. *Bull. Chem. Soc. Jpn.* **2000**, *73* (10), 2389–2394.

(8) Krayushkin, M. M.; Kalik, M. A.; Migulin, V. A. *Russ. Chem. Rev.* **2009**, *78* (4), 329–336.

(9) Ephritikhine, M. *Chem. Commun.* **1998**, No. 23, 2549–2554.

(10) Guirado, G.; Coudret, C.; Hliwa, M.; Launay, J.-P. *J. Phys. Chem. B* **2005**, *109* (37), 17445–17459.

(11) Sevez, G.; Pozzo, J.-L. *Dye. Pigment.* **2011**, *89* (3), 246–253.

(12) Sud, D.; McDonald, R.; Branda, N. R. *Inorg. Chem.* **2005**, *44* (17), 5960–5962.

(13) Li, Z.; Yin, J.; Wu, X.; Lin, Y.; Zeng, Q.; Fan, F.; Liu, S. H. *J. Photochem. Photobiol. A* **2011**, *218* (2–3), 192–198.

(14) Pu, S.; Tang, H.; Chen, B.; Xu, J.; Huang, W. *Mater. Lett.* **2006**, *60* (29–30), 3553–3557.

(15) Miyaura, N.; Yamada, K.; Suzuki, A. *Tetrahedron Lett.* **1979**, *20* (36), 3437–3440.

(16) Carey, J. S.; Laffan, D.; Thomson, C.; Williams, M. T. *Org. Biomol. Chem.* **2006**, *4* (12), 2337.

(17) Suzuki, A. *J. Organomet. Chem.* **1999**, *576* (1–2), 147–168.

(18) Badone, D.; Baroni, M.; Cardamone, R.; Ielmini, A.; Guzzi, U. *J. Org. Chem.* **1997**, *62* (c), 7170–7173.

(19) Amatore, C.; Jutand, A.; Le Duc, G. *Chem. Eur. J.* **2011**, *17* (8), 2492–2503.

(20) Torborg, C.; Beller, M. *Adv. Synth. Catal.* **2009**, *351* (18), 3027–3043.

(21) Nicolaou, K. C.; Bulger, P. G.; Sarlah, D. *Angew. Chem. Int. Ed.* **2005**, *44* (29), 4442–4489.

(22) de Jong, J. J. D.; Lucas, L. N.; Hania, R.; Pugzlys, A.; Kellogg, R. M.; Feringa, B. L.; Duppen, K.; van Esch, J. H. *Eur. J. Org. Chem.* **2003**, 1887–1893.

(23) Weidner, T.; Baio, J.; Seibel, J.; Siemeling, U. *Dalton Trans.* **2012**, *41* (5), 1553.

(24) Yagai, S.; Ohta, K.; Gushiken, M.; Iwai, K.; Asano, A.; Seki, S.; Kikkawa, Y.; Morimoto, M.; Kitamura, A.; Karatsu, T. *Chem. Eur. J.* **2012**, *18* (8), 2244–2253.

(25) Smith, G. B.; Dezeny, G. C.; Hughes, D. L.; King, A. O.; Verhoeven, T. R. *J. Org. Chem.* **1994**, *59* (26), 8151–8156.

(26) Boyer, J. C.; Carling, C. J.; Chua, S. Y.; Wilson, D.; Johnsen, B.; Baillie, D.; Branda, N. R. *Chem. Eur. J.* **2012**, *18* (11), 3122–3126.

(27) Qin, B.; Yao, R.; Zhao, X.; Tian, H. *Org. Biomol. Chem.* **2003**, *1* (12), 2187–2191.

(28) Tsivgoulis, G. M.; Lehn, J. M. *Chem. Eur. J.* **1996**, *2* (11), 1399–1406.

(29) van Leeuwen, T.; Pijper, T. C.; Areephong, J.; Feringa, B. L.; Browne, W. R.; Katsonis, N. *J. Mater. Chem.* **2011**, *21* (9), 3142–3146.

(30) Hermes, S.; Dassa, G.; Toso, G.; Bianco, A.; Bertarelli, C.; Zerbi, G. *Tetrahedron Lett.* **2009**, *50* (14), 1614–1617.

(31) Lucas, L. N.; Jong, J. J.; Esch, J. H.; Kellogg, R. M.; Feringa, B. L. *Eur. J. Org. Chem.* **2003**, *2003*, 155–166.

(32) Xiao, S.; Zou, Y.; Yu, M.; Yi, T.; Zhou, Y.; Li, F.; Huang, C. *Chem. Commun. (Camb).* **2007**, No. 45, 4758–4760.

(33) Matsuda, K.; Shinkai, Y.; Irie, M. *Inorg. Chem.* **2004**, *43* (13), 3774–3776.

(34) Matsuda, K.; Shinkai, Y.; Yamaguchi, T.; Nomiyama, K.; Isayama, M.; Irie, M. *Chem. Lett.* **2003**, *32* (12), 1178–1179.

(35) Price, J. H.; Williamson, A. N.; Schramm, R. F.; Wayland, B. B. *Inorg. Chem.* **1972**, *11* (6), 1280–1284.

(36) Farrell, N.; Kiley, D. M.; Schmidt, W.; Hacker, M. P. *Inorg. Chem.* **1990**, *29* (3), 397–403.

(37) Marqués-Gallego, P.; Den Dulk, H.; Brouwer, J.; Kooijman, H.; Spek, A. L.; Roubeau, O.; Teat, S. J.; Reedijk, J. *Inorg. Chem.* **2008**, *47* (23), 11171–11179.

(38) Fuks, L.; Samochocka, K.; Anulewicz-Ostrowska, R.; Kruszewski, M.; Priebe, W.; Lewandowski, W. *Eur. J. Med. Chem.* **2003**, *38* (7–8), 775–780.

(39) Leijen, S.; Burgers, S. A.; Baas, P.; Pluim, D.; Tibben, M.; Van Werkhoven, E.; Alessio, E.; Sava, G.; Beijnen, J. H.; Schellens, J. H. M. *Invest. New Drugs* **2015**, *33* (1), 201–214.

(40) Bitzer, R. S.; Nascimento, M. A. C.; Filgueiras, C. A. L. *Polyhedron* **2015**, *102*, 329–336.

(41) Del Solar, V.; Quiñones-Lombraña, A.; Cabrera, S.; Padrón, J. M.; Ríos-Luci, C.; Alvarez-Valdés, A.; Navarro-Ranninger, C.; Alemán, J. *J. Inorg. Biochem.* **2013**, *127*, 128–140.

(42) Tomé, M.; López, C.; González, A.; Ozay, B.; Quirante, J.; Font-Bardía, M.; Calvet, T.; Calvis, C.; Messeguer, R.; Baldomé, L.; Badía, J. *J. Mol. Struct.* **2013**, *1048*, 88–97.

(43) Stepanenko, I. N.; Cebrián-Losantos, B.; Arion, V. B.; Krokhin, A. A.; Nazarov, A. A.; Keppler, B. K. *Eur. J. Inorg. Chem.* **2007**, *2* (3), 400–411.

(44) Lo, W. K. C.; Huff, G. S.; Cubanski, J. R.; Kennedy, A. D. W.; McAdam, C. J.; McMorran, D. A.; Gordon, K. C.; Crowley, J. D. *Inorg. Chem.* **2015**, *54* (4), 1572–1587.

(45) Martín Santos, C.; Cabrera, S.; Ríos-Luci, C.; Padrón, J. M.; López Solera, I.; Quiroga, A. G.; Medrano, M. A.; Navarro-Ranninger, C.; Alemán, J. *Dalton Trans.* **2013**, *42* (37), 13343–13348.

CHAPTER 3

Spectroscopic, structural and computational analyses

3.1. Photochromic properties

Given its crucial importance towards their potential application in photoactivated chemotherapy, the photochromic behavior of all the synthesized ligands and metal complexes, namely their capacity to undergo reversible photocyclization, was thoroughly studied by irradiation with a xenon light source at selected wavelength ranges. The resulting photochemical reactions were monitored by means of UV-Vis and ^{1}H NMR spectroscopies.

The UV-Vis absorption of a 20 μM solution of ligand **L1^{H}** in dichloromethane was firstly studied. As expected for this kind of molecular switch, the starting open form of the ligand exhibits intense absorption bands in the UV region of the spectrum, centered around λ_{max1} = 286 nm and λ_{max2} = 322 nm. This latter absorption corresponds to the HOMO→LUMO transition that, according to the Woodward-Hoffmann rules, is required for the photocyclization process to occur.[1] Thus, the irradiation of the system with UV light (λ < 365 nm) led to the apparition of an increasingly intense new absorption band in the visible region of the spectrum, located around λ_{max} = 544 nm, indicative of the formation of the more conjugated closed-ring species. This photochemical transformation was accompanied by a clear color change of the solution, turning from colorless to deep purple, and proceeded until a photostationary

state (PSS) was reached after a few minutes of UV light exposure. As previously discussed (see Chapter 1), this PSS corresponds to the final equilibrium situation of the photocyclization reaction and, although complete photoconversion is rarely achieved, it is generally assumed to represent the closed form of the molecular switch.[2] A summary of these spectral changes is shown in Figure 3.1, which depicts the absorption spectra of both the open form and the PSS of **L1^{H}** in organic solvent.

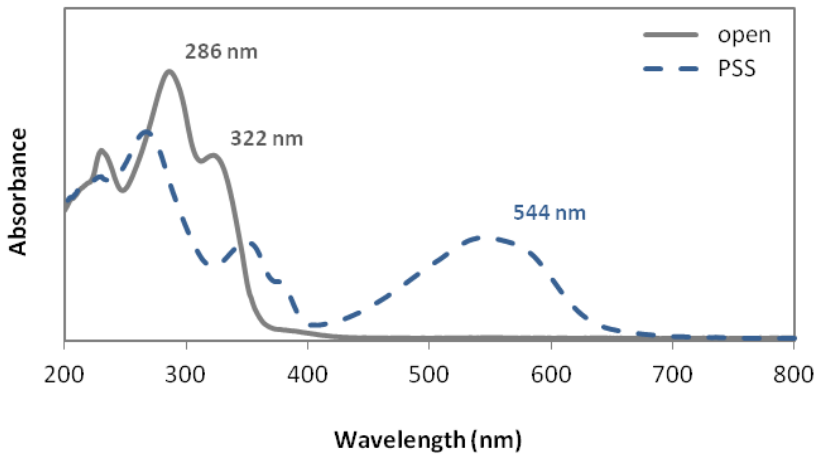

Figure 3.1. *Absorption spectral changes of a CH_2Cl_2 solution of ligand **L1^{H}** before (solid line) and after (dashed line) photoirradiation at λ < 365 nm*.

While the closed isomer remained in this state if kept in the dark at room temperature for several days, irradiation with visible light (λ > 425 nm) produced a progressive bleaching of the colored solution as well as the full recovery of the original absorption spectrum, corresponding to the open form of the ligand. This process, however, took a noticeably longer time than the photocyclization reaction, in agreement with the well-known lower quantum yield of such ring-opening reactions.[3] Additionally, despite its lesser relevance towards potential biological applications, the fatigue resistance of the system was briefly assessed by performing up to five consecutive coloring/bleaching cycles, after which no significant spectral changes were detected.

Analogous studies with the rest of the photochromic ligands prepared produced similar results. All the open-ring systems display strong absorption bands in the UV region, the less energetic one corresponding to the photoreactive HOMO→LUMO

transition. In contrast, the closed isomers present characteristic visible absorption bands within the 525-600 nm range, which confer them purple or blue colorations. The UV-Vis absorption data for all the studied systems, including the position and intensity of all the relevant bands, are summarized in Table 3.1.

Some interesting trends can be noticed by comparing the position of the photoreactive bands of the perfluorinated and hydrogenated switches bearing identical functional groups, as a result of the different electronic density of the central double bond. The HOMO→LUMO transition of the open form of compounds **L1^{F}**, **L2^{F}** and **L5^{F}** is systematically located at shorter wavelengths with respect to that of their corresponding non-fluorinated counterparts, with a hypsochromic shift of about 20-30 nm. For the closed species, this trend is inverted and a significant bathochromic shift is observed for the perfluoro compounds, amounting to 40-60 nm. Such results are in agreement with those obtained by Feringa and co-workers in their comparative studies between hydrogenated and perfluorinated dithienylcyclopentenes,[4] and hence indicate that the photochemical reaction window of these molecules can indeed be tuned to some extent through chemical modification of the central ring. Since light-penetration depth in living tissues is highly dependent on the wavelength of the incident radiation,[5] such considerations may thus be of paramount importance for forthcoming investigations, when the fine tuning of other DTC-based ligands for specific biological applications will be eventually undertaken.

Ligand **L4^{H}** stands out as a striking exception among the studied systems, due to its apparent lack of photoreactivity. Contrary to what was observed for all other molecules, prolonged irradiation of a dichloromethane solution of this methylimidazole-containing compound only produced very minor coloration and spectral changes, hence indicating that its photoisomerization is seemingly hindered. Further investigation of the properties of this peculiar system was specifically addressed on account of these observations.

The photochemical transformation of all these molecules, as well as the unexpected behavior of ligand **L4^{H}**, was subsequently monitored by means of ^{1}H NMR spectroscopy. For instance, a series of ^{1}H NMR spectra of a $CDCl_3$ solution of ligand **L1^{F}** after different photoirradiation times is illustrated in Figure 3.2. In this way, the

Table 3.1. *UV-Vis absorption λ_{max} (nm) and ε (10^3 M^{-1} cm^{-1}) values for all the photochromic ligands in CH_2Cl_2 solutions. The photoreactive transitions are indicated in bold; shoulder peaks are noted with [s].*

Ligand	λ_{max} and ε, open form	λ_{max} and ε, PSS
$L1^H$	230 (21.5), 286 (30.4), **322** (20.9)	267 (23.6), 346 (11.0), 353 (10.9), **544** (11.6)
$L1^F$	277 (32.7), **303** (36.7)	274 (28.3), 299 (25.7), 377 (7.7), **593** (10.1)
$L2^H$	229 (54.5), 275 (50.9), **353** (23.4)	229 (44.8), 266 (43.2), 309 (31.5), **558** (25.4)
$L2^F$	229 (29.7), 273 (36.4), **320** (23.9)	230 (33.6), 275 (21.0), 335 (23.6), **600** (12.3)
$L3^H$	229 (24.2), 278 (29.1), **312** (23.0)	229 (24.6), 273 (24.4), **526** (12.4)
$L4^H$	250 (23.3), 283 (31.0), ca. **310**$_{[s]}$ (24.4)	309 (24.6), **518** (6.8)
$L5^H$	230 (21.9), 282 (29.6), ca. **325**$_{[s]}$ (16.9)	229 (18.9), 269 (21.8), 340 (11.0), **532** (9.4)
$L5^F$	**294** (34.1)	277 (23.8), 303 (23.6), 375 (8.0), **595** (10.8)
$L6^H$	241 (42.8), 281 (46.2), **332** (31.7)	241 (42.8), 278 (39.4), 377 (19.1), **566** (19.5)

photoisomerization of the ligand upon UV light exposure was easily followed via the gradual disappearance of the original NMR signals, which was concomitantly accompanied by the progressive apparition of a new set of peaks ascribed to the closed-ring species. The occurrence of the expected electrocyclic reaction was corroborated by the observed upfield shift of the proton at the 4-position of the thiophene ring, from 7.47 to 6.85 ppm. This is indicative of the loss of aromaticity

caused by the progressive formation of the new intramolecular bond at the proximal 2-position. This transformation continued until the PSS was reached; after 5 minutes of light exposure, no further variation of the peaks was observed, and in the resulting equilibrium situation, a photoconversion ratio of 0.86 could be directly determined from the relative intensity of the two sets of signals.

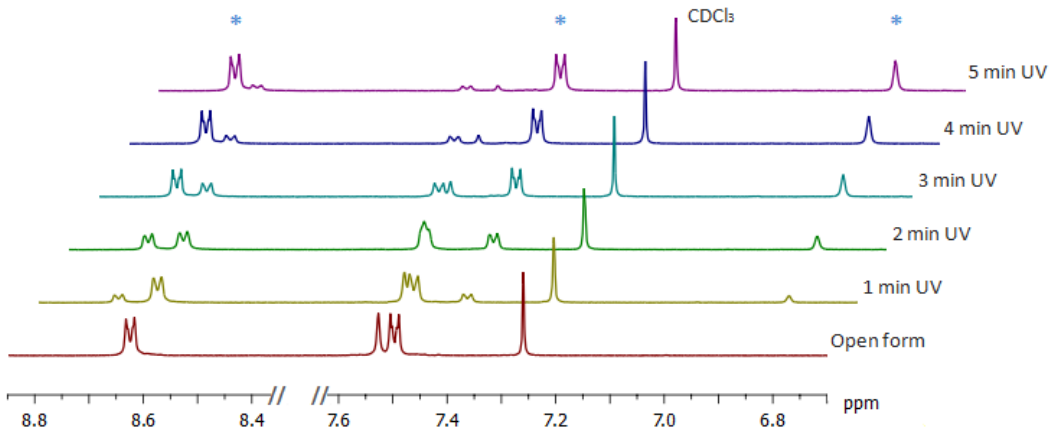

Figure 3.2. *^{1}H NMR spectra of a $CDCl_3$ solution of **L1^{F}** before (red) and after different photoirradiation times at λ < 365 nm. Signals corresponding to the closed isomer are indicated with blue asterisks.*

^{1}H NMR spectroscopy measurements conducted with the rest of the photoswitches produced, with the notable exception of ligand **L4^{H}**, similar results that are summarized in Table 3.2. For these systems, a stable PSS was also reached within 5 minutes of UV light irradiation, and although ligand **L2^{F}** showed a particularly lower ring-closing efficiency, high photoconversion rates were generally obtained. Furthermore, in addition to the quite remarkable upfield shift of the thiophene signal that was observed for all closed species (as discussed for **L1^{F}**), a substantial modification of the methyl signal was also noted for —and only for— all perfluorinated ligands upon ring-closure. A downfield shift of the CH_3 singlet, of about 0.2 ppm, was systematically observed in these cases; this fact evidences a stronger electron-withdrawing inductive effect of the fluorine substituents over the methyl groups in the closed species, most likely arising from the more effective electronic conjugation of these photoisomers.

In contrast, experiments carried out with the methylimidazolic ligand **L4^{H}** were consistent with the previously obtained UV-Vis absorption data, and disclosed an almost entire lack of photochromic behavior; even after extended photoirradiation times, less than 10% of the starting compound could be converted into its closed isomer. Considering that the underlying cause of this anomalous performance could have a remarkable impact on the future design of similar molecules for biological applications, the distinct properties of this system were then further investigated computationally. The results obtained in this theoretical study are fully discussed at the end of this chapter.

After successfully completing the photochromic characterization of the series of ligands, equivalent studies were subsequently performed with all the platinum complexes, with the aim of assessing any potential alterations of the photochemical properties of these systems induced by the coordination to the metal centers.

Table 3.2. *Characteristic ^{1}H NMR chemical shifts of the open and closed forms of the studied ligands in $CDCl_3$, and maximum photoconversion efficiency.*

Ligand	Conversion	δCH$_3$ open	δ CH open	δCH$_3$ closed	δCH closed
L1^{H}	0.82	2.03	7.22	2.02	6.61
L1^{F}	0.86	2.00	7.47	2.22	6.85
L2^{H}	0.74	2.10	7.23	2.09	6.69
L2^{F}	0.42	2.08	7.47	2.27	6.92
L3^{H}	> 0.95	2.02	7.05	2.02	6.62
L4^{H}	0.09	2.10	6.96	2.10	6.36
L5^{H}	0.78	1.99, 2.07	7.01, 7.29	2.03	6.42, 6.69
L5^{F}	0.88	1.98, 2.04	7.26	2.21	6.71, 6.88
L6^{H}	0.84	2.07	7.41	2.12	6.84

As an illustration, Figure 3.3 shows the UV-Vis absorption spectra of the open form and the PSS of a dichloromethane solution of complex **C1^{H}**. Akin to the corresponding free ligand, **C1^{H}** exhibited strong UV absorption in the form of two major bands located at λ_{max1} = 312 nm and λ_{max2} = 359 nm, the latter one corresponding to the photoreactive HOMO→LUMO transition. Irradiation with UV light (λ < 365 nm) produced the immediate formation of the closed form of the complex, which presented a characteristic absorption in the visible region of the spectrum, around λ_{max} = 624 nm. As observed for its metal-free counterpart, an intense color change of the solution accompanied the photochemical reaction of the complex, whereas subsequent irradiation with visible light (λ < 425 nm) produced its bleaching and the full recovery of the original absorption spectrum.

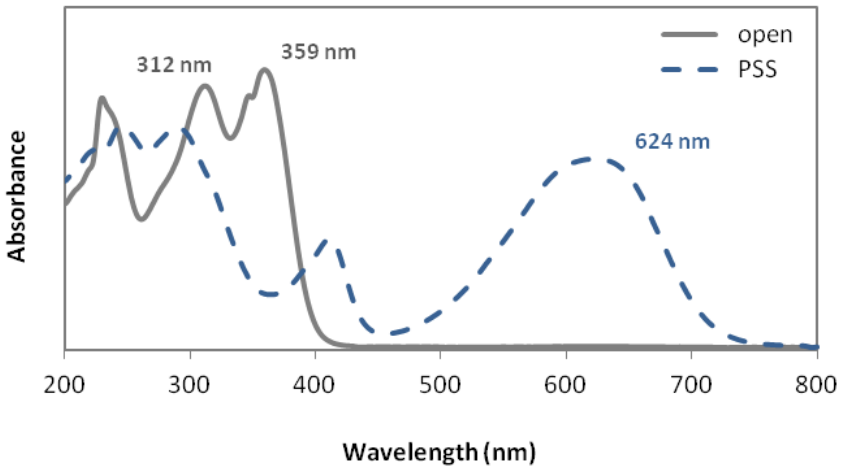

Figure 3.3. *Absorption spectral changes of a CH_2Cl_2 solution of complex **C1^{H}** before (solid line) and after (dashed line) photoirradiation at λ < 365 nm.*

In addition, the complementary ^{1}H NMR spectroscopy measurements revealed that the photochromic performance of **C1^{H}** is in fact more efficient than that of ligand **L1^{H}**. Less than 3 minutes of UV light irradiation were in this case sufficient to attain the PSS of the system, hence implying a higher quantum yield for the photocyclization reaction of the metal complex. Furthermore, an almost quantitative photoconversion into the closed species was achieved, in contrast with the 0.82 conversion ratio displayed by the free ligand.

Table 3.3. *UV-Vis absorption λ_{max} (nm) and ε (10^3 M^{-1} cm^{-1}) values for all photochromic platinum(II) complexes in CH_2Cl_2 solutions. The photoreactive transitions are indicated in bold; shoulder peaks are noted with [s].*

Complex	λ_{max} and ε, open form	λ_{max} and ε, PSS
C1^{H}	230 (40.5), 312 (42.5), **359** (45.1)	245 (36.0), 289 (35.8), 411 (17.8), **624** (30.6)
C1^{F}	230 (29.2), 275 (29.8), **332** (64.1)	229 (31.1), 283 (33.3), 399 (13.9), **627** (19.6)
C2^{H}	233 (69.8), 294 (49.5), **380** (16.1)	230 (58.5), 276 (49.1), 375 (14.6), **591** (26.9)
C2^{F}	232 (61.1), 275 (61.4), **359** (21.9)	232 (62.5), 288 (45.4), $330_{[s]}$ (36.3), **610** (20.1)
C3^{H}	231 (41.4), 286 (37.9), **334** (23.0)	231 (48.2), 276 (35.1), 364 (13.0), **559** (21.8)
C4^{H}	230 (35.8), 249 (31.4), 275 (33.2)	n/a
C5^{H}	232 (31.0), 301 (32.0), **358** (20.2)	239 (26.9), 284 (31.4), 391 (14.2), **604** (23.0)

With the exception of complex **C4^{H}**, which was obtained from the non-switching ligand **L4^{H}** and turned out to be completely photoinactive, such an enhanced photochromic performance was also displayed by all other platinum complexes. Higher ring-closing reaction times and efficiencies, compared to those of the corresponding free ligands, were achieved for all the systems, including a two-fold photoconversion rate improvement for the perfluorinated, quinoline-bearing complex **C2^{F}** (see Tables 3.2 and 3.4). Furthermore, it is worth noting that the ring-closing reaction was in all cases a clean process; no additional signals (which would be indicative of the formation of undesired species) were detected after irradiation of all complexes, other than those corresponding to the photocyclization products. All these promising results contrast

with those of previous reports on similar DTC-based N-donor systems coordinated to various transition metals such as ruthenium, iron or copper, whose photochromic performance was affected or even inactivated upon metal binding.[6,7] Accordingly, platinum(II) coordination appears to be a more promising synthetic approach for the preparation of novel photoactivatable metallodrugs incorporating this kind of molecular devices.

Given the intended biological application of these transition-metal systems, their photochromic performance was also evaluated in buffered aqueous media containing small amounts of DMSO, which was needed for the complete solubilization of all compounds. Absorption data obtained under these conditions, summarized in Table 3.5, show a general decrease of the absorbance of all the metal complexes, compared to that displayed in organic solution. Regarding the position of the photoreactive bands, no major differences were noted for the open isomers, with the exception of a slight shift towards higher energies of the ring-closing transition of the quinoline-bearing complexes **C2^{H}** and **C2^{F}**. For the closed isomers, in contrast, a hypsochromic displacement of the ring-opening band, of about 15-40 nm, was systematically

Table 3.4. *Characteristic ^{1}H NMR chemical shifts of the open and closed forms of the studied platinum(II) complexes in $CDCl_3$, and maximum photoconversion efficiency.*

Complex	Conversion	δCH$_3$ open	δCH open	δCH$_3$ closed	δCH closed
C1^{H}	> 0.95	2.03	7.28	2.01	6.67
C1^{F}	0.84	2.03	7.55	2.22	6.89
C2^{H}	> 0.95	2.09	7.30	2.06	6.74
C2^{F}	0.82	2.12	7.51	2.27	6.97
C3^{H}	> 0.95	2.02	7.10	1.99	6.50
C4^{H}	n/a	2.23	7.25	n/a	n/a
C5^{H}	0.82	1.97, 2.07	6.99, 7.31	2.01, 2.02	6.41, 6.69

Table 3.5. *UV-Vis absorption λ_{max} (nm) and ε (10^3 M^{-1} cm^{-1}) values for all photochromic platinum(II) complexes in aqueous solution. Photoreactive transitions are indicated in bold; shoulder peaks are noted with [s].*

Complex	λ_{max} and ε, open form	λ_{max} and ε, PSS
C1^{H}	238 (25.2), 314 (23.6), **358** (19.5)	239 (23.5), 280 (21.3), 404 (9.0), **601** (15.3)
C1^{F}	237 (22.9), 279 (24.4), **325** (30.3)	237 (22.8), 277 (23.6), 393 (9.0), **608** (12.0)
C2^{H}	238 (45.1), 273 (38.0), **357** (14.6)	238 (43.0), 307 (23.0), 363 (10.8), **559** (15.8)
C2^{F}	237 (36.6), 271 (41.8), **315** (24.7)	238 (42.0), 335 (24.9), **597** (14.5)
C3^{H}	238 (28.3), 280 (24.2), ca. **335**$_{[s]}$ (13.1)	238 (27.4), 274 (21.9), 365 (9.7), **545** (13.3)
C4^{H}	238 (24.4), 274 (25.9)	n/a
C5^{H}	237 (23.3), 283 (23.8), ca. **360**$_{[s]}$ (8.8)	238 (19.7), 278 (20.3), 378 (9.3), **568** (12.1)

observed. Most importantly, the previously noted differences in the photoreactive band positioning between perfluorinated and hydrogenated switches remained unaltered in buffered aqueous media. Hence, this interesting structure-activity outcome may be of particular use for the future spectral tuning of biologically relevant DTC-based metal complexes.

Finally, the photocyclization of the complexes in pure dimethylsulfoxide solutions was also briefly assayed, obtaining photoconversion rates and optimal irradiation times comparable to those obtained in other organic solvents. This was examined in view of their subsequent evaluation in a series of biological interaction studies, requiring their solubilization in aqueous media from DMSO stock solutions.

3.2. Crystallographic analysis

In addition to common spectroscopic and spectrometric characterization, the crystal structure of some of the synthesized metal complexes could be determined by means of single-crystal X-ray diffraction measurements (see experimental section for details). The data obtained corroborated the proposed structure for all compounds, and in particular the *trans* disposition of the anionic chlorido ligands coordinated to each platinum(II) center.

3.2.1. Crystal structure of open complex C1^{F}

Single crystals of the open form of complex **C1^{F}**, suitable for X-ray diffraction studies, were obtained by slow evaporation of a concentrated dimethylsulfoxide solution. A representation of the molecular structure of this compound is depicted in Figure 3.4; crystallographic data and selected bond lengths and angle values are listed in Tables 3.6 and 3.7, respectively.

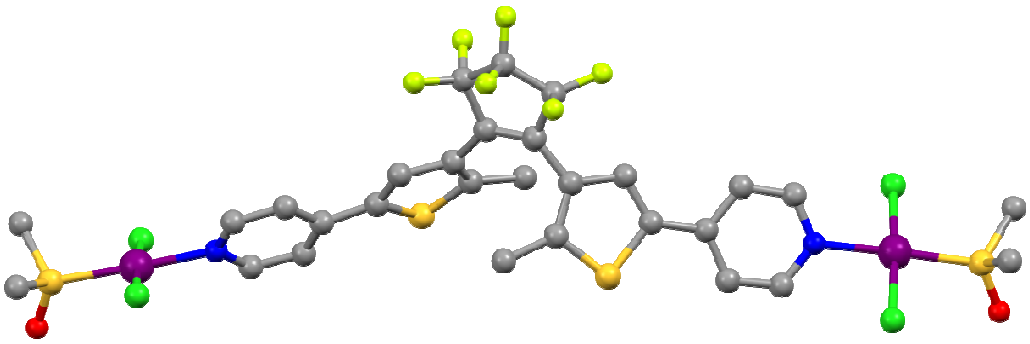

Figure 3.4. *Crystal structure of the open form of complex **C1^{F}**. Hydrogen atoms are omitted for clarity.*

As expected, **C1^{F}** is a dinuclear platinum(II) complex, with two symmetry-related metal centers exhibiting a slightly distorted square-planar geometry. The coordination sphere of these platinum centers is composed of two chlorido ligands in *trans*

disposition, a dimethylsulfoxide molecule bound through its sulfur atom and one of the pyridine residues of the bridging photochromic ligand. The slight distortion of each of these square planes is evidenced by the unequal values of the Cl–Pt–S angles, which amount to ca. 94 and 88 degrees, and most likely arises from steric hindrance induced by the methyl groups of the DMSO ligand.

The extended conjugation of the system is illustrated by the high coplanarity of the thiophene and pyridine rings, which exhibit a relative torsion angle of approximately 4 degrees. The pyridine moieties are not orientated in a fully perpendicular disposition with respect to the square-planar coordination plane, as would be expected for minimal repulsion; instead, the corresponding torsion angle amounts to ca. 48 degrees, most likely as a result of the numerous short-contact interactions with vicinal molecules. Regarding the tridimensional crystal packing, no significant high-order structuring can be noted.

Table 3.6. *Selected data for the crystal structure of the open form of complex* ***C1^F***.

Open complex C1^F	
Crystal data	
Formula	$C_{29}H_{28}Cl_4F_6N_2O_2Pt_2S_4$
Fw (g mol^{-1})	1210.75
Crystal system, space group	Orthorhombic, Pbcn
a, b, c (Å)	26.845(1), 8.8724(4), 15.5304(6)
α, β, γ (°)	90, 90, 90
V (Å^3)	3699.0(3)
Z	4
μ (mm^{-1})	8.132
Data collection and refinement	
Temperature (K)	100
T_{min}, T_{max}	0.49, 0.75
No. of measured, independent and observed [I > 2σ(I)] reflections	23958, 5628, 4072
R[I > 2σ(I)], wR(I), *S*	0.0439, 0.1204, 1.044
No. of parameters	252

Table 3.7. *Selected structural parameters for the crystal structure of the open form of complex* ***C1***^{F}.

Bond distances (Å)		Angle values (degrees)	
$Pt_1—Cl_1$ $Pt_2—Cl_3$	2.305(2)	$Cl_1—Pt_1—N_1$ $Cl_3—Pt_2—N_2$	88.38(1)
$Pt_1—Cl_2$ $Pt_2—Cl_4$	2.306(2)	$Cl_1—Pt_1—S_1$ $Cl_3—Pt_2—S_2$	94.23(6)
$Pt_1—N_1$ $Pt_2—N_2$	2.061(5)	$Cl_2—Pt_1—N_1$ $Cl_4—Pt_2—N_2$	89.05(1)
$Pt_1—S_1$ $Pt_2—S_2$	2.219(2)	$Cl_2—Pt_1—S_1$ $Cl_4—Pt_2—S_2$	88.36(6)

3.2.2. Crystal structure of open and closed complex C2^{H}

Single crystals of complex **C2**^{H}, suitable for X-ray diffraction measurements, were obtained by slow diffusion of diethyl ether into a concentrated solution of the complex in dichloromethane. Interestingly, the structural resolution revealed that the crystals obtained were composed of a mixture of the open and closed isomers of the compound, both being depicted in Figure 3.5. Crystallographic data and selected structural parameters, obtained as mean values for both isomers, are listed in Tables 3.8 and 3.9, respectively.

C2^{H} is also a dinuclear platinum(II) complex containing two slightly distorted square-planar metal centers, with chemical connectivity and structural parameters analogous to those of complex **C1**^{F}. The enhanced electronic delocalization along the extended conjugated system is again evidenced by the low torsion angles between the thiophene and the quinoline moieties, which amount to ca. 10 degrees. The almost completely parallel relative disposition of the quinoline planes at each side of the bridging ligand is another significant feature of the crystal structure of this complex, since it accounts for effective π–π stacking between adjacent molecules. As shown in

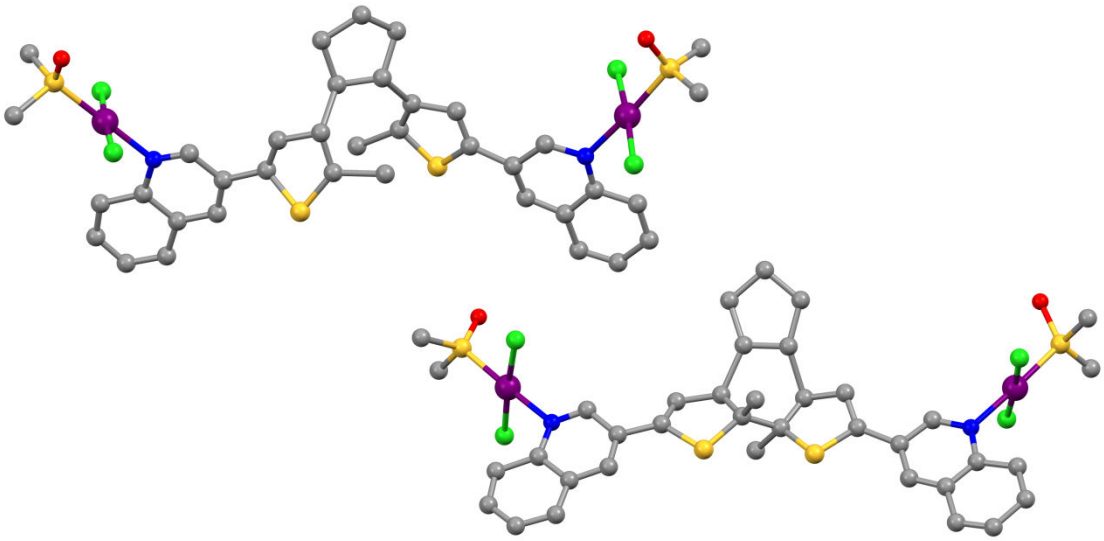

Figure 3.5. *Crystal structure of the open (top) and closed (bottom) forms of complex* ***C2^{H}***. *Hydrogen atoms are omitted for clarity.*

Table 3.8. *Selected data for the crystal structure of the open and closed forms of complex* ***C2^{H}***.

	Open and closed complex C2^{H}
Crystal data	
Formula	$C_{37}H_{38}Cl_4N_2O_2Pt_2S_4$
Fw (g mol^{-1})	1202.91
Crystal system, space group	Triclinic, P-1
a, b, c (Å)	7.4854(8), 13.993(2), 19.545(2)
α, β, γ (°)	86.078(7), 83.201(7), 86.543(8)
V (Å^3)	2025.2(4)
Z	2
μ (mm^{-1})	9.190
Data collection and refinement	
Temperature (K)	200
T_{min}, T_{max}	0.26, 0.75
No. of measured, independent and observed [I > 2σ(I)] reflections	7783, 7783, 5448
R[I > 2σ(I)], wR(I), *S*	0.1089, 0.2676, 1.082
No. of parameters	614

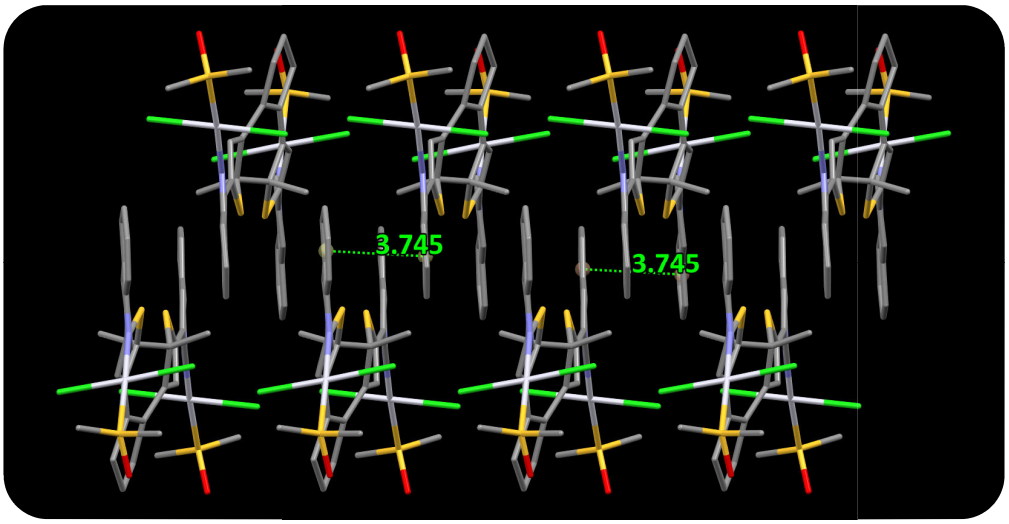

Figure 3.6. *π–π stacking interactions established between the quinoline rings of adjacent molecules of complex* ***C2***^{H}*, separated by a distance of 3.745* Å*. Hydrogen atoms are omitted for clarity.*

Figure 3.6, this interaction facilitates a continuous ordering of intercalated molecules, with mean distances between nearby ring centroids of about 3.75 Å. This intermolecular distance is found within the common range for this kind of π-stacking association, as discussed in Janiak's extensive study on ring interactions in metal complexes bearing aromatic N-donor ligands.[8]

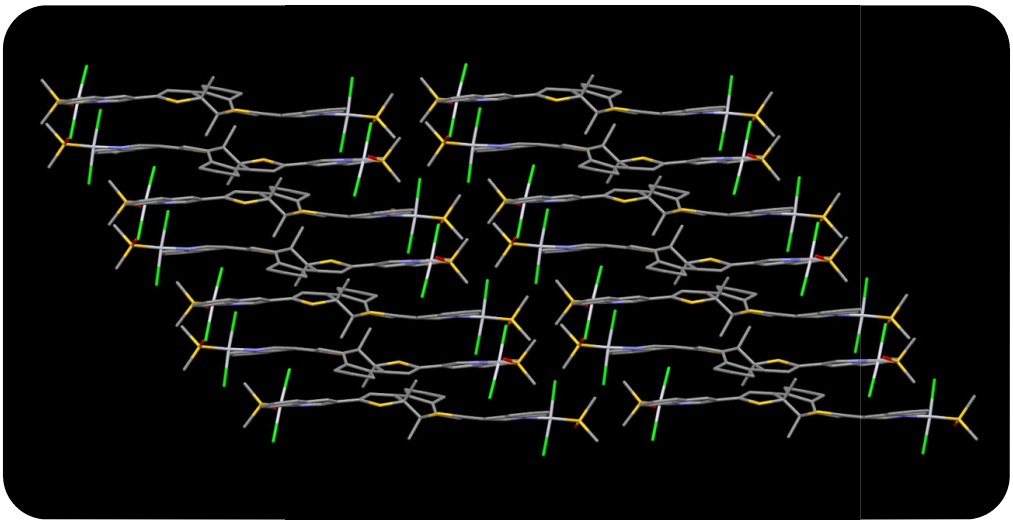

Figure 3.7. *Bidimensional layered framework observed in the crystal structure of complex* ***C2***^{H}*. Hydrogen atoms are omitted for clarity.*

Moreover, the association of several chains of stacked complex molecules gives rise to a two-dimensional network of offset parallel molecular layers, which is depicted in Figure 3.7. This supramolecular 2D structure is further sustained through several short-contact interactions between the anionic chlorido ligands and the electron-deficient hydrogen atoms from the DMSO groups in the vicinity, with mean H···Cl distances ranging from 2.65 to 2.85 Å.

Table 3.9. *Selected structural parameters for the crystal structure of the open and closed forms of complex* ***C2^{H}***.

Bond distances (Å)		Angle values (degrees)	
Pt_1—Cl_1	2.29(1)	Cl_1—Pt_1—N_1	87(1)
Pt_2—Cl_3	2.28(1)	Cl_3—Pt_2—N_2	88(1)
Pt_1—Cl_2	2.27(1)	Cl_1—Pt_1—S_1	89.6(5)
Pt_2—Cl_4	2.26(1)	Cl_3—Pt_2—S_2	89.2(5)
Pt_1—N_1	2.08(3)	Cl_2—Pt_1—N_1	90(1)
Pt_2—N_2	2.11(4)	Cl_4—Pt_2—N_2	88(1)
Pt_1—S_1	2.22(1)	Cl_2—Pt_1—S_1	93.2(5)
Pt_2—S_2	2.28(2)	Cl_4—Pt_2—S_2	94.3(5)

3.2.3. Crystal structure of open complex C2^{F}

Single crystals of complex **C2^{F}**, suitable for X-ray diffraction studies, were obtained by slow diffusion of diethyl ether into a concentrated solution of the complex in dichloromethane. A representation of the molecular structure of this compound is depicted in Figure 3.8; crystallographic data and selected bond lengths and angle values are listed in Tables 3.10 and 3.11, respectively.

In the crystalline state, complex **C2^{F}** exhibits analogous structural features to those of its hydrogenated equivalent, i.e. compound **C2^{H}**, including very similar bond distances and angles around the platinum(II) metal centers (see Table 3.9). In addition,

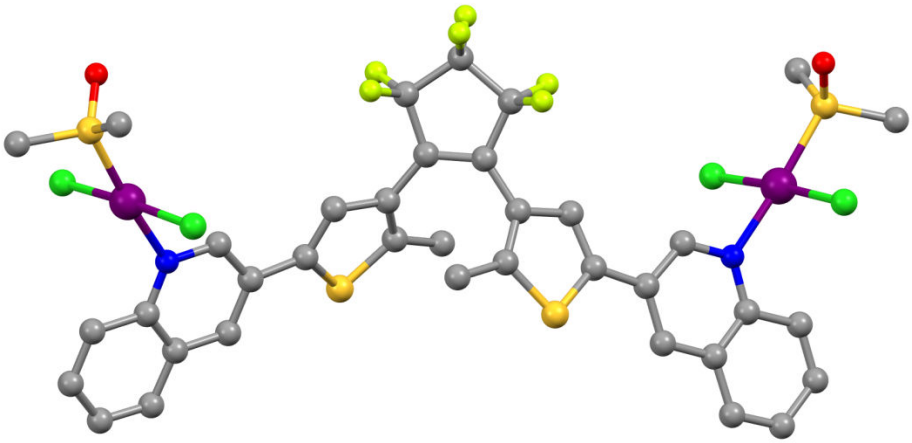

Figure 3.8. *Crystal structure of the open form of complex* ***C2***^{F}. *Hydrogen atoms are omitted for clarity.*

it is worth noticing that the presence of fluorine atoms on the central cyclopentene ring does not seem to substantially alter the electronic conjugation of the whole molecule, as shown by almost identical torsion angles between the cyclopentene and quinoline units, of about 10 degrees.

However, noticeable differences are found in the crystal packing of **C2**^{F}, compared to that of its hydrogenated analogue. Although similar π–π stacking interactions are again established between adjacent molecular entities, the higher relative torsion angle between the quinoline planes of the complex hinders the generation of a layered 2D structure like that observed for **C2**^{H}. Instead, monodimensional molecular chains are in this case formed, displaying a distance of 3.730 Å between π–π interacting rings that is comparable to the separation of 3.745 Å observed for the previous complex. This particular feature is illustrated in Figure 3.9.

Besides, the presence of halogen-bonding interactions between the stacked molecular chains is also noteworthy. This unusual interaction arises from the anisotropic distribution of the electronic density of covalently bound halogen atoms. Under these circumstances, a region of lower electron density, known as σ hole, is generally formed along the projection of the covalent bond. This electrophilic spot is able to attractively interact with neighboring electron-rich regions, such as those surrounding the corresponding σ hole of neighboring halogens, hence producing halogen bonding.[9]

Table 3.10. *Selected data for the crystal structure of the open form of complex* ***C2^F***.

Open complex $C2^F$	
Crystal data	
Formula	$C_{37}H_{32}Cl_4F_6N_2O_2Pt_2S_4$
Fw (g mol^{-1})	1310.85
Crystal system, space group	Monoclinic, C2/c
a, b, c (Å)	25.739(1), 22.713(1), 9.9361(5)
α, β, γ (°)	90, 90.957(3), 90
V ($Å^3$)	5808.2(5)
Z	8
μ (mm^{-1})	5.186
Data collection and refinement	
Temperature (K)	100
T_{min}, T_{max}	0.53, 0.75
No. of measured, independent and observed [I > 2σ(I)] reflections	51558, 8893, 6776
R[I > 2σ(I)], wR(I), *S*	0.0797, 0.2229, 1.066
No. of parameters	261

Table 3.11. *Selected structural parameters for the crystal structure of the open form of complex* ***C2^F***.

Bond distances (Å)		Angle values (degrees)	
Pt_1—Cl_1 Pt_2—Cl_3	2.288(2)	Cl_1—Pt_1—N_1 Cl_3—Pt_2—N_2	86.8(1)
Pt_1—Cl_2 Pt_2—Cl_4	2.303(2)	Cl_1—Pt_1—S_1 Cl_3—Pt_2—S_2	94.51(7)
Pt_1—N_1 Pt_2—N_2	2.062(5)	Cl_2—Pt_1—N_1 Cl_4—Pt_2—N_2	89.9(1)
Pt_1—S_1 Pt_2—S_2	2.212(2)	Cl_2—Pt_1—S_1 Cl_4—Pt_2—S_2	89.00(7)

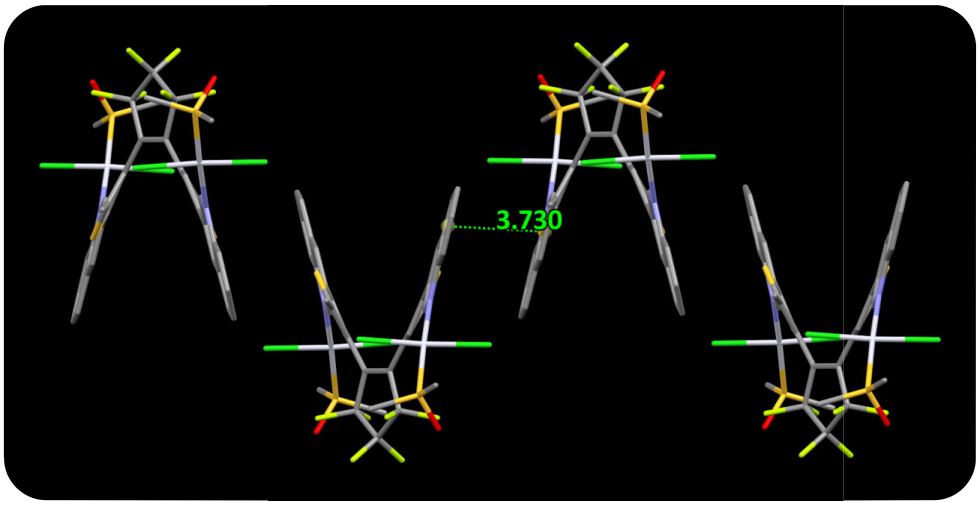

Figure 3.9. *π–π stacking interactions established between the quinoline rings of adjacent molecules of complex* ***C2***^{F}*, separated by an intermolecular distance of 3.730 Å and generating a 1D chain. Hydrogen atoms are omitted for clarity.*

Such supramolecular association can be seen in Figure 3.10, in which the halogen bonding between the cyclopentene rings of opposing **C2**^{F} molecules, with an intermolecular F···F distance of 3.015 Å, are depicted. This interaction gives rise to a multidimensional, ordered framework, which is extended along the axis of the π-π ring stacking.

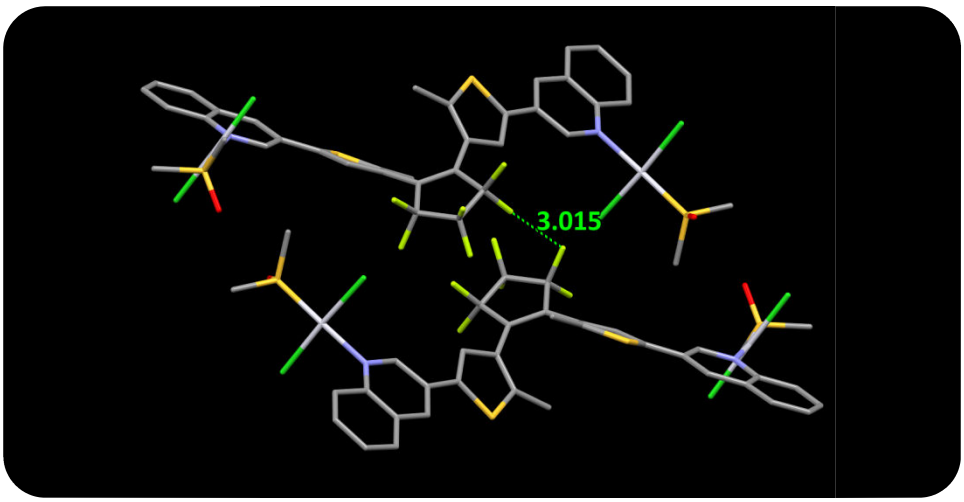

Figure 3.10. *Halogen-bonding interaction between fluorine atoms of two molecules of complex* ***C2***^{H} *belonging to different molecular chains, characterized by a F···F distance of 3.015 Å. Hydrogen atoms are omitted for clarity.*

3.2.4. Crystal structure of open complex C4^{H}

Twinned crystals of **C4^{H}**, suitable for X-ray diffraction studies using a synchrotron source, were obtained by slow diffusion of diethyl ether into a concentrated solution of the complex in dichloromethane. A representation of the molecular structure of this compound is depicted in Figure 3.11; crystallographic data and selected parameters are listed in Tables 3.12 and 3.13, respectively.

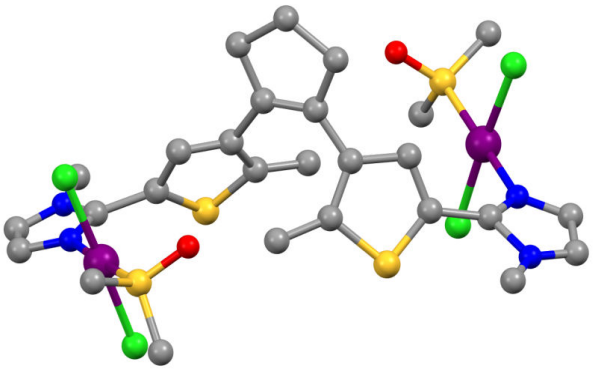

Figure 3.11. *Crystal structure of the open form of complex **C4^{H}**. Hydrogen atoms are omitted for clarity.*

The crystal structure of **C4^{H}**, which is also a dinuclear platinum(II) complex, exhibits the same chemical connectivity as all previously described complexes, as well as comparable bond distances and angle values around the metal centers. However, significant differences regarding the electronic delocalization of this system may be expected from the much higher torsion angles between the thiophene and imidazole rings (amounting to ca. 55 degrees), in contrast to the high ligand planarity displayed by all other compounds.

Although this distortion could be partially attributed to steric hindrance due to the presence of the methyl group at the *ortho* position of the imidazole ring, this was further investigated through computational analysis of the electronic structure of the free ligand (discussed in the next section). These studies revealed a much less effective electronic delocalization for this particular system, which may account for the structural differences observed for the metal complex.

Table 3.12. *Selected data for the crystal structure of the open and closed forms of complex* ***C2^{H}***.

Open complex C4^{H}	
Crystal data	
Formula	$C_{27}H_{36}Cl_4N_4O_2Pt_2S_4$
Fw (g mol^{-1})	1108.82
Crystal system, space group	Triclinic, P-1
a, b, c (Å)	13.339(2), 16.241(3), 17.767(3)
α, β, γ (°)	109.26(1), 90.81(1), 101.45(1)
V (Å^3)	3548(1)
Z	4
μ (mm^{-1})	10.481
Data collection and refinement	
Temperature (K)	100
T_{min}, T_{max}	0.22, 0.68
No. of measured, independent and observed [I > 2σ(I)] reflections	43733, 8076, 6142
R[I > 2σ(I)], wR(I), *S*	0.1163, 0.3369, 1.040
No. of parameters	442

.

Table 3.13. *Selected structural parameters for the crystal structure of the open form of complex* ***C4^{H}***.

Bond distances (Å)		Angle values (degrees)	
Pt_1—Cl_1	2.30(2)	Cl_1—Pt_1—N_1	89(1)
Pt_2—Cl_3	2.34(1)	Cl_3—Pt_2—N_2	90(1)
Pt_1—Cl_2	2.30(2)	Cl_1—Pt_1—S_1	87.4(5)
Pt_2—Cl_4	2.31(2)	Cl_3—Pt_2—S_2	88.5(5)
Pt_1—N_1	2.02(4)	Cl_2—Pt_1—N_1	89(1)
Pt_2—N_2	2.02(4)	Cl_4—Pt_2—N_2	88(1)
Pt_1—S_1	2.24(1)	Cl_2—Pt_1—S_1	94.9(5)
Pt_2—S_2	2.21(1)	Cl_4—Pt_2—S_2	93.6(6)

3.3. Computational study of the photoinactive ligand $L4^H$

The unexpected photochemical behavior of the imidazole-containing ligand **$L4^H$**, which is unable to undergo photocyclization upon irradiation with UV light, was extensively analyzed by means of density functional theory (DFT) calculations (see experimental section for details), in order to get a better understanding of the structural and electronic effects related to this particularly ineffective process.

A comparative structural study of **$L4^H$** and **$L1^H$**, the latter one being used as a reference photoswitchable ligand, was initially addressed through their geometry optimization in the gas phase. Close inspection of the models obtained revealed no significant structural differences; for instance, the distance between the carbon positions prone to forming the new intramolecular C-C bond amounted to about 3.69 Å in both cases. Besides, subsequent inclusion of solvent effects (namely dichloromethane, in which both compounds are highly soluble) by means of a polarizable continuum model did not give rise to significant variations in the optimized structures, as evidenced in Figure 3.12. Accordingly, with the aim of attaining a proper simulation of the experimental conditions, all successive calculations were carried out under the presence of solvent modeling.

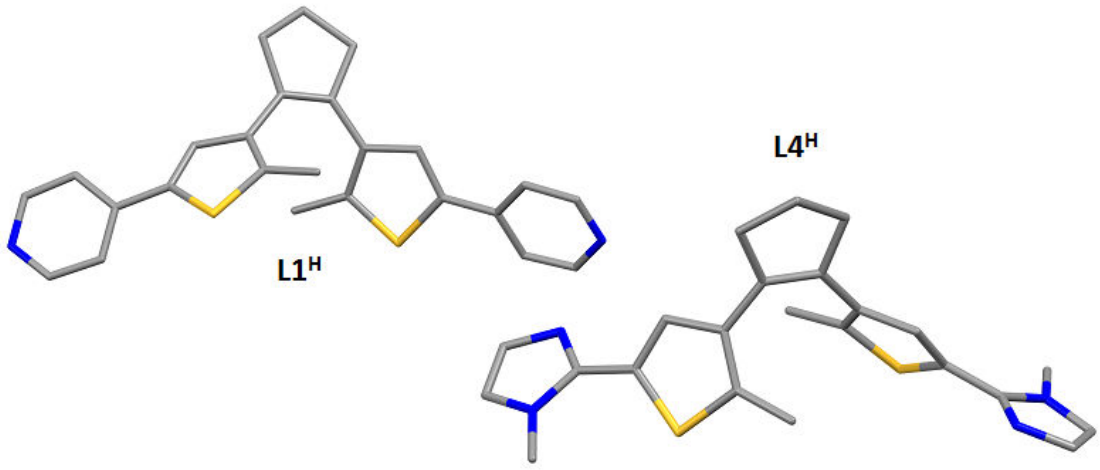

Figure 3.12. *Optimized structures of the open form of ligands **$L1^H$** (top) and **$L4^H$** (bottom). Hydrogen atoms are omitted for clarity.*

Following these initial observations, the change in free energy upon ring closing was subsequently calculated for both systems, so as to assess any potential differences regarding their thermodynamic stability. For that purpose, the corresponding closed isomers of **L4^{H}** and **L1^{H}**, shown in Figure 3.13, were also structurally optimized and their relative free energy was compared to that of their open form, thus obtaining the computed $\Delta_r G°$ values associated to the photocyclization process. In agreement with their structural equivalence, the change in free energy for both systems was indeed quite similar, amounting to 13.75 and 15.17 kcal·mol^{-1} for **L1^{H}** and **L4^{H}**, respectively. Consequently, this would indicate that the photoreaction should be almost equally favorable for both systems, hence implying that the non-occurrence of the ring-closing process for **L4^{H}** is not a thermodynamic issue, but rather a kinetic one.

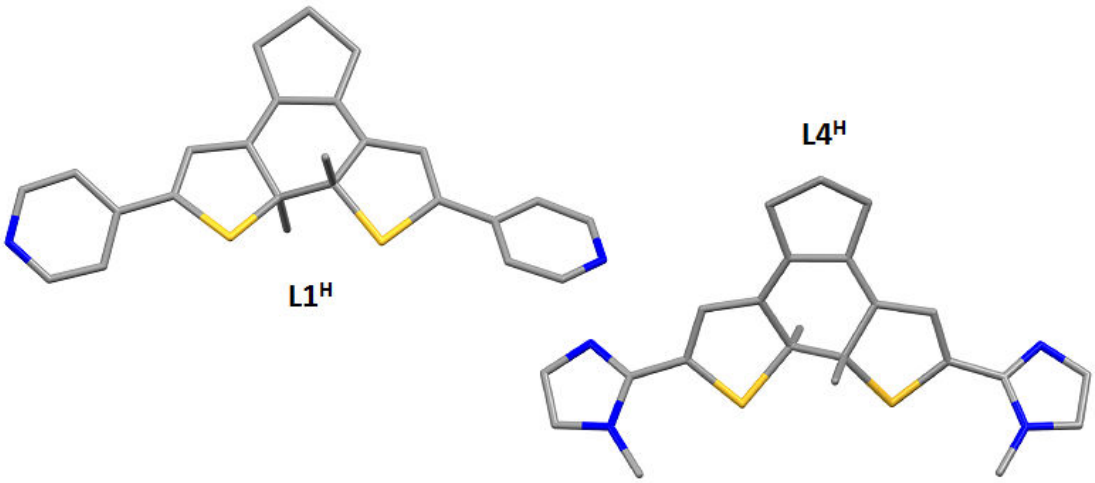

Figure 3.13. *Optimized structures of the closed form of ligands **L1^{H}** (top) and **L4^{H}** (bottom). Hydrogen atoms are omitted for clarity.*

A comparative analysis of the absorption spectra and molecular orbital distribution of both molecules, in their starting open forms, was then performed using Time-Dependant Density Functional Theory (TD-DFT) calculations, with the objective of gaining a deeper insight into the photoreaction mechanism of each system at the electronic level. For that purpose, a survey of different density functionals was firstly carried out to determine the most adequate method to reproduce experimental evidence, using as a reference value the experimental position of the HOMO→LUMO

Table 3.14. *TD-DFT calculated position and oscillator strength values for the HOMO→LUMO transition of open ligand* ***L1^{H}*** *in dichloromethane, using different computational methods.*

HOMO→LUMO transition for L1^{H}			
Functional	**λ_{calc} (nm)**	**f**	**$\Delta\lambda_{exp}$ (nm)**
B3LYP	**351.63**	**0.2668**	**30.63**
BLYP	452.16	0.0728	131.16
BP86	455.32	0.0727	134.32
PBEPBE	455.42	0.0694	134.42
TPSSh	382.73	0.1539	61.73
ωB97xD	288.44	0.7671	-32.56

band for ligand **L1^{H}** in the chosen solvent (λ_{exp} = 322 nm). Among all the tested methods (TPSSh, PBEPBE, BP86, BLYP, B3LYP and ωB97xD), the one that better reproduced this value was the B3LYP functional, which in fact had already been used for obtaining the ground-state optimizations. The calculated position of the studied HOMO→LUMO transition of **L1^{H}** using each of these methods are listed in Table 3.14.

Table 3.15. *Allowed TD-DFT calculated absorption transitions for the open form of* ***L1^{H}*** *and* ***L4^{H}*** *in dichloromethane. The most relevant transitions are indicated in blue.*

Absorption data for L1^{H}				Absorption data for L4^{H}			
Band	**f**	**Energy (nm)**	**Transition**	**Band**	**f**	**Energy (nm)**	**Transition**
1	**0.2668**	**351.63**	**109B → 110B**	**1**	**0.1897**	**320.37**	**111B → 112B**
2	0.0015	345.61	109A → 111A	2	0.0503	312.71	111A → 113A
3	0.3489	306.44	108B → 110B	3	0.0266	300.41	110A → 112A
4	0.4694	305.74	108B → 111B	**4**	**0.9487**	**295.79**	**109B → 112B**
5	0.2959	293.23	107A → 110A	5	0.0195	285.47	110B → 113B
6	0.0556	286.96	107B → 111B	6	0.1701	273.78	109B → 113B
7	0.1132	280.29	109A → 112A	7	0.2178	273.53	111A → 114A
8	0.0017	273.61	109B → 113B	8	0.0572	259.89	110B → 114B
9	0.0084	272.51	105A → 110A	9	0.0307	245.89	111B → 115B
10	0.0024	272.29	104B → 111B	10	0.0008	242.42	111B → 116B
11	0.0507	268.99	109B → 114B	11	0.0892	238.48	108B → 112B

Following this determination, the absorption transitions of each of the open-ring forms of the studied systems, i.e. **L1^{H}** and **L4^{H}**, were then calculated using the selected B3LYP density functional. The values obtained are collated in Table 3.15.

In the case of ligand **L1^{H}**, the most interesting feature arising from the calculated absorption data is the distribution of the most relevant transitions into two well-differentiated regions of the spectrum. As already stated above, the computed HOMO→LUMO transition of this system is located at λ_{calc} = 352 nm (f = 0.2668); this is noticeably separated from other transitions of significant intensity that are unrelated to the expected ring-closing process, which appear to be mainly centered around the 300 nm region (see Table 3.15). These computed data are in good agreement with the experimental absorption spectrum of the ligand, which, as previously discussed at the beginning of this chapter, shows two major well-defined bands located at λ_{max1} = 286 nm and λ_{max2} = 322 nm (see Figure 3.1).

In contrast, substantial differences emerge upon close inspection of the absorption data corresponding to ligand **L4^{H}**. As experimentally observed, the computed HOMO→LUMO transition of this system is found at a slightly higher energy with respect to that of **L1^{H}**, namely at λ_{calc} = 320 nm (f = 0.1897), while a second relevant transition, exhibiting a much higher oscillator-strength associated value, is in this case found closer to the former one, at λ_{calc} = 296 nm (f = 0.9487). This neighboring band, which was partially forbidden for the previous system, corresponds to a non-photoreactive HOMO-2→LUMO transition, which becomes fully allowed in the particular case of **L4^{H}**.

Such a remarkable difference between the computed oscillator strength values of the HOMO→LUMO and HOMO-2→LUMO bands implies that the non-reactive latter transition has indeed a much higher probability of absorbing the incident UV radiation, which is most likely the cause of the blockage of the photocyclization process. These results correlate well with the experimental absorption spectrum of **L4^{H}**, which is shown in Figure 3.14; a shoulder peak, which may correspond to the HOMO→LUMO transition, is easily noticeable at slightly lower energy values with respect to the band of highest intensity, which may be ascribed to the computed HOMO-2→LUMO transition.

Nevertheless, although there is little doubt that the presence of the strongly absorbing HOMO-2 to LUMO transition may severely contribute to hindering the photocyclization process of ligand **L4^{H}**, it may also be noticed that, under these circumstances, the gradual formation of the closed species should still be to some extent expected upon continuous UV light exposure. Consequently, since these observations were not sufficient to thoroughly explain the complete inertness of the ligand towards the ring-closing reaction, the relevant molecular orbitals involved in the photoisomerization of both **L1^{H}** and **L4^{H}** were subsequently analyzed, in order to assess potential key differences between their electronic structures.

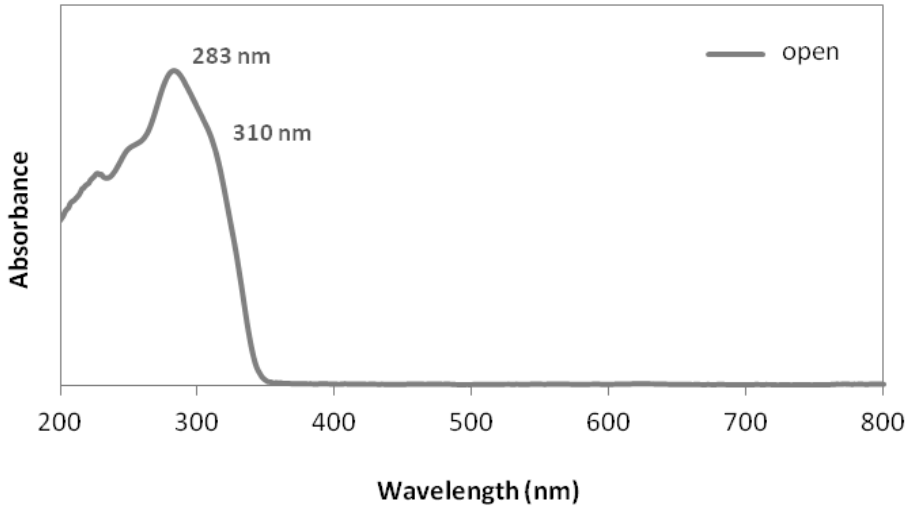

Figure 3.14. *Experimental absorption spectrum of a CH_2Cl_2 solution of **L4^{H}***, showing a shoulder peak next to the band of highest intensity.

As seen in Figure 3.15, the composition of the HOMO is comparable for both systems. Despite the occurrence of some minor delocalization over the imidazole rings in the case of ligand **L4^{H}**, the electronic density of the orbital is mainly localized over the central [4n+2] π-electrons system for both molecules. According to the Woodward-Hoffmann rules, this electronic structure should lead to the adoption of a conrotatory rearrangement mechanism for the electrocyclic reaction under photochemical control, via the corresponding excited-state orbital rotation at the 2-position of the thiophene moieties.[1,10]

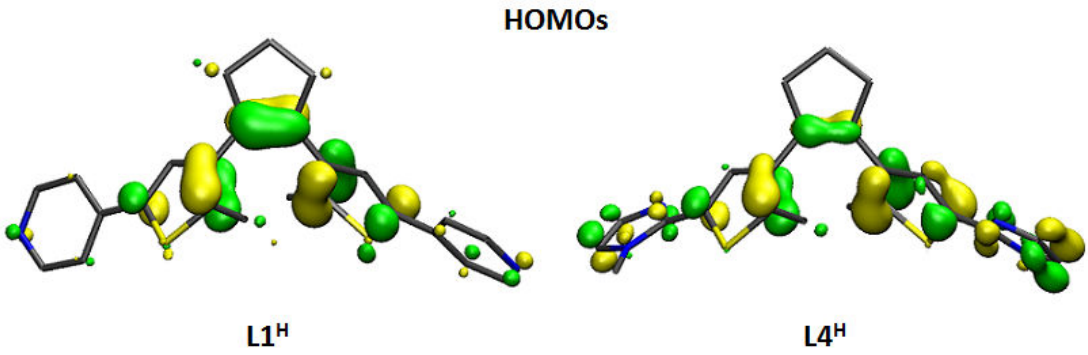

Figure 3.15. *Calculated HOMOs for the open form of ligands* ***L1***^{H} *and* ***L4***^{H}.

On the contrary, the corresponding excited-state molecular orbitals of each of the studied systems exhibit key divergences that further help explaining the photoreactive behavior disparity between these compounds. As evidenced in Figure 3.16, the LUMO of **L1**^{H} exhibits a major delocalization over the pyridine groups anchored to the photoswitchable synthon, whereas in the case of **L4**^{H} the electronic density of the LUMO is strongly localized over the central cyclopentene moiety and the thiophene structure. This unexpected feature, which is more easily appraised in the schematic representation depicted in Figure 3.17, greatly increases the antibonding character of the frontier orbital of **L4**^{H}, as a result of the larger nodal *p* contribution of the carbon and sulfur atoms surrounding the photoreactive 2-position of the thiophene rings. Therefore, and as already reported by Staykov and co-workers for a closely related series of diarylperfluorocyclopentenes,[11] it appears that this strong antibonding

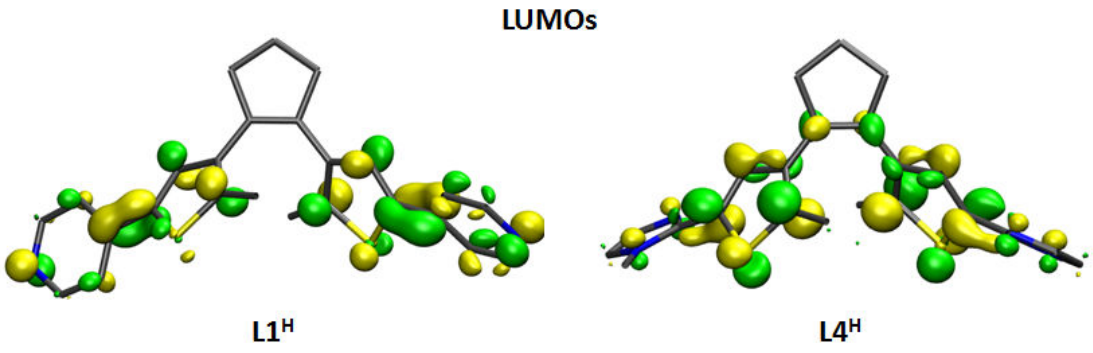

Figure 3.16. *Calculated LUMOs for the open form of ligands* ***L1***^{H} *and* ***L4***^{H}.

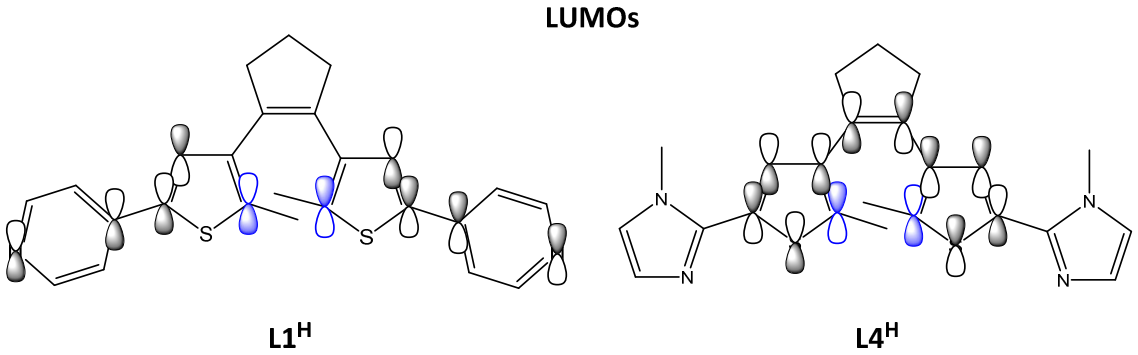

Figure 3.17. *Schematic representation of the most relevant contributions of the calculated LUMOs. Orbitals prone to rotation are indicated in blue.*

interaction with the adjoining atomic orbitals is the main cause of the blockage of the conrotatory orbital rearrangement, which impedes ligand **L4^{H}** to effectively undergo ring closure.

With the aim of further verifying these observations, the electronic structures of two additional systems were subsequently studied using the same computational methods. The quinoline-substituted igand **L2^{H}** was chosen as a second reference photoswitching molecule, for which an electronic structure comparable to that of **L1^{H}** was expected. In addition, a modeled derivative of ligand **L4^{H}** with non-methylated imidazole rings (symbolized as **L4^{H} (HxMe)**, see Figure 3.18) was also investigated. The aim of this model was to confirm whether the distinct LUMO distribution of **L4^{H}** was indeed an intrinsic feature of this particular system, and not an artifact originated by the lower ring coplanarity of the initially optimized structure, due to steric hindrance imposed by the methyl groups.

The corresponding LUMOs of these two additionally considered systems, which are shown in Figure 3.18, were in agreement with the previously obtained results. In this way, the LUMO of ligand **L2^{H}** certainly presents features comparable to those of **L1^{H}**; it exhibits a significant electronic delocalization over its extended aromatic system, as well as little to no contribution from the atomic orbitals surrounding the key 2-position of the thiophene rings. On the contrary, the non-methylated model of **L4^{H}** does maintain, with slight variations, the already discussed orbital distribution that leads to an increased antibonding character able to hinder the required rotation. Most

importantly, considering that the structurally modified model of **L4^{H}** indeed displays an appreciably lower torsion angle between the thiophene and imidazole rings (from ca. 24° for **L4^{H}** to about 12° for **L4^{H} (HxMe)**, compared to the angle of ca. 17° observed for **L1^{H}**), it is thus safe to assert that this defining orbital differentiation does not arise from optimization deviations, but from the intrinsic structural and electronic features of the imidazolic ligand.

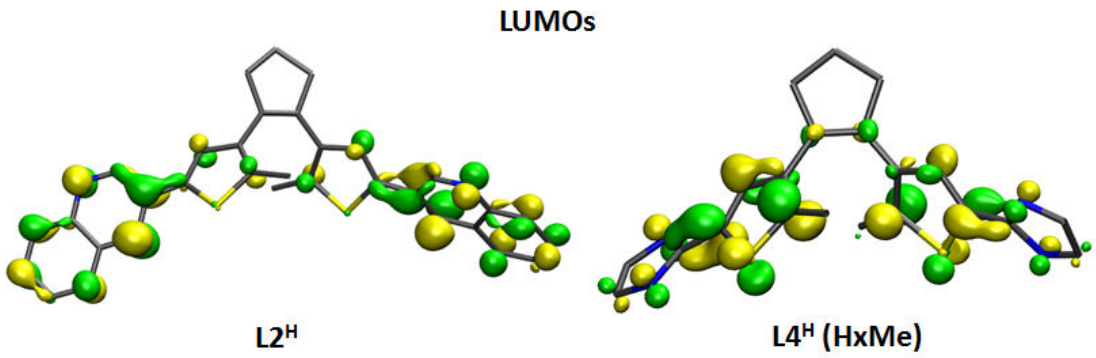

Figure 3.18. *Calculated LUMOs for the open form of ligand **L2^{H}** and the **L4^{H} (HxMe)** model.*

In conclusion, the herein reported computational studies support the proposal of the distinct shape and antibonding interactions of the LUMO of the particular five-membered system of ligand **L4^{H}** as the cause of its striking photochemical inertness. The results obtained hence emphasize that the chemical modification of the dithienylcyclopentene backbone may have a crucial impact not only on the spectroscopic features of the resulting molecular switches, but also on their most elementary photochromic performance. At the same time, it is also worth noting that, in light of the good experimental correlation displayed by the studies carried out, computational analysis may thus be considered an invaluable tool for the prediction of the photochemical functioning of DTC derivatives. This might become especially useful in future investigations aimed at the rational design of novel photoresponsive systems with specific properties, resulting in a much more efficient approach, in terms of time and resources, to the synthetic chemical work.

3.4. Experimental section

3.4.1. Materials and methods

HPLC grade solvents for the spectroscopic measurements were purchased from Sigma-Aldrich and used as received. Spectroscopic measurements in buffered aqueous media were performed in cacodylate buffer solution (1 mM sodium cacodylate, 20 mM NaCl, pH = 7.2), which was prepared from ultrapure water. The UV and visible irradiation experiments were carried out with a MAX-303 light source from Asahi Spectra, using appropriate bandpass filters. UV-Vis absorption spectra were recorded on a Varian Cary 100 Bio spectrophotometer. Nuclear magnetic resonance (NMR) spectra were registered at 298 K on a Varian Mercury 400 MHz spectrometer; proton chemical shifts (δ) are reported in ppm and are referenced to the corresponding non-deuterated solvent peak ($CHCl_3$: 7.26 ppm).

3.4.2. X-Ray crystallography

Data reduction and absorption corrections were commonly performed with the SAINT and SADABS software packages, respectively; the structures were then solved and refined using SHELXL2014 or SHELXTL.[12]

Data for the open form of complex **C1^{F}** were collected on a blue block at 100 K on a Bruker APEX II QUAZAR diffractometer, equipped with a microfocus multilayer monochromator with Mo Kα radiation (λ = 0.71073 Å). Non-hydrogen atoms were refined anisotropically. Hydrogen atoms were placed in calculated positions and refined isotropically. Five fluorine atoms and one carbon atom of the perfluorocyclopentene motif were disordered over two equivalent positions due to the existence of two possible conformations of the ring, and were refined with displacement parameters restraints.

Data for the open and closed forms of complex **C2^{H}** were collected on an orange block at 200 K on a Bruker PHOTON100 CMOS diffractometer at beamline 11.3.1 of the

Advanced Light Source (Synchrotron radiation, λ = 0.7749 Å). Non-hydrogen atoms were refined anisotropically. The central part of the ligand was heavily disordered as a result of the presence of both photoisomers, which were defined from electron-density peaks and refined with both distance and displacement parameters restraints. Hydrogen atoms were placed in calculated positions and refined with a riding model.

Data for the open form of complex **C2^{F}** were collected on a colorless plate at 100 K on a Bruker SMART CCD 6000 diffractometer, equipped with a graphite crystal monochromator with Mo Kα radiation (λ = 0.71073 Å). Non-hydrogen atoms were refined isotropically. Hydrogen atoms were placed in calculated positions and refined isotropically using a riding model.

Data for the open form of complex **C4^{H}** were collected on a colorless plate at 100 K on a Bruker PHOTON100 CMOS diffractometer at beamline 11.3.1 of the Advanced Light Source (Synchrotron radiation, λ = 0.7749 Å). Absorption, twinning and other effects were corrected using the Multi-Scan method (TWINABS). Only the heavy atoms were refined anisotropically, while all light atoms were refined isotropically. Hydrogen atoms were found in the difference map for the methyl groups, and placed in calculated positions for all other carbon atoms. All hydrogen atoms were then constrained and refined using a riding model. Bond distance restraints were used in modeling one of the ligands.

3.4.3. Computational details

All calculations were performed using the Gaussian 09 electronic structure code (rev. D01).[13] Cartesian coordinates for the optimized structures of all the studied complexes can be found in Tables 3.16 to 3.21. A survey of different density functional methods was done using as a reference value the experimental position of the HOMO-LUMO band for **L1^{H}** (λ_{exp} = 321 nm). From the different tested functionals (TPSSh, PBEPBE, BP86, BLYP, B3LYP and ωB97xD), the one that better reproduced this value was the B3LYP functional, which was therefore used to perform all ground-state optimizations.[14–16] The fully optimized contracted triple-ζ all-electron Gaussian basis set with added polarization functions, developed by Ahlrichs and co-workers, was used

for all the elements in the molecule.[17] The studied systems were fully optimized in vacuum and modeling the dichloromethane solvent properties using a polarizable continuum model (self-consistent reaction field approximation); subsequently, the vibrational analysis was performed. The UV-Vis spectra were calculated by means of the Time-Dependent Density Functional Theory (TD-DFT) methodology,[18] using the same functional as for the optimizations. The number of excited states included in the TDDFT calculation was 30.

Table 3.16. *Cartesian coordinates for the optimized structure of the open form of ligand* ***L1^{H}***.

Cartesian coordinates for open L1^{H} (CH_2Cl_2)							
Atom	**X**	**Y**	**Z**	**Atom**	**X**	**Y**	**Z**
S	1.22066	3.73129	2.21339	H	4.52030	5.17145	2.23390
S	2.80872	1.35213	7.00374	H	-0.36682	4.53286	4.51441
N	3.80137	3.20853	-2.51701	H	0.88290	5.18418	5.58661
N	-0.04890	1.19628	11.60019	H	0.70397	3.44265	5.40523
C	2.75623	4.17264	1.51660	H	2.26624	4.60579	8.44547
C	3.51537	4.82611	2.43678	H	4.83188	1.37471	4.91821
C	2.89612	4.96491	3.71608	H	4.96133	3.10855	4.58072
C	1.63522	4.43300	3.74645	H	3.59103	2.19506	3.96125
C	0.65458	4.39476	4.87087	H	1.75475	2.15823	-0.07147
C	3.57456	5.60957	4.84807	H	2.41440	1.69425	-2.39169
C	4.15991	6.99786	4.71301	H	5.12306	4.78219	-2.41051
C	4.97687	7.17136	6.00297	H	4.55348	5.42345	-0.10704
C	4.35974	6.17385	6.99641	H	2.21252	0.01063	9.42011
C	3.70971	5.14445	6.09708	H	0.87299	-0.62934	11.37703
C	2.18852	2.47271	8.18559	H	-0.84558	3.09348	11.62142
C	2.53025	3.74478	7.84621	H	0.37651	3.89316	9.64460
C	3.27145	3.84910	6.62981				
C	3.51631	2.62793	6.06154				
C	4.26679	2.30149	4.81362				
C	3.10068	3.83990	0.13341				
C	2.50047	2.78165	-0.54856				
C	2.87716	2.51495	-1.85391				
C	4.37557	4.21852	-1.86238				
C	4.06198	4.57428	-0.56285				
C	1.42246	2.02356	9.34948				
C	1.53826	0.73234	9.86374				
C	0.78884	0.37314	10.97109				
C	-0.15717	2.43074	11.10777				
C	0.53740	2.88426	10.00059				
H	5.09751	5.73085	7.66812				
H	3.60099	6.65076	7.62771				
H	6.01533	6.89268	5.81295				
H	4.97223	8.19633	6.37265				
H	4.76497	7.11293	3.81096				
H	3.34721	7.72946	4.63963				

Table 3.17. *Cartesian coordinates for the optimized structure of the closed form of ligand* ***L1^{H}***.

Cartesian coordinates for closed L1^{H} (CH_2Cl_2)							
Atom	**X**	**Y**	**Z**	**Atom**	**X**	**Y**	**Z**
S	0.08077	1.82761	2.09838	H	2.21240	-0.00111	1.71754
S	-0.06294	-1.85374	2.07611	H	-0.00676	-3.53256	-1.18396
N	-0.24921	-7.23557	2.37112	H	0.29028	-2.13040	-3.31793
N	0.32403	7.20302	2.45305	H	-1.28291	-1.33611	-3.37435
C	-0.43042	0.64931	0.75448	H	1.43823	-0.10783	-3.98173
C	0.38024	-0.65643	0.72513	H	-0.02743	0.02876	-4.95118
C	-0.08107	0.74058	-1.69628	H	-0.99375	1.62821	-3.41478
C	-0.16332	1.41863	-0.54084	H	0.70373	2.05729	-3.24451
C	-0.08936	2.83698	-0.31961	H	-0.58056	4.13508	3.47610
C	-0.09711	-0.71556	-1.70527	H	0.91752	5.43592	-0.33929
C	-0.05828	-3.21418	0.92786	H	-0.37943	6.46594	4.23965
C	0.05041	-1.40941	-0.56583	H	1.02215	7.71037	0.58443
C	-1.94724	0.43119	0.87266	H	0.67972	-4.17388	3.39118
C	1.90110	-0.43848	0.77057	H	-0.98643	-5.43747	-0.36664
C	-0.22616	-1.18987	-3.12678	H	0.53187	-6.51587	4.13238
C	0.03343	3.20257	0.96902	H	-1.03062	-7.72434	0.53073
C	-0.00053	-2.83131	-0.36011				
C	-0.01306	1.24553	-3.11487				
C	0.35163	-0.00964	-3.93070				
C	0.13919	4.57121	1.48542				
C	-0.21264	4.89178	2.79539				
C	0.59923	5.61384	0.67908				
C	-0.10429	6.20519	3.22333				
C	0.66638	6.89242	1.20163				
C	-0.12935	-4.59009	1.43068				
C	0.28590	-4.92465	2.71844				
C	-0.61910	-5.62595	0.63317				
C	0.20742	-6.24430	3.13357				
C	-0.65220	-6.91162	1.14134				
H	-0.11971	3.54895	-1.13357				
H	-2.29451	-0.22299	0.07114				
H	-2.45558	1.39123	0.78205				
H	-2.21230	-0.01655	1.82878				
H	2.20761	0.22485	-0.03994				
H	2.40473	-1.39692	0.64406				

Table 3.18. *Cartesian coordinates for the optimized structure of the open form of ligand* ***L4^{H}***.

Cartesian coordinates for open L4^{H} (CH_2Cl_2)							
Atom	**X**	**Y**	**Z**	**Atom**	**X**	**Y**	**Z**
S	0.73926	4.25059	2.22242	H	2.32454	4.27461	8.39321
S	2.28105	1.16272	6.58817	H	4.15167	1.11967	4.36606
N	1.24989	0.65326	9.76029	H	4.52212	2.84265	4.19002
N	1.70048	4.61253	-0.99778	H	2.99545	2.20929	3.58927
C	2.26925	4.54648	1.43896	H	1.77816	-1.08233	8.69092
C	3.18733	4.96713	2.34705	H	3.13674	-0.06269	9.21425
C	2.69028	5.05353	3.68399	H	2.25773	-1.04196	10.39755
C	1.36777	4.71549	3.77435	H	-0.38089	4.63438	-0.67741
C	0.47568	4.70295	4.97131	H	0.48563	6.10460	-0.18107
C	3.53731	5.47122	4.80881	H	0.23169	5.76470	-1.89910
C	4.31245	6.76889	4.75785	H	0.23894	-0.12325	11.48070
C	5.23443	6.68592	5.98460	H	1.85940	4.35552	-3.11759
C	4.54755	5.68373	6.92646	C	3.49057	3.63061	-1.77212
C	3.68853	4.86021	5.99131	H	4.24909	3.19000	-2.39903
C	1.93971	2.21980	7.93252	N	3.61694	3.66977	-0.41118
C	2.44025	3.45955	7.69222	N	0.22757	2.61445	9.64015
C	3.09734	3.59086	6.43004	C	-0.26256	1.91269	10.70627
C	3.11303	2.41951	5.72300	H	-1.03114	2.31677	11.34541
C	3.72838	2.12440	4.39540				
C	2.15768	-0.44823	9.49215				
C	1.13698	1.83359	9.08673				
C	2.52534	4.26573	0.03112				
C	0.43166	5.31592	-0.92905				
C	0.35118	0.69812	10.79352				
C	2.31217	4.20184	-2.15283				
H	5.25721	5.07072	7.48553				
H	3.91550	6.19087	7.66459				
H	6.20412	6.28642	5.68073				
H	5.40792	7.65564	6.45038				
H	4.86293	6.89278	3.82267				
H	3.61499	7.61173	4.82452				
H	4.21005	5.18828	2.07423				
H	-0.53656	5.02069	4.71880				
H	0.87053	5.37450	5.73345				
H	0.42035	3.70490	5.41302				

Table 3.19. *Cartesian coordinates for the optimized structure of the closed form of ligand* ***L4^{H}***.

Cartesian coordinates for closed L4^{H} (CH_2Cl_2)							
Atom	**X**	**Y**	**Z**	**Atom**	**X**	**Y**	**Z**
S	-0,18365	1,85051	2,14858	H	1,80845	-0,19023	-3,72242
S	-0,42315	-1,82107	2,13748	H	0,46853	-0,02110	-4,85496
N	0,06375	-5,12666	2,56434	H	-0,61668	1,62526	-3,45319
N	0,55260	5,06765	2,58951	H	1,06214	2,00370	-3,09037
C	-0,56660	0,67353	0,75953	H	-0,04764	-7,09444	3,39737
C	0,20674	-0,65264	0,83440	H	0,74104	7,03352	3,41088
C	0,06338	0,72871	-1,63346	H	1,70912	-3,89543	2,95506
C	-0,13318	1,42312	-0,50193	H	0,47995	-3,91429	4,23496
C	-0,04343	2,84039	-0,28324	H	1,54565	-5,31478	4,00093
C	0,00616	-0,72694	-1,63237	H	0,62522	3,77170	4,24672
C	-0,29445	-3,19507	1,01096	H	1,98309	3,62703	3,10699
C	0,00640	-1,41297	-0,47942	H	1,87486	5,02666	4,18331
C	-2,09265	0,49738	0,70539	C	-1,17318	-6,60038	1,53004
C	1,71754	-0,47370	1,05347	H	-1,70055	-7,49170	1,23041
C	0,02451	-1,21267	-3,05586	N	-1,25989	-5,43991	0,81486
C	-0,05672	3,21473	1,00810	N	-0,58869	5,58837	0,76314
C	-0,09483	-2,83228	-0,26644	C	-0,33875	6,72345	1,47755
C	0,30979	1,21563	-3,03858	H	-0,68059	7,69021	1,14457
C	0,72657	-0,05915	-3,79726				
C	-0,36159	-6,42645	2,61332				
C	0,36318	6,42244	2,60889				
C	-0,50673	-4,56772	1,45910				
C	-0,04240	4,60260	1,45321				
C	1,00154	-4,52058	3,49546				
C	1,29843	4,32163	3,58964				
H	0,05529	3,55734	-1,08650				
H	-2,36265	-0,15415	-0,12730				
H	-2,55941	1,47036	0,55169				
H	-2,47834	0,06416	1,62655				
H	2,13306	0,17086	0,27701				
H	2,20564	-1,44685	0,99460				
H	1,92990	-0,03261	2,02575				
H	-0,04831	-3,55593	-1,06882				
H	0,52915	-2,17073	-3,18000				
H	-1,00130	-1,32942	-3,42103				

Table 3.20. *Cartesian coordinates for the optimized structure of the open form of ligand* ***L2^{H}***.

Cartesian coordinates for open L2^{H} (CH_2Cl_2)							
Atom	**X**	**Y**	**Z**	**Atom**	**X**	**Y**	**Z**
S	1,08736	4,00823	2,18554	H	1,94693	-0,13035	9,31117
S	2,48601	1,20058	6,80443	H	0,27275	3,81542	9,44256
C	2,64978	4,31478	1,47583	C	-0,32429	1,28759	11,41587
C	3,49453	4,82548	2,41050	C	0,51165	-1,00690	11,44516
C	2,91900	4,95559	3,71311	C	-1,11999	0,98271	12,54358
C	1,60915	4,56339	3,74827	C	-0,26686	-1,27490	12,53562
C	0,65350	4,56135	4,89481	H	1,14581	-1,77388	11,01609
C	3,68823	5,45650	4,85961	C	-1,09008	-0,27018	13,08981
C	4,42158	6,77742	4,78242	H	-1,74555	1,76491	12,95481
C	5,27986	6,78797	6,05693	H	-0,25588	-2,26160	12,98124
C	4,57630	5,81127	7,01280	H	-1,70098	-0,49910	13,95409
C	3,79656	4,91100	6,07849	N	-0,37944	2,54475	10,89141
C	2,02629	2,31478	8,06343	C	2,92333	4,03184	0,06595
C	2,50272	3,55694	7,78352	C	2,30446	3,02864	-0,63311
C	3,22723	3,64460	6,55356	C	3,87745	4,82193	-0,63540
C	3,32144	2,43900	5,91445	C	2,62461	2,81261	-1,99033
C	4,00553	2,10026	4,63194	H	1,57571	2,38342	-0,15427
H	5,27406	5,25311	7,64006	H	4,36496	5,64037	-0,11393
H	3,88919	6,33332	7,68883	C	3,60117	3,64922	-2,58219
H	6,27641	6,40715	5,82428	C	2,02444	1,79366	-2,76869
H	5,39779	7,78514	6,48012	C	3,95165	3,45152	-3,93710
H	5,01626	6,87558	3,87152	C	2,38241	1,62328	-4,07634
H	3,69391	7,59689	4,77035	H	1,27866	1,15408	-2,31119
H	4,52784	5,06865	2,20138	C	3,35528	2,46030	-4,66561
H	-0,35415	4,82998	4,57523	H	4,69865	4,10331	-4,37240
H	0,98051	5,27665	5,64919	H	1,92047	0,84328	-4,66840
H	0,60993	3,57885	5,37175	H	3,62721	2,31209	-5,70323
H	2,35091	4,40762	8,43449	N	4,21128	4,64826	-1,88347
H	4,46016	1,10966	4,67111				
H	4,78570	2,83325	4,42653				
H	3,30697	2,12295	3,79156				
C	1,23570	1,88645	9,21878				
C	1,29084	0,61990	9,73934				
C	0,35774	2,81230	9,85000				
C	0,50029	0,28131	10,85794				

Table 3.21. *Cartesian coordinates for the optimized structure of the open form of* ***L4^{H} (HxMe)***.

Cartesian coordinates for open L4^{H} (HxMe) (CH_2Cl_2)							
Atom	**X**	**Y**	**Z**	**Atom**	**X**	**Y**	**Z**
S	0,81356	4,24316	2,19384	H	4,52694	2,84387	4,24341
S	2,23784	1,21854	6,64026	H	3,00696	2,19546	3,64084
N	0,97207	0,60735	9,52212	H	-0,05427	-0,29847	11,17471
N	1,60444	4,19955	-0,90913	H	1,62520	3,89111	-3,03245
C	2,35859	4,51860	1,43727	C	3,53673	3,96437	-1,87379
C	3,26410	4,95270	2,35136	H	4,34151	3,81994	-2,57634
C	2,74318	5,05824	3,67826	N	3,77630	4,14069	-0,53555
C	1,41737	4,73020	3,75130	N	0,48581	2,71776	9,93523
C	0,50439	4,73297	4,93182	C	-0,07893	1,92045	10,89716
C	3,57460	5,48355	4,81207	H	-0,66422	2,33597	11,70144
C	4,36542	6,77151	4,75354	H	1,38350	-0,20444	9,09231
C	5,26747	6,69673	5,99544	H	0,61626	4,30271	-0,74912
C	4,55382	5,71815	6,94201				
C	3,70010	4,88972	6,00630				
C	1,88564	2,30445	7,95578				
C	2,40843	3,53338	7,71081				
C	3,08864	3,63418	6,45731				
C	3,10467	2,45147	5,77015				
C	3,73247	2,12848	4,45548				
C	1,11718	1,89861	9,12011				
C	2,59197	4,28317	0,02254				
C	0,20713	0,60868	10,65864				
C	2,19722	3,99424	-2,12707				
H	5,24687	5,10584	7,52219				
H	3,91609	6,24451	7,66151				
H	6,23661	6,28062	5,71285				
H	5,44588	7,67146	6,44864				
H	4,93152	6,87489	3,82531				
H	3,67674	7,62298	4,79665				
H	4,28882	5,17707	2,09015				
H	-0,49755	5,06845	4,66155				
H	0,89782	5,39879	5,69956				
H	0,42386	3,73643	5,37333				
H	2,30077	4,35701	8,40273				
H	4,15775	1,12416	4,45150				

3.5. References

(1) Woodward, R. B.; Hoffmann, R. *J. Am. Chem. Soc.* **1965**, *87* (1959), 395–397.

(2) Feringa, B. L. *Molecular Switches*; Wiley-VCH: Darmstadt, 2001.

(3) Kobatake, S.; Shibata, K.; Uchida, K.; Irie, M. *J. Am. Chem. Soc.* **2000**, *122* (49), 12135–12141.

(4) de Jong, J. J. D.; Lucas, L. N.; Hania, R.; Pugzlys, A.; Kellogg, R. M.; Feringa, B. L.; Duppen, K.; van Esch, J. H. *Eur. J. Org. Chem.* **2003**, 1887–1893.

(5) Wang, L. V.; Wu, H.-I. *Biomedical Optics: Principles and Imaging*; Wiley, 2007.

(6) Zhong, Y. W.; Vila, N.; Henderson, J. C.; Flores-Torres, S.; Abruña, H. D. *Inorg. Chem.* **2007**, *46* (25), 10470–10472.

(7) Matsuda, K.; Shinkai, Y.; Irie, M. *Inorg. Chem.* **2004**, *43* (13), 3774–3776.

(8) Janiak, C. *J. Chem. Soc., Dalton Trans.* **2000**, No. 21, 3885–3896.

(9) Cavallo, G.; Metrangolo, P.; Milani, R.; Pilati, T.; Priimagi, A.; Resnati, G.; Terraneo, G. *Chem. Rev.* **2016**, *116* (4), 2478–2601.

(10) Hoffmann, R.; Woodward, R. B. *Science* **1970**, *167* (3919), 825–831.

(11) Staykov, A.; Yoshizawa, K. *J. Phys. Chem. C* **2009**, *113* (9), 3826–3834.

(12) Sheldrick, G. M. *Acta Crystallogr. Sect. A* **2008**, *64*, 112–122.

(13) Frisch, M. J.; Trucks, G. W.; Schlegel, H. B.; Scuseria, G. E.; Robb, M. A.; Cheeseman, J. R.; Scalmani, G.; Barone, V.; Mennucci, B.; Petersson, G. A.; Nakatsuji, H.; Caricato, M.; Li, X.; Hratchian, H. P.; Izmaylov, A. F.; Bloino, J.; Zheng, G.; Sonnenberg, J. L.; Hada, M.; Ehara, M.; Toyota, K.; Fukuda, R.; Hasegawa, J.; Ishida, M.; Nakajima, T.; Honda, Y.; Kitao, O.; Nakai, H.; Vreven, T.; Montgomery, J. A., J.; Peralta, J. E.; Ogliaro, F.; Bearpark, M.; Heyd, J. J.; Brothers, E.; Kudin, K. N.; Staroverov, V. N.; Kobayashi, R.; Normand, J.; Raghavachari, K.; Rendell, A.; Burant, J. C.; Iyengar, S. S.; Tomasi, J.; Cossi, M.;

Rega, N.; Millam, J. M.; Klene, M.; Knox, J. E.; Cross, J. B.; Bakken, V.; Adamo, C.; Jaramillo, J.; Gomperts, R.; Stratmann, R. E.; Yazyev, O.; Austin, A. J.; Cammi, R.; Pomelli, C.; Ochterski, J. W.; Martin, R. L.; Morokuma, K.; Zakrzewski, V. G.; Voth, G. A.; Salvador, P.; Dannenberg, J. J.; Dapprich, S.; Daniels, A. D.; Farkas, Ö.; Foresman, J. B.; Ortiz, J. V.; Cioslowski, J.; Fox, D. J. *Gaussian 09 (Revision D.01)*; Gaussian Inc.: Wallingford, CT, 2009.

(14) Chai, J. D.; Head-Gordon, M. *Phys. Chem. Chem. Phys.* **2008**, *10* (44), 6615–6620.

(15) Becke, A. D. *J. Chem. Phys.* **1993**, *98* (7), 5648–5652.

(16) Lee, C.; Yang, W.; Parr, R. G. *Phys. Rev. B* **1988**, *37* (2), 785–789.

(17) Schäfer, A.; Huber, C.; Ahlrichs, R. *J. Chem. Phys.* **1994**, *100* (8), 5829–5835.

(18) Casida, M. E.; Jamorski, C.; Casida, K. C.; Salahub, D. R. *J. Chem. Phys.* **1998**, *108* (11), 4439–4449.

CHAPTER 4

Biological evaluation

4.1. DNA interaction studies

4.1.1. Metal-complex interactions with DNA

Nuclear DNA is generally considered to be the primary biological target of most chemotherapeutical drugs, both in current clinical use and under several development stages.[1] Although the detailed mechanism through which many nucleic acid-drug interactions proceed still remains to be fully understood, DNA targeting with small molecules is a particularly efficient way of interfering with a number of paramount biological processes, including gene expression, protein synthesis and cell division. Such DNA-interacting agents thus may find their utility in the treatment of several diseases for which the inhibition of the normal DNA function may be of particular interest, among which cancer stands in a paradigmatic position.

The vast range of possibilities offered by DNA-drug interactions arises not only from the inherent structural complexity of this biomolecule, but also from its polymorphic nature. Aside from the well-known, double-stranded helical structure of the most common B-DNA form described by Watson and Crick, a number of alternative DNA conformations and even non-duplex structures can also be found. All these structures take part of a number of relevant biological processes, and each one of them

represents a potential chemotherapeutic target through which the regulation of a particular function may be eventually achieved.[2]

When addressing the study of the specific interaction of small molecules with DNA, including that of transition-metal complexes such as those reported in this thesis, both covalent and non-covalent binding modes may be considered.[3] Covalent binding, in particular, is a common mode of DNA interaction for most metal complexes, providing that one or more of the ligands surrounding the metal center are labile enough to be readily hydrolyzed, and hence generate vacant binding sites. As previously described for cisplatin in the introductory chapter of this thesis, metallic covalent binders generally coordinate to the electron-rich N7 position of the purine residues of DNA, forming monofunctional adducts, and/or bifunctional inter- and intrastrand crosslinks.[4] This generally results in the local bending and unwinding of the double helix, which in turn blocks the replication and transcription processes; ultimately, following the failure of DNA-repair and nucleotide-excision mechanisms, programmed cell death occurs.[5]

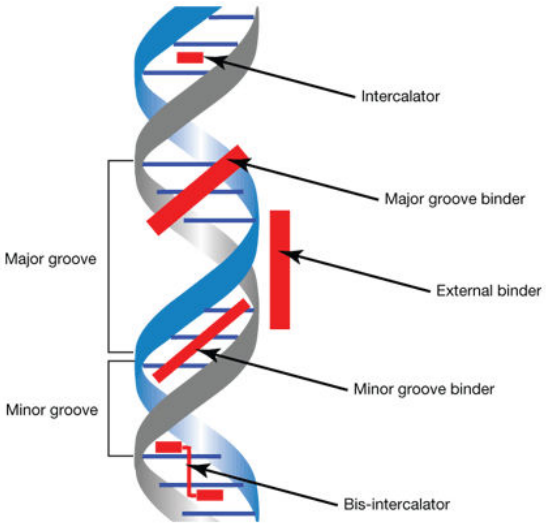

Figure 4.1. *Schematic representation of non-covalent DNA-drug interactions.*

Non-covalent DNA binding, on the other hand, encompasses three fundamentally different intermolecular interactions depicted in Figure 4.1: intercalation between DNA base pairs; minor and major groove binding; and, to a much lesser extent, non-specific backbone association.[6] Being governed by a combination of Van der Waals forces,

hydrogen bonding, electrostatic attraction or hydrophobic effects, non-covalent binding activity has an interesting reversible nature from the perspective of drug metabolism and hence of side-effect reduction, and in the case of transition-metal complexes, it typically arises from particular interactions between the organic ligands and the double helix.

Intercalation can be defined as the insertion of a planar, electron-deficient aromatic ring system between the stacked base pairs of DNA.[7] Several conformational changes take place as a result of this interaction, which is stabilized by the overlap of the π orbitals of both the intercalator and the adjoining nucleobases; DNA must dynamically open a space between its base pairs for intercalation to occur, which results in the local unwinding, lengthening and stiffening of the double helix. Blockage of transcription, replication and DNA-repair mechanisms result from this insertion, which is why most intercalating agents are considered strong mutagens; for the same reasons, they can also be successfully applied as strong cancer cell-growth inhibitors.[8,9]

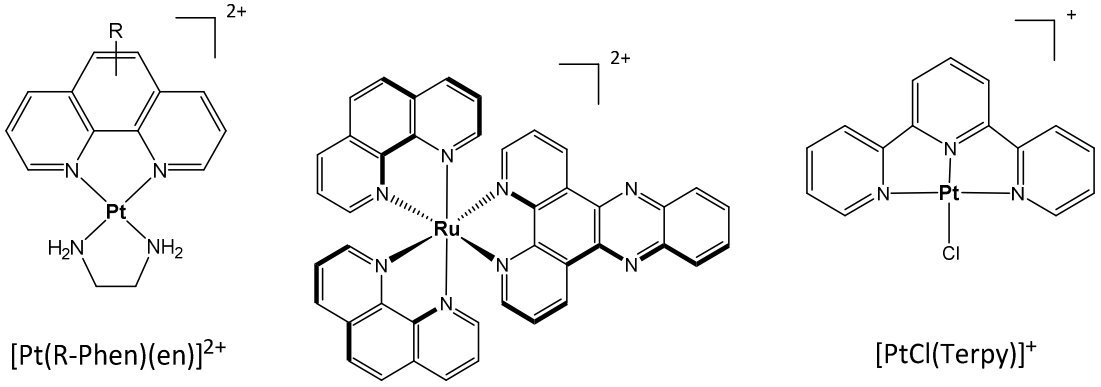

$[Pt(R\text{-}Phen)(en)]^{2+}$ $[Ru(Phen)_2(dppz)]^{2+}$ $[PtCl(Terpy)]^{+}$

Figure 4.2. *Illustrative examples of Pt(II) and Ru(II) intercalating metal complexes.*[10–12]

Many metal complexes bearing a variety of polyaromatic ligands, like those depicted in Figure 4.2, typically exhibit strong intercalating and anticancer properties. For instance, planar-shaped platinum(II) complexes of the type $[Pt(R\text{-}Phen)(en)]^{2+}$ have been extensively studied and are known to display noteworthy antitumoral activity.[10] Polypyridyl ruthenium(II) compounds such as $[Ru(Phen)_2(dppz)]^{2+}$ (dppz =

dipyridophenazine) are also potent intercalators exhibiting interesting potential applications as diagnosis agents,[11] and copper(II) porphyrin-based systems have been described to induce redox-mediated DNA cleavage after intercalative DNA association.[13] Other interesting examples include platinum(II) terpyridyl complexes able to covalently bind to DNA after being inserted, or even polynuclear compounds displaying multiple intercalating moieties tethered by a flexible linker; such additional interactions usually account for increased antiproliferative capacity.[12,14]

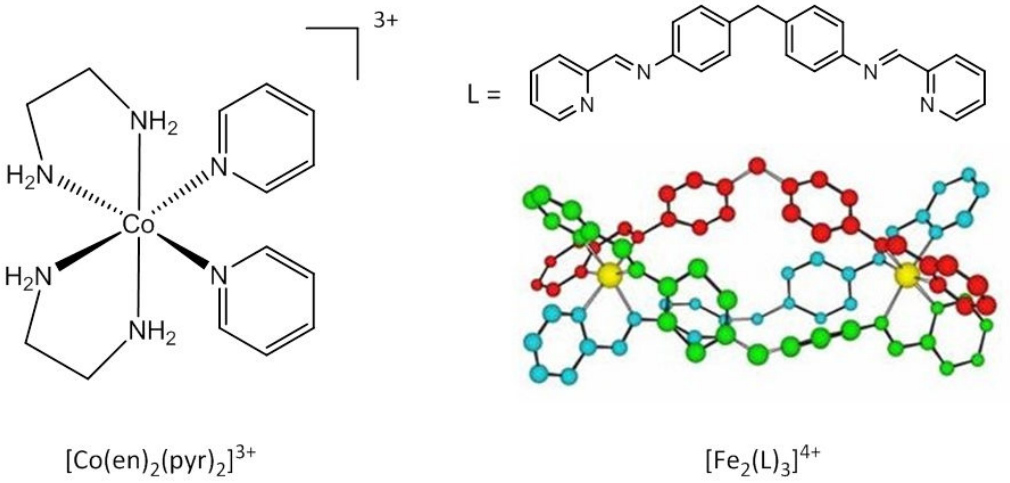

Figure 4.3. *Illustrative examples of Ru(II) and Fe(II) groove-binding metal complexes.*[15,16]

Groove binding is the other main non-covalent nucleic acid interaction mode. Just as most DNA-binding proteins, long-shaped molecules or metal complexes with a certain degree of conformational flexibility may exhibit particular affinity for either the major or minor grooves of DNA, owing to complementary hydrophobic and electrostatic effects.[17] Although this intermolecular association does not generally induce any particular rearrangement of the double helix, groove binders are able to inhibit several DNA-protein readout processes and the expression of specific gene sequences. In other cases, groove association is a required prior step for metal complexes to cause further DNA damage. Ruthenium(II) and cobalt(III) complexes such as $[Ru(Me_4Phen)_3]^{2+}$ (Me_4Phen = 3,4,7,8-tetramethylphenanthroline) or $[Co(en)_2(py)_2]^{3+}$ are illustrative examples of compounds capable of binding electrostatically within the grooves of DNA, and of subsequently inducing strand cleavage upon light irradiation.[18,15] Some

iron or copper supramolecular metallohelicates are also known as major-groove binders and have received notable attention in recent years, due to their particular ability to induce dramatic DNA supercoiling.[16,19] A few of these compounds are shown in Figure 4.3.

In summary, metal-containing molecules are able to induce an array of notable effects on the structure and conformation of DNA, which may have a defining impact on an even wider range of cellular processes. Since DNA stands as the main and most effective biological target for many antiproliferative agents, evaluating the nature of these interactions is a crucial step in the early development of novel metallodrugs. Such investigations are crucial to get a better understanding of both their mechanism of action and their key structural features, which may eventually lead to rational design refinement and hence an activity enhancement.

With these objectives in mind, the thorough evaluation of the DNA-interacting capabilities of both the open and closed isomers of the synthesized photoswitchable complexes was subsequently addressed using various techniques. The results obtained successfully corroborated the suitableness of the innovative DTC-based approach for the design of novel light-activatable metallodrugs, and are discussed below.

4.1.2. Agarose gel electrophoresis studies

Gel electrophoresis is a fairly simple technique that is commonly used to separate and analyze charged biomolecules, such as nucleic acids, according to their size and conformation.[20] This separation takes place by application of an electric field through a porous gel matrix generally made of agarose or polyacrylamide, which is loaded with the studied samples. Due to the negatively charged nature of their phosphate backbone, DNA molecules are attracted by the opposite electrode and move across the gel, displaying distinct migration rates through the porous network based on their structural features. In practice, gel electrophoresis can be used to qualitatively assess the activity of a DNA binder as a function of its effect over the electrophoretic mobility of nucleic acid samples, which will be directly related to the induced conformational changes.

Plasmidic DNA is typically used in gel electrophoresis experiments. Plasmids are small, double-stranded and circular DNA sequences, which akin to chromosomal DNA are generally found *in vivo* in a tightly compacted supercoiled conformation. This compact state, however, may be altered by the action of either topoisomerase enzymes or accidental single-strand breaking, producing in both cases the unwinding of the supercoils and the adoption of a relaxed, open circular conformation. These two naturally-occurring supercoiled and relaxed topologies of plasmidic DNA are also respectively known as forms I and II. Strong DNA-cleaving agents, in addition, may be able to induce double-strand breaking of the circular structure, which then results in a linear DNA chain commonly denoted as form III. As could be expected, each of these plasmid DNA topologies, which are schematically represented in Figure 4.4, displays a distinct electrophoretic mobility and may be affected in different ways by DNA-interacting agents.

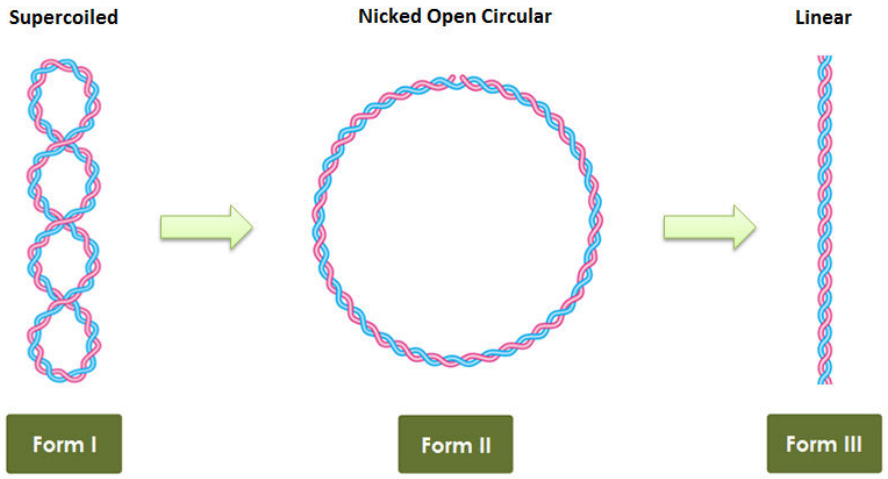

Figure 4.4. *Schematic representation of the three main plasmid DNA topologies.*

Gel electrophoresis experiments were thus performed for an initial screening of the DNA-interacting behavior of the open and closed forms of all the synthesized photoswitchable platinum(II) complexes. Native pBR322 plasmid DNA samples were separately treated with increasing quantities of both isomers of each compound, and the effect on their electrophoretic mobility was subsequently evaluated after an incubating period of 24 h at 37 °C, during which all samples were kept in the dark (see

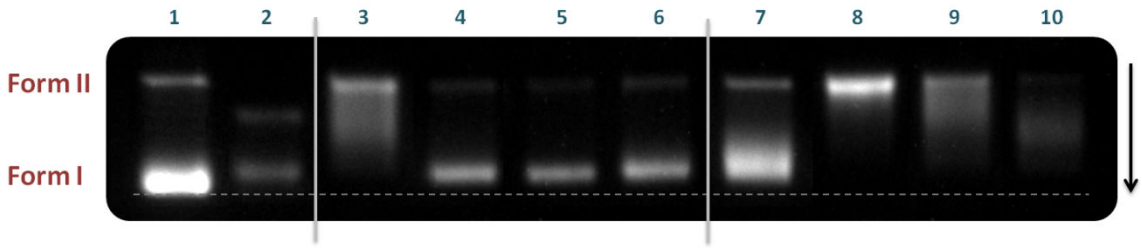

Figure 4.5. *Agarose gel electrophoresis image for pBR322 DNA incubated for 24 h at 37 °C with increasing quantities of complex* ***C1^{H}*** *in its open and closed forms. Lane 1: Native plasmid DNA; lane 2: DNA + 0.5 equiv. cisplatin; lanes 3-6: DNA + 0.5 to 2.0 equiv.* ***C1^{H}*** *(open form); lanes 7-10: DNA + 0.5 to 2.0 equiv.* ***C1^{H}*** *(closed form).*

experimental section for details). Following the mobility shift assays, the resulting gels were then treated with an appropriate DNA marker for visualization.

Figure 4.5 shows the agarose gel electrophoresis image obtained after incubating plasmid DNA samples with the open and closed forms of complex **C1^{H}**. Lane 1 corresponds to native pBR322 DNA, which, as stated above, is principally found in its supercoiled conformation (form I). A small presence of nicked circular conformation (form II) is also appreciated, exhibiting a lesser electrophoretic mobility due to its more voluminous nature. Lane 2 corresponds to a sample of DNA incubated with 0.5 equivalents of cisplatin, which affects the mobility of both DNA conformations and was used as a positive control. As observed in the gel, cisplatin's binding to supercoiled DNA causes the unwinding of the double helix, hence producing the removal of negative supercoils; as a result, the electrophoretic mobility of form I is reduced.[21] The same unwinding process, on the contrary, does increase the mobility of the open circular conformation upon platinum binding, due to a shortening effect on the DNA contour length that results in a more compact structure.[22] These effects are known to become more pronounced in a dose-response fashion, up to the point that all metal/DNA adducts would co-migrate in the form of a single broad band in the presence of increasing amounts of cisplatin.

Lanes 3 to 6 and 7 to 10 correspond to plasmid DNA samples incubated with increasing quantities of the open and closed isomers of the complex, respectively. A promising and clearly distinct DNA-interacting behavior of the two isomeric forms can easily be

appreciated. Low concentrations of the open form of **C1^{H}** appear to produce a variable decrease of the electrophoretic mobility of supercoiled DNA, as observed in lane 3. This effect could be ascribed to the gradual unwinding of the double helix, although it becomes apparently much less pronounced at higher complex concentration; indeed, lanes 4-6 exhibit a much better defined form I band, whose mobility diminution is comparable to that of supercoiled DNA treated with cisplatin. These results suggest that the open isomer of complex **C1^{H}** is able to interact with the double strand of DNA in multiple ways, most probably as a result of cooperative effects between the platinum centers and the organic ligand, leading to an equilibrium governed by compound concentration. It is likely that intercalative interaction may have a role at lower complex concentrations, generating the observed partial unwinding, whereas increasing quantities of the complex seem to lead to typical DNA-platination effects.

On the contrary, the closed isomer of complex **C1^{H}** exhibits a strong intercalative interaction with DNA, most likely arising from its much higher stiffness, planarity and electronic conjugation. As previously discussed, DNA intercalation is known to induce stronger local unwinding of the double helix than covalent binding; this may result in the relaxation of the negatively supercoiled plasmid sequences until virtually reaching an open circular conformation, whereas further addition of the intercalating agent will then lead to positive supercoiling.[23] Such features are clearly observed in lanes 7-10, containing increasing concentrations of closed **C1^{H}**. Lane 7 exhibits an initial decrease of the mobility of negatively supercoiled DNA (form I), due to partial twist reduction of the biomolecule; increasing the amount of complex enhances this effect, up to the point that, in lane 8, all initially supercoiled DNA appears to be completely relaxed and co-migrates with the unaffected nicked DNA fraction. Finally, a mobility increase is then observed in lanes 9 and 10, as a result of the subsequent induction of positive supercoiling to the previously relaxed structure.

Moreover, the distinguishable vanishing of the bands accompanying this mobility increase is also worth mentioning, as it most likely arises from the precipitation of highly platinated DNA adducts. This suggests that covalent binding of the metal centers may take place following the insertion of the compound between base pairs, which, as in the case of the previously described terpyridine platinum(II) complexes, may account for a stronger antiproliferative activity of this closed species.

Different DNA interactions of their open and closed photoisomers, thereby supporting their potential application as photoactivatable drugs, were also observed for some other tested compounds like the perfluorinated complex **C1^{F}**. The corresponding agarose gel electrophoresis results are shown in Figure 4.6. As for the previous compound, incubation of DNA with increasing quantities of the open isomer of **C1^{F}** produces the unwinding of the supercoiled circular structure, the complete conversion into form II being now observed at the highest complex concentration (lane 6). This may be explained by single-strand cleavage of the plasmid induced by platinum binding, resulting in the complete relaxation of supercoiled DNA fragments through free rotation around the nicked strand.

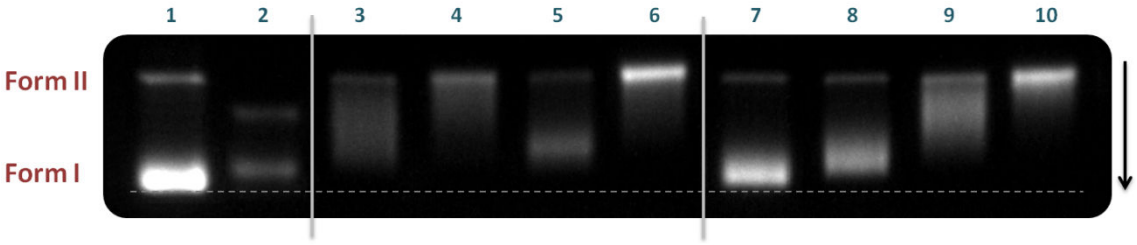

Figure 4.6. *Agarose gel electrophoresis image for pBR322 DNA incubated for 24 h at 37 °C with increasing quantities of complex **C1^{F}** in its open and closed forms. Lane 1: Native plasmid DNA; lane 2: DNA + 0.5 equiv. cisplatin; lanes 3-6: DNA + 0.5 to 2.0 equiv. **C1^{F}** (open form); lanes 7-10: DNA + 0.5 to 2.0 equiv. **C1^{F}** (closed form).*

The closed-ring form of complex **C1^{F}**, on the other hand, presents well-defined intercalating properties comparable to those of the previous compound, even though higher concentrations are in this case needed to produce similar results. Indeed, whereas 1.0 equivalent of closed **C1^{H}** is sufficient to give rise to the complete relaxation of supercoiled circular DNA (Figure 4.5, lane 8), twice that amount of closed **C1^{F}** is required in order to achieve the same effect (Figure 4.6, lane 10). Such a decrease in the activity of the complex can be justified by its potentially repulsive interactions with the phosphate backbone, due to the presence of the fluorine atoms in the inserted ligand. These results thus indicate that the favored DNA interaction mode for these cyclized photoisomers is intercalation.

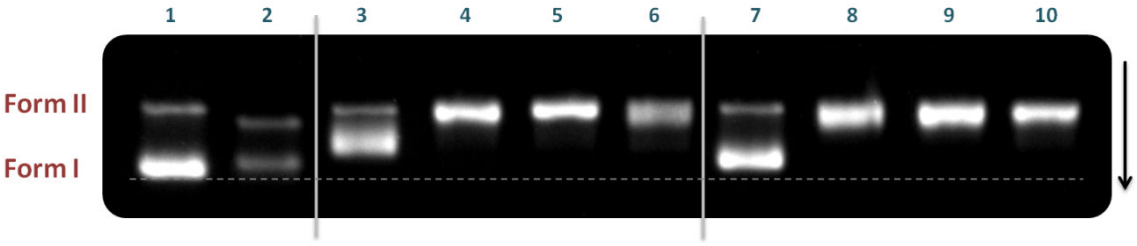

Figure 4.7. *Agarose gel electrophoresis image for pBR322 DNA incubated for 24 h at 37 °C with increasing quantities of complex* ***C2^{H}*** *in its open and closed forms. Lane 1: Native plasmid DNA; lane 2: DNA + 0.5 equiv. cisplatin; lanes 3-6: DNA + 0.5 to 2.0 equiv.* ***C2^{H}*** *(open form); lanes 7-10: DNA + 0.5 to 2.0 equiv.* ***C2^{H}*** *(closed form).*

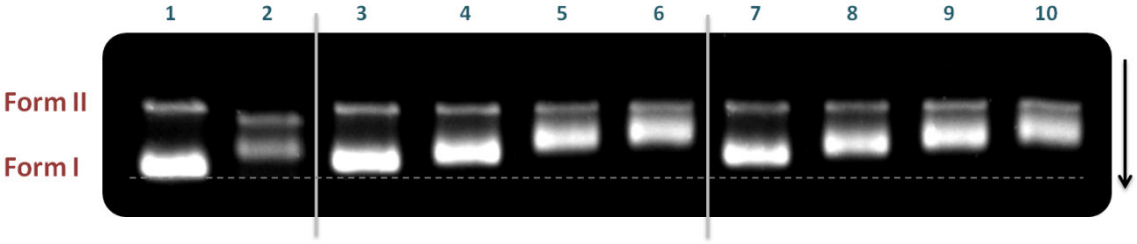

Figure 4.8. *Agarose gel electrophoresis image for pBR322 DNA incubated for 24 h at 37 °C with increasing quantities of complex* ***C2^{F}*** *in its open and closed forms. Lane 1: Native plasmid DNA; lane 2: DNA + 0.5 equiv. cisplatin; lanes 3-6: DNA + 0.5 to 2.0 equiv.* ***C2^{F}*** *(open form); lanes 7-10: DNA + 0.5 to 2.0 equiv.* ***C2^{F}*** *(closed form).*

The assays carried out with complexes **C2^{H}** and **C2^{F}**, however, revealed minor differences regarding the DNA-interacting capabilities of their open and closed forms. As seen in Figures 4.7 and 4.8, a noticeable decrease of the electrophoretic mobility of supercoiled DNA is observed for all samples treated with increasing quantities of each compound, even producing its co-migration with open circular DNA in the case of both the open and closed isomers of complex **C2^{H}** (Figure 4.7, lanes 4-6 and 8-10). This feature may be attributed to the presence of the planar-shaped quinoline rings in both ligands, which apparently confers a comparable intercalating activity to all these species regardless of the state of the photoswitchable core (i.e. open or closed).

It is nevertheless worth noting that, as observed for the first tested complexes, both the open and closed isomers of **C2^{F}** show a weaker affectation of supercoiled DNA

compared with their non-fluorinated counterparts (Figure 4.8, lanes 3-10). Altogether, these findings suggest that the fluorination of the ligand backbone has a negative impact on the affinity of the resulting complexes towards the double helix, probably due to its incompatibility with the otherwise favored intercalating binding mechanism. Therefore, in the absence of complementary interactions, it is likely that complexes bearing this structural motif might be prone to display poorer antiproliferative properties.

Figures 4.9 and 4.10 show the agarose gel electrophoresis images obtained after incubating pBR322 plasmid DNA with increasing amounts of complex **C3^{H}** and the non-photoreactive complex **C4^{H}**, respectively. If the previously examined compounds allowed evaluating the influence of the perfluorinated backbone on their DNA-interacting performance, complexes **C3^{H}** and **C4^{H}** were considered of particular interest to analyze both the role of the metal-binding unit in DNA association and the effects produced by slight chemical modifications, by comparison with compound **C1^{H}**.

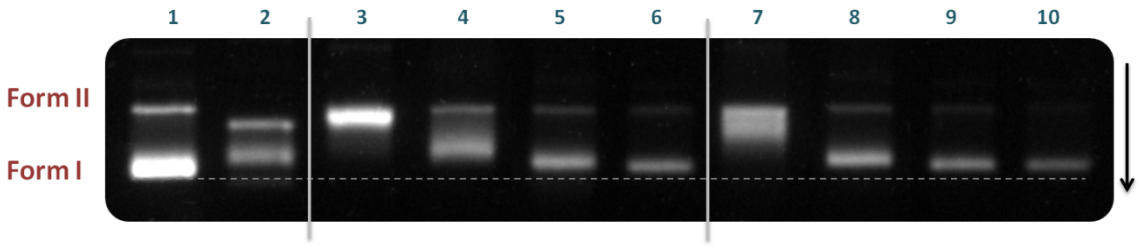

Figure 4.9. *Agarose gel electrophoresis image for pBR322 DNA incubated for 24 h at 37 °C with increasing quantities of complex **C3^{H}** in its open and closed forms.*
*Lane 1: Native plasmid DNA; lane 2: DNA + 0.5 equiv. cisplatin; lanes 3-6: DNA + 0.5 to 2.0 equiv. **C3^{H}** (open form); lanes 7-10: DNA + 0.5 to 2.0 equiv. **C3^{H}** (closed form).*

The results obtained show that the alteration of the electrophoretic mobility of plasmid DNA induced by the open forms of either **C3^{H}** or **C4^{H}** follows a similar dose-dependent pattern, as that observed for complex **C1^{H}**. 0.5 equivalents of **C3^{H}** or **C4^{H}** clearly produce the complete unwinding of supercoiled circular DNA and hence its conversion to form II, whereas higher complex concentrations lead again to effects comparable to those of cisplatin, therefore suggesting a metal covalent binding. Such

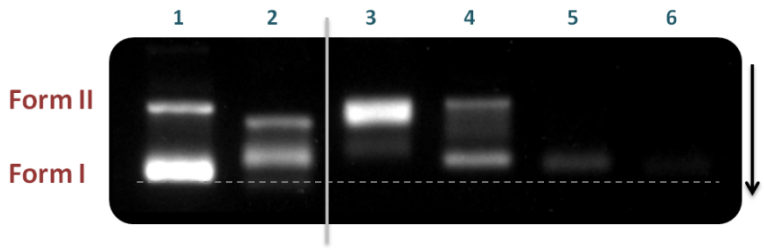

Figure 4.10. *Agarose gel electrophoresis image for pBR322 DNA incubated for 24 h at 37 °C with increasing quantities of complex* ***C4***^{H}*. Lane 1: Native plasmid DNA; lane 2: DNA + 0.5 equiv. cisplatin; lanes 3-6: DNA + 0.5 to 2.0 equiv.* ***C4***^{H} *(open form).*

covalent binding, in addition, seems to be particularly strong in the case of complex **C4**^{H}, for which a clear vanishing of the bands (indicative of adduct precipitation) is noticed at the highest concentrations (Figure 4.10, lanes 5-6).

Clear differences, however, arise when comparing the DNA-binding behavior of closed **C3**^{H} and that of closed **C1**^{H}. Despite their similar chemical structure, the former compound does not seem to show the strong intercalative activity displayed by the latter one; instead, its effects on the electrophoretic mobility of supercoiled circular DNA are comparable to those of its non-cyclized counterpart (Figure 4.9). Albeit it is unclear whether the alteration of the activity of closed **C3**^{H} stems from the presence of the methyl group or from the variation of the relative disposition of the metal centers, the results obtained for these complexes plainly indicate that solely the activity of the closed-ring species is significantly altered by the subtle modification of the metal-binding unit of the ligands. Consequently, this further corroborates that the DNA-binding activity of the open and closed photoisomers does actually proceed via two different mechanisms.

Finally, Figure 4.11 depicts the agarose gel corresponding to the mobility shift assays performed with the mononuclear complex **C5**^{H}. This complex allowed assessing the extent to which the dinuclear nature of the platinum compounds has a significant impact on the DNA-binding performance of these systems. Surprisingly, no isomeric differentiation was observed upon treating pBR322 plasmid samples with the open and closed forms of this complex, which produce in both cases solely a comparable retardation of the mobility of supercoiled DNA. The induction of such a slight

unwinding of the double helix may be expected for the open covalently-binding isomer, as a result of the loss of one of the active metal centers, but in the case of the closed-ring species this fact may have key implications. Closed **C5**^{H} does not display such a strong intercalating activity as closed **C1**^{H}, despite the fact that the substitution of a metal-binding unit with a phenyl ring may have somewhat favored the insertion of the organic ligand between DNA base pairs; consequently, covalent platinum binding appears to be crucial. It may thus be inferred that the strong DNA-unwinding activity displayed by most of the closed complexes is due to not only their insertion between DNA base pairs, but also to subsequent platinum covalent anchoring. Actually, this was already suggested by the band disappearance taking place when high amounts of closed complex **C1**^{H} are used (see Figure 4.5), which can thus be ascribed to the precipitation of covalent metal/DNA adducts.

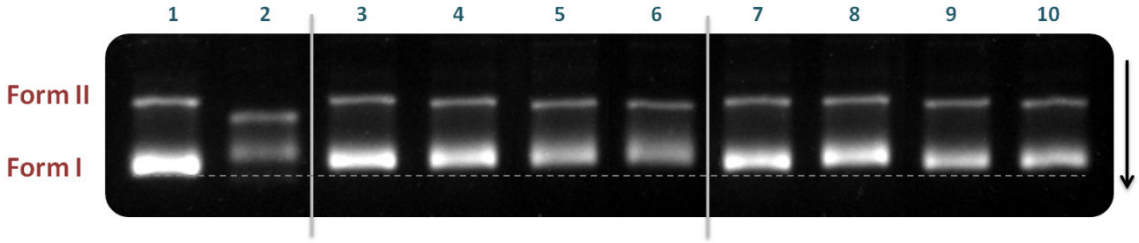

Figure 4.11. *Agarose gel electrophoresis image for pBR322 DNA incubated for 24 h at 37 °C with increasing quantities of complex* ***C5***^{H} *in its open and closed forms.*
Lane 1: Native plasmid DNA; lane 2: DNA + 0.5 equiv. cisplatin; lanes 3-6: DNA + 0.5 to 2.0 equiv. ***C5***^{H} *(open form); lanes 7-10: DNA + 0.5 to 2.0 equiv.* ***C5***^{H} *(closed form).*

In summary, the agarose gel electrophoresis experiments disclosed two fundamental facts concerning the herein presented series of platinum(II) metalloswitches. First and foremost, the two interchangeable photoisomers of these complexes possess an inherently different DNA-binding behavior, seemingly governed by either metal-mediated covalent binding or ligand-mediated base-pair insertion. This important feature, consequently, validates the use of DTC-based ligands as a novel approach to design photoactivated chemotherapeutics. Secondly, and as a result of their distinct comportment, the activity of the open and closed isomers of these DNA-interacting

agents can be independently fine-tuned by means of chemical modification of the metal environment or the bridging photoswitchable ligand, opening up a whole new way of designing metal-based anticancer drugs. After these initial observations, and with the aim of fully characterizing these unprecedented systems, the distinct properties of their open and closed photoisomers were then investigated using competitive binding assays, which allowed to further evaluating the base-pair association exhibited by most of the cyclized species.

4.1.3. Fluorescent intercalator displacement assays

Following the gel electrophoresis assays, the intercalating activity of the closed form of the metalloswitches was further examined using ethidium bromide displacement experiments. Ethidium bromide (EB), depicted in Figure 4.12, is a phenanthridine-based organic dye that acts as a strong intercalating agent; this results from its ability to efficiently bind between stacked base pairs of DNA, adopting a parallel disposition with respect to the base-pair axis.[24,25]

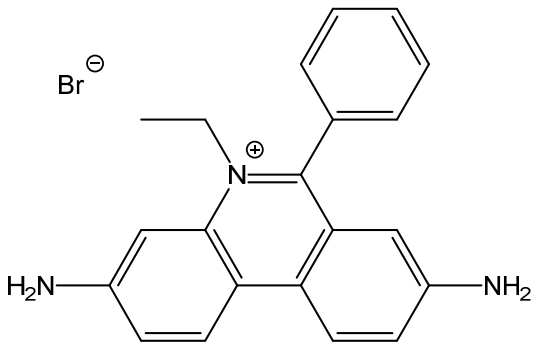

Figure 4.12. *Chemical structure of the fluorescent dye, ethidium bromide (EB).*

The binding of this pigment to double-stranded DNA does not only inhibit a wide range of relevant biological functions due to its interference with gene expression, but it also produces a great increase of its fluorescent emission intensity and lifetime, which can thus be used to monitor the binding process.[26,27] The explanation to this impactful fluorescence enhancement upon binding to duplex DNA can be found in the loss of

solvation produced by the dye's insertion within the hydrophobic base-pair environment. The resulting absence of surrounding water molecules causes the inactivation of the proton-transfer quenching mechanism, to which ethidium bromide's excited state is particularly susceptible due to its remarkably long radiative lifetime.[28,29]

Because of the singular fluorescent features of the DNA/EB system, ethidium bromide is a very convenient spectroscopic probe of nucleic acid conformation and interactions, being widely used to study the binding properties of other DNA-interacting agents through competitive assays.[30] In such studies, based on the ability of the tested species to compete with the dye for intercalation positions, the partial displacement of DNA-bound ethidium bromide produces an emission decrease of the monitored system, whose magnitude can directly be related to the interacting capability of the competing agent.

In the present work, this fluorescence assay was used to further investigate the DNA-interacting behavior of the open and closed photoisomers of the platinum metalloswitches, with the objective to corroborate the results obtained in the agarose gel electrophoresis experiments (see above). For that purpose, samples containing linear *calf thymus* DNA (*ct*-DNA) and ethidium bromide (15 μM and 75 μM, respectively) were incubated at 37 °C for a small period of time, sufficient to promote the occupation of all intercalation sites by the fluorescent dye. The resulting solutions were then treated with increasing amounts of either the open or closed isomers of the photoswitching complexes, and after an additional incubation period of 24 h in the dark, fluorescence emission spectra of all samples were recorded in the range 530-800 nm, using an excitation wavelength of λ_{exc} = 514 nm (see experimental section for details).

Representative results corresponding to the treatment of DNA/EB samples with the open and closed forms of the pyridine-containing complex **C1^{H}** are shown in Figures 4.13 and 4.14, respectively. Although a decrease of the fluorescent emission of the DNA/EB adduct —indicative of the dye's displacement— is easily appreciable in both graphs, the quenching effect is drastically more pronounced in the case of the closed species, hence implying its much higher capacity to expel DNA-bound ethidium

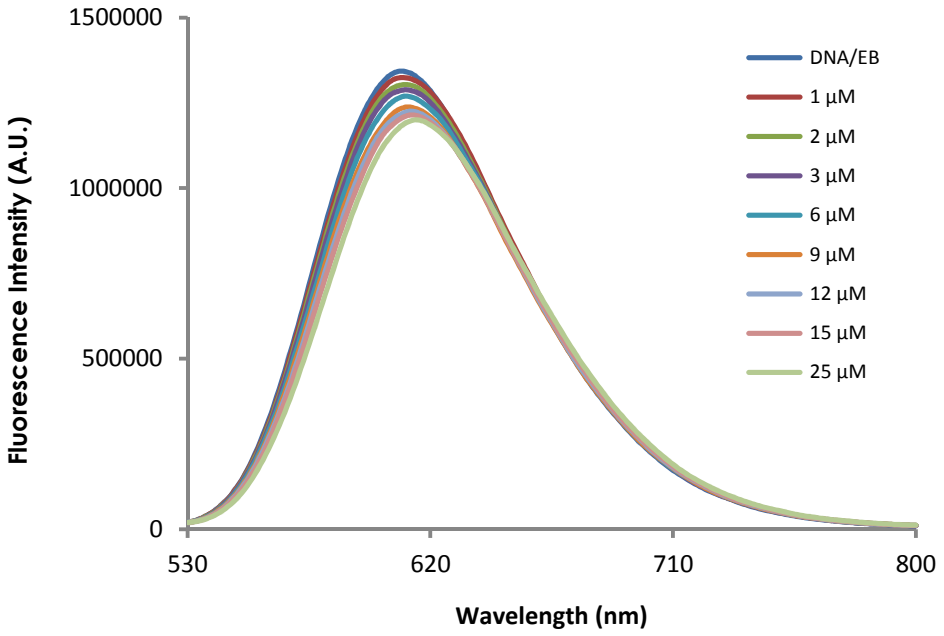

Figure 4.13. *Fluorescence emission spectra of ct-DNA/EB samples ($[DNA]_{bp}$ = 15 µM, [EB] = 75 µM) treated with increasing quantities (1-25 µM) of the open form of* ***C1^{H}****, registered after incubation for 24 h at 37 °C.*

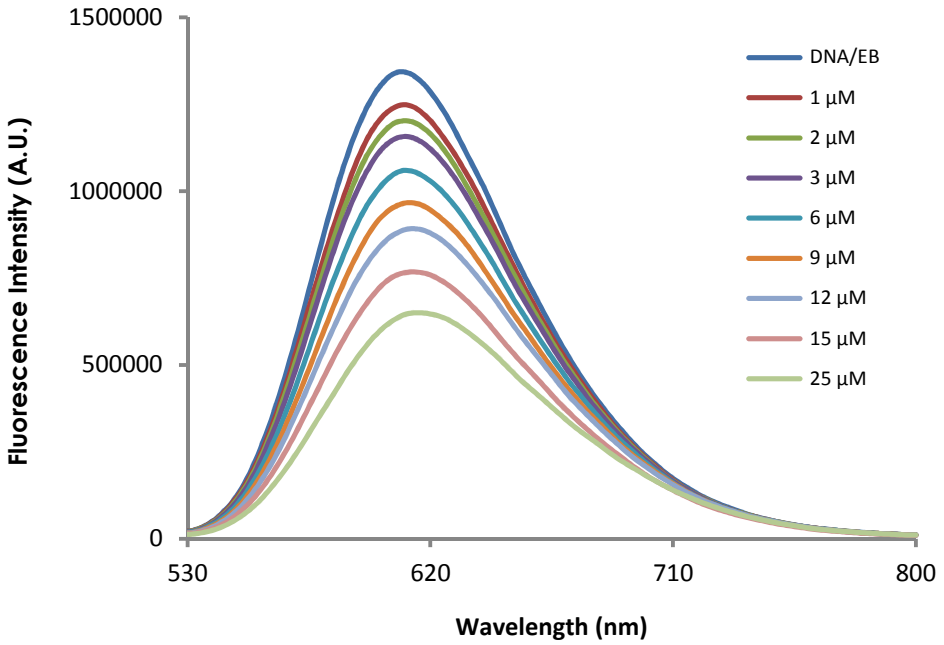

Figure 4.14. *Fluorescence emission spectra of ct-DNA/EB samples ($[DNA]_{bp}$ = 15 µM, [EB] = 75 µM) treated with increasing quantities (1-25 µM) of the closed form of* ***C1^{H}****, registered after incubation for 24 h at 37 °C.*

bromide. Accordingly, these data further evidence that, contrary to its open-ring isomer, closed **C1^{H}** exhibits a remarkably strong intercalating behavior owing to its distinct structural and electronic features, which is in good agreement with the previous gel electrophoresis observations.

Additionally, in order to establish a proper comparison between the DNA binding affinity of all studied species, these fluorescent emission results have been used to determine the corresponding Stern-Volmer quenching constants (K_{SV}) for intermolecular deactivation, by applying the Stern-Volmer equation (4.1).[31]

$$\frac{I_0}{I} = 1 + K_{SV}[Q] \qquad (4.1)$$

In this expression, I_0 represents the initial fluorescence emission intensity of the system; I represents the fluorescence emission intensity after the addition of a quencher; and Q represents the quencher, which in this particular case corresponds to the tested complex. Accordingly, a plot of I_0/I versus [complex] at the maximum emission wavelength (λ_{max} = 610 nm) can be adjusted to a straight line, whose slope is equal to the K_{SV} value. In this manner, Stern-Volmer constants of $K_{SV} = 6.6 \pm 0.8 \cdot 10^3$ M^{-1} and $K_{SV} = 42.5 \pm 0.6 \cdot 10^3$ M^{-1} were respectively calculated for the open and closed isomers of complex **C1^{H}**; the corresponding plots, obtained after three independent experimental sets of measurements, are shown in Figure 4.15.

Similar trends were observed for the open and closed isomers of all the studied metalloswitches, whose corresponding calculated Stern-Volmer constants are summarized in Table 4.1. As evidenced by the remarkably higher constant values obtained, the closed species exhibit in all cases a greatly enhanced capability of displacing the fluorescent dye from stacking interbase positions of DNA, therefore corroborating that an intercalative binding mode is in effect inherent to the cyclized form of all the complexes. In addition, noticeably lower quenching constants were systematically achieved for the fluorinated closed-ring species, compared with their corresponding non-halogenated analogues, which is also in agreement with the data achieved by electrophoretic mobility shift assays. Whilst the Stern-Volmer constants obtained from the titration of the DNA/EB system with closed **C1^{H}** and **C2^{H}** are of

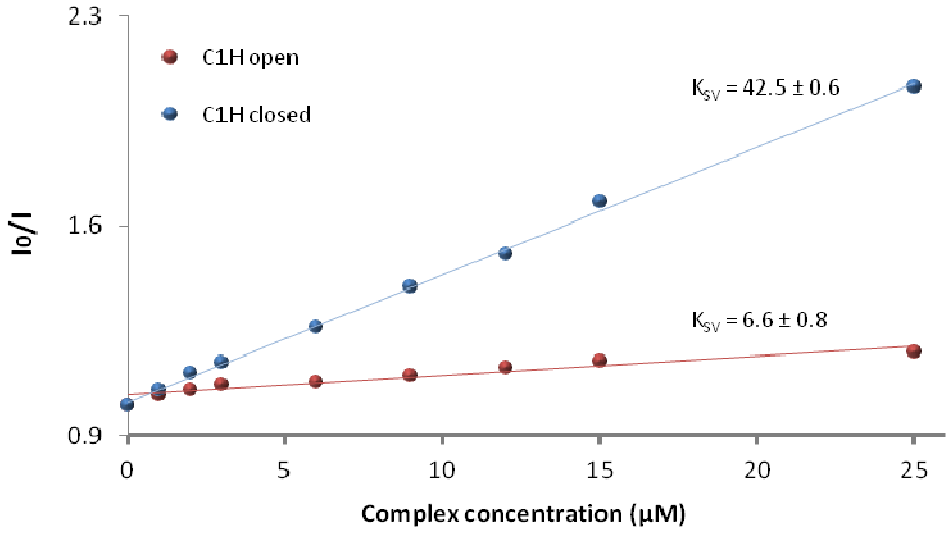

Figure 4.15. *Plots of I_0/I vs [complex] for the titration of ct-DNA/EB samples ($[DNA]_{bp}$ = 15 μM, [EB] = 75 μM) with the open (red) and closed (blue) isomers of* ***C1^H*** *at λ_{exc} = 514 nm and λ_{em} = 610 nm: experimental data points, obtained in triplicate, and linear fitting of the data. K_{SV} values are indicated in 10^3 M^{-1}.*

Table 4.1. *Calculated Stern-Volmer quenching constants for the titration of ct-DNA/EB samples ($[DNA]_{bp}$ = 15 μM, [EB] = 75 μM) with the open and closed isomers of all the synthesized metalloswitches, at λ_{exc} = 514 nm and λ_{em} = 610 nm.*

Complex	K_{SV} (10^3 M^{-1}), open form	K_{SV} (10^3 M^{-1}), closed form
C1^H	6.6 ± 0.8	42.5 ± 0.6
C1^F	4.8 ± 0.9	26.8 ± 0.9
C2^H	13.7 ± 0.7	58 ± 3
C2^F	18.4 ± 0.7	45 ± 3
C3^H	9.9 ± 0.4	37.4 ± 0.8
C4^H	17.1 ± 0.9	n/a
C5^H	1.4 ± 0.3	21.7 ± 0.6

respectively K_{SV} = 42.5 ± 0.6 · 10^3 M^{-1} and K_{SV} = 58 ± 3 · 10^3 M^{-1}, these values are correspondingly reduced to K_{SV} = 26.8 ± 0.9 · 10^3 M^{-1} and K_{SV} = 45 ± 3 · 10^3 M^{-1} for closed **C1^F** and **C2^F**. Hence, these results corroborate former observations on the negative impact of the fluorination of the cyclopentene backbone towards the DNA intercalation of these compounds. As previously speculated, these differences may originate from the probable induction of unfavorable electrostatic repulsion between the fluorine atoms and the negatively charged phosphate backbone of the double helix, which may cause slight destabilization of the resulting DNA/complex adducts.[32]

Moreover, a noticeably reduced dye-displacement ability is exhibited by the mononuclear complex **C5^H**, whose Stern-Volmer quenching constants for the open and closed isomers amount to K_{SV} = 1.4 ± 0.3 · 10^3 M^{-1} and K_{SV} = 21.7 ± 0.6 · 10^3 M^{-1}, respectively. The latter value, noticeably lower than that of closed **C1^H**, is again in line with earlier results obtained with plasmid DNA, confirming that the binding of the dinuclear species to neighboring nucleobases (subsequent to the compounds' insertion) is crucial with regard to the stabilization of the resulting DNA/complex adducts.

To sum up, the data achieved by the fluorescent intercalator displacement experiments allowed confirming the distinct DNA-binding activity and the structure-activity relationships that had previously been assessed by means of agarose gel electrophoresis assays. Moreover, the results obtained clearly support the fact that closed photoisomers are capable of inducing a stronger alteration of the double helix conformation, through a combination of intercalative and covalent associations. Consequently, it may be expected that such closed-ring species are able to induce a stronger inhibition of gene expression and DNA replication processes, which may eventually be reflected by a more potent antiproliferative activity. Therefore, further investigation on this issue was subsequently carried out applying several *in vivo* cell viability assays.

However, apart from all these somewhat expected findings, the outcome of the titration of the EB/DNA system with the non-photoreactive complex **C4^H** requires special attention. As indicated by its associated Stern-Volmer quenching constant, i.e. K_{SV} = 17.1 ± 0.9 · 10^3 M^{-1}, this imidazolic species exhibits a far superior degree of interaction with the DNA chain than other structurally similar complexes, like the open

forms of **C1^{H}** and **C3^{H}**. Its dye-displacement activity, in fact, is comparable or even greater than that of the open isomers of **C2^{H}** and **C2^{F}** (see Table 4.1), whose reasonably stronger intercalative binding capacity can be directly related to their planar-shaped quinoline metal-binding units. Nevertheless, this is not the case for the open form of complex **C4^{H}**, whose lack of potentially intercalating structural motifs hence suggests that it is presumably able to expel ethidium bromide through a different type of DNA interaction.

A possible explanation for this fact lies in the potential induction of strong alterations of the double-helix conformation through metal binding; local modifications of the secondary or tertiary structure of the DNA chain, such as those produced by the formation of 1,3-interstrand crosslinks, may indeed force the dye to abandon the nearby interbase positions due to the destabilization of the π-stacking interactions, and thereby cause fluorescence emission decrease. Such a distinctly strong binding effect, moreover, could also justify the high degree of platination and band fading observed by electrophoretic mobility shift assays of circular DNA treated with **C4^{H}**, which as aforementioned is far superior to that of all the other open-ring complexes. With a view to the future design of a subsequent generation of novel DTC-based metalloswitches with improved biological performances, this particularly interesting structure-activity relationship was further investigated using circular dichroism spectroscopy, which was expected to disclose potential key alterations of the DNA structure induced by the imidazole-bearing metallodrug.

4.1.4. Circular dichroism measurements

Circular dichroism (CD) spectroscopy is a light-absorption technique extensively used for the conformational analysis of a wide variety of optically active samples in solution, even though it is in the study of large biomolecules such as DNA and proteins where it finds its most important applications.[33]

The experimentally measured parameter in CD spectroscopy is the difference in absorbance of left- and right-handed circularly polarized light; this phenomenon, which is what the term "circular dichroism" stands for, is inherent to chiral samples

and can be defined as $\Delta A = A_L - A_R$, although for historical reasons most CD measurements are commonly reported in degrees of ellipticity (θ). Since a detailed explanation of this parameter surpasses the purpose of this brief introduction and can be found elsewhere,[34] it suffices to say that ellipticity is a measure of the distortion experienced by the circularly polarized light beam after going through a sample (due to the unequal absorption of its linear components), and that it can be easily obtained from differential absorbance as $\theta = 32.98\ \Delta A$.

Being a light-absorption phenomenon, circular dichroism is in fact tightly related to conventional UV-Vis spectroscopy, which means that the chromophores that contribute to both spectra are exactly the same. This fact, along with its high sensitivity to structural changes of the studied sample, whatever their origin, makes it an incredibly valuable tool for the structural analysis of a variety of biological systems, with common application fields including the estimation of protein secondary-structure content or the monitoring of protein and nucleic acid unfolding processes. Additionally, CD is also useful for the assessment of protein and nucleic acid interaction with small molecules, such as organic ligands, short-chain peptides or metal complexes, which is highly valuable for the present study.

As illustrated in Figure 4.16, the main naturally-occurring DNA conformations (namely A-DNA, B-DNA and Z-DNA) possess distinct CD spectra in the near-UV region, owing to their unique structural parameters and electronic interactions.[35] The spectrum of the

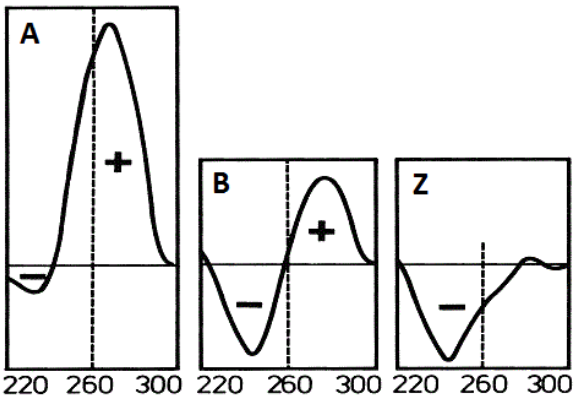

Figure 4.16. *Characteristic CD spectra corresponding to the A, B and Z conformations of DNA.*[35]

most common B conformation, in particular, is characterized by the presence of two bands of similar intensity and opposite sign, with a crossover point located at ca. 260 nm. These positive and negative bands, centered around 275 and 245 nm, act as conformational fingerprints, respectively ascribed to the asymmetry derived from the base-pair alignment and the right-handed helicity of the molecule. Thus, they can be monitored to qualitatively assess the nature and magnitude of the changes related to the secondary structure of B-DNA, such as those induced by the binding of a metal complex.

CD measurements were hence carried out with the aim of further analyzing the distinct interaction of open complex **C4^{H}** with B-DNA, compared with that of the other open-ring metalloswitches. To that end, linear *calf thymus* DNA (*ct*-DNA) solutions were treated with increasing quantities of the open form of all the platinum complexes, and the CD spectra of all the resulting samples were subsequently recorded in the near-UV region, between 235 and 315 nm, after an incubating period of 24 h in the dark at 37 °C (see experimental section for details).

Direct comparison of the CD spectra obtained after titration of B-DNA solutions with the open forms of **C1^{H}** and **C4^{H}** clearly reveals noticeable differences regarding their ability to induce structural alterations of the double helix. As shown in Figure 4.17, the

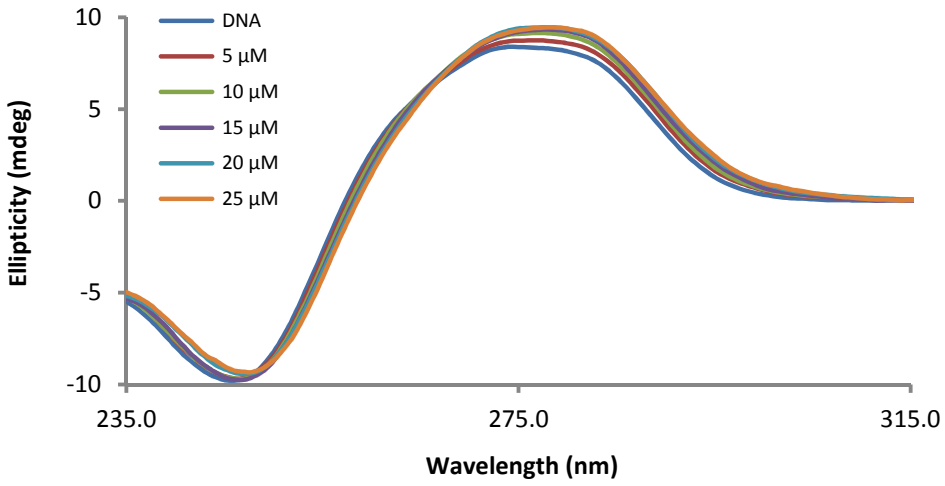

Figure 4.17. *CD spectra of ct-DNA samples ([DNA]$_{bp}$ = 50 µM) treated with increasing concentrations (5-25 µM) of the open form of complex **C1^{H}**, registered after incubation for 24 h at 37 °C.*

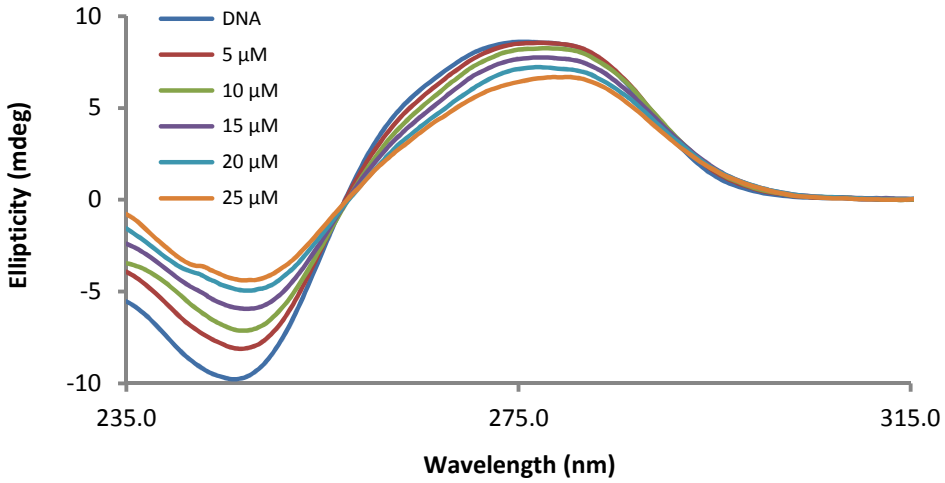

Figure 4.18. *CD spectra of ct-DNA samples ($[DNA]_{bp}$ = 50 µM) treated with increasing concentrations (5-25 µM) of the open form of complex* ***C4^{H}***, *registered after incubation for 24 h at 37 °C.*

addition of increasing amounts of open **C1^{H}** to *ct*-DNA results in a small bathochromic shift of both the positive and the negative characteristic bands of its CD spectrum, as well as a progressive slight increase of the ellipticity of the positive signal, until reaching saturation. Such spectroscopic features, which are known to be indicative of the covalent binding of monodentate platinum(II) drugs to the DNA structure,[36] are thus in agreement with the previously proposed metal-mediated activity of the open photoisomers, and corroborate as well that the binding of the complex does not have a significant impact on the helical conformation nor on the base-pair stacking of the biomolecule. In the same way, the open forms of all other complexes, apart from **C4^{H}**, do also display CD spectroscopic features comparable to those of open **C1^{H}**, hence evidencing that no significant alteration of the B-DNA topology is produced upon their covalent binding. The corresponding results are summarized in Table 4.2, which gathers the spectral changes induced upon the treatment of *ct*-DNA samples with the highest tested concentration of each complex.

The open isomer of **C4^{H}**, on the contrary, induces a drastically distinct alteration of the conformation of the double helix. The progressive binding of this imidazolic species leads to a severe decrease of the whole CD signal of B-DNA, which is especially pronounced in the case of the negative band (see Figure 4.18). These spectral changes

clearly evidence that **C4^{H}** fixation on DNA has a distinct incidence on the secondary structure of the biomolecule, generating local disruptions of the helical turn and destabilization of the alignment of adjacent base pairs. This effect is plainly consistent with the efficient expulsion of ethidium bromide noted by fluorescence assays.

Due to **C4^{H}** being the only metal complex exhibiting such a distinct DNA-interacting behavior, this comportment may necessarily arise from the presence of the

Table 4.2. *CD spectral changes induced upon the treatment of 50 μM$_{bp}$ ct-DNA samples with a 25 μM concentration of the open form of the studied complexes, after incubation for 24 h at 37 °C. Mean values for free DNA samples are given in the top row as a reference.*

Sample	CD data, negative band	CD data, positive band
DNA (50 μM$_{bp}$)	λ_{min} = 245.0 nm θ_{min} = -9.85 mdeg	λ_{max} = 275.5 nm θ_{max} = 8.65 mdeg
DNA + C1^{H} (25 μM)	λ_{min} = 247.5 nm $\Delta\theta$ = +0.87 mdeg	λ_{max} = 279.0 nm $\Delta\theta$ = +0.95 mdeg
DNA + C1^{F} (25 μM)	λ_{min} = 247.0 nm $\Delta\theta$ = +0.53 mdeg	λ_{max} = 278.0 nm $\Delta\theta$ = +0.74 mdeg
DNA + C2^{H} (25 μM)	λ_{min} = 247.5 nm $\Delta\theta$ = +0.33 mdeg	λ_{max} = 280.5 nm $\Delta\theta$ = +0.59 mdeg
DNA + C2^{F} (25 μM)	λ_{min} = 247.0 nm $\Delta\theta$ = +0.42 mdeg	λ_{max} = 278.0 nm $\Delta\theta$ = +1.35 mdeg
DNA + C3^{H} (25 μM)	λ_{min} = 247.5 nm $\Delta\theta$ = +1.85 mdeg	λ_{max} = 279.5 nm $\Delta\theta$ = -0.46 mdeg
DNA + C4^{H} (25 μM)	λ_{min} = 247.0 nm **$\Delta\theta$ = +5.41 mdeg**	λ_{max} = 280.0 nm **$\Delta\theta$ = -1.92 mdeg**
DNA + C5^{H} (25 μM)	λ_{min} = 247.5 nm $\Delta\theta$ = +0.40 mdeg	λ_{max} = 278.5 nm $\Delta\theta$ = +0.80 mdeg

methylimidazole units in the photoswitching ligand, albeit the exact mechanism through which this platinum compound induces such a structural alteration of B-DNA remains to be elucidated. Although the alkylating potential of the N-methyl group should not be completely overlooked, it is probable that the singular electronic structure of this ligand, as supported by theoretical calculations (see Chapter 3), has a direct effect on the ligand-exchange kinetics and/or the binding affinity of the platinum(II) centers, which may thus become more prone to mediate DNA cross-links. Accordingly, efforts shall be made in future investigations to assess any potential benefits of using other imidazolic structures towards the development of biologically active DTC-based ligands. The aim of such upcoming studies shall be to reach a compromise between efficient DNA interaction and optimal photochemical control, which may eventually lead to more potent photoactivatable metallodrugs.

4.2. *In vitro* studies against selected cancer cell lines

4.2.1. Cell viability assays

After successfully completing all the DNA interaction studies, which revealed interesting distinct DNA binding affinities and properties for the open and closed forms of the photochromic complexes, the potential application of such metalloswitches as novel photochemotherapeutic agents was subsequently examined. This was addressed through a series of cell viability assays, in which the effect of the open and closed isomers of each complex on cancer cell proliferation and survivability was thoroughly evaluated.

The cancer cell viability was analyzed with the MTT assay.[37,38] In this colorimetric method, the living cell population of a sample after drug treatment is determined by the addition of 3-(4,5-dimethylthiazol-2-yl)-2,5-diphenyltetrazolium bromide (MTT), a pale-yellow dye, and the monitoring of its subsequent mitochondrial reduction into its deep-purple formazan derivative. Since this reduction process (shown in Figure 4.19) is exclusively carried out by living cells, the remaining population —and therefore the cytotoxic effect of the tested drug— can be directly estimated from the relative

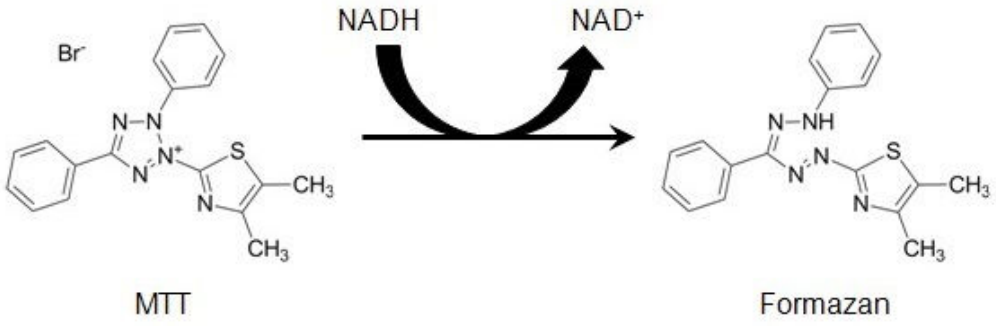

Figure 4.19. *Mitochondrial reduction of MTT (yellow) into Formazan (purple).*

absorbance of the sample near the formazan's absorption maximum, which is compared to that displayed by non-treated control cells.

Up to five cancer cell lines, with different characteristics, were selected for the initial screening of the compounds, namely A549 (lung adenocarcinoma), A375 (melanoma), MCF7 (breast carcinoma), SW620 (colorectal adenocarcinoma) and SKOV3 (ovarian adenocarcinoma). Single-point screening assays at constant complex concentrations (10 and 50 µM) were first conducted, in order to get a general estimation of the cytotoxic potential and isomeric differentiation of all species. Following the chemical treatment, all cell samples were incubated for 48 h under standardized conditions, after which the resulting viability was determined with the MTT method (see experimental section for details). The results obtained for each complex, out of three independent measurements, are depicted in Figures 4.20 to 4.26.

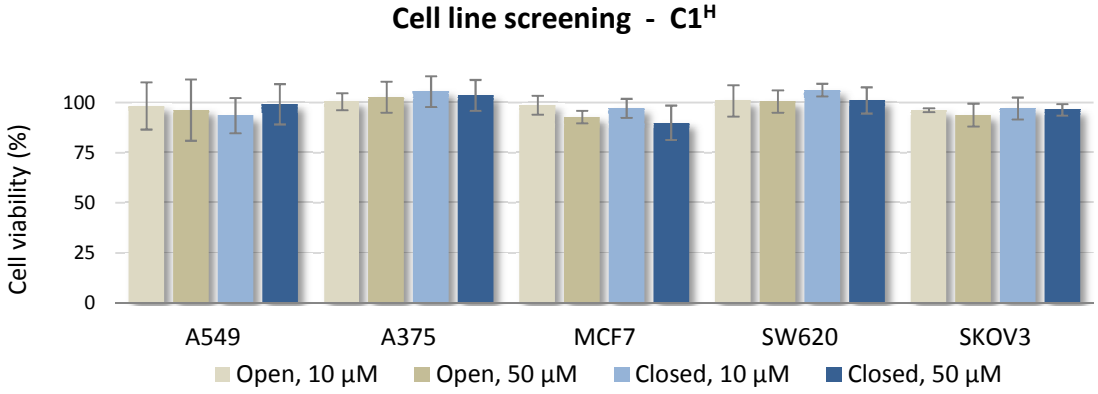

Figure 4.20. *Cell viability assays for the open and closed forms of* ***C1^{H}*** *at constant complex concentrations (10 and 50 µM), after treatment for 48 h. Results are given in % of cell viability.*

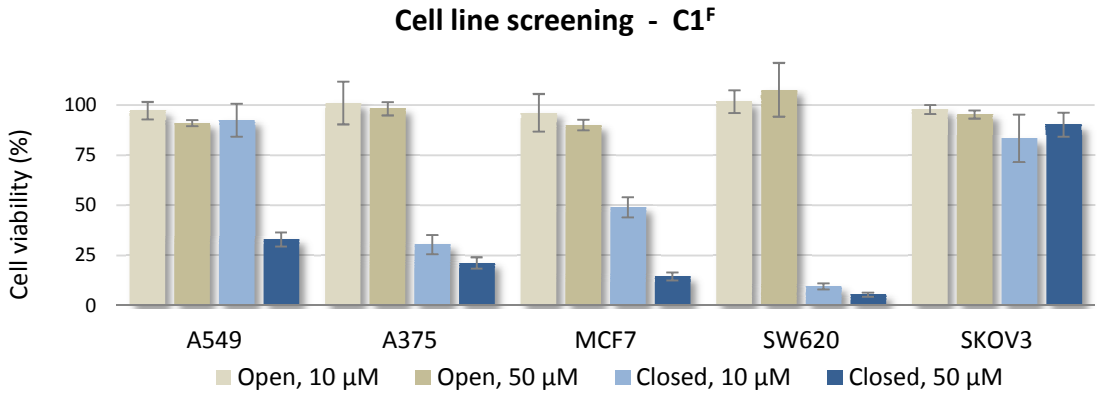

Figure 4.21. *Cell viability assays for the open and closed forms of* ***C1^{F}*** *at constant complex concentrations (10 and 50 µM), after treatment for 48 h. Results are given in % of cell viability.*

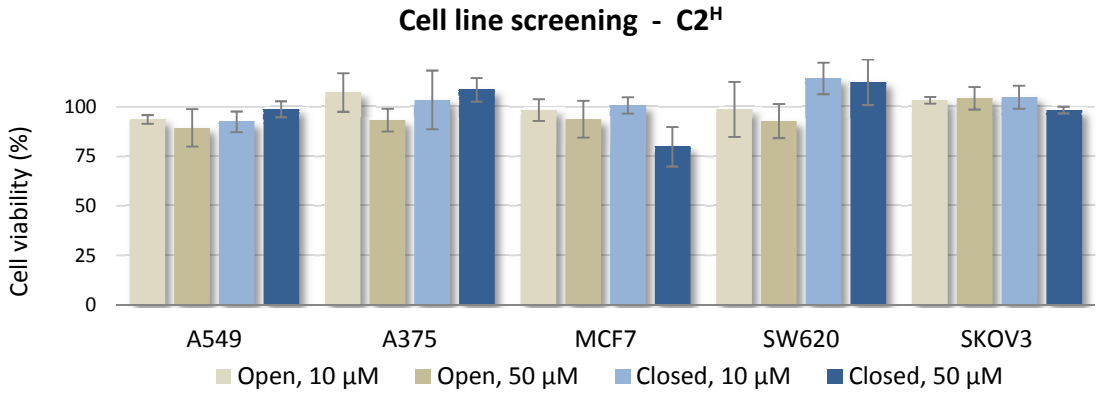

Figure 4.22. *Cell viability assays for the open and closed forms of* ***C2^{H}*** *at constant complex concentrations (10 and 50 µM), after treatment for 48 h. Results are given in % of cell viability.*

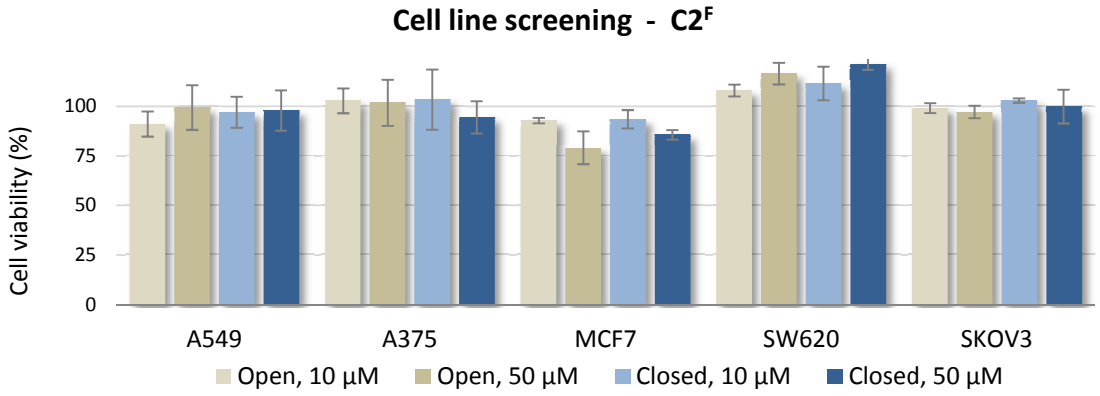

Figure 4.23. *Cell viability assays for the open and closed forms of* ***C2^{F}*** *at constant complex concentrations (10 and 50 µM), after treatment for 48 h. Results are given in % of cell viability.*

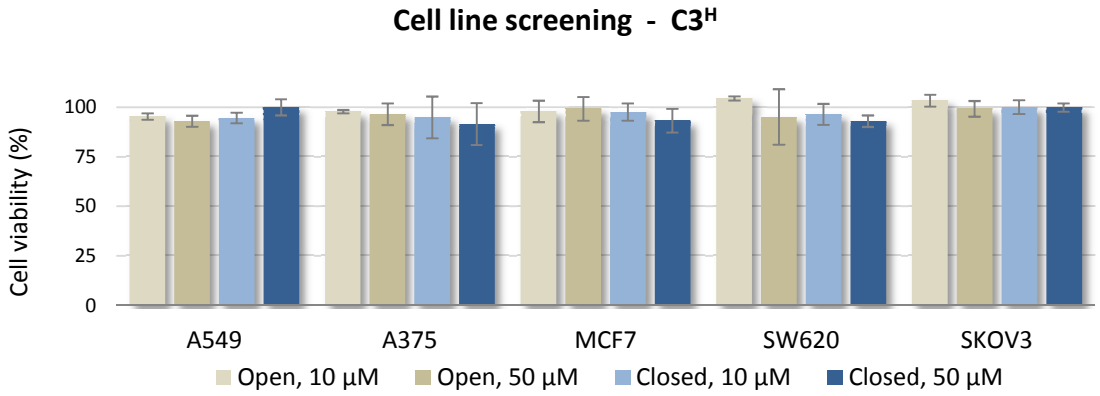

Figure 4.24. *Cell viability assays for the open and closed forms of* ***C3^{H}*** *at constant complex concentrations (10 and 50 µM), after treatment for 48 h. Results are given in % of cell viability.*

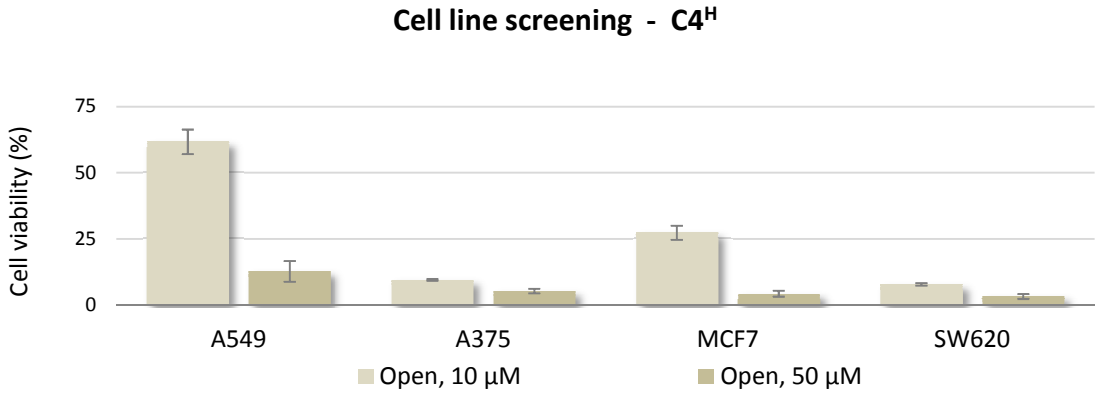

Figure 4.25. *Cell viability assays for the open form of* ***C4^{H}*** *at constant complex concentrations (10 and 50 µM), after treatment for 48 h. Results are given in % of cell viability.*

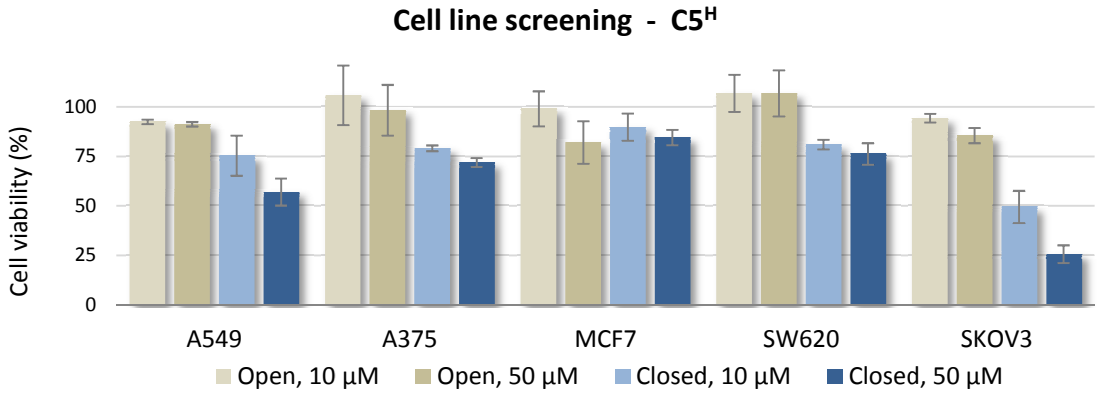

Figure 4.26. *Cell viability assays for the open and closed forms of* ***C5^{H}*** *at constant complex concentrations (10 and 50 µM), after treatment for 48 h. Results are given in % of cell viability.*

Strikingly, most of the screened platinum(II) complexes exhibit very poor cytotoxicity towards all the selected cancer cell lines, along with the absence of noticeable discrimination between the activity of their open and closed isomers. In spite of the noteworthy results achieved in the DNA interaction assays, above 75% survival of the cancer cell populations were systematically obtained after treatment with either the open or closed forms of complexes **C1^{H}**, **C2^{H}**, **C2^{F}** or **C3^{H}**. Among all these poorly-active agents, only the mononuclear complex **C5^{H}** shows slightly better results. Its closed isomer is somewhat more active than the open one, and in particular it is able to induce 50% growth inhibition of SKOV3 ovarian cancer cells at a 10 μM concentration (see Figure 4.26).

Much more promising results were achieved with complex **C1^{F}** (see Figure 4.21). Whereas the open form of this pyridine-bearing, fluorinated species is also ineffective in all tested cancer cell lines, its closed-ring counterpart presents a remarkably high cytotoxic activity against most of them, which corroborates the data obtained from all the previous DNA interaction studies. Specifically, treatment with a 50 μM concentration of closed **C1^{F}** led to cell survival levels below 35% in all cases, except for the ovarian SKOV3 line. Even more interesting is the fact that such high cancer-cell death ratios were also achieved with the melanoma, breast carcinoma and colorectal adenocarcinoma cell lines when using a therapeutically more relevant dose, namely 10 μM. Consequently, these results constitute the ultimate proof of concept for the rational design of metal-containing DTC-based photoswitches as potential photochemotherapeutic agents, confirming that the structural and electronic changes taking place upon their light-mediated transformation can effectively translate into drastically different antiproliferative activities.

Additionally, the cell viability results achieved with the photochemically inert complex **C4^{H}** were also noteworthy (see Figure 4.25). In accordance with the notably distinct features exhibited by this compound in all the previous DNA interaction studies, **C4^{H}** displays a highly cytotoxic activity, far beyond that of any other open-ring species and even slightly better than that of closed **C1^{F}**. In fact, **C4^{H}** was able to induce cell death ratios of over 85% in all the screened cancer cell lines at a 50 μM dose, and most remarkably, similarly high antiproliferative levels were achieved even at a complex concentration of 10 μM. In addition to further supporting previous evidence on a

different mechanism of action taking place with this complex, these biological data hence highlight the promising cytotoxic potential of such imidazole-based ligands, which accordingly should be further evaluated in forthcoming investigations.

To gain a better insight of the chemotherapeutic potential of complexes **C1^{F}** and **C4^{H}** after this initial screening, half maximal inhibitory concentrations (IC_{50}) in selected cell lines were subsequently determined. This parameter can be defined as the minimum concentration of a drug that is required to produce an *in vitro* 50% inhibition of a specific biological function, such as cancer cell proliferation. The cell lines chosen for this determination, performed by means of dose-response cell viability assays, were A375 and SW620; not only because both closed **C1^{F}** and open **C4^{H}** had exhibited remarkably high cytotoxicity against them, but also due to their particular interest, owing to their intrinsic characteristics. On the one hand, melanoma cells constitute the most suitable target for PACT drug candidates such as those presented in this thesis, due to the inherent accessibility to the treatment area,[39] whereas the interest in the colorectal cancer line mostly arose from its bad prognosis and current shortfall of effective therapies.[40] In addition, the IC_{50} values of cisplatin in these cell lines were determined as well under exactly the same experimental conditions, with the aim of setting out a proper comparison of the activity of the complexes with a well-established clinical reference.

Table 4.3. *Half inhibitory concentrations (IC_{50}, μM) of cisplatin and the selected complexes for the A375 and SW620 cell lines, after incubation for 48 h. The results are expressed as mean values ± SD out of three independent experiments.*

Compound	IC_{50}, A375 cells (μM)	IC_{50}, SW620 cells (μM)
Cisplatin	6.6 ± 0.6	14 ± 2
C1^{F} (open)	> 75	> 75
C1^{F} (closed)	3.1 ± 0.2	2.4 ± 0.2
C4^{H}	3.4 ± 0.6	1.8 ± 0.3

The outcome of these experiments, summarized in Table 4.3, not only further corroborate the results obtained by single-point cell viability assays, but also show that the cytotoxic potential of these complexes in the selected cancer cell lines is even greater than that of cisplatin. The determined IC_{50} values for closed **C1^{F}** and the non-photoreactive complex **C4^{H}**, all in the low micromolar range, reveal that both compounds are twice as effective as the classical platinum drug against malignant A375 melanoma cells. Moreover, the antiproliferative activity is even better against SW620 colorectal cancer cells, for which the IC_{50} values obtained for **C4^{H}** and closed **C1^{F}** are almost an order of magnitude lower than those of cisplatin.

In summary, the paramount fact regarding the *in vitro* cell viability studies performed is that they allowed validating the initial challenging and innovative research proposal developed in the present thesis. Despite the preliminary nature of these results, the fact that photoresponsive metallodrugs based on a DTC ligand-activation approach exhibit such antitumoral activities, especially against melanoma cells, is indeed highly promising. The pioneering data achieved, thus, clearly open up new perspectives in the field of PACT, which shall be further explored in future investigations through the rational design and fine-tuning of additional members of this class of metal-containing switches.

However, in view of all the results obtained from the DNA interaction studies, the explanation to the drastically distinct antitumoral activity of the closed isomer of complex **C1^{F}** still remained unclear. Actually, neither complex **C1^{F}** nor the mononuclear compound **C5^{H}** —whose closed-ring form is particularly active against ovarian SKOV3 cancer cells— had shown the most prominent DNA-interacting capabilities, compared to those of all other systems designed and prepared in this work. Consequently, to better understand the origin of their cytotoxic behavior, it was decided to carry out a comparative analysis of the cellular uptake and location of the highly active closed isomer of complex **C1^{F},** as well as the structurally analogous, but inactive, closed form of **C1^{H}**. The main idea behind this study was to try to assess whether the antitumoral activity of **C1^{F}** might be due to any potential affinity towards an alternative cellular target, apart from nuclear DNA. This investigation was performed by fluorescence confocal miscroscopy imaging.

4.2.2. Fluorescence confocal microscopy studies

Fluorescence confocal microscopy is an optical imaging technique widely used in biomedical research, especially for the detailed analysis of fixed cells and tissues that have been labeled with fluorescent probes.[41] In contrast with a conventional optical microscope, a confocal microscope is designed to exclude most of the out-of-focus light emitted by the sample, by adding a pinhole aperture before the detector that rejects any rays not directly coming from the focal plane.[42] This setup is illustrated in Figure 4.27. The resulting imaging, accordingly, is restrained to a thin cross-section of the specimen, being thus able to provide a more accurate local analysis, as well as a better contrast and optical resolution. Moreover, it even enables the reconstruction of three-dimensional models, which can be attained by progressively sectioning the sample at different depths along a vertical axis.

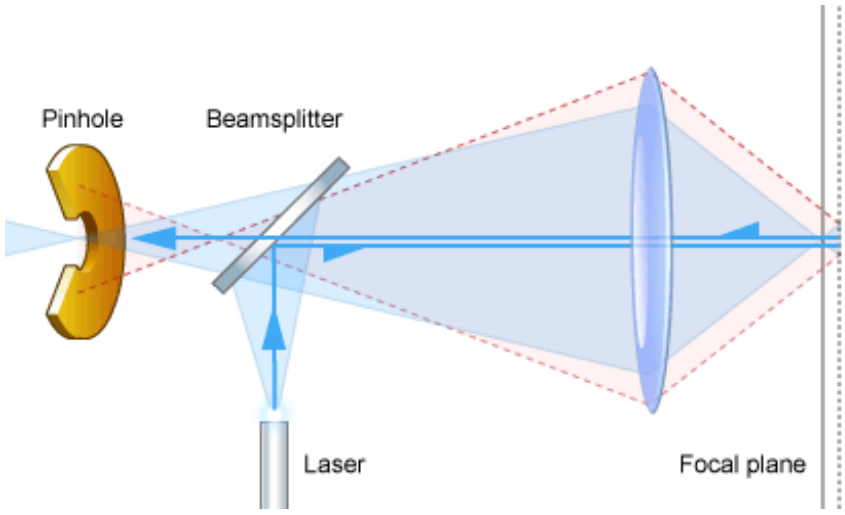

Figure 4.27. *Schematic confocal microscopy setup, displaying laser excitation and fluorescent emission collection. The red-dotted shape represents out-of-focus emitted light that gets excluded by the pinhole.*

Since the highly conjugated closed isomers of the metal complexes exhibit reasonable fluorescence emission under excitation at the standard λ_{exc} = 488 nm channel of the confocal microscope laser source, this was used to monitor the cellular uptake and distribution of closed **C1^{H}** and **C1^{F}**. To that end, A375 melanoma samples were

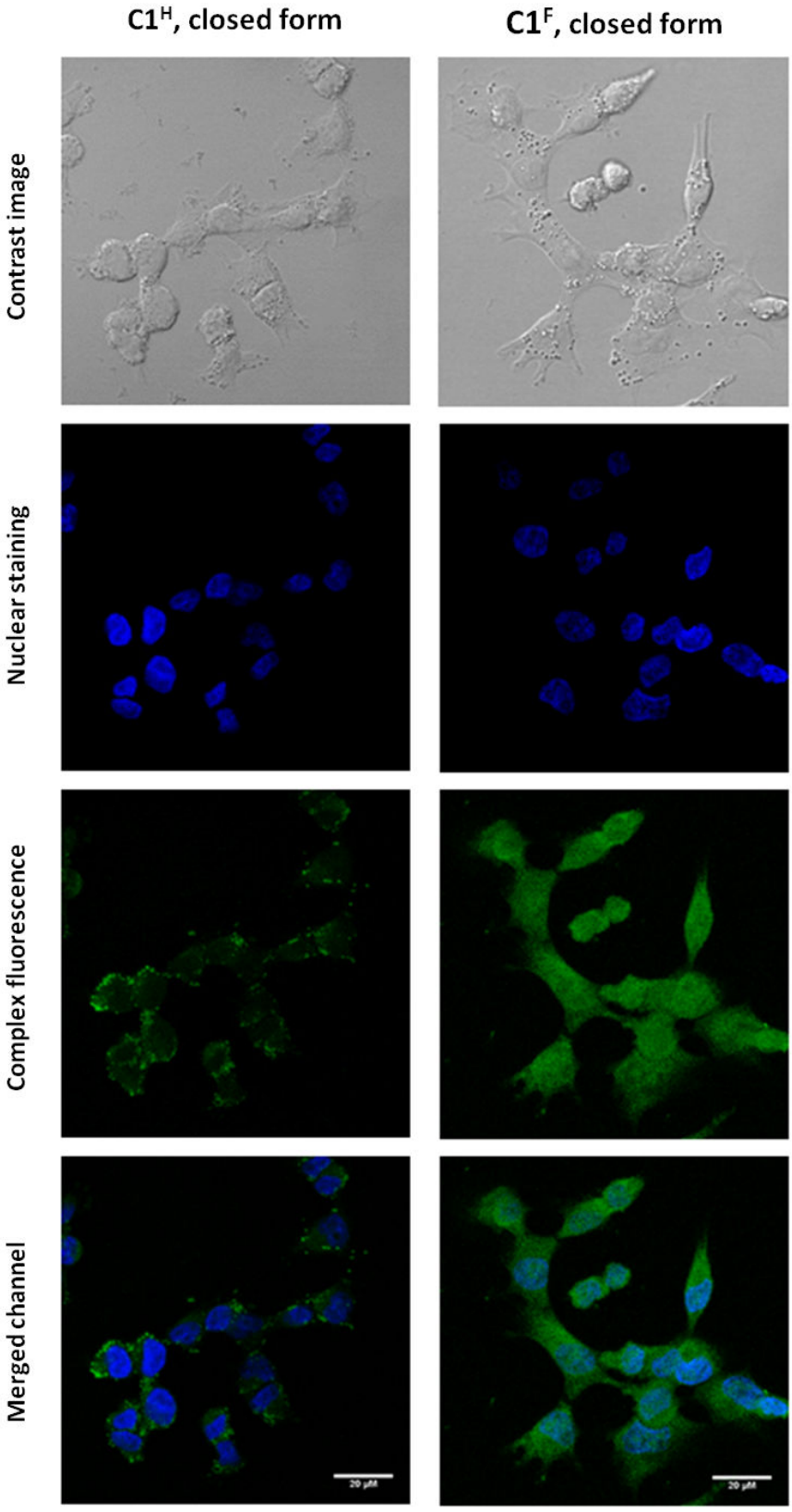

Figure 4.28. *Confocal microscopy images showing the uptake of closed* ***C1^{H}*** *(left) and closed* ***C1^{F}*** *(right) in A375 cells, after 24 h. The white bar symbolizes a length of 20 µm.*

incubated with the closed complexes for 24 h (using a concentration of 25 μM), and subsequently treated with an appropriate nuclear fluorescent staining prior to imaging (see experimental section for details). A comparative view of the resulting confocal microscopy images is shown in Figure 4.28.

The obtained fluorescent emission data clearly indicate that both complexes are capable of crossing the cell membrane and entering the cytoplasmic matrix. However, their intracellular distribution is notably different. While the highly active closed isomer of **C1^{F}** appears to be uniformly scattered across the cytosol and even in the cell nucleus, being thus able to reach its main biological target, this is not the case for the closed form of **C1^{H}**. Instead, a clearly distinguishable vesicular pattern is detected for this inactive compound, which is confined in small circular areas, unable to reach the nucleus. These observations hence suggest that, after entering the cell, closed **C1^{H}** is apparently recognized and systematically captured by secretory vesicles, most likely producing its subsequent excretion. This efflux mechanism would therefore justify its lack of significant toxicity, and probably that of some other tested complexes.

Moreover, since most platinum(II) drugs are expected to primarily target nuclear DNA, intensity profile line scans were also performed to confirm whether the efficacy of closed complex **C1^{F}** may effectively be associated with its actual localization within the cancer cell nucleus. Hence, the emission of the nuclear staining and of the tested complexes in the cell samples was measured separately as a function of the distance along a thin cross-section comprising both the nuclear and the cytoplasmic matrices, with the aim of assessing whether both signals converged. The outcome of these measurements, along with an image of the corresponding scanned area, is shown in Figures 4.29 and 4.30.

The resulting fluorescence intensity profile scans further explain the different cytotoxic activity exhibited by closed **C1^{H}** and closed **C1^{F}**. As seen in Figure 4.29, for **C1^{H}**, only the nuclear staining signal is seen during the scan of the nuclear matrix, along the white arrow. The fluorescence emission due to the closed complex is solely observed when the focal point reaches the cytosol, at about 14 μm from the starting scanning point. These data indicate that the compound is exclusively localized outside of the cell nucleus, and is therefore unable to reach its biological target.

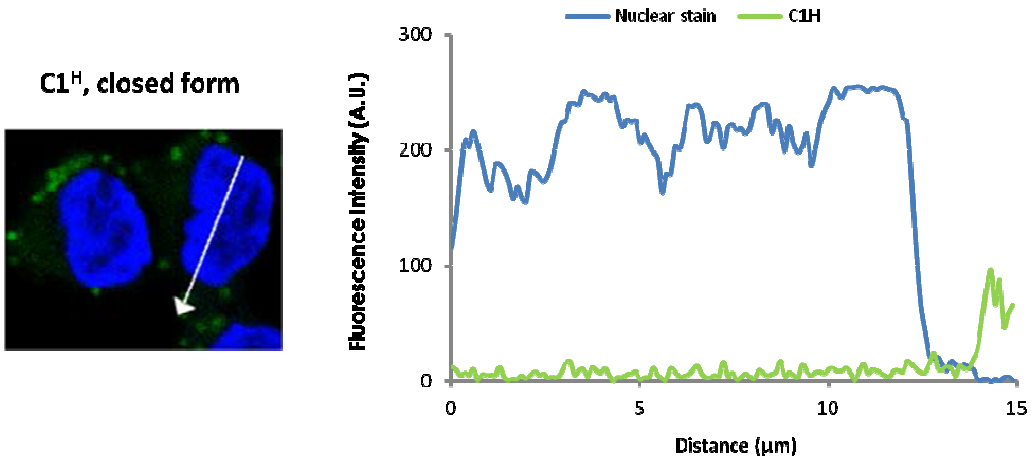

Figure 4.29. *Fluorescence intensity profile for TO-PRO-3 nuclear staining (blue) and closed complex* ***C1***^{H} *(green) in A375 cells. The scanning direction is indicated with a white arrow.*

On the contrary, for closed **C1**^{F} (Figure 4.30), a continuous significant contribution of the fluorescence emission of the compound was detected along the full scan, the first half of which, as evidenced by both the depicted arrow and the staining contribution, corresponded to the analysis of the cellular nucleus. The observed full superimposition of both signals (i.e. from the nuclear staining and from closed **C1**^{F}) unequivocally implies that the complex is in this case able to cross the nuclear membrane and effectively bind to DNA, thus explaining its high cytotoxic activity.

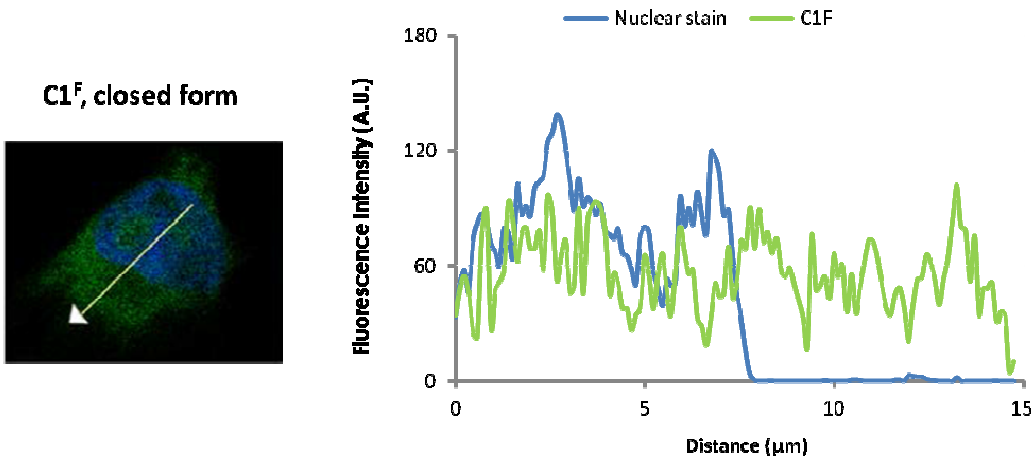

Figure 4.30. *Fluorescence intensity profile for TO-PRO-3 nuclear staining (blue) and closed complex* ***C1***^{F} *(green) in A375 cells. The scanning direction is indicated with a white arrow.*

In conclusion, the confocal microscopy studies carried out demonstrate that the singularly distinct antiproliferative activity of the closed form of complex **C1^{F}** is not strictly related with its particular interaction with biological targets, but with its ability to actually reach nuclear DNA. In fact, it is likely that this perfluorinated species may be the only closed-ring complex able to efficiently avoid vesicle-mediated excretion, and to enter the cancer cell nucleus.

Most importantly, these interesting findings leave room for more research. For instance, the use of different nuclear internalization strategies for the so-far ineffective DTC-based platinum(II) photoswitches may help to achieve more potent antiproliferative activities, as suggested by the higher degree of DNA interaction displayed by some of these complexes. Hence, the pioneering investigations carried out in this PhD thesis work bring new scientific questions to the ever-growing field of inorganic photoactivated chemotherapy, which will have to be addressed in the near future.

4.3. Experimental section

4.3.1. Materials

Ethidium bromide, sodium cacodylate, TAE (Tris Acetate-EDTA) buffer solution and *calf thymus* DNA were purchased from Sigma-Aldrich and were used as received. Plasmid pBR322 DNA was purchased from Roche. Ultrapure water was used for the preparation of all buffer and sample solutions. The pH of the prepared cacodylate buffer solution (1 mM sodium cacodylate, 20 mM NaCl, pH = 7.2) was adjusted with an ultrapure aqueous solution of hydrochloric acid. Fluorescence and circular dichroism spectra were collected in 1 cm pathlength quartz cuvettes. All reagents used during the various *in vitro* studies were purchased from Sigma-Aldrich and Invitrogen.

4.3.2. DNA interaction studies

Stock solutions - Commercial plasmid pBR322 stock solution (250 μg/mL, ca. 385 μM_{bp}) was used as received. A 150 μM *ct*-DNA stock solution was prepared by dissolution of the highly polymerized sodium salt in cacodylate buffer, and its exact concentration was established by absorbance at 260 nm (ε_{bp} = 13200 M^{-1} cm^{-1}). 5 mM stock solutions of the studied complexes were freshly prepared in DMSO before each experiment, and further diluted in DMSO/buffer mixtures as needed. Closed complex stock solutions were obtained by irradiation of the initial stock solution for 3 min at $\lambda < 365$ nm (see Chapter 3).

Agarose gel electrophoresis - Samples containing 15 μM (base pair) pBR322 plasmid DNA, 0.5-2.0 equivalents of the complexes (7.5-30 μM) and a constant 5% DMSO content in a 20 μL final volume of cacodylate buffer solution were incubated in the dark for 24 h at 37 °C. Analogous samples of free plasmid DNA and DNA bound to cisplatin (0.5 equiv., no DMSO content) were also prepared and used as controls. Following incubation, all samples were treated with 4 μL of xylene cyanol 1x aqueous solution (containing 30% glycerol) and subsequently electrophoretized in agarose gel (1% in TAE buffer, Tris-Acetate-EDTA) for 1 h at 6.25 V cm^{-1}, using a Bio-Rad horizontal

tank connected to a Consort EV231 variable potential power supply. Afterwards, the gel was treated with SYBR® Safe DNA gel stain and subsequently photographed with a Bio-Rad Gel Doc EZ imager.

Ethidium bromide displacement assays - Samples containing 15 μM (base pair) *ct*-DNA and 75 μM ethidium bromide in cacodylate buffer solution were incubated for 1 h at 37 °C, after which they were subsequently treated with increasing amounts of the complex stock solutions. The resulting samples, containing 1-25 μM of the studied complexes and up to a 5% DMSO content in a 3 mL final volume, were then incubated in the dark for 24 h at 37 °C. Following incubation, the fluorescence emission spectra of all samples were recorded at room temperature in the range 530-800 nm, using a Horiba Jovin Yvon SPEX Fluorolog 3-22 spectrofluorometer and applying an excitation wavelength of λ_{exc} = 514 nm. Non complex-containing *ct*-DNA/EB solutions in cacodylate buffer were used as control references.

Circular dichroism spectroscopy - Samples containing 50 μM (base pair) *ct*-DNA, 5-25 μM of the studied complexes and up to a 5% DMSO content in a 3 mL final volume of cacodylate buffer solution were incubated for 24 h at 37 °C. Following incubation, the circular dichroism spectra of all samples were recorded at room temperature using a Jasco J-815 CD spectropolarimeter. The spectra were measured over the 235-315 nm wavelength range in order to minimize DMSO interference, using a bandwidth of 2 nm, a data pitch of 0.5 nm, scanning speed of 50 nm min^{-1}, response time of 1 s and 4 accumulations. Non complex-containing *ct*-DNA solutions in cacodylate buffer were used as control references.

4.3.3. *In vitro* studies

Cell lines and culture - Human lung adenocarcinoma (A549), melanoma (A375), breast adenocarcinoma (MCF7), colorectal adenocarcinoma (SW620) and ovarian adenocarcinoma (SKOV3) cell lines used in this study were purchased from the American Type Culture Collection (ATCC). A549, A375, SW620 and SKOV3 cells were cultured in DMEM medium supplemented with 10% (v/v) fetal bovine serum (FBS), 100 unit/mL penicillin, 100 μg/mL streptomycin and 2 mM L-glutamine. MCF7 cells were

cultured in DMEM-F12 (Ham) media (1:1) supplemented with 5% horse serum (v/v), 100 µM sodium pyruvate, 10 µg/mL insulin, 100 unit/mL penicillin, 100 µg/mL streptomycin and 2 mM L-glutamine. All cell lines were grown at 37 °C under a 5% CO_2 atmosphere.

Cell viability assays - Cell proliferation was evaluated by the 3-(4,5-dimethylthiazol-2-yl)-2,5-diphenyl-tetrazolium bromide (MTT) assay. Cells were plated in 96-well sterile plates at a density of 10^5 cells per mL (100 µL) and allowed to grow for 24 h. After attachment to the surface, cells were then incubated with various concentrations of the studied complexes (10 and 50 µM for single-point experiments and a 0.5-5 µM range for dose-response curves), freshly dissolved in DMSO and diluted in the corresponding culture medium (DMSO final concentration = 1%), for 48 h at 37 °C. Control cells were cultured in the corresponding culture medium plus the carrier (DMSO final concentration = 1%). Following the treatment, 10 µM MTT was added to each well for an additional 4 h. Afterwards, the medium was aspirated, the purple formazan precipitate was dissolved in 100 µL of DMSO, and the absorbance at 570 nm was measured in a multi-well plate reader (Multiskan FC, Thermo Scientific). Cell viability was expressed as percentage values with respect to control cells, and data are shown as the mean value ± SD of three independent experiments. Dose-response curves and the corresponding IC_{50} values were obtained by means of non-linear fitting, calculated with GraphPad Prism 5.0 software. For comparison purposes, the cytotoxic effect of cisplatin was also evaluated under identical experimental conditions.

Confocal microscopy - A375 cells were seeded on glass coverslips at a density of 10^5 cells per mL (100 µL) and allowed to grow for 24 h. After attachment to the surface, cells were then incubated with a 25 µM concentration of the studied complexes, freshly dissolved in DMSO and diluted in the corresponding culture medium (DMSO final concentration = 1%), for 48 h at 37 °C. Control cells were cultured in the corresponding culture medium plus the carrier (DMSO final concentration = 1%). Following the treatment, cells were washed twice with 1x PBS (phosphate buffer solution) and fixed with 4% paraformaldehyde for 20 min, after which they were permeabilized with 0.2% Triton X-100 for 15 min at room temperature and washed twice with 1x PBS. Finally, 15 min incubation with 2 µM of TO-PRO®-3 iodide was performed to stain the cell nuclei, and the coverslips were then placed on the slides

using Mowiol® 4-88 mounting medium. The Z-stack images were captured using a Leica TCS-SL filter-free spectral confocal microscope equipped with a 488 nm argon laser and a 633 nm helium/neon laser, using a 63x oil immersion objective (1.4 numerical aperture), with a z voxel size of 0.56 µm and an image resolution of 1024x1024 pixels. Images were projected into a single layer and the resulting two-dimensional data set was merged using the ImageJ software package. In a first instance, the microscope was set up appropriately taking into account the autofluorescence of the studied cell line.

4.4. References

(1) Chaires, J. B. *Curr. Opin. Struct. Biol.* **1998**, *8* (3), 314–320.

(2) Hurley, L. H. *Biochem. Soc. Trans.* **2001**, *29* (6), 692–696.

(3) Pages, B. J.; Ang, D. L.; Wright, E. P.; Aldrich-Wright, J. R. *Dalton Trans.* **2015**, *44* (8), 3505–3526.

(4) Wang, D.; Lippard, S. J. *Nat. Rev. Drug. Discov.* **2005**, *4* (4), 307–320.

(5) Cepeda, V.; Fuertes, M. A.; Castilla, J.; Alonso, C.; Quevedo, C.; Pérez, J. M. *Anticancer. Agents Med. Chem.* **2007**, *7* (1), 3–18.

(6) Sirajuddin, M.; Ali, S.; Badshah, A. *J. Photochem. Photobiol. B* **2013**, *124*, 1–19.

(7) Lerman, L. S. *J. Mol. Biol.* **1961**, *3* (1), 18–30.

(8) Keck, M. V; Lippard, S. J. *J. Am. Chem. Soc.* **1992**, *114* (9), 3386–3390.

(9) Werner, M. H.; Gronenborn, A. M.; Clore, G. M. *Science* **1996**, *271* (5250), 778–784.

(10) Brodie, C. R.; Collins, J. G.; Aldrich-Wright, J. R. *Dalton Trans.* **2004**, No. 8, 1145–1152.

(11) Vos, J. G.; Kelly, J. M. *Dalton Trans.* **2006**, No. 41, 4869–4883.

(12) Jennette, K. W.; Lippard, S. J.; Vassiliades, G. A.; Bauer, W. R. *Proc. Natl. Acad. Sci.* **1974**, *71* (10), 3839–3843.

(13) Lainé, M.; Richard, F.; Tarnaud, E.; Bied-Charreton, C.; Verchère-Béaur, C. *J. Biol. Inorg. Chem.* **2004**, *9* (5), 550–562.

(14) Duskova, K.; Sierra, S.; Fernández, M.-J.; Gude, L.; Lorente, A. *Bioorg. Med. Chem.* **2012**, *20* (24), 7112–7118.

(15) Nagababu, P.; Kumar, D. A.; Reddy, K. L.; Kumar, K. A.; Mustafa, M. B.; Shilpa, M.; Satyanarayana, S. *Met. Based. Drugs* **2008**, *2008*, ID 275084.

(16) Hannon, M. J.; Painting, C. L.; Jackson, A.; Hamblin, J.; Errington, W. *Chem. Commun.* **1997**, No. 18, 1807–1808.

(17) Oguey, C.; Foloppe, N.; Hartmann, B. *PLoS One* **2011**, *5* (12), e15931.

(18) Kelly, J. M.; Tossi, A. B.; McConnell, D. J.; OhUigin, C. *Nucleic Acids Res.* **1985**, *13* (17), 6017–6034.

(19) Hannon, M. J.; Moreno, V.; Prieto, M. J.; Moldrheim, E.; Sletten, E.; Meistermann, I.; Isaac, C. J.; Sanders, K. J.; Rodger, A. *Angew. Chem. Int. Ed.* **2001**, *40* (5), 879–884.

(20) Aaij, C.; Borst, P. *Biochim. Biophys. Acta - Nucleic Acids Protein Synth.* **1972**, *269* (2), 192–200.

(21) Cohen, G. L.; Bauer, W. R.; Barton, J. K.; Lippard, S. J. *Science* **1979**, *203* (4384), 1014–1016.

(22) Sherman, S. E.; Lippard, S. J. *Chem. Rev.* **1987**, *87* (5), 1153–1181.

(23) Bates, A. D.; Maxwell, A. *DNA Topology*; Oxford University Press: Oxford, 2005.

(24) Nafisi, S.; Saboury, A. A.; Keramat, N.; Neault, J. F.; Tajmir-Riahi, H. A. *J. Mol. Struct.* **2007**, *827* (1–3), 35–43.

(25) Tsai, C. che; Jain, S. C.; Sobell, H. M. *J. Mol. Biol.* **1977**, *114* (3), 301–315.

(26) Waring, M. J. *J. Mol. Biol.* **1965**, *13* (1), 269–282.

(27) Heller, D. P.; Greenstock, C. L. *Biophys. Chem.* **1994**, *50* (3), 305–312.

(28) Olmsted, J.; Kearns, D. R. *Biochemistry* **1977**, *16* (16), 3647–3654.

(29) LePecq, J. B.; Paoletti, C. *J. Mol. Biol.* **1967**, *27* (1), 87–106.

(30) Chen, W.; Turro, N. J.; Tomalia, D. A. *Langmuir* **2000**, *16* (1), 15–19.

(31) Permyakov, E. A. *Luminescent Spectroscopy of Proteins*; CRC Press: Boca Raton, FL, 1992.

(32) Martín-Pintado, N.; Yahyaee-Anzahaee, M.; Deleavey, G. F.; Portella, G.; Orozco, M.; Damha, M. J.; González, C. *J. Am. Chem. Soc.* **2013**, *135* (14), 5344–5347.

(33) Berova, N.; Nakanishi, K.; Woody, R. W. *Circular Dichroism: Principles and Applications, Second Edition*; Wiley-VCH: New York, 2000.

(34) Kelly, S. M.; Jess, T. J.; Price, N. C. *Biochim. Biophys. Acta - Proteins Proteomics* **2005**, *1751* (2), 119–139.

(35) Fasman, G. D. *Circular Dichroism and the Conformational Analysis of Biomolecules*; Springer US: Boston, MA, 1996.

(36) Macquet, J.-P.; Butour, J.-L. *Eur. J. Biochem.* **1978**, *83* (2), 375–387.

(37) Mosmann, T. *J. Immunol. Methods* **1983**, *65* (1–2), 55–63.

(38) Marshall, N. J.; Goodwin, C. J.; Holt, S. J. *Growth Regul.* **1995**, *5* (2), 69–84.

(39) Horbert, R.; Pinchuk, B.; Davies, P.; Alessi, D.; Peifer, C. *ACS Chem. Biol.* **2015**, *10* (9), 2099–2107.

(40) Aklilu, M.; Eng, C. *Nat. Rev. Clin. Oncol.* **2011**, *8* (11), 649–659.

(41) Semwogerere, D.; Weeks, E. R. In *Encyclopedia of Biomaterials and Biomedical Engineering, Second Edition*; CRC Press, 2008; pp 705–714.

(42) Pawley, J. B. *Handbook of Biological Confocal Microscopy, Third Edition*; Springer: New York, 2006.

CONCLUSIONS

Summary and conclusions

The main aim of this PhD thesis was to examine whether potential photoactivatable metal compounds for anticancer application could be achieved through the photomodification of coordinated ligands. For that purpose, a series of photoswitchable platinum(II) complexes based on photoresponsive dithienylcyclopentene moieties were designed, synthesized and fully characterized, and their biological properties were subsequently evaluated.

Hence, following different established procedures, various heterocyclic, N-donor metal-binding units were connected to dithienylcylopentene synthons, bearing either a hydrogenated or a perfluorinated backbone. In this manner, ten photoresponsive ligands were obtained with reasonable yields, most of them being hitherto unreported in the literature. These molecules were then used to yield up to six dinuclear Pt(II) complexes, as well as a mononuclear Pt(II) species. All compounds were fully characterized by means of common techniques, i.e. ^{1}H NMR spectroscopy, mass spectrometry and elemental analysis.

The connectivity of all metal complexes was further confirmed via X-ray determination of several crystal structures. These measurements actually revealed the *trans* disposition of the chlorido ligands coordinated to the Pt(II) centers, as well as the

ability of some of the complexes to generate distinct supramolecular associations in the solid state, as a result of their fluorinated cyclopentene backbone.

The photochemical properties of all the ligands and metal complexes synthesized were evaluated through UV-Vis absorption and ^{1}H NMR spectroscopies. The photochemical window of the ligands, in both their open and closed states, was found to be dependent on both the metal-binding units and the bridging cycloalkene moiety. With the exception of ligand **L4^{H}**, which turned out to be photoinactive, all other ligands showed thermally-stable photochromic performances. Most remarkably, the coordination to the Pt(II) metal centers produced an enhancement of these capabilities, as evidenced by the higher photoconversion rates and quantum yields displayed by the corresponding metal complexes.

DFT calculations were carried out to investigate the distinct photochemical properties of the imidazolic ligand **L4^{H}**, which was unable to undergo light-mediated cyclization. The results obtained pointed to a distinct electronic distribution of the LUMO of this system as the main cause of its photoinertness. In fact, the larger *p* contribution of the atoms next to the reactive 2-position of the thiophene rings of this species confers a much higher antibonding character to the frontier orbital, which ultimately blocks the required orbital rotation leading to the formation of the new carbon-carbon bond. Furthermore, the applied calculation methods evidenced a remarkable capacity of accurately reproducing the experimental features of the systems studied. Hence, computational analysis shall be considered as a highly valuable tool for the future design of novel DTC-based systems with specific spectroscopic characteristics.

DNA-interaction studies performed with the platinum(II) metal complexes confirmed that the overall activity of these unprecedented class of photoactivatable agents can be efficiently modified through their light-mediated conversion. Clearly distinct DNA-interacting properties for the open and closed forms of the metal complexes were observed. Different metal covalent binding and ligand intercalative association for the two forms were established by agarose gel electrophoresis and fluorescent dye-displacement assays. Accordingly, these very important results imply that the activity of each photoisomer may be independently tailored through appropriate structural modifications, which opens up new synthetic possibilities for the future development of more specific DTC-based metallodrugs.

Circular dichroism measurements were performed to assess the particular alteration of the DNA structure induced by the binding of the non-photoswitching complex **C4^{H}**. The experiments carried out suggest that this compound displays a prominent ability to produce covalent DNA cross-linking. Hence, these observations demonstrate that the electronic structure of the bridging ligand has a direct impact on the binding properties of the metal centers, which can be exploited to selectively modify their activity.

In the last part of this study, the antiproliferative activity of the open and closed forms of the complexes prepared was tested against several cancer cell lines. Although the distinct DNA-interacting capability of each photoisomer did not translate into noticeable cytotoxic performances for most of the compounds, highly promising results were achieved for complex **C1^{F}**. The closed form of this platinum(II) complex exhibited better cytotoxic activity than cisplatin against melanoma and colorectal cells, while its open form remained non-toxic. This outstanding outcome thus represents a 'proof of concept' regarding the potential application of DTC photoswitches in the development of novel PACT agents.

In addition, very high cytotoxic activities were also presented by the non-photoreactive complex **C4^{H}**. This fact, may be directly related to the strong DNA cross-linking capacity displayed by this complex, as revealed through circular dichroism measurements. Consequently, the potential benefits of incorporating other imidazolic structures in DTC-based metal complexes constitute a promising perspective requiring further thorough investigation.

Finally, confocal microscopy experiments carried out to analyze the cellular uptake of these novel metallodrugs suggest that the inactivity of most of the complexes studied may stem from their inability to actually reach their primary target, i.e. nuclear DNA. Accordingly, the exploration of the possible internalization of these compounds through their incorporation into drug-delivery systems represents another very challenging topic for forthcoming investigations.

In summary, the results obtained during this PhD validated the proposed approach, as the objective set at the beginning of the work was reached. Indeed, the data obtained have allowed to clearly demonstrate that DTC-based systems can be considered as an alternative new class of molecules in the area of PACT. However, a number of new

scientific questions opened up by the pioneering work presented in this thesis need to be addressed in future studies. For instance, the biological photoactivation of the compounds so far prepared takes place in the UV region, which is not ideal for real *in vivo* applications. Therefore, modification of these systems is necessary to shift the photocyclization process towards visible light (or even towards near IR). This may be achieved through the modification of the ligands (for example by incorporating withdrawing and/or donating groups) and/or the metal complexes (different metal ions can be used or the preparation of organometallic compounds can be envisaged), as well as their potential combination with light-upconverting carriers.